Genetische Charakterisierung und Therapieüberwachung von fortgeschrittenen Tumorerkrankungen mit Hilfe der Hochdurchsatzsequenzierung und Liquid Biopsy

Dissertation

der Mathematisch-Naturwissenschaftlichen Fakultät

der Eberhard Karls Universität Tübingen

zur Erlangung des Grades eines

Doktors der Naturwissenschaften

(Dr. rer. nat.)

vorgelegt von

Dipl. biol. Franz Joachim Hilke

aus Berlin

Tübingen

2020

Gedruckt mit Genehmigung der Mathematisch-Naturwissenschaftlichen Fakultät der Eberhard Karls Universität Tübingen.

Tag der mündlichen Qualifikation: 21.12.2020

Stellvertretender Dekan: Prof. Dr. József Fortágh

1. Berichterstatter: Prof. Dr. Olaf Horst Riess

2. Berichterstatter: Prof. Dr. Hans-Georg Rammensee

Inhaltsverzeichnis

Abbildungsverzeichnis

Tabellenverzeichnis

Abkürzungsverzeichnis

WHO	World Health Organization
HNSCC	Head and neck squamous cell carcinoma/ Kopf-Hals-Tumoren
ctDNA	Zellfreie zirkulierende Tumor DNA
WES	Whole exome sequencing
UV	Ultraviolett
DNA	Desoxyribonukleinsäure
ICGC	International Cancer Genome Consortium
TCGA	The Cancer Genome Atlas Project
NGS	Next-generation sequencing
WGS	Whole genome sequencing
dNTP	Desoxyribonukleosidtriphosphat
CRT	Cyclic reversible termination
TIRF	Total internal reflection flourescense
cfDNA	Circulating cell-free DNA
CNV	Copy number variant/ Kopienzahlveränderung
ddPCR	Digital droplet PCR
PCR	Polymerase Chain reaction
MRD	Molecular residual disease/ molekulare Resterkrankung
HPV	Humanes Papillomavirus
SKCM	Human skin cutaneous melanoma
CT	Computertomographie
IMRT	Intensity Modulated Radiation Therapy
DKTK-ROG	Deutsches Konsortium für Translationale Krebsforschung, Radiation Oncology Group

CRP	C-reaktives Protein
PEG	Perkutane endoskopische Gastronomie
G-CFS	Granulocyte colony stimulating factor/ Granulozyten-Kolonie-stimulierender Faktor
RTOG	Radiation Therapy Oncology Group
RCTX	Radiochemotherapie
cvDNA	Circulating virus DNA
UMI	Unique molecular identifer
CTLA-4	Zytotoxisches T-Lymphozyten-assoziiertes Protein 4
PD-1	Programmiertes Zelltod Protein 1
PD-L1	Programmiertes Zelltod Protein 1 Ligand
SNV	Single nucleotide variant/ Einzelnukleotidmutationen
INDEL	Insertions and deletions/ kleine Insertionen und Deletionen
TMB	Tumor mutational burden/ Tumormutationslast
RECIST	Response Evaluation Criteria In Solid Tumors
PD	Progressive disease
SD	Stable disease
PR	Partial response
EGFR	Endothelialer Wachstumsfaktor-Rezeptor
HPD	Hyper progressive disease
HR	Hazard ratio
CI	Confidence interval/ Konfidenzintervall
IFN-γ	Interferon gamma
TNF	Tumornekrosefaktors
CIS	Cytokine induced senescence/ Zytokin-induzierte Seneszenz

Zusammenfassung

Laut Angaben der Weltgesundheitsorganisation (World Health Organization, WHO) sind Krebserkrankungen die zweithäufigste Todesursache weltweit. Im Jahr 2018 belief sich die Anzahl der Todesfälle in Folge einer Krebserkrankung auf ca. 9,6 Millionen Menschen (1). Weltweit ist jeder sechste Tod die Folge einer Krebserkrankung. Zwei Fortschritte der jüngeren Vergangenheit haben die Krebstherapie revolutioniert. Die genetische Analyse von Tumoren hat zur Identifikation von Zielstrukturen geführt, die eine personalisierte und tumorspezifische Therapie erlaubt. Zudem zielen neuartige Ansätze der Immuncheckpoint-Blockade darauf ab eine Anti-Tumor-Immunität zu fördern. Trotz dieser Fortschritte profitiert die Mehrheit der Tumorpatienten im fortgeschrittenen Stadium nicht von den derzeit zugelassenen Therapien.

Im Rahmen der Promotion wurden zwei Tumorentitäten untersucht: das Maligne Melanom und die Kopf-Hals-Tumoren. In beiden Fällen wurden Patienten in einem fortgeschrittenen Krankheitsstadium untersucht mit dem Ziel Treibermutationen mittels Hochdurchsatzsequenzierung zu identifizieren, die mit dem Therapieansprechen korrelieren oder sich als Behandlungsziel eignen. Die soliden Tumoren der Patienten mit einem Kopf-Hals-Tumor (HNSCC) wurden mit Hilfe eines Tumorgenpanels genetisch charakterisiert. Die dabei gefundenen Treibermutationen dienten im Rahmen der *Liquid Biopsy* als Surrogatmarker für den Tumor, um das Therapieansprechen der Radiochemotherapie zu beobachten. Die Dynamik der ctDNA korrelierte mit der Tumorlast vor Therapiebeginn und nahm im Rahmen der Behandlung ab. Konnte nach Abschluss der Therapie ctDNA detektiert werden, kam es zu einem Rezidiv. Die zirkulierende zellfreie Tumor DNA (ctDNA) erwies sich als zuverlässiger Surrogatmarker für den Tumor.

Die Patienten mit einem Malignen Melanom wurden ebenfalls mittels Panel- oder Gesamt-Exom-Sequenzierung (WES) genetisch charakterisiert und das Therapieansprechen dokumentiert. Als potentielle genetische Resistenzmarker wurden schwere Mutationen in den Genen der Zellzykluskontrolle identifiziert. Insbesondere der MDM-p53-p21Cip1- und p16Ink4a-CDK4/6-Rb1-Signalweg waren bei den Therapieversagern gestört. Des Weiteren konnten durch die umfassende genetische Charakterisierung Mutationen identifiziert werden, die spezifisch für den jeweiligen histopathologischen Subtypen sind.

Summary

The World Health Organization (WHO) states cancer the second most common cause of death worldwide. In 2018 the number of deaths due to cancer amounted to approximately 9.6 million people (1). Worldwide every sixth death is due to cancer. Two recent advances have revolutionized cancer therapy. The genetic analysis of tumors has led to the identification of target structures that allow for personalized and tumor-specific therapy. In addition, novel approaches of immune checkpoint blockade aim to promote anti-tumor immunity. Despite these advances, the majority of advanced cancer patients do not benefit from currently approved therapies.

Two tumor entities were investigated in the course of the PhD: melanoma and head and neck tumors. In both cases, the patients had at an advanced stage of the disease. For a better understanding of the factors that control the response to treatment as well as the identification of new therapeutic targets (driver mutations) high-throughput sequencing was applied. For this purpose the solid tumor biopsies of patients with head and neck cancer (HNSCC) were genetically characterized using a tumor panel. The identified driver mutations were used in Liquid Biopsy to monitor the response of the patients to radiochemotherapy. It was shown that the dynamics of Liquid Biopsy correlate with the course of therapy. The circulating cell-free tumor DNA (ctDNA) proved to be a reliable surrogate marker for the tumor. And the ctDNA dynamics correlated with the tumor load prior to therapy and decreased during treatment. If ctDNA could be detected after completion of therapy, a recurrence occurred.

Patients with malignant melanoma were also genetically characterized by panel or whole exome sequencing (WES) and the response to therapy was documented. The in-vivo and in-vitro shown association between the anti-proliferative effect of immune checkpoint therapy by induction of the p16Ink4a-CDK4/6-Rb1 and MDM-p53-p21Cip1 signaling was disturbed in patients with treatment failures. Serious mutations in the cell cycle control genes were identified as potential genetic resistance markers. Furthermore, comprehensive genetic characterization allowed the identification of mutations specific to the respective histopathological subtypes.

Liste der Publikationen der Dissertation

a) Akzeptierte Publikationen

Kerstin Zwirner, **Franz J Hilke**, German Demidov, Stephan Ossowski, Cihan Gani, Olaf Rieß, Daniel Zips, Stefan Welz, Christopher Schroeder. *"Circulating Cell-Free DNA: A Potential Biomarker to Differentiate Inflammation and Infection During Radiochemotherapy"*, Radiother Oncol, 129 (3), 575-581 Dec 2018

Andrea Forschner, **Franz-Joachim Hilke**, Irina Bonzheim, Axel Gschwind, German Demidov, Teresa Amaral, Stephan Ossowski, Olaf Riess, Christopher Schroeder, Peter Martus, Bernhard Klumpp, Irene Gonzalez-Menendez, Claus Garbe, Heike Niessner, Tobias Sinnberg. *"MDM2, MDM4 and EGFR Amplifications and Hyperprogression in Metastatic Acral and Mucosal Melanoma"*, Cancers (Basel), 12 (3) 2020 Feb 26

Ellen Brenner, Barbara F Schörg, Fatima Ahmetlić, Thomas Wieder, **Franz Joachim Hilke**, Nadine Simon, Christopher Schroeder, German Demidov, Tanja Riedel, Birgit Fehrenbacher, Martin Schaller, Andrea Forschner, Thomas Eigentler, Heike Niessner, Tobias Sinnberg, Katharina S Böhm, Nadine Hömberg, Heidi Braumüller, Daniel Dauch, Stefan Zwirner, Lars Zender, Dominik Sonanini, Albert Geishauser, Jürgen Bauer, Martin Eichner, Katja J Jarick, Andreas Beilhack, Saskia Biskup, Dennis Döcker, Dirk Schadendorf, Leticia Quintanilla-Martinez, Bernd J Pichler, Manfred Kneilling, Ralph Mocikat, Martin Röcken. *"Cancer Immune Control Needs Senescence Induction by Interferon-Dependent Cell Cycle Regulator Pathways in Tumours"*, Nat Commun, 11 (1), 1335 2020 Mar 12

b) Eingereichte Manuskripte

Franz J. Hilke*, Francesc Muyas*, Jakob Admard, Beate Kootz, Dominik Nann, Stefan Welz, Olaf Rieß, Daniel Zips, Stephan Ossowski, Christopher Schroeder, Kerstin Clasen. "*Dynamics of cell-free tumour DNA correlate with treatment response of head and neck cancer patients receiving radiochemotherapy"*, Radiother Oncol (major revision)

c) Noch nicht eingereichte Manuskripte

Franz J. Hilke, T. Sinnberg, A. Gschwind, H. Niessner, G. Demidov, T. Amaral, S. Ossowski, I. Bonzheim, O. Riess, C. Garbe, C. Schroeder, A. Forschner. *"Next-generation sequencing in a real world cohort of 82 advanced melanoma patients identifies distinct mutation pattern in different melanoma subtypes"*

1. Einleitung

1.1 Tumorerkrankungen

Der Begriff Tumor ist lateinisch und bedeutet Schwellung oder Geschwulst. Im Folgenden wird er als Synonym für Tumorerkrankungen oder auch Krebs genutzt. Am Anfang jeder Krebserkrankung steht die Transformation einer normalen Zelle zu einer neoplastischen Tumorzelle. Im Rahmen der Transformation kommt es in einem mehrschrittigen Prozess zu einem immer stärkeren Verlust der eigentlichen Funktionen der Zelle.

Dieser Prozess lässt sich histologisch in drei Phasen einteilen. Die Hyperplasie ist der Beginn der Transformation, die Zellen weisen einen normalen Phänotyp auf, liegen aber in exzessiver Anzahl vor. Es folgt eine immer stärker werdende Varianz des Zellwachstums, die Dysplasie. Das bedeutet, im Vergleich zu normalen Zellen unterscheiden sich die dysplastischen Zellen in ihrer Größe und Form sowie dem Verhältnis von Nukleus zum Zytoplasma. Am Ende des Prozesses steht die neoplastische Zelle (Abbildung 1). Als Neoplasie werden sowohl gutartige (benigne) als bösartige (maligne) Tumorzellen bezeichnet. Krebszellen sind maligne Tumorzellen und besitzen als elementares Unterscheidungsmerkmal zu den benignen Tumorzellen die Fähigkeit in das umliegende Gewebe einzuwachsen und zu metastasieren.

Man unterscheidet Tumoren entsprechend ihres Ursprungsgewebes in epitheliale und nicht-epitheliale Tumoren. Als Karzinom werden alle Tumoren bezeichnet, die aus Epithelzellen hervorgehen. Dazu gehören sowohl die Plattenepithelkarzinome z.B. der Haut, Lunge, des Ösophagus und Gebärmutterhalses, sowie die Adenokarzinome, hervorgehend aus dem Drüsengewebe des Gastrointestinaltraktes, der Lunge, Brust, Prostata oder des Eierstocks. Zu den nicht-epithelialen Tumoren gehören die Sarkome, dessen Ursprung in den verschiedenen Bindegeweben liegt, die Tumoren des blutbildenden Gewebes wie Lymphome und Leukämien, sowie die die neuroektodermalen Tumoren des peripheren und zentralen Nervensystems wie z.B. das Gliom, Glioblastom, Schwannom, Medulloblastom oder Neuroblastom.

Die Ursachen für die Entstehung von Malignomen lassen sich in zwei Gruppen zusammenfassen: Als extrinsische Faktoren bezeichnet man alle Umwelteinflüsse

sowie den Lebenswandel. Es werden alle chemischen und physikalischen Substanzen berücksichtigt, die karzinogen wirken, also einen Tumor verursachen können. Zu den bekanntesten chemischen Risikofaktoren gehören das Rauchen und ein übermäßiger Alkoholkonsum. Die ionisierende Strahlung sowie das sich exzessive Aussetzen gegenüber UV-Licht sind die bekanntesten physikalischen Faktoren. Nicht zu vergessen sind Infektionen mit Viren, wie z.B. dem human Papilloma-Virus oder das Hepatitis-B/C-Virus. Unter intrinsischen Risikofaktoren versteht man Keimbahnmutationen, also bereits in der befruchteten Eizelle angelegte Mutationen, die von den Eltern über ihre Keimzellen vererbt werden. Ebenfalls als intrinsischer Risikofaktor müssen somatische Mutationen verstanden werden. Diese Mutationen entstehen spontan in einzelnen Zellen und sind die Folge der kontinuierlichen Stammzellteilung und den dabei unvermeidbar auftretenden Fehlern bei der Replikation der Desoxyribonukleinsäure (DNA). Als mutagen werden Mutationen bezeichnet, die das Erbgut einer Zelle so verändern, dass sie beginnt sich unkontrolliert zu teilen, ihre eigentliche Funktion verliert und in das umgebende Gewebe einwächst und metastasiert.

1.2 Krebs als genetische Erkrankung

Die genomische Instabilität ist ein wesentliches Merkmal von Tumorzellen. Durch sie häufen Zellen schrittweise Mutationen an, die es ihnen ermöglichen, Wachstumsvorteile gegenüber den umliegenden Zellen zu erlangen (2, 3). Den Grundstein für diese Erkenntnis legten die Arbeiten zum Einfluss von Viren bei der Tumorentstehung von Peyton Rous, Gross und Stewart (4, 5). Sie konnten zeigen, dass es in der Folge einer Virusinfektion zu einer Transformation der normalen Zellen zu Tumorzellen kommt. Verantwortlich für die Tumorgenese waren einzelne Virusgene, die sogenannten viralen Onkogene (5). In der Folge stellte sich heraus, dass es im menschlichen Genom homologe Kopien dieser Onkogene gibt, die man als Proto-Onkogene bezeichnete. Weisen diese eine aktivierende Mutation auf, kommt es zur Transformation der Zelle (5).

Einen weiteren Hinweis auf die Beteiligung bestimmter Gene und Signalwege bei der Tumorentstehung gaben die Arbeiten von Knudson und Nordling. Sie zeigten, dass eine Kombination mehrerer genetischer Veränderungen zur Malignomentstehung führt. Es stellte sich heraus, dass die Schädigung eines Allels nicht ausreichend für die Tumormanifestation ist. Erst der Verlust der Heterozygotie, also beider Allele, führt zur

unkontrollierten Proliferation (6). Aus dieser Feststellung formulierte Knudson 1971 die „Two-Hit-Hypothese“ und legte damit den Grundstein für die weitere Entdeckung und Erforschung sogenannter Tumorsuppressorgene. Heute wissen wir, dass nicht nur der Verlust der Kopienzahl, sondern auch die Aktivitätsreduzierung zum Beispiel durch die Methylierung regulatorisch wichtiger Regionen des zweiten Allels zur Tumorgenese beitragen können (2, 5, 7).

Mit der Entdeckung der Onko- und Tumorsuppressorgene war die Grundlage für die Betrachtung von Tumoren als genetische Erkrankung gelegt. Um möglichst alle Mutationen und die dazugehörigen Gene zu identifizieren, wurden das *International Cancer Genome Consortium* (ICGC) und *The Cancer Genome Atlas Project* (TCGA) gegründet. Im Ergebnis dieser beiden Bestrebungen ist eine umfassende genomische Landkarte der häufigsten Tumorerkrankungen entstanden (8, 9). Die umfassende genetische Analyse von 33 Tumorentitäten und 9.423 Tumorproben durch das TCGA detektierte 299 relevante Gene in der Tumorgenese, die sich auf 12 Signalwege verteilen (9-13).

Im Rahmen der Tumorentstehung häuft jeder Tumor tausende genetische und epigenetische Alterationen an, die nicht in der Keimbahn nachweisbar sind. Nur wenige dieser Mutationen haben das Potential, die Transformation zu initiieren und voranzutreiben (8). Daher ist es wichtig, zwischen sogenannten *Passenger* und *Driver* Mutationen zu unterscheiden, da ausschließlich die *Driver* (Treibermutationen) ein onkogenes Potential besitzen (7, 14). Im Zuge dieser Definition stellte sich heraus, dass es von der Initiation bis hin zu einem invasiven Tumor nur weniger Treibermutationen bedarf. Bert Vogelstein unterteilte diesen Prozess in drei Phasen (15): Am Beginn steht die *breakthrough phase*. Hier erfährt die Zelle ihre erste Treibermutation in einem Onko- oder Tumorsuppressorgen und beginnt, sich abnormal zu teilen. Es folgt die *expansion phase* mit der zweiten Treibermutation. Die Anzahl an Tumorzellen nimmt trotz der Unterversorgung mit Nährstoffen und Sauerstoff weiter zu. Am Ende der Transformation, als Resultat der dritten Treibermutation, steht die *invasive phase* (Abbildung 1). Im weiteren Verlauf der Tumorgenese können zusätzliche Treibermutationen hinzukommen (8). Sie sind häufig das Ergebnis der Tumorzellevolution durch die Fernmetastasierung und/oder einer Tumortherapie. Der gesamte Prozess von der Tumorzellinitiation bis hin zum invasiven Tumor dauert in den meisten adulten Tumoren vermutlich bis zu drei Jahrzehnte (7, 15).

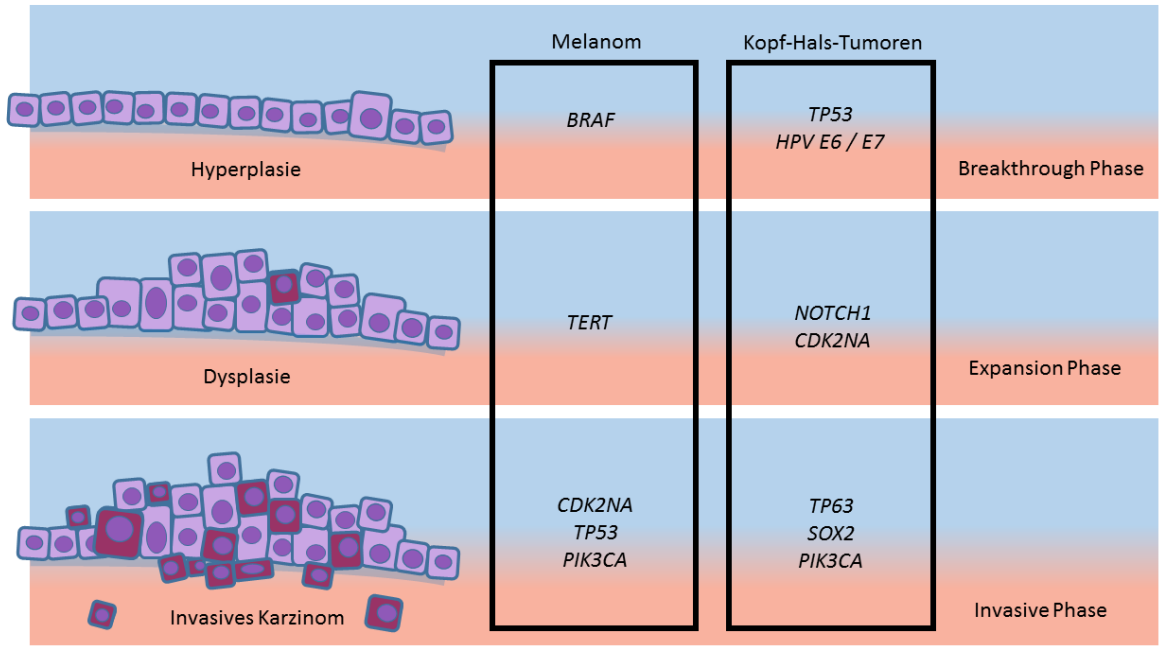

Abbildung 1: Die Entstehung von Tumoren

Die Abbildung illustriert die schrittweise Entstehung eines Tumors am Beispiel des Malignen Melanoms und Kopf-Hals-Tumoren. Histologisch beginnt die Tumorgenese mit einer Hyperplasie, gefolgt von einer Dysplasie der Zellen und schließlich der Entstehung eines malignen Tumors. Dieser ist in der Lage ist in das umliegende Gewebe einzuwachsen und Fernmetastasen zu bilden. Damit die Tumortransformation der Zellen beginnt, bedarf es in aller Regel genetischer bzw. epigenetischer Treibermutationen in Onko- bzw. Tumorsuppressorgenen. Die Akkumulation von Treibermutationen lässt sich in drei Phasen einteilen, die *Breakthrough*, *Expansion* und *Invasive* Phase. Die schrittweise Anhäufung von Treibermutationen steht in enger Verbindung zu den beobachteten histologischen Veränderungen der Zelle. Die Abbildung ist angelegt an die Arbeit von B. Vogelstein et al. und F. Faraji et al. (15, 16). Teile der Abbildung wurden mit Graphiken von Smart Servier Medical Art erstellt (https://smart.servier.com/).

1.3 Genetische Analyse von Tumoren

In der Arbeit *Hallmarks of Cancer* sowie der Neuauflage *Hallmarks of Cancer: The Next Generation* beschreiben Hanahan und Weinberg die sechs wesentlichen biologischen Fähigkeiten, die sich Tumorzellen im Rahmen ihrer karzinogenen Transformation aneignen (2, 3). Als einen der Treiber bei dem mehrschrittigen Erwerb der *Cancer Hallmarks* identifizieren die Autoren die genomische Instabilität. Das bedeutet, dass Tumoren durch die Akkumulation von Mutationen in Genen entstehen, die für das Zellüberleben und Wachstum, die Proliferation und Differenzierung kodieren (Wachstumsvorteil erhalten). Die Mutationen, im folgenden Treibermutationen genannt, führen zu einer Aktivierung bzw. Überaktivierung oder Inhibition der eigentlichen Funktion des Genproduktes. Die Identifikation der Treibermutationen, die zur Aktivierung von Onkogenen bzw. Inaktivierung von Tumorsuppressorgenen führen, hat in der heutigen Onkologie einen enormen

Stellenwert eingenommen (9). Dies ist unter anderem auf die Weiterentwicklung und gleichzeitige Kostenreduktion der Sequenziermethoden zur Bestimmung der Treibermutation zurückzuführen. Sie werden unter dem Begriff *next-generation sequencing* zusammengefasst (14).

Unter dem Begriff *next-generation sequencing* (NGS; Hochdurchsatzsequenzierung) werden alle Sequenziertechnologien zusammengefasst, die das automatisierte Sanger-Sequenzieren abgelöst haben (17). Diese unterscheidet man aktuell in die Analyse von langen DNA Fragmenten (*long-read NGS*; > 1kb) und kurzen DNA Fragmenten (*short-read NGS*; 35-700bp) (17-19). Die long-read Technologie wird vor allem in den Bereichen der de novo Kartierung von Genomen, der Detektion komplexer Strukturveränderungen (Translokationen, Inversionen, Fusionen) und Untersuchung von Einzelzellsuspensionen angewendet. Die *short-read* Technologien erlauben ebenfalls die Untersuchung gesamter Genome (*whole genome sequencing* = WGS), Exome (*whole exome sequencing* = WES), sowie Transkriptome und Methylome. Auf Grund der gesunkenen Kosten finden *short-read* Technologien sowohl in der klinischen Routine als auch in diversen Forschungsbereichen eine breite Anwendung.

Allen *short-read* Technologien ist gemein, dass der experimentelle Ablauf folgendem Schema entspricht (Abbildung 2A): (1) DNA Isolation, (2) DNA Fragmentierung, (3) Herstellung der DNA Bibliothek, (4) Sequenzierung und Datenanalyse. Auf den Teil der DNA Isolation soll hier nicht näher eingegangen werden. Die sich daran anschließende Fragmentierung generiert DNA Abschnitte, die die maximale Leselänge des verwendeten Gerätes nicht überschreiten und legiert Adapter, die eine spätere Amplifikation und Sequenzierung im Gerät erst möglich machen. Das wesentliche Merkmal jeder *short-read* Hochdurchsatzsequenzierung ist die Möglichkeit, innerhalb von wenigen Stunden Sequenzrohdaten im Giga- bzw. Terabasen-Bereich zu generieren. Das ist nur durch zwei wesentliche Schritte in Vorbereitung auf die Sequenzierung möglich: zum einen die klonale Amplifikation der DNA Moleküle und zum anderen die Parallelisierung dieses Prozesses (18, 19). Je nach Hersteller und Gerät werden für die klonale Amplifikation, Parallelisierung und Sequenzierung unterschiedliche Techniken verwendet. Im Rahmen der Promotion wurden ausschließlich Geräte des Herstellers *Illumina* verwendet. Die klonale Amplifikation geschieht hier in einer Festphase auf einem Glasträger, der *solid-state amplification*

(Abbildung 2B). Weitere Möglichkeiten für die klonale Amplifikation sind die *bead based* Methode und die *DNA nanoball generation*.

Die klonale Amplifikation stellt ausgehend von einem Originaltemplate tausende identischer Kopien des gleichen DNA Moleküls her, die gleichzeitig untersucht werden können. Die Parallelisierung ist die Separierung dieses Prozesses in Reaktionszentren (*Cluster*). Daraus resultiert die gleichzeitige Untersuchung mehrerer Millionen unterschiedlicher DNA Moleküle in nur einem Lauf (*run*). Im Fall der verwendeten Geräte von Illumina erfolgt die klonale Amplifikation der DNA Fragmente mittels *solid-state* in der *bridge PCR* (20). Die einzelsträngigen DNA Moleküle aus der *library preparation* hybridisieren über eine komplementäre Adaptersequenz an den festgebundenen Primern auf der Oberfläche des Glasträgers (*flowcell*). Am Ende der *bridge-PCR* Amplifikation erhält man *Cluster* bestehend aus Millionen Kopien klonal amplifizierter einzelsträngiger Fragmente (Abbildung 2B).

Die eigentliche Sequenzierung, also die Detektion der Basensequenz, erfolgt entweder in Form von *sequencing by synthesis* oder als *sequencing by ligation* (17, 18).

Die von *Illumina* verwendete Methode ist das *Sequencing by synthesis*. Es beruht auf einer Weiterentwicklung der Kettenabruchsequenzierung (*cyclic reversible termination* = CRT). Ein Zyklus besteht aus drei Schritten: (1) der Inkorporation eines mit Fluorophor markierten und an der 3´- OH Gruppe geblockten Nukleotids (dNTP), (2) einem Waschschritt zum Entfernen aller nicht eingebauten dNTPs und (3) der Detektion durch laserinduzierte Fluoreszenz (*total internal reflection flourescense*, TIRF). Im Anschluss wird der Fluorophor sowie die Blockierung am 3´- OH Ende entfernt und der Zyklus beginnt erneut. Am Ende der Sequenzierung werden die Bilddaten in eine Nukleotidsequenz übersetzt (Abbildung 2B).

Diese Sequenz wird mit dem Referenzgenom verglichen und Veränderungen annotiert. Anhand der Annotation werden die Unterschiede zwischen dem Referenzgenom und der sequenzierten Probe ermittelt. Die Unterschiede (Polymorphismen, Varianten oder Mutationen) sollen dabei helfen, die Entstehung und Progression der untersuchten Krankheit zu verstehen.

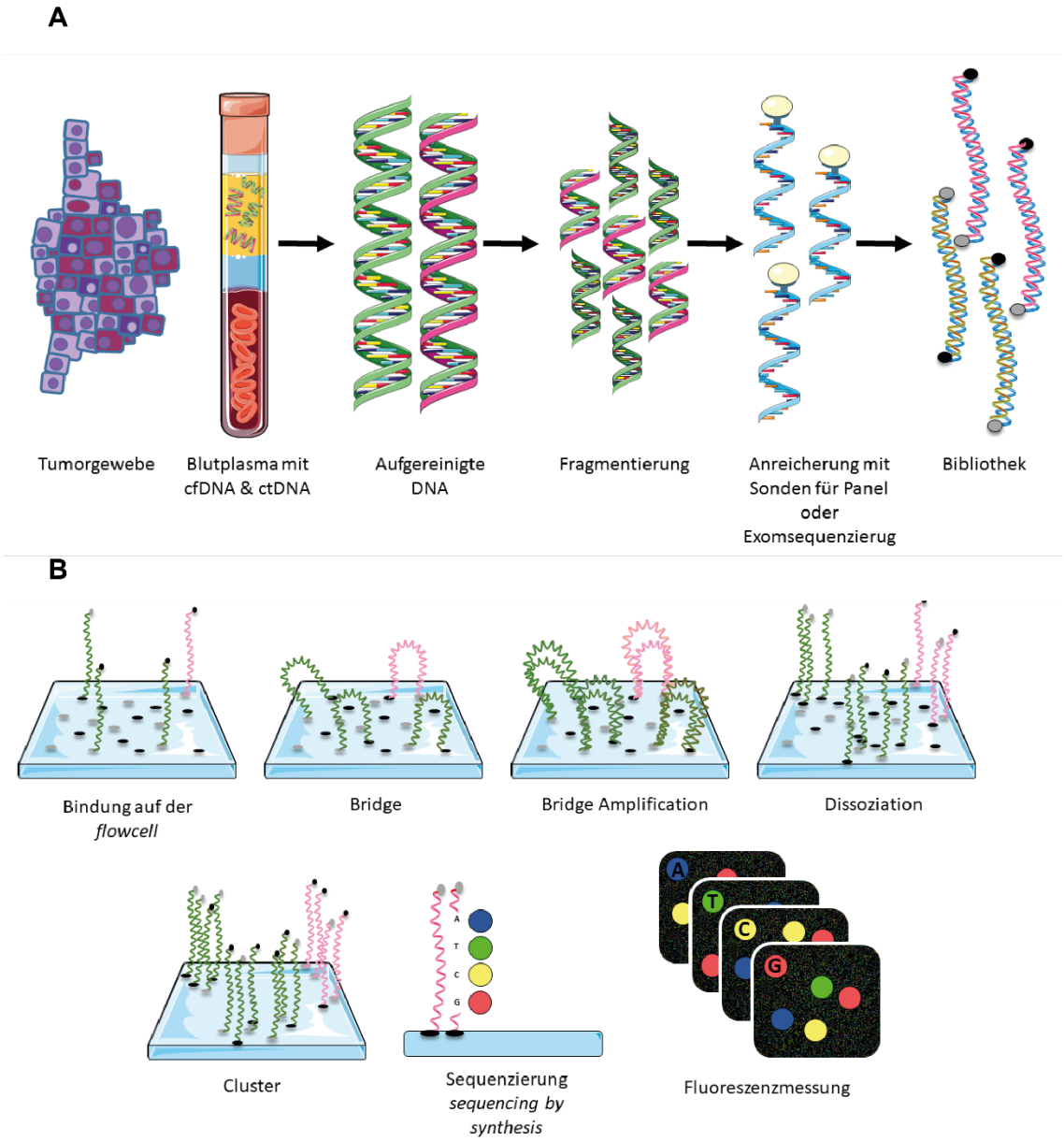

Abbildung 2: Next-generation sequencing (Hochdurchsatzsequenzierung)

(**A**) Die Abbildung zeigt den schematischen Ablauf von der Probengewinnung über die DNA-Isolation bis zur Herstellung der DNA-Bibliothek. Die isolierte DNA wird ein einem ersten Schritt fragmentiert, damit sie die richtige Länge für die folgenden Schritte bei der Herstellung der DNA-Bibliothek hat. Es folgt die Anreicherung (*capture*) der DNA-Bereiche von Interesse (Panel, Exom, Genome, ect) mit Biotyn-markierten Sonden. Die angereicherte DNA wird dann in einem mehrschrittigen Verfahren vervielfältigt, ein Adapter angehängt für die Bindung im Gerät und aufgereinigt, sodass am Ende die fertige DNA-Bibliothek (*library*) entsteht. Sie enthält nur die genomischen Bereiche von Interesse. (**B**) Es folgt die Hochdurchsatzsequenzierung. In diesem Schritt binden alle DNA-Moleküle mit einem Adapter an eine definierte und räumlich voneinander gentrennten Position auf der *flowcell* und es folgt die bridge-Amplifikation. Das bedeutet, die gebundenen DNA-Moleküle werden extrem stark vervielfältigt, sodass die sogenannten *cluster* entstehen. Jedes *cluster* besteht aus Millionen Kopien des gleichen DNA-Moleküls. Die Sequenzierung jedes einzelnen *cluster* erfolgt im *sequencing by synthesis* Verfahren. Hierbei kommt es zum Einbau eines mit Fluorophor markierten und an der 3´- OH Gruppe geblockten Nukleotids (dNTP), gefolgt von einem Waschschritt zum Entfernen aller nicht eingebauten dNTPs. Im Anschluss wird das eingebaute Nukleotid über seinen spezifischen Fluorophor bestimmt. Nach der Detektion wird der Fluorophor sowie die Blockierung am 3´- OH Ende der Nukleotide entfernt und der Zyklus beginnt erneut. Am Ende wird die Fluoreszenzabfolge bioinformatisch in eine Nukleotidsequenz übersetzt. Die Abbildung ist angelegt an die Arbeit von S. Goodwin et al. und M. L. Metzker et al. (17, 18).

1.4 Liquid Biopsy

Der Begriff *Liquid Biopsy* geht auf die ersten Arbeiten von Klaus Pantel zurück, in denen er das Vorhandensein von Mikrometastasen und zirkulierenden Tumorzellen bei Patienten mit soliden Tumoren beschrieben hat (21). Heute steht *Liquid Biopsy* für die Detektion von zirkulierenden Tumorzellen, sowie aller im Blut nachweisbaren Tumorzell-assoziierten Produkte, wie den zirkulierenden Exosomen, Tumor DNA und microRNA (22, 23). Neben dem Blut können diese Tumorprodukte auch aus anderen Körperflüssigkeiten wie Urin, Speichel, Pleura- und Zerebrospinalflüssigkeit gewonnen werden (24-27). Erstmals detektiert wurden Nukleinsäuren im Blut von Patienten im Jahr 1948 von den französischen Wissenschaftlern Mandel und Metais (28). Zwei Jahrzehnte später konnte gezeigt werden, dass eine Korrelation zwischen der Menge an zirkulierender zellfreier DNA (circulating cell-free DNA, cfDNA) und chronisch entzündlichen Erkrankungen, sowie Tumorerkrankungen besteht (29, 30). Auch in Folge einer Verletzung, eines Schlaganfalles, einer Operation, eines Infektes, körperlicher Anstrengung oder im Rahmen einer Schwangerschaft kann es zu einem Anstieg der cfDNA kommen (23, 31-36).

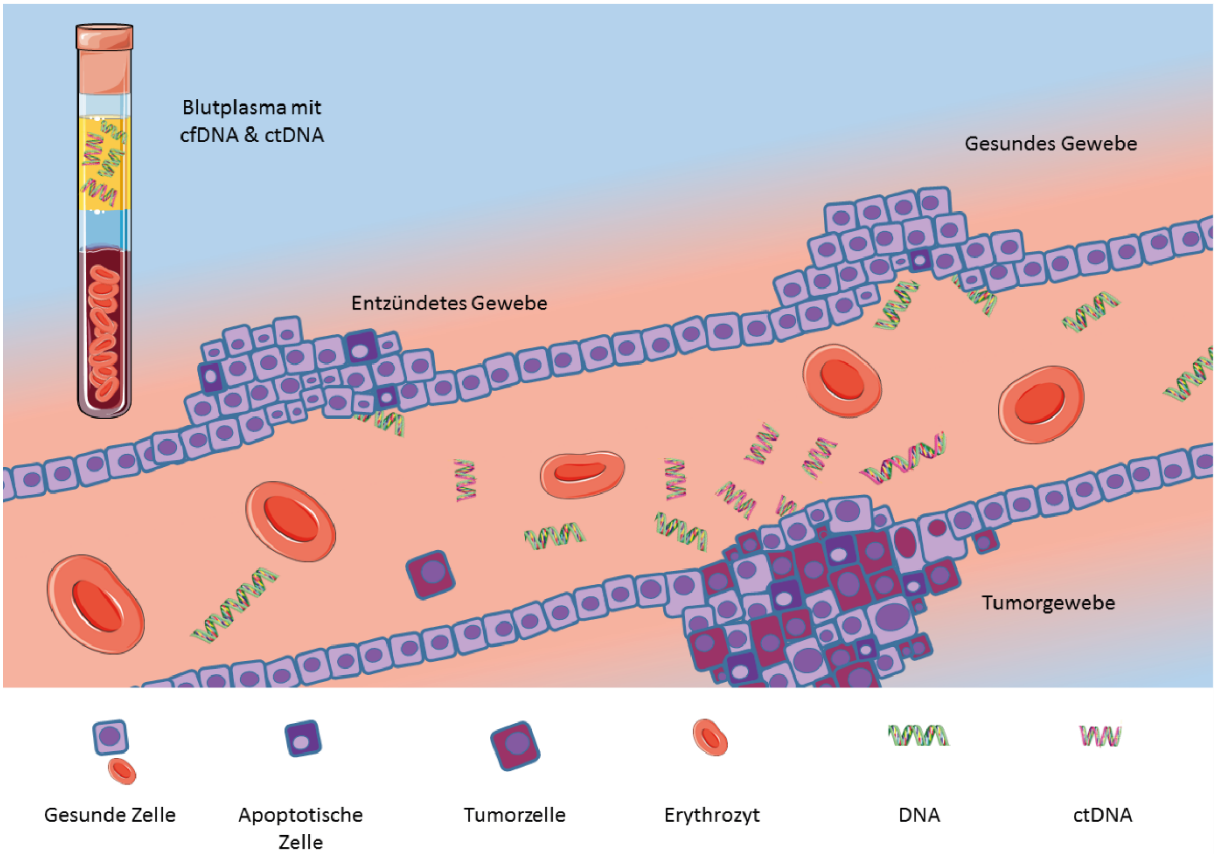

Abbildung 3: Die Liquid Biopsy

Die zellfreie DNA (cfDNA) wird von normalen, entzündeten und karzinogenen Zellen (ctDNA) durch Apoptose und Nekrose in die Zirkulation des Blutkreislaufes entlassen. Die ctDNA kann aus der Blutprobe eines Tumorpatienten extrahiert werden und in der Folge mittels Hochdurchsatzsequenzierung analysiert werden. Es ist möglich, somatische Einzelbasenaustausche (SNVs), Kopienzahlveränderungen (CNVs) und Strukturveränderungen wie Fusion aus der ctDNA nachzuweisen. Die Abbildung ist in Anlehnung an die Arbeit von Crowley et al. entstanden (37). Teile der Abbildung wurden mit Graphiken von Smart Servier Medical Art erstellt (https://smart.servier.com/).

Im Normalfall werden absterbende und tote Zellen mittels Phagozytose von Makrophagen beseitigt und die dabei freigesetzte DNA von Leber, Nieren und Milz aus der Zirkulation entfernt (38). Bei Tumorpatienten ist dieser Mechanismus gestört, sodass es zu einem messbaren Anstieg von cfDNA Molekülen in der Zirkulation kommt (37). Als Ursprung der cfDNA wurden auch hier apoptotische und nekrotische Zellen identifiziert (39). Diese Hypothese wird durch die Beobachtung gestützt, dass cfDNA Fragmente eine Länge von ca. 140-160 Basenpaaren haben (40). Das entspricht der Fragmentierungslänge einer Windung/Umwicklung um das Nukleosom inklusive *Linker* Sequenz als Folge der Apoptose (41, 42).

Bei onkologischen Patienten wird die zellfreie zirkulierende Tumor DNA (ctDNA) anhand von Tumor-spezifischen Mutationen identifiziert (22, 23, 37, 43). Mit der Weiterentwicklung der modernen Sequenziermethodik ist es heute möglich, aus der ctDNA einzelne Mutationen, mehrere Gene oder sogar das gesamte Tumorexom bzw. -genom zu untersuchen. Für die Detektion und Quantifikation von *hotspot* Mutationen werden vorwiegend PCR-basierte Methoden, namentlich *ddPCR* (*digital droplet PCR*) und *BEAMing* (*beads, emulsion, amplification, magnetics*) verwendet (41, 44, 45). Durch die Vereinzelung und Parallelisierung in hunderte bis tausende Reaktionen können seltene Mutationen mit einer Sensitivität von bis zu 1:10.000 Molekülen detektiert werden. Daneben gibt es NGS-basierte Ansätze, die sich für die Untersuchung mehrerer genetischer Loci und des gesamten Tumorexoms eignen (46-48). Durch die Kombination mit *unique molecular barcodes*, der Markierung jedes untersuchten DNA Moleküls mit einem spezifischen Barcode, ist es möglich, Mutationen mit einer Allelfrequenz von 0.1% und geringer zu detektieren (47, 49). Ab einem ctDNA-Anteil von 5-10% ist es auch möglich, Tumor-spezifische chromosomale Kopienzahlveränderungen (*copy number variants*) des Genoms zu detektieren (50-52). Hierbei kommt das *shallow WGS* zum Einsatz, bei dem das Gesamtgenom mit einer durchschnittlichen Tiefe von 0.1X sequenziert und im Anschluss mit dem Genom von gesunden Patienten vergleichen wird.

Auf Grund des minimal invasiven Charakters der *Liquid Biopsy*, bestehend aus einer einfachen Blutentnahme, sowie den Fortschritten im Bereich der Sequenziertechnologien, kann die ctDNA in den aktuellen Forschungsarbeiten als sensitiver und dynamischer Biomarker in der Diagnostik von Tumorpatienten eingesetzt werden (53). Die Früherkennung von Tumorerkrankungen, das Therapieansprechen, die Detektion von Therapieresistenzen sowie die Erkennung von einer residuellen Tumorerkrankung nach Therapie (*Minimal Residual Disease*) stehen hier im Fokus (22, 23, 37, 54). Darüber hinaus geht man davon aus, dass die ctDNA deutlich besser die genetische Inter- und Intraheterogenität von Tumor und Metastasen abbilden kann (55).

1.5 HNSCC

Der Begriff Kopf-Hals-Tumoren (*Head and neck squamous cell carcinoma = HNSCC*) fasst verschiedene Karzinome zusammen, die im Bereich des Kopfes und Halses entstehen. Im Jahr 2018 wurden unter diesem Sammelbegriff ca. 890.000 Neuerkrankungen diagnostiziert. Damit ist das *HNSCC* die siebthäufigste Tumorerkrankung weltweit (1).

Histologisch handelt es sich um ein Plattenepithelkarzinom, dass aus den Epithelzellen der Schleimhäute der Mundhöhle, des Oropharynx, Larynx und Hypopharynx entsteht und sehr heterogen ist (56). Die drei wesentlichen Risikofaktoren für die Entstehung von Kopf-Hals-Karzinomen sind ein regelmäßiger Nikotinabusus, übermäßiger Alkoholkonsum und die Infektion mit dem humanen Papillomavirus (HPV), insbesondere HPV16 (57, 58). Vor allem beim Oropharynxkarzinom nimmt die Anzahl der Patienten mit einer HPV Infektion zu. Dies führte zum einen zu der Unterteilung in HPV-positive und -negative Oropharynxkarzinome und zum anderen zu der Feststellung das Patienten mit HPV-positiven Tumoren mit einer besseren Prognose assoziiert sind (59, 60). Auch beim *HNSCC* konnte gezeigt werden, dass die Karzinogenese schrittweise abläuft (61). Zu Beginn können Veränderungen der Schleimhäute, sogenannte Leukoplakien und Erythroplakien beobachtet werden. Ausgehend von diesen Vorläuferläsionen kommt es durch die Akkumulation von weiteren Mutationen zu hyperplastischen und dysplastischen Läsionen, aus denen sich ein Carcinoma in situ und ultimativ ein invasives *HNSCC* entwickeln kann (62, 63).

Durch die umfassende genetische Charakterisierung durch das *TCGA* wurden die wesentlichen Treibermutationen des *HNSCC* identifiziert, die zu einer Einteilung in Subgruppen führte (64). Die Studie identifizierte zwei genetische Subgruppen innerhalb der HPV-negativen *HNSCCs*. Auf der einen Seite Tumoren mit vielen Mutationen und chromosomalen Kopienzahlveränderungen (CNVs) und auf der anderen Seite Tumoren mit wenigen bis gar keinen CNVs (64). Die zuletzt genannte Gruppe zeichnet sich zusätzlich durch aktivierende Mutationen in dem Gen *HRAS* sowie inaktivierenden Mutationen in *TRAF3* aus, sowie einem *TP53* Wildtypstatus (64, 65). Die zweite Gruppe der HPV-negativen *HNSCC* ist geprägt durch zahlreiche aktivierende und inaktivierende Mutationen in den Genen der Zellzykluskontrolle, des PI3K-, Wnt- und RTK-Signalweges sowie der epigenetischen Regulation (57, 64). Hier

sind vor allem Mutationen in den Genen *TP53*, *CDKN2A*, *EGFR*, *PIK3CA*, *FAT1*, *AJUBA*, *NOTCH1*, *KMT2A* und *NSD1* zu finden.

Die Gruppe der HPV-positiven Tumoren hat ein anderes Mutationsspektrum mit insgesamt weniger Veränderungen und einer deutlichen viralen Signatur, APOBEC genannt (57, 66). Das am häufigsten mutierte Gen ist *PIK3CA* und ähnlich wie beim Zervixkarzinom ist seine chromosomale Region (3q26) häufig amplifiziert. Zusätzlich gibt es noch zwei weitere Loci, die vermehrt chromosomale Verluste aufzeigen. Es handelt sich dabei um die Region 14q32 mit dem Gen *TRAF3* und 9q mit dem Gen *ATM*. Die für das *HNSCC* typischen inaktivierenden Mutationen der Gene *TP53* und *CDKN2A* findet man beim HPV-positiven Typ nicht. Stattdessen entfaltet die Interaktion der viralen Onkoproteine E6/7 mit p53 und pRB ebenfalls eine inaktivierende Wirkung (57, 66).

1.6 Melanom

Maligne Melanome sind bösartige Tumoren der Haut. Sie entstehen durch die karzinogene Transformation von Pigmentzellen, den Melanozyten. Man findet sie vor allem in der Epidermis der Haut, aber auch in der Aderhaut (Uvea), sowie im Haarschaft der Haarfollikel, den Meningen und der Schleimhaut (67, 68). Im Jahr 2018 wurden weltweit ca. 300.000 neue Fälle des Melanoms diagnostiziert und 61.000 Todesfälle (1). Damit liegt das Melanom auf Platz 19 der Tumorerkrankungen weltweit und tritt besonders häufig bei Menschen mit einem hellen Hauttyp auf (67, 69).

Melanozyten leiten sich aus den Zellen der Neuralleiste ab und wandern von dort während der Embryogenese in die Haut. Dort lagern sie sich in der Basalmembran an. Ihre Funktion ist die Produktion von Pigment (Melanin) zum Schutz der Keratinozyten vor zu starker Sonneneinstrahlung. Damit ist insbesondere die ultraviolette (UV) Strahlung gemeint, die zu DNA-Schäden der Hautzellen führen kann (67, 70). Daraus leitet sich die Schlussfolgerung ab, dass die UV-Strahlung als einer der Hauptrisikofaktoren für die Entstehung von Melanomen angesehen werden kann (67, 71, 72). Neben dem Hauttyp spielen die Anzahl und Größe kongenitaler Nävi, genetische Prädisposition (familiäre Häufung) oder Störungen der DNA Reparatur (Xeroderma pigmentosum) eine Rolle (67, 69).

Abhängig von der Lokalisation, also dem Entstehungsort des Primarius, werden die Melanome in vier Subtypen eingeteilt: das kutane, das akrolentiginöse, das mukosale

und uveale Maligne Melanom, (71). Das kutane Melanom ist der häufigste Subtyp. Es entsteht entweder neu (*de novo*) oder aus einer Vorläuferläsion, wie zum Beispiel einem dysplastischen Nävus oder dem Melanom *in situ* (67, 70, 72-74). Kutane Melanome haben eine hohe Mutationslast, die eine deutliche UV-Signatur trägt (C>T Transitionen an Dipyrimidinen). Als Folge kommt es häufig zu aktivierenden Mutationen der Gene des MAPKinase Signalweges, wie z.B. *BRAF*, *NRAS* und *NF1* (71, 75, 76). Dies führte zu der genetischen Klassifikation des kutanen Melanoms in die genomischen Subtypen des *BRAF*- (V600E), *RAS*- (*NRAS*, *KRAS*, *HRAS*; G12D & Q61N) oder *NF1*-mutierten Melanom, sowie dem *triple wildtype* (75). Mutationen in den Genen *BRAF* und *NRAS* sind in aller Regel nicht gemeinsam zu finden. Im weiteren Verlauf der Tumorgenese folgen Mutationen in den Genen der Zellzykluskontrolle (*CDKN2A*del, *TP53*del), dem *PI3K*/*AKT* Signalweg (*PTEN*del) und dem SWI/SNF- (*ARID2*) sowie dem Wnt-Signalweg (*CTNNB1*) (71, 75, 76).

Das akrolentiginöse Melanom hat eine deutlich geringere Inzidenz, dafür eine erhöhte Mortalitätsrate im Vergleich zum kutanen Melanom. Es entsteht an den Palmae, Plantae und dem Nagelbett und hat eine deutlich geringere Mutationslast als das kutane Melanom (69, 77). Statt der seltener zu findenden Treibermutation in den Genen *BRAF/NRAS/NF1* finden sich bei diesem Subtyp vermehrt chromosomale Kopienzahlveränderungen in den Genen *TERT*, *PAK1*, *CDK4*, *CCND1* und *KIT* (71, 76, 77).

Das mukosale Melanom ist eher selten, hat aber einen besonders aggressiven Verlauf (76, 78). Es entsteht aus den Melanozyten der Schleimhäute der Nase, Mundhöhle, und des Genitaltrakts sowie der anorektalen Region (71, 76, 78). Ähnlich wie das akrolentiginöse Melanom ist die Anzahl der somatischen Mutationen sehr gering und es besitzt keine UV-Signatur. Auch dieser Subtyp ist vor allem durch somatische Kopienzahlveränderungen geprägt. Sie betreffen vor allem die Gene der Zellzykluskontrolle (*CCND1*, *CDK4*, *MDM2, CDKN2A, ATM)*, des RTK-RAS-Signalweges (*KIT*, *MITF*, *NF1*), der Telomerkontrolle (*TERT*) und des PI3K-Signalweges (*PTEN*). Aktivierende Mutationen in den Genen *BRAF*, *NRAS* und *NF1* sind deutlich seltener im Vergleich zum kutanen Melanom (76, 78, 79). Allerdings finden sich neben Amplifikationen auch häufiger Treibermutationen in dem Gen *KIT*, einer Rezeptor-Tyrosinkinase. Zusätzlich finden sich gehäuft Mutationen in dem Gen

SF3B1. Es handelt sich hier um einen Spleißfaktor der ebenfalls gehäuft mutiert im uvealen Melanom zu finden ist (76, 78).

Das uveale Melanom entsteht aus den Pigmentzellen der Aderhaut und hat die geringste Mutationslast aller vier Subtypen (71). Zu den häufigsten somatischen Veränderungen gehören die aktivierenden Mutationen in den Genen *GNAQ* und *GNA11*. Es handelt sich um zwei Guaninnukleotid-gekoppelte Proteine, die eine Aktivierung des MAPKinase Signalweges nach sich ziehen (80, 81). Darüber hinaus finden sich gehäuft Mutationen in den Genen *BAP1* und *SF3B1*, die sich gegenseitig ausschließen (82, 83). Auch bei diesem Subtyp finden sich zusätzlich chromosomale Kopienzahlveränderungen. Dabei spielt das Chromosom 3 eine wichtige Rolle bei der Einteilung dieses Tumors in zwei Subgruppen. Man findet entweder eine Mono- oder Disomie des Chromsom 3. Weitere Kopienzahlveränderungen betreffen die Gene *MYC* und *EIF1AX.*

2. Zielsetzung

Die genomische Instabilität von Tumoren ist ein wesentlicher Faktor bei ihrer Entstehung und Evolution. Durch die schrittweise Anhäufung von Treibermutationen erwerben die Tumorzellen Wachstums- und Überlebensvorteile gegenüber den Zellen des umliegenden Gewebes. Daher spielt die Identifikation von Treibermutationen eine wichtige Rolle bei der Erforschung und Diagnostik von Tumorerkrankung. Neben der genetischen Analyse aus soliden Tumorbiopsien kann zu diesem Zweck auch die *Liquid Biopsy* eingesetzt werden.

Ziel der Promotion war es, bei Patienten mit einem fortgeschrittenen Melanom (*SKCM*) oder Kopf-Hals-Tumoren (*HNSCC*) umfassende genetische Tumorprofile zu erstellen und potentielle genetische Biomarker zu identifizieren, die mit dem Therapieansprechen korrelieren. Darüber hinaus sollten umfassende genetische Landkarten der Tumorgenome erstellt werden, die die Unterteilung der Tumoren in Subgruppen ermöglicht und die Möglichkeit gibt weitere genetische Marker für eine gezielte Therapie zu identifizieren.

Zu diesem Zweck wurden die soliden Tumorbiopsien unter Anwendung der Exom- und Panelsequenzierung genetisch charakterisiert und mit klinischen Parametern, wie der Tumorlast, dem progressionsfreien Überleben und dem Auftreten eines Rezidivs korreliert. Gleichzeitig wurde bei den Patienten mit einem fortgeschrittenen *HNSCC* eine Therapiebegleitende *Liquid Biopsy* durchgeführt. Die Analyse der zellfreien zirkulierenden Tumor-DNA sollte als dynamischer Marker für die Beobachtung des Therapieansprechen und der Detektion einer minimalen Resterkrankung im Anschluss an die Therapie etabliert werden.

3. Ergebnisse und Diskussion

3.1 Kopf-Hals-Tumoren

Die meisten Patienten mit Kopf-Hals-Tumoren (*HNSCC*) weisen bei Erstdiagnose ein fortgeschrittenes Krankheitsstadium auf (84). Ihre leitliniengerechte Behandlung basiert auf bildgebenden Verfahren wie der Computertomographie (CT) und bedeutet entweder die chirurgische Exzision, soweit operabel, gefolgt von einer adjuvanten Radio(chemo)therapie oder alternativ bei Inoperabilität die primäre Radiochemotherapie (85, 86). Trotz der intensiven Therapie sind Rezidive in fortgeschrittenen Stadien häufig (84, 87). Daher ist es notwendig, komplementäre Methoden für die Stratifikation, Prognose und Therapieprädiktion der Patienten im klinischen Alltag zu entwickeln.

Eine Möglichkeit ist der Einsatz der *Next-Generation-Sequencing* Technologie in Kombination mit der *Liquid Biopsy*. Sie ermöglichen es, Tumor-spezifische Treibermutationen zu identifizieren und im Plasma als zirkulierenden zellfreie Tumor-DNA zu detektieren und zu quantifizieren. Die Zusammenführung der Informationen aus der *Liquid Biopsy*, dem genetischen Profil des Tumors und den klinischen Daten könnten in Zukunft dazu beitragen, Tumoren umfassender zu charakterisieren.

Die Ergebnisse aus der umfassenden genetischen Charakterisierung und der Beobachtung des Therapieverlaufes mittels *Liquid Biopsy* im Zusammenhang mit den klinischen Verläufen sind in zwei Publikationen zusammengefasst, die sich in folgende Themenschwerpunkte gliedern:

1. cfDNA als Marker für Infektion vs. Inflammation
2. *Liquid Biopsy* als Surrogatmarker für das Therapieansprechen und die Detektion einer minimalen Resterkrankung (MRD)

3.1.1 Studiendesign

Alle Patienten wurden mit intensitätsmodulierter Strahlentherapie (*Intensity Modulated Radiation Therapy*, IMRT) mit einer kumulativen Strahlendosis von 70-77Gy behandelt. Begleitend wurde wöchentlich eine Chemotherapie mit Cisplatin oder einer Kombinationstherapie aus 5-FU und MMC verabreicht.

Für die Analyse der zellfreien zirkulierenden DNA (cfDNA) bzw. Tumor DNA (ctDNA) wurden insgesamt fünf Blutproben zu fünf Zeitpunkten gewonnen (Abbildung 4). Der

Zeitpunkt *t1* markiert den Studieneinschluss vor Beginn der Therapie als *baseline*. Im Verlauf der Radiochemotherapie wurden drei weitere Blutproben (*t2-4*) entnommen, wobei der Zeitpunkt *t2* am Beginn der Behandlung, 4-7 Tage nach Therapieinitiation liegt. Der Zeitpunkt *t3* markiert die dritte Woche der Therapie und Zeitpunkt *t4* liegt am Ende des Behandlungszyklus. Die erste Nachuntersuchung findet sechs bis zwölf Wochen nach dem Behandlungsende statt und markiert den Zeitpunkt *t5*. Hier wurde neben der Blutentnahme auch eine klinische Untersuchung zusammen mit einer Computertomographie (CT) durchgeführt. Das Auftreten eines Rezidivs bzw. einer Progression im weiteren Verlauf der Nachsorge wurde durch bildgebende Verfahren und endoskopische Nachsorge diagnostiziert.

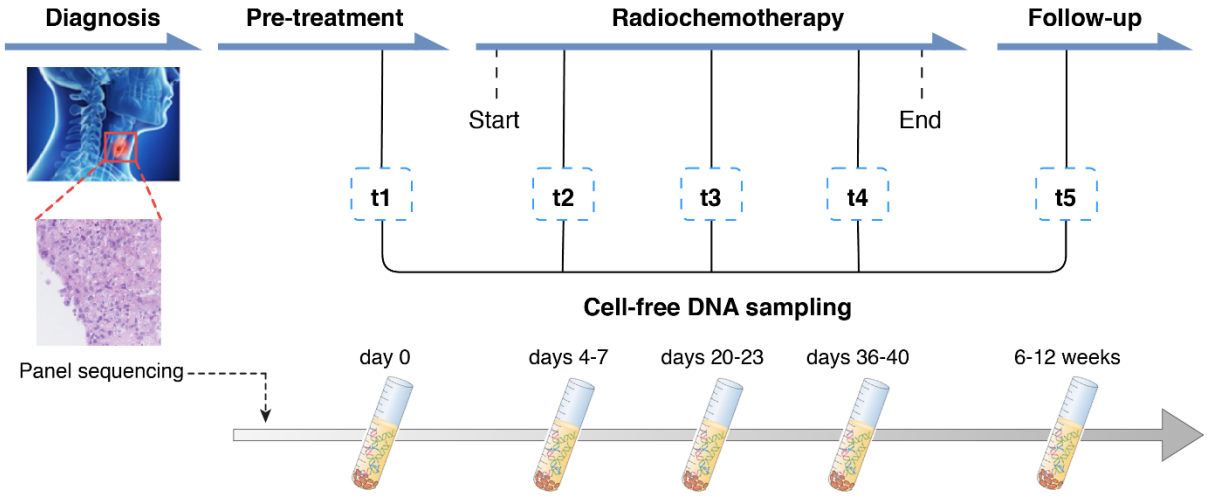

Abbildung 4: Studiendesign

Nach der Diagnosestellung eines lokal fortgeschrittenen Kopf-Hals-Tumors (*HNSCC*) wird der Patient in die Studie eingeschlossen und aus der soliden Tumorbiopsie eine Panelsequenzierung zur Identifikation von Treibermutationen durchgeführt. Alle Patienten wurden im Rahmen der Studie fünf Blutproben für die Quantifikation der cfDNA und Analyse der ctDNA sowie cvDNA entnommen. Die erste Probe t1 wurde vor Beginn der Radiochemotherapie entnommen. Im Verlauf der Therapie wurden weitere drei Proben (t2-t4) entnommen. Im Anschluss an die Therapie erfolgte die letzte Blutentnahme (t5). Die Abbildung ist Teil des Manuskripts „Dynamics of cell-free tumour DNA correlate with treatment response of head and neck cancer patients receiving radiochemotherapy" und für die Promotion modifiziert.

3.1.2 Patientenkohorte

Im Rahmen der Promotion wurden 20 Patienten mit einem lokal fortgeschrittenen *HNSCC*, lokalisiert im Oropharynx (n=14), Hypopharynx (n=4) oder der Mundhöhle (n=2), in dem Zeitraum von 2015 bis 2016 eingeschlossen (Tabelle 1). Das mediane Alter der Kohorte lag bei 60 Jahren und der Großteil der Patienten (90%) war männlich. Als weitere für die Prognose wichtige Faktoren wurden der HPV-Status und Nikotinkonsum untersucht. Insgesamt waren 17 der 20 Patienten Raucher (85%) und fünf Patienten mit der Tumorlokalisation im Oropharynx wurden positiv auf eine HPV

Infektion getestet. Bei der Hälfte der Patienten trat innerhalb von 2 Jahren ein Rezidiv auf.

Tabelle 1: Klinische Parameter der Kohorte

	Alter in Jahren	**Altersspanne**
Median	60	49-75
Geschlecht (N, %)		
Männlich	18	90%
Weiblich	2	10%
HPV Status (N, %)		
Positiv	5	25%
Negativ	14	70%
Nicht getestet	1	5%
Lokalisation (N, %)		
Mundhöhle	2	10%
Oropharynx	14	70%
Hypopharynx	4	20%
Raucher (N, %)		
Ja	17	85%
nein	3	15%
Rezidiv (N, %)		
Ja	10	50%
nein	10	50%

3.1.3 Genetisches Profil der Kohorte

Die genetische Analyse des soliden Tumorgewebes wurde mittels eines Tumorpanels durchgeführt, bestehend aus 327 Genen. Das Panel ist spezifisch auf die Analyse von *HNSCCs* abgestimmt und vom DKTK-ROG Kooperationspartner (Deutsches Konsortium für Translationale Krebsforschung, Radiation Oncology Group) in Berlin entworfen (88). Es wurden 20 Tumorbiopsien von 20 Patienten und ihre entsprechenden Referenzproben (Blut) mit einer durchschnittliche Sequenzierungstiefe von 190X für die Tumorproben und 186X für die Referenzenproben sequenziert. Die Sequenzierung detektierte insgesamt 667 somatische Mutationen, synonyme und nicht-synonyme, im kodierenden Bereich. Daraus resultiert ein Median von 18 somatischen Mutationen pro Patient (min. 6, max. 282). Die Annotation mit Hilfe der Internetplattform *Cancer Genome Interpreter*

klassifizierte 127 Varianten als Treibermutationen (89). Daraus ergibt sich ein Median von vier Treibermutationen pro Patient. (min. 1, max. 52).

Die zehn häufigsten mutierten Gene mit Treibermutationen gehören zum TP53-, NOTCH-, HIPPO- und PI3K–Signalweg oder sind Teil der Chromatinmodifikation (Abbildung 5). Das Tumorsuppressorgen *TP53* ist in 16 der 20 Patienten mutiert und damit das am häufigsten mutierte Gen der Kohorte. Es folgen die beiden Tumorsuppressorgene *FAT1* und *NOTCH1* die in 30% (7 von 20) bzw. 20% (4 von 20) der Patienten mutiert sind. Darüber hinaus sind die Gene *ATM*, *KMT2D*, *NCOR1* und *ZNF750* in jeweils 15% (3 von 20) der Patienten von einer Treibermutation betroffen. In mindestens 2 von 20 Patienten (10%) wurden Treibermutationen in den Genen *KMT2C*, *MTOR*, *PIK3CA* gefunden.

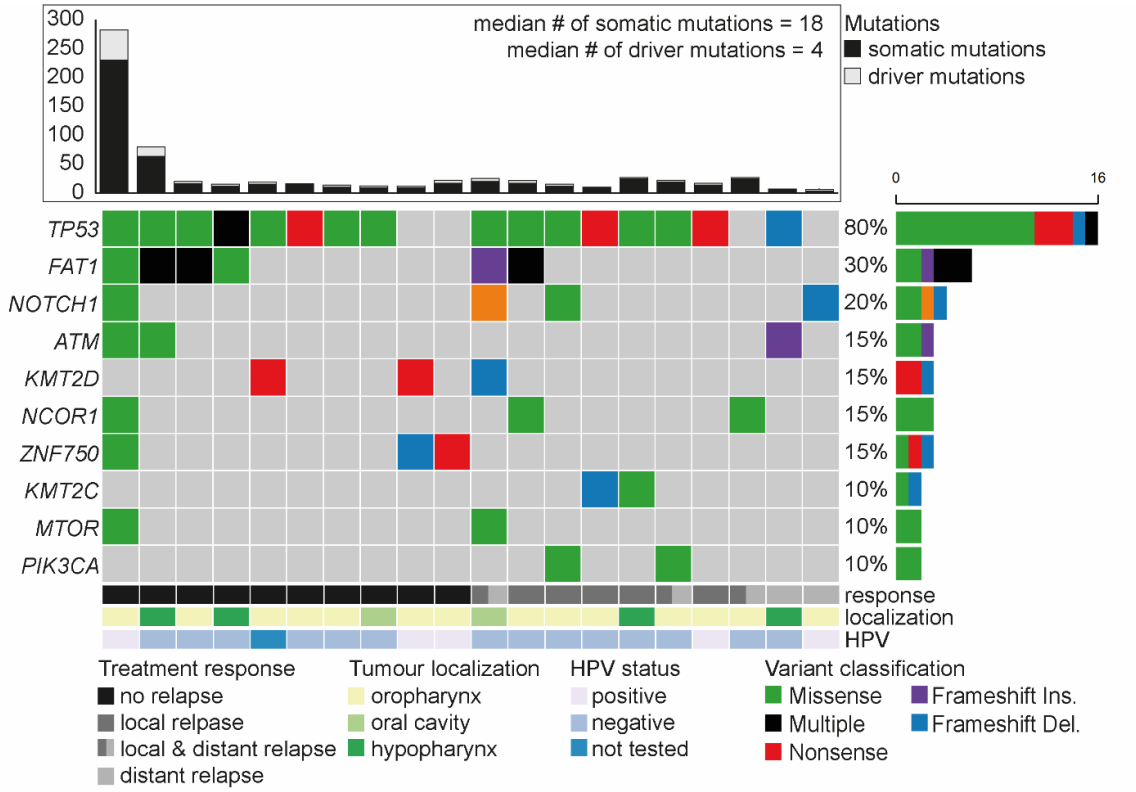

Abbildung 5: Oncoplot der zehn häufigsten mutierten Gene des *HNSCC*

Die Abbildung fasst die zehn am häufigsten mutierten Gene der Kohorte zusammen. Bei den Mutationen handelt es sich ausschließlich um Treibermutationen. Im oberen Teil der Abbildung ist ein Balkendiagramm, das die Gesamtzahl aller Mutationen pro Patient darstellt. In schwarz sind alle somatischen Veränderungen anzeigt und in grau die vom *Cancer Genome Interpreter* identifizierten Treibermutationen. Jede Spalte im *Oncoplot* repräsentiert einen Patienten und die für ihn spezifischen Mutationen. In den Zeilen ist die Häufigkeit, mit der ein Gen mutiert ist, sowie die Art der Mutationen erfasst. In der Analyse wurden nur Einzelbasenaustausche untersucht. Unterhalb der Gene wird zusätzlich das Therapieansprechen in einer Grauskala dargestellt, sowie die Tumorlokalisation (gelb-grüne Skala) und der durch die Pathologie bestimmte HPV-Status (violett-blaue Skala). Die Abbildung entstammt dem Manuskript „Dynamics of cell-free tumour DNA correlate with treatment response of head and neck cancer patients receiving radiochemotherapy".

3.1.4 cfDNA als potentieller Marker zur Unterscheidung zwischen Inflammation und Infektion

Die leitliniengerechte Therapie bei Patienten mit einem fortgeschritten HNSCC ist die Radiotherapie mit einer begleitenden Chemotherapie (85). Während der Radiochemotherapie kommt es häufig zu lokalen Nebenwirkungen, wie z.B. der radiogenen Dermatitis und Mukositis oder Infektionen (90). Die Unterscheidung zwischen Inflammation und Infektion ist wichtig für die optimale Anpassung und Fortführung der Therapie. Aktuell werden sowohl das C-reaktive Protein (CRP) als auch Änderungen in der Anzahl der weißen Blutkörper für die Unterscheidung zwischen Infektion und Inflammation herangezogen (91, 92).

Die zellfreie zirkulierenden DNA (cfDNA) als Produkt aller apoptotischen und nekrotischen Zellen ist möglicherweise ein weiterer sinnvoller Parameter, da neben der Tumorerkrankung auch eine Inflammation oder Infektion zur Erhöhung der cfDNA führen können (93, 94). Zu diesem Zweck wurde in der Studie „*Circulating cell-free DNA: A potential biomarker to differentiate inflammation and infection during radiochemotherapy*“ untersucht, ob eine Änderung des cfDNA-Spiegels vor und während der Radiochemotherapie von *HNSCC*-Patienten ein zusätzlicher Biomarker für die Erkennung von Entzündungen (mäßige Toxizität) oder einer schweren Infektion sein kann.

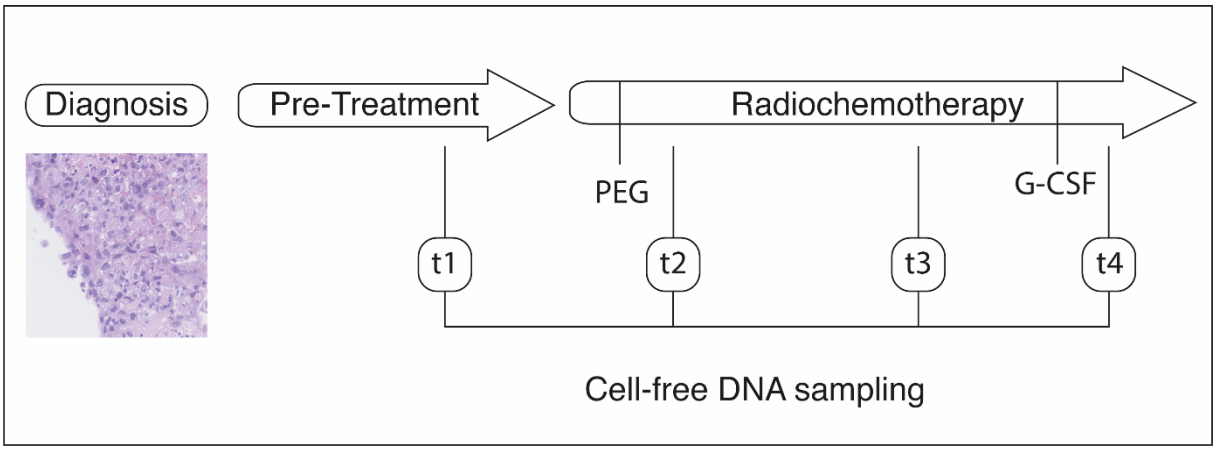

Abbildung 6: Studiendesign für die Qualifikation der cfDNA – Inflammation vs. Infektion

Die Abbildung illustriert die Zeitpunkte (t1-t4) der Blutentnahme vor und während der Radiochemotherapie. Die Blutentnahme t1 markiert den Zeitpunkt 1 und erfolgte 0-15 Tage vor Beginn der Therapie. Die Blutprobe t2 wurde während der ersten Woche nach dem Start der Radiochemotherapie (4-7 Tage) entnommen. Die Probe t3 ist in der dritten Therapiewoche (20-23) entnommen und die Probe t4 am Ende der Behandlung (37-40 Tage). Das Einbringen einer PEG-Sonde (perkutane endoskopische Gastronomie) erfolgte in der ersten Behandlungswoche. Vier Patienten erhielten G-CSF vor der letzten Blutentnahme (t4). Die Abbildung entstammt der Arbeit „Circulating cell-free DNA: A potential biomarker to differentiate inflammation and infection during radiochemotherapy” (95).

3.1.4.1 cfDNA Quantifikation

In der Studie wurden insgesamt 77 Blutproben von 20 Patienten mit einem *HNSCC* entnommen und quantifiziert (Abbildung 7). Das mediane Niveau der cfDNA unterscheidet sich zwischen den Zeitpunkten T1-T4 nur gering, wobei ein minimaler Anstieg von T1 zu T4 (Min = 8,97 ng/ml, Max = 12,65 ng/ml) zu beobachten ist. Darüber hinaus kann man eine Schwankungsbreite der DNA Menge, sowohl innerhalb eines Patienten aber auch zwischen den Patienten feststellen (Min = 2,89 ng/ml, Max = 172,9 ng/ml).

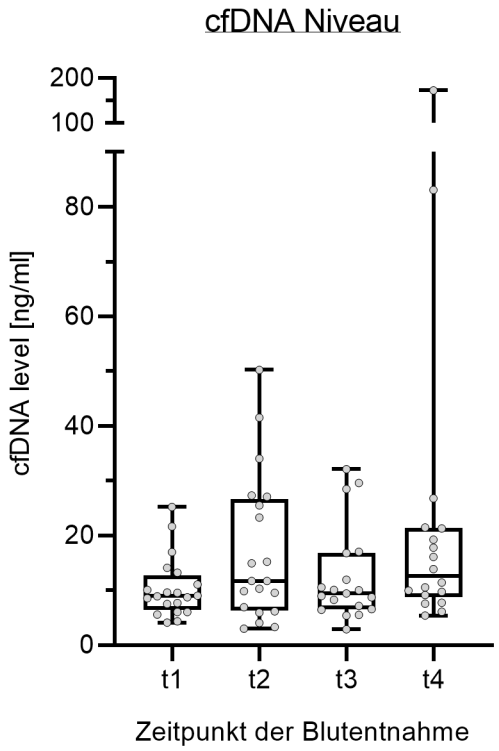

Abbildung 7: Quantifikation der cfDNA zu den Zeitpunkten t1 bis t4

Insgesamt wurde in der Studie von 77 cfDNA Proben die DNA-Konzentration mittels Fluoreszenzspektroskopie bestimmt. Zum Zeitpunkt T1 wurden 20 Proben untersucht. Die mediane Konzentration betrug vor dem Beginn der Therapie 8,9 ng/ml (T1, n = 20) und steigerte sich im Verlauf der Therapie über 11,7 ng/ml (T2, n = 20), 9,4 ng/ml (T3, n = 19) auf 12,65 ng/ml (T4, n = 18).

3.1.4.2 Klinische Einflussgrößen auf die cfDNA Menge im Plasma

Zur genaueren Charakterisierung der Einflüsse auf die cfDNA-Konzentration wurde sie im nächsten Schritt mit klinischen und serologischen Parametern verglichen. Als Einflussgrößen wurden folgende klinische Parameter einzeln untersucht:

a) die Notwendigkeit der Hospitalisierung
b) das Einbringen einer PEG Sonde (perkutane endoskopische Gastronomie)
c) die Gabe von Antibiotika im Rahmen von Infekten

d) die Gabe von G-CSF (Granulozyten-Kolonie-stimulierenden Faktor) im Rahmen einer Neutropenie

Das Einbringen einer PEG-Sonde, die Gabe von G-CSF auf Grund einer Neutropenie und die Gabe von Antibiotika im Rahmen einer nachgewiesenen Infektion korrelierten alle mit einem signifikanten Anstieg der cfDNA-Menge (Abbildung 8). Die Notwendigkeit der Hospitalisierung zeigte einen Anstieg der cfDNA Menge, dieser war aber nicht signifikant. Zusätzlich zur cfDNA-Menge wurde als etablierter Marker für die Unterscheidung von Infektion und Inflammation die Änderung des CRP-Spiegels untersucht. In allen untersuchten Fällen - der Gabe von Antibiotika, dem Einbringen einer PEG Sonde und der Notwendigkeit der Hospitalisierung – zeigte sich ein signifikanter Anstieg des CRP (Abbildung 8).

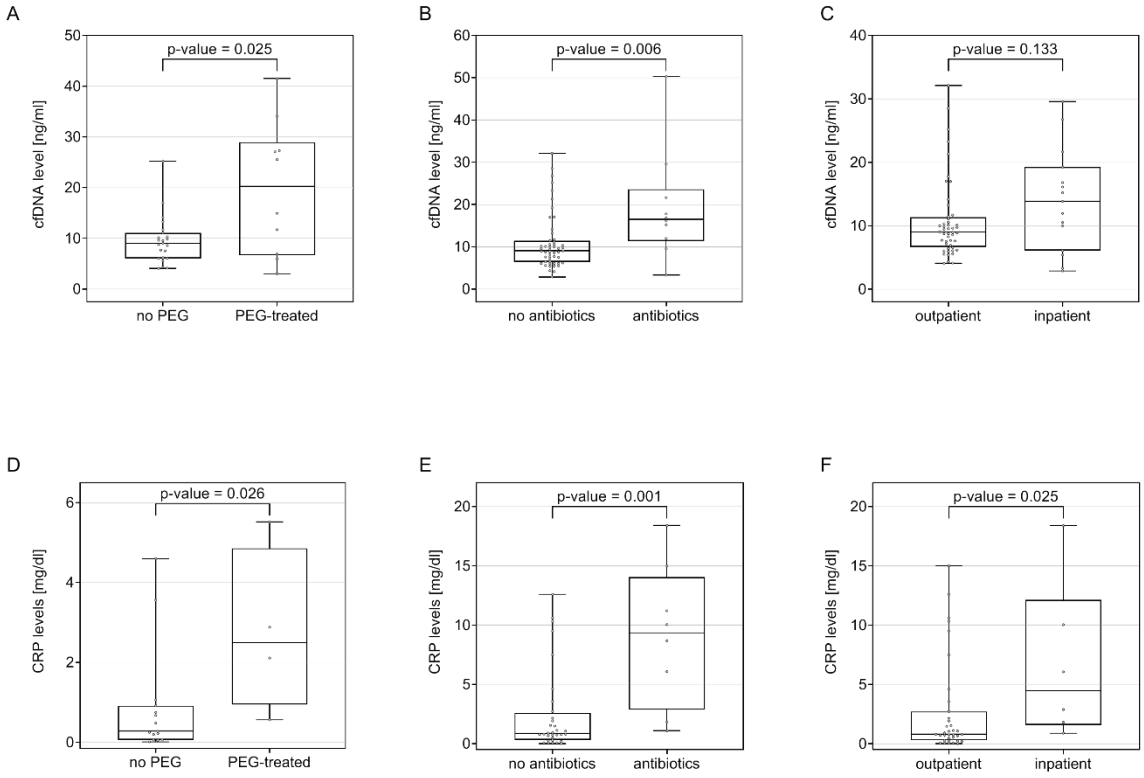

Abbildung 8: Klinische Parameter und Relation zur cfDNA und CRP Konzentration

Dargestellt ist der Einfluss der einzelnen klinischen Parameter (Einbringen einer PEG Sonde, Antibiotikagabe und Hospitalisierung) auf die Konzentration der cfDNA (A-C) und CRP (D-F). A & D) Die Notwendigkeit einer PEG Sonde führte sowohl zu einem signifikanten Anstieg der cfDNA Konzentration als auch des CRP-Spiegels. B & E) Kam es im Rahmen der Radiochemotherapie zur Gabe von Antibiotika, stiegen der cfDNA- und CRP-Spiegel signifikant an. C & F) Nur der CRP-Spiegel stieg signifikant an, sollte im Rahmen der Radiochemotherapie eine Hospitalisierung des Patienten notwendig sein. Alle Werte, die im Zusammenhang mit G-CSF Gaben stehen, wurden bei den übrigen drei Parametern exkludiert. Die Abbildung basiert auf den Daten aus der Arbeit von Zwirner et al. (95).

3.1.4.3 Inflammation versus Infektion

Zur Unterscheidung zwischen Inflammation und Infektion wurde die Änderung der cfDNA Konzentration im Vergleich zu den bereits etablierten blutbasierten Markern wie dem CRP und der Leukozytenzahl gemessen. Die Patienten wurden in drei klinische Kategorien eingeteilt: chronische Entzündung (*baseline inflammation*), mäßige Entzündung (*moderate inflammation*) und Infektion (*manifest infection*). Folgend wurden diese Subpopulationen jeweils mit den gemessenen cfDNA-, CRP- und Leukozytenwerten korreliert.

Als mögliche Störfaktoren wurden die Gabe von G-CSF und das Einbringen der PEG-Sonde identifiziert. Alle im zeitlichen Zusammenhang mit der Gabe von G-CSF und dem Einbringen der PEG-Sonde erhobenen Werte wurden in der Analyse daher nicht berücksichtigt. Im Fall von G-CSF zeigte sich, dass die beiden höchsten cfDNA-Werte (172,9 ng/ml und 83,5 ng/ml) ein bis zwei bzw. acht bis neun Tage nach der Gabe des Medikaments gemessen wurden. Darüber hinaus ließ sich eine zeitliche Korrelation zwischen der Gabe von G-CSF und der cfDNA Konzentration beobachten (Abbildung 9). Für das Einsetzen einer PEG-Sonde konnte eine ähnliche Beobachtung gemacht werden. Erfolgte die Messung der cfDNA-Konzentration bzw. des CRP-Levels innerhalb von drei Tagen nach der Implantation, war eine signifikante Erhöhung zu beobachten (Abbildung 9).

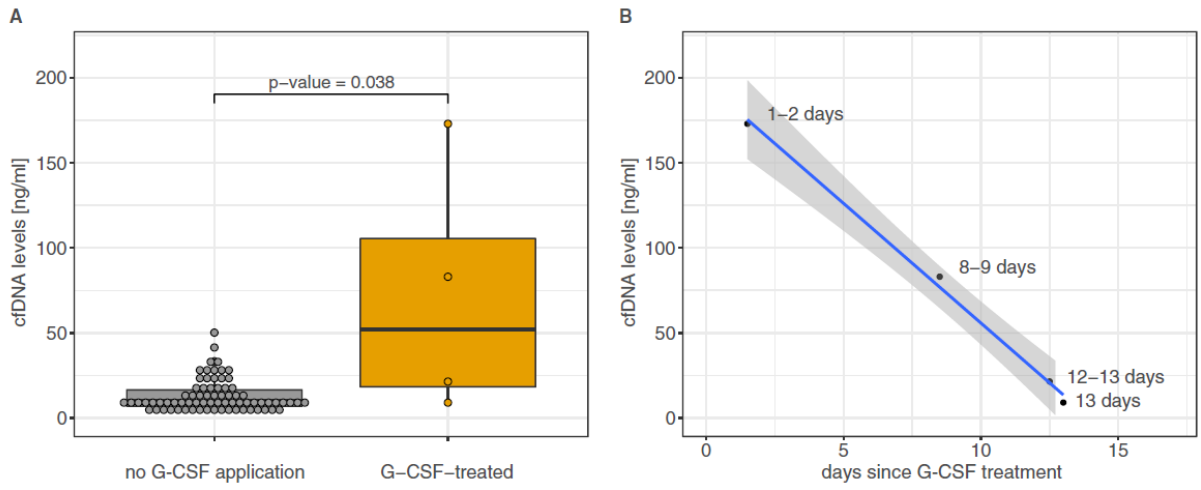

Abbildung 9: Der Einfluss von G-CSF auf die cfDNA Konzentration

Die Gabe von Gabe von G-CSF (Granulozyten-Kolonie-stimulierenden Faktor) wurde im Rahmen der Radiochemotherapie bei Neutropenie gegeben. A) Die Gabe von G-CSF führte zu einem deutlichen Anstieg der cfDNA-Konzentration im Vergleich zu den unbehandelten Patienten. B) Darüber hinaus zeichnete sich ein klarer zeitlicher Zusammenhang zwischen der Gabe von G-CSF und der gemessenen cfDNA-Konzentration ab. Die Gabe von G-CSF wurde als möglicher Störfaktor identifiziert und die cfDNA-Werte nicht weiter berücksichtigt. Die Abbildung entstammt der Arbeit von Zwirner et al. (95).

In der folgenden Analyse war eine eindeutige Differenzierung zwischen chronischer Inflammation (*baseline*) und einer schweren Infektion (*manifest infection*) sowohl mit Hilfe der cfDNA Quantifizierung als auch der Bestimmung des CRP-Levels möglich (Abbildung 10). Die Unterscheidung zwischen Toxizität (*moderate inflammation*) und schwerer Infektion war ausschließlich durch die Messung der cfDNA Konzentration gegeben (Abbildung 10A). Sie zeigte signifikant erhöhte Werte in Verbindung mit einer Infektion. Eine breite Streuung der CRP-Werte war innerhalb der *moderate inflammation* Gruppe zu beobachten. Dennoch zeigte sich ein signifikanter Unterschied der CRP Werte zwischen den Patienten der *baseline* und der *moderate inflammation* Gruppe (Abbildung 10B). Die Leukozytenzahl zeigte einen signifikanten Unterschied zwischen den Werten der *baseline* und *moderate inflammation* Gruppe (Abbildung 10C). Im Rahmen einer schweren Infektion variierte die Leukozytenzahl zwischen den Patienten stark und war somit zugleich ein Hinweis auf eine Leukopenie bzw. Leukozytose.

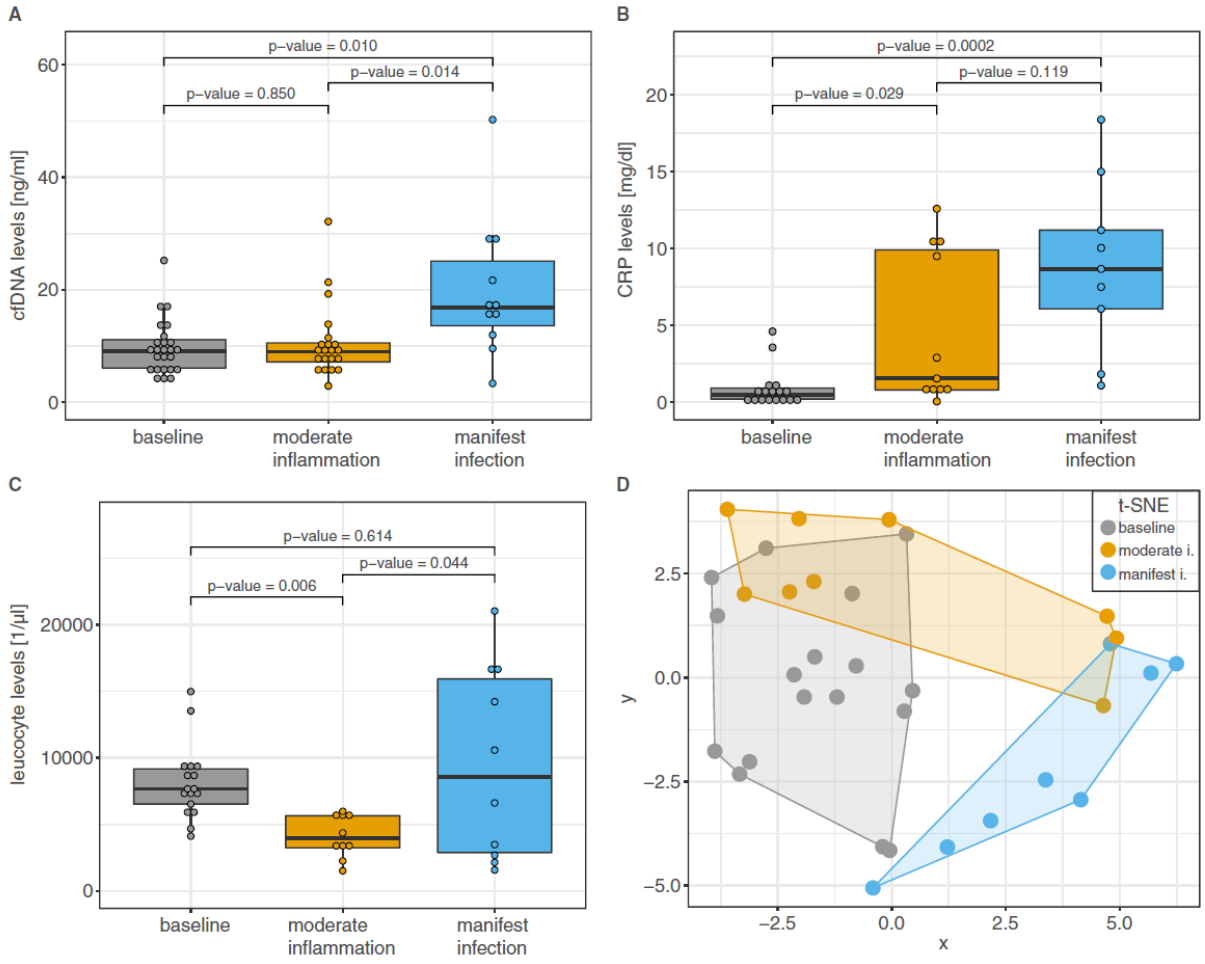

Abbildung 10: Infektion vs Inflammation

Für die Unterscheidung zwischen einer chronischen Inflammation (*baseline*), der Toxizität durch die Radiochemotherapie (*moderate inflammation*) und einer schweren Infektion (*manifest infection*) wurden die folgenden Parameter berücksichtigt: *manifest infection* = Patienten mit Fieber und Antibiotikagabe oder Fieber in Kombination mit einem mikrobiologischen Keimnachweis; Inflammation/Toxizität im Rahmen der Radiotherapie wurde über die Toxicity criteria of the Radiation Therapy Oncology Group definiert (96). Es wurde zwischen RTOG Grad ≤ 1 (*Baseline Inflammation*) und einem RTOG Grad 2 und 3 (*moderate inflammation*) unterschieden. A) Der cfDNA Spiegel ermöglicht die Unterscheidung zwischen einer chronischen Inflammation und einer scheren Infektion, sowie einer toxischen Inflammation und einer schweren Infektion. B) Die Bestimmung des CRP-Spiegels ermöglicht die Unterscheidung zwischen einer chronischen Inflammation und einer schweren Infektion sowie einer Tumor-bedingten und toxischen Inflammation. C) Deutliche Änderungen in der Anzahl der weißen Blutkörperchen können bei der Unterscheidung zwischen einer Tumor-bedingten Inflammation und der durch die Radiochemotherapie verursachten Inflammation festgestellt werden. D) tSNE (*unsupervised stochastic nonlinear dimensionality reduction technique*) der Plot zeigt die Gruppierung der klinischen Zustände. Die Abbildung entstammt der Arbeit von Zwirner et al. (95).

3.1.5 CtDNA als potentieller Biomarker bei Patienten mit einem HNSCC

Neben den beschriebenen Nebenwirkungen im Rahmen einer Radiochemotherapie (RCTX) auf Grund des intensiven Behandlungsregimes stellt die Rezidivrate von 50-60% der Patienten eine Herausforderung dar (84, 97). Aktuell gibt es keine Strategie für die aktive Überwachung des Behandlungserfolges unter RCTX und die Nachsorge basiert auf der klinischen Untersuchung des Patienten und bildgebenden Verfahren. Daher wäre es wünschenswert Verfahren zu entwickeln, die sowohl eine dynamische Kontrolle des Behandlungserfolges als auch die Detektion einer minimalen Resterkrankung am Ende der Therapie ermöglichen.

In der Studie *„Dynamics of cell-free tumour DNA correlate with treatment response of head and neck cancer patients receiving radiochemotherapy“* untersuchten wir daher den Einsatz der *Liquid Biopsy* als Biomarker für die Therapieüberwachung und die Detektion einer minimalen Resterkrankung nach Therapie. In der Studie wurde sowohl die zellfreie zirkulierende Tumor DNA (ctDNA) als auch zirkulierende DNA der humanen Papillomavirenstämme HPV16 und 18 (cvDNA) untersucht (Abbildung 11).

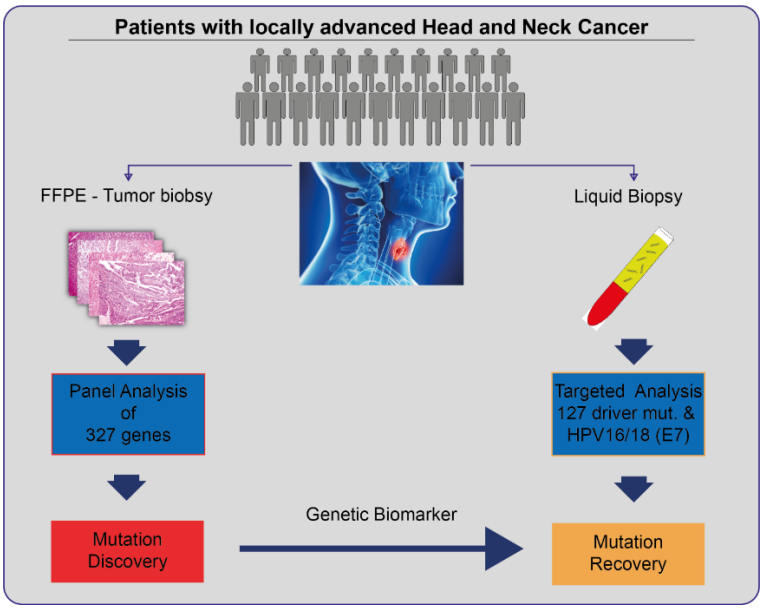

Abbildung 11: Studiendesign für die Untersuchung der zellfreien zirkulierenden Tumor DNA (ctDNA)

Im Rahmen der Studie wurden 20 Patienten mit einem fortgeschrittenen Kopf-Hals-Tumor (HNSCC) eingeschlossen. Das Tumorgewebe der Patienten wurde vor Beginn der Therapie mit einem *HNSCC*-spezifischen Genpanel (327 Gene) analysiert. Die dabei identifizierten Treibermutationen und die Sequenz des viralen Onkogen E7 wurden für die gezielte Analyse im Rahmen der Liquid Biopsie eingesetzt.

3.1.5.1 Detektion der ctDNA und Korrelation mit der Tumormasse

Wie in Abschnitt 2.1.3 beschrieben, wurde von jedem der 20 Patienten eine umfassende Panelsequenzierung aus der soliden Tumorbiopsie durchgeführt und 127 Treibermutationen identifiziert. Für die Detektion der ctDNA und cvDNA wurde ein spezifisches Panel entworfen, das sowohl alle 127 Treibermutationen abdeckt, als auch die Sequenz des Onkoproteins E7 der Virusstämme HPV16 und 18. Um auch sehr niedrige ctDNA-Spiegel detektieren zu können, verwendeten wir einen ultra-sensitiven NGS-Ansatz unter Verwendung von Template-spezifischen Barcodes (*unique molecular identifer,* UMI). Dadurch war es uns möglich, bei einer durchschnittlichen Sequenziertiefe von 23.206X vor und 2.049X nach UMI-basierter Deduplikation ein mutiertes ctDNA Molekül aus 2000 Wildtypmolekülen zu detektieren. Das entspricht einem mittleren Detektionslimit von 0,05 Prozent.

Zur Detektion der Treibermutationen im Plasma wurden von jedem Patienten fünf Blutproben (N = 99) über den Therapieverlauf (t1-5) hinweg gesammelt (Abbildung 12). In 17 von 20 Patienten konnte an mindestens einem Zeitpunkt ctDNA detektiert werden. In drei Patienten konnte zu keinem Zeitpunkt ctDNA detektiert werden. Dies entspricht einer Detektionsrate von 85%.

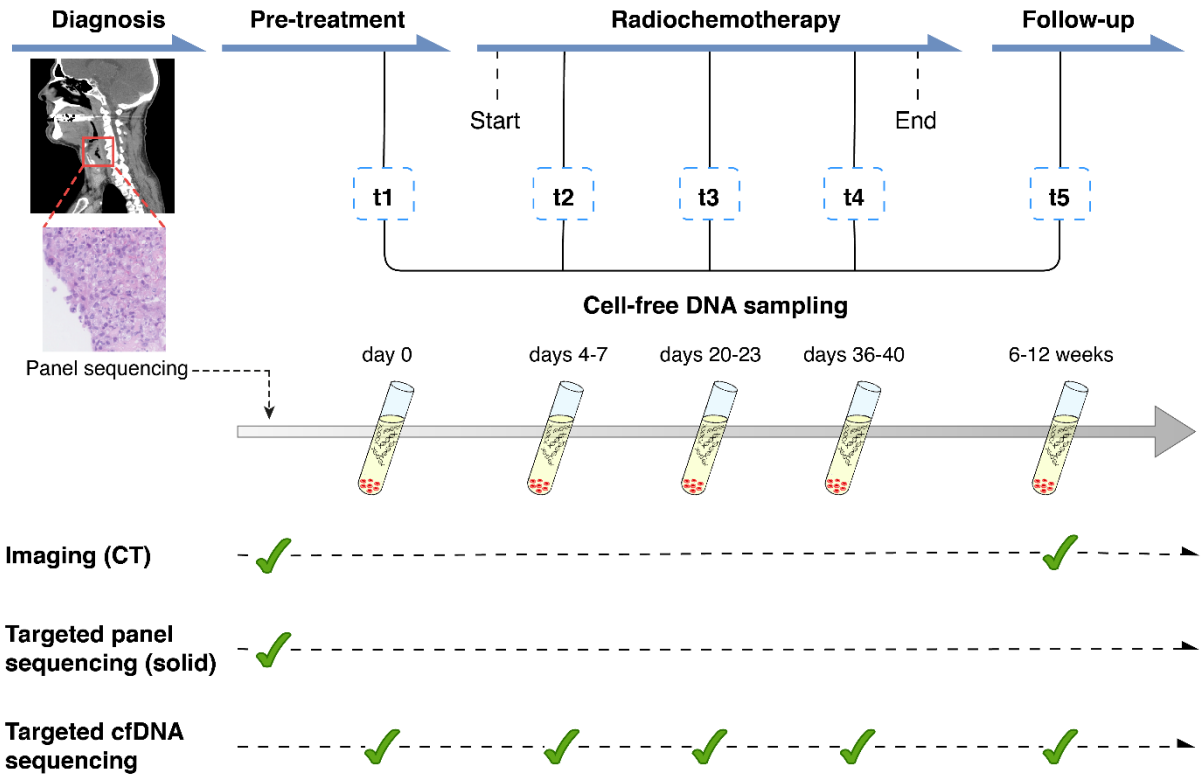

Abbildung 12: Probensammlung und Analyseverfahren

Das im Rahmen der Diagnosestellung gewonnene Tumormaterial wurde mittels Panelsequenzierung auf Treibermutationen untersucht. Jeder Patient erhielt vor und nach der Therapie eine CT-gestützte Aufnahme des Tumors zur Bestimmung der Tumorlast. Es wurden insgesamt fünf Blutproben für die Analyse der ctDNA gesammelt. Eine Probe vor Beginn der Therapie als Ausgangswert. Im Verlauf wurden drei weitere Proben gesammelt zur Beobachtung des Therapieansprechens. Die letzte Probe wurde als Teil der ersten Nachuntersuchung gewonnen für die Bestimmung einer residuellen Tumorerkrankung. Die Abbildung entstammt dem Manuskript „Dynamics of cell-free tumour DNA correlate with treatment response of head and neck cancer patients receiving radiochemotherapy".

Zwischen der makroskopischen Tumorlast und der Allelfrequenz der Treibermutationen im Plasma (im Folgenden als ctDNA-Spiegel bezeichnet) gemessen vor dem Therapiebeginn (t1) konnte eine positive Korrelation beobachtet werden. Größere Volumina der Primärtumoren und ihrer beteiligten Lymphknoten waren mit höheren ctDNA-Spiegeln assoziiert (Abbildung 13).

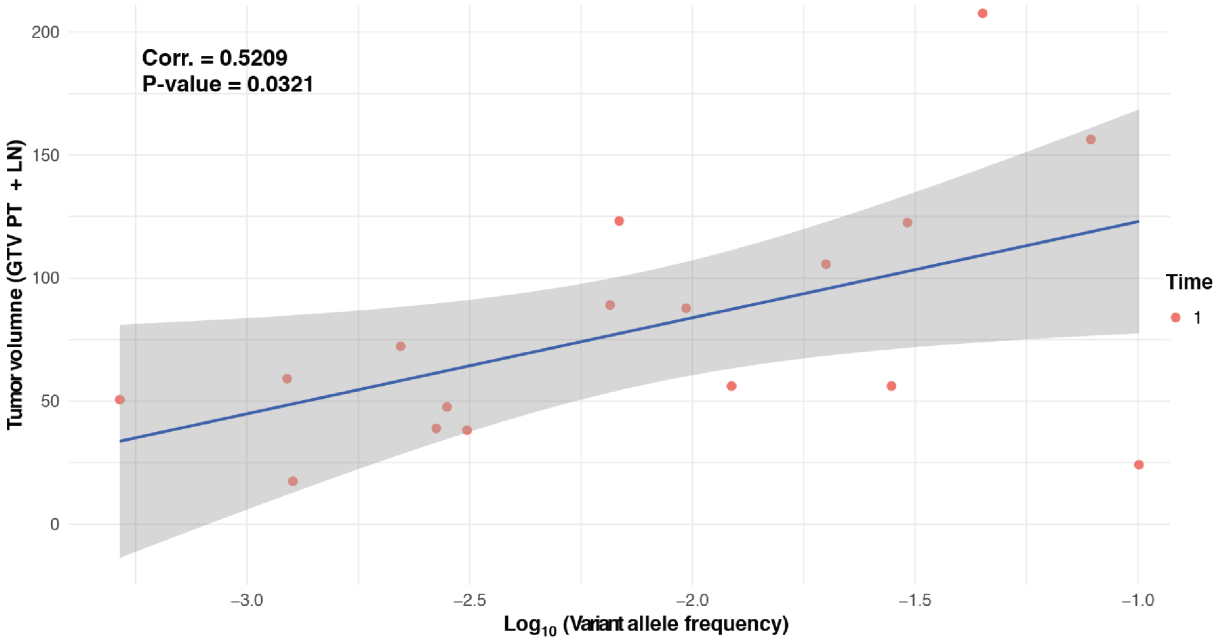

Abbildung 13: Korrelation zwischen der Tumorlast und des ctDNA-Spiegel zu Therapiebeginn

Korrelation des Gesamttumorvolumens (GTV PT + LN) mit dem ctDNA-Spiegel der Treibermutationen im Plasma vor der Behandlung (t1). Die Häufigkeit der Allel-Varianten im Plasma korrelierte (p-Wert < 0,05, Pearson-Korrelationstest) mit der Gesamtgröße des Tumors (GTV PT + LN). Die Abbildung entstammt dem Manuskript „Dynamics of cell-free tumour DNA correlate with treatment response of head and neck cancer patients receiving radiochemotherapy".

3.1.5.2 ctDNA-Spiegel als dynamischer Marker und Therapieüberwachung

Um eine Aussage über einen möglichen Zusammenhang zwischen der ctDNA Kinetik und dem Therapieansprechen treffen zu können, wurde der ctDNA-Spiel in zeitlicher Relation zur RCTX untersucht. Wie bereits oben beschrieben, gibt es Einflussgrößen, die den Anteil der ctDNA an der Gesamtmenge der cfDNA variieren lassen können. Daher wurde in der Betrachtung die Gesamtmenge der cfDNA sowie das Vorhandensein einer schweren Infektion als Störfaktoren berücksichtigt und aus der Betrachtung der ctDNA-Dynamik ausgeschlossen. So konnte eine deutliche Zeit- und Dosisabhängigkeit gezeigt werden (Tabelle 2).

Tabelle 2: Regressionsanalyse - Korrelation zwischen dem Therapieverlauf und dem ctDNA Spiegel

Pat	Number of Mutations	Time – ctDNA AF correlation	Spearman correlation	p-value Spearman correlation	Confounder Model	p-value Confounder model
13	3	Sign. decrease	-0.8963	0.00001	Non-significant	0.1907
18	3	Sign. decrease	-0.9069	0.00005	Significant	0.0189
7	7	Sign. decrease	-0.5161	0.00150	Significant	0.0113
3	2	Sign. decrease	-0.8370	0.00252	Significant	0.0441
20	2	Sign. decrease	-0.7878	0.00681	Significant	0.0971
14	2	Sign. decrease	-0.8486	0.00772	Non-significant	0.7704
16	2	Sign. decrease	-0.7139	0.02039	Significant	0.0253
21	1	No sign. change	-0.7000	0.23333	Non-significant	0.2266
10	2	No sign. change	-0.4238	0.25566	Significant	0.087

Pat	Number of Mutations	Time – ctDNA AF correlation	Spearman correlation	p-value Spearman correlation	Confounder Model	p-value Confounder model
5	5	No sign. change	0.2563	0.27534	Significant	0.0005
17	1	No sign. change	-0.8000	0.33333	Non-significant	0.8246
15	1	No sign. change	-0.4000	0.75000	Non-significant	0.7596
9	4	No sign. change	-0.0552	0.81713	Significant	0
4	3	No sign. change	-0.0328	0.90773	Non-significant	0.1697
19	1	No sign. change	-0.2000	0.91667	Non-significant	0.4281
22	1	No sign. change	0.20000	0.91667	Non-significant	0.446
2	1	Inconclusive	NA	NA	Inconclusive	NA
8	0	Inconclusive	NA	NA	Inconclusive	NA
11	1	Inconclusive	NA	NA	Inconclusive	NA
23	0	Inconclusive	NA	NA	Inconclusive	NA

Der ctDNA-Spiegel sank im Verlauf der Beobachtung von einem Median von 1% zum Zeitpunkt *t1* auf 0,01% zum Zeitpunkt *t5* ab (Abbildung 14). Bei sieben Patienten (3, 7, 13, 14, 16, 18 und 20) beobachteten wir eine signifikant negative Korrelation (p-Wert < 0,05) zwischen der Tumorallelfrequenz im Plasma und dem Behandlungsverlauf (Tabelle 2). Bei den übrigen acht Patienten zeigte sich ebenfalls eine Abnahme der ctDNA-Spiegel, allerdings ohne Signifikanz. Darüber hinaus zeigte ein Patient bereits während der Behandlung Anzeichen eines Therapieversagens. Dies spiegelte sich auch durch einen Anstieg des ctDNA-Spiegels im Laufe der Behandlung wider (Patient 5; fortschreitende Erkrankung bei *t5*). Patient 11 wurde von der Korrelationsanalyse ausgeschlossen, da nur eine Mutation überwacht wurde, die nicht zu jedem Zeitpunkt die minimale Sequenzierungstiefe für den Mutationsnachweis erreichte (Abbildung 14).

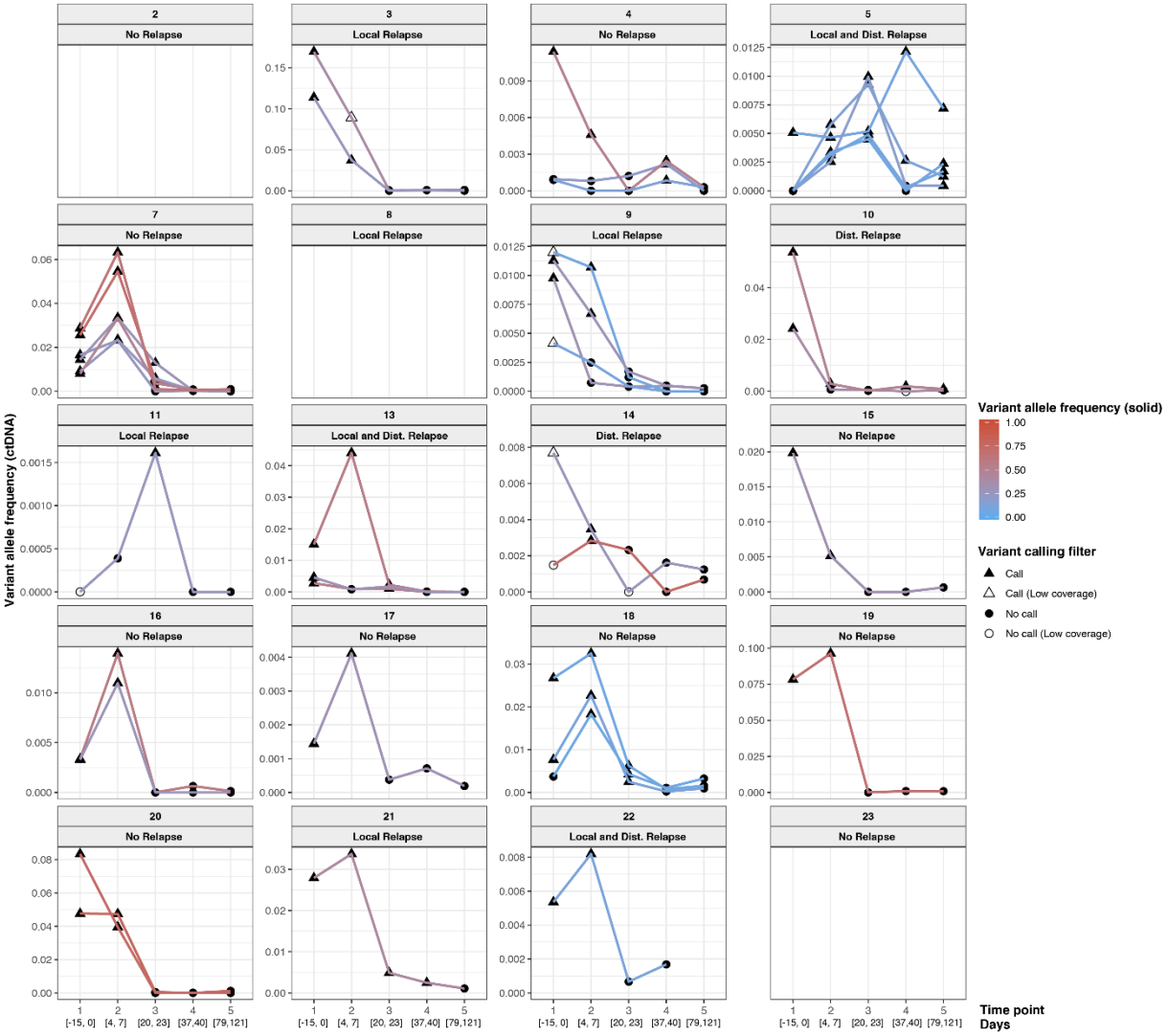

Abbildung 14: Beobachtung des ctDNA Spiegels im Verlauf der Therapie

Dargestellt ist die Allelfrequenz der Patienten-spezifischen Treibermutationen (VAF). Jedes einzelne Bild repräsentiert einen Patienten und die Allelfrequenz der Treibermutationen zu den Zeitpunkten t1-t5. Die Linien verbinden die einzelnen Messungen der gleichen Mutation. Ihre Farben repräsentieren die detektierte Allelfrequenz der Varianten im soliden Tumor. Die Formen zeigen, ob die Treibermutation detektiert wurde (schwarzes Dreieck = *call*), die Treibermutation detektiert wurde, die Abdeckung aber gering war (leeres Dreieck = *call with low coverage*), die Treibermutation nicht detektiert wurde (schwarzer Kreis = *no call*) oder die Abdeckung zu gering war für die Detektion der Treibermutation (leerer Kreis = *no call with low coverage*). Die Abbildung entstammt dem Manuskript „*Dynamics of cell-free tumour DNA correlate with treatment response of head and neck cancer patients receiving radiochemotherapy*".

3.1.5.3 HPV

Neben den Treibermutationen wurde auch das diagnostische Potenzial zirkulierender cvDNA (circulating viral DNA) im Plasma evaluiert. Daher wurde die gesamte Kohorte zu allen fünf Zeitpunkten auf die Existenz der E7-Sequenz aus den HPV16- und HPV18-Stämmen untersucht. Die Untersuchung der *Liquid Biopsy* konnte cvDNA Fragmente bei allen drei Patienten nachweisen, die zuvor auch immunhistochemisch positiv in der p16INK4a-Proteinfärbung waren. Die Anzahl der Virusfragmente zum

Zeitpunkt t1 lag zwischen 2.229 - 11.671 normalisierten cvDNA Fragmenten pro Patient (Abbildung 15). Bei einem weiteren Patienten, mit einem negativen p16INK4a-Test, konnte ein niedriger cvDNA-Spiegel von 352 Fragmenten zum Zeitpunkt *t1* festgestellt werden. Die Schätzung der HPV-Kopien pro Krebszelle bei allen drei Patienten ergab 3,86, 2,95 und 11,69 HPV-Kopien pro Krebszelle bei den Patienten 4, 14 und 15. Es war zu beobachten, dass der cvDNA-Spiegel bei allen drei Patienten ab dem Zeitpunkt t3 oder *t4* nicht mehr nachweisbar war und dies auch zum Zeitpunkt *t5* so blieb (Abbildung 15).

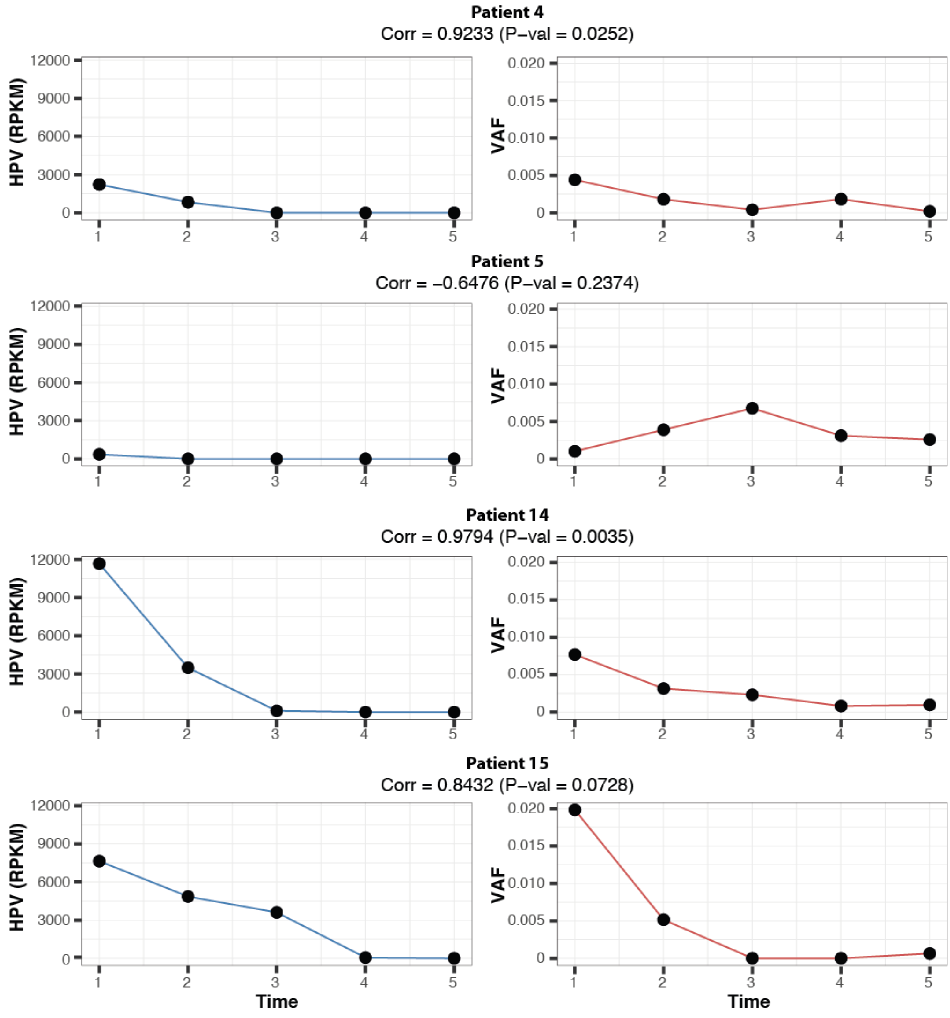

Abbildung 15: Detektion und Verlauf von viraler DNA (HPV 16/18 E7) im Plasma

In der Abbildung sind die longitudinalen Verläufe der cvDNA-Spiegel im Plasma der Patienten 4, 5, 14 und 15 dargestellt. Die Anzahl der viralen DNA Fragmente ist auf die Anzahl der Sequenziereereignisse (reads) in einem Bereich von einer Kilobase auf eine Millionen Sequenziereereignisse normalisiert (RPKM = *reads per kilobase per millionen mapped reads*). Im Vergleich dazu (rechts) ist der longitudinale Verlauf der Allelfrequenz der Treibermutationen (VAF) im Plasma dargestellt. Untersucht wurden in beiden Fällen alle fünf Zeitpunkte t1-t5. Die Pearson-Korrelationswerte zwischen VAF und HPV (RPKM) sind unter der Patientenbezeichnung angegeben. Die Abbildung entstammt dem Manuskript „*Dynamics of cell-free tumour DNA correlate with treatment response of head and neck cancer patients receiving radiochemotherapy*".

Zusätzlich untersuchten wir die cvDNA-Kinetik der drei Patienten (4, 14 und 15) während der RCTX-Behandlung. Alle drei Patienten zeigten eine stetige Abnahme der Viruslast während der gesamten Therapie. Die Korrelation zwischen der longitudinalen Abnahme der normalisierten cvDNA-Fragmente und der Behandlungsdauer war signifikant (p-Wert < 0,05 mit Spearman-Korrelationstest). Darüber hinaus korrelierte die zeitliche Abnahme der normalisierten cvDNA-Fragmente mit der Abnahme der ctDNA-Spiegel bei den jeweiligen Patienten (p-Wert < 0,05 bei den Patienten 4 und 14, p-Wert = 0,07 bei Patient 15, unter Verwendung des Pearson-Korrelationstests, Abbildung 15).

3.1.5.4 Detektion einer minimalen Resterkrankung (*molecular residual disease*; MRD)

Das zweite Ziel dieser Studie war das Auftreten eines lokalen Progresses oder eines Rezidivs möglichst frühzeitig mit Hilfe der Liquid Biopsy zu erkennen. Das heißt, die Detektion minimaler Mengen zirkulierenden ctDNA-Moleküle als möglichen Marker einer molekularen Resterkrankung (*molecular residual disease*, MRD) nachzuweisen. Es wurden 16 Patienten in die MRD-Analyse einbezogen, bei denen erfolgreich Plasma zum Zeitpunkt *t5* gewonnen wurde und mindestens für einen früheren Zeitpunkt (*t1-t4*) ctDNA nachgewiesen wurde. Bei zwei von acht Patienten, die einen Rückfall erlitten (Abbildung 16), konnte eine MRD festgestellt werden, während keiner der acht Rezidiv freien Patienten eine MRD zeigte. Es hatten folglich 100% der Patienten mit nachweisbarer MRD ein Rezidiv, aber 75% dieser Patienten zeigten nach der Behandlung keine molekulare Resterkrankung.

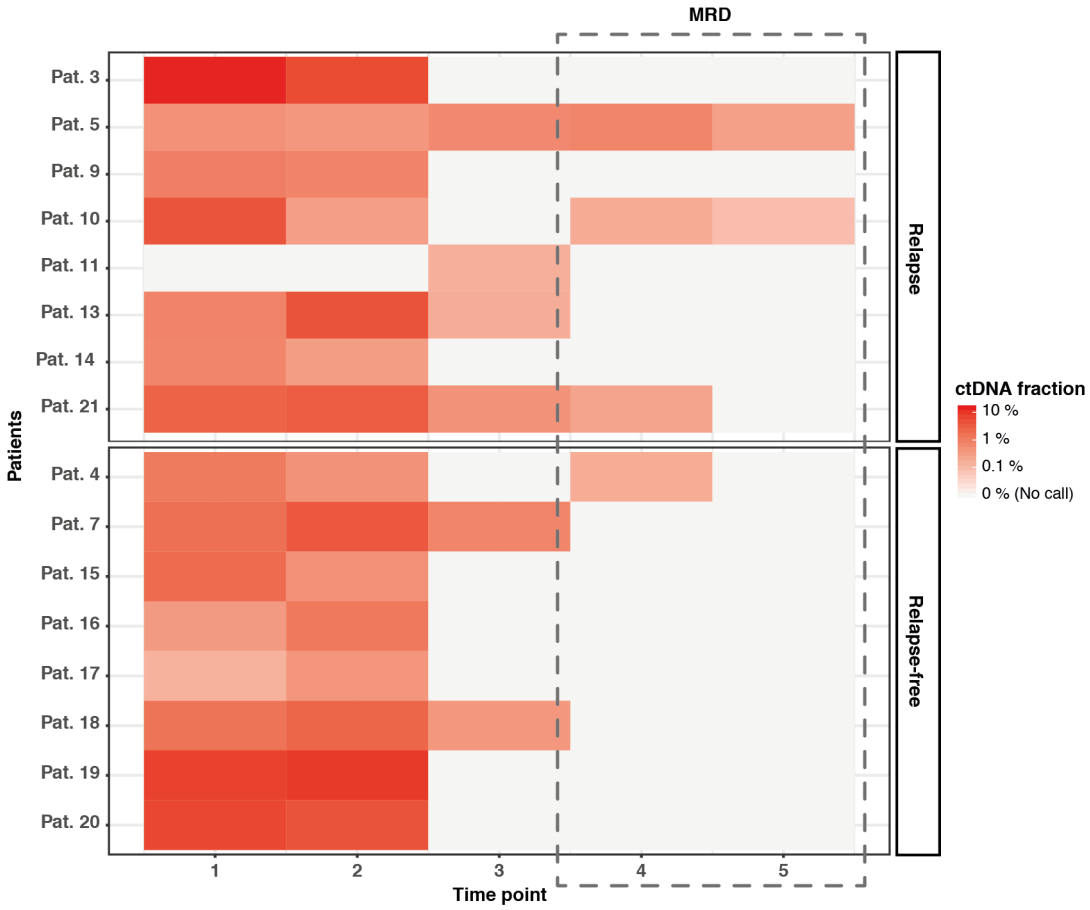

Abbildung 16: ctDNA Heatmap

Die Heatmap ist eine Zusammenfassung aller Patienten und Zeitpunkte. Die rote Farbskala zeigt ein positives Ergebnis in Relation zum detektiert ctDNA-Anteil in der Plasmaprobe an. Die graue Farbe steht für ein negatives Ergebnis, d.h. es wurde keine ctDNA nachgewiesen. Die Zeitpunkte t4 und t5 wurden für die Untersuchung einer minimalen Resterkrankung (MRD = *molecular residual disease*) berücksichtigt. Nur wenn auch zum Zeitpunkt t5 noch ctDNA nachweisbar war, wurde der Patient als MRD-positiv betrachtet. Die Abbildung entstammt dem Manuskript „Dynamics of cell-free tumour DNA correlate with treatment response of head and neck cancer patients receiving radiochemotherapy".

Beide MRD-positive Patienten wiesen eine signifikante Anzahl von Tumorfragmenten mit MRD-Scores von 12,16 ($p < 10\text{-}12$) bzw. 2,44 ($p < 0{,}004$) auf (siehe Abbildung 17). Sie zeigten entweder eine progressive Erkrankung innerhalb von 101 Tagen bei Patient 5 oder eine Fernmetastase nach 833 Tagen bei Patient 10. Die Analyse der residuellen ctDNA-Fragmente ergab, dass Patient 5 immer noch ctDNA-Fragmente von fünf mutierten Treibergenen mit einer globalen Allelfrequenz von 0,27% hatte (Abbildung 17A). Bei Patient 10 wurde nur die Mutation in *TP53* detektiert (VAF = 0,09%), während die Mutation in *ATM* nicht mehr nachweisbar war (Abbildung 17B).

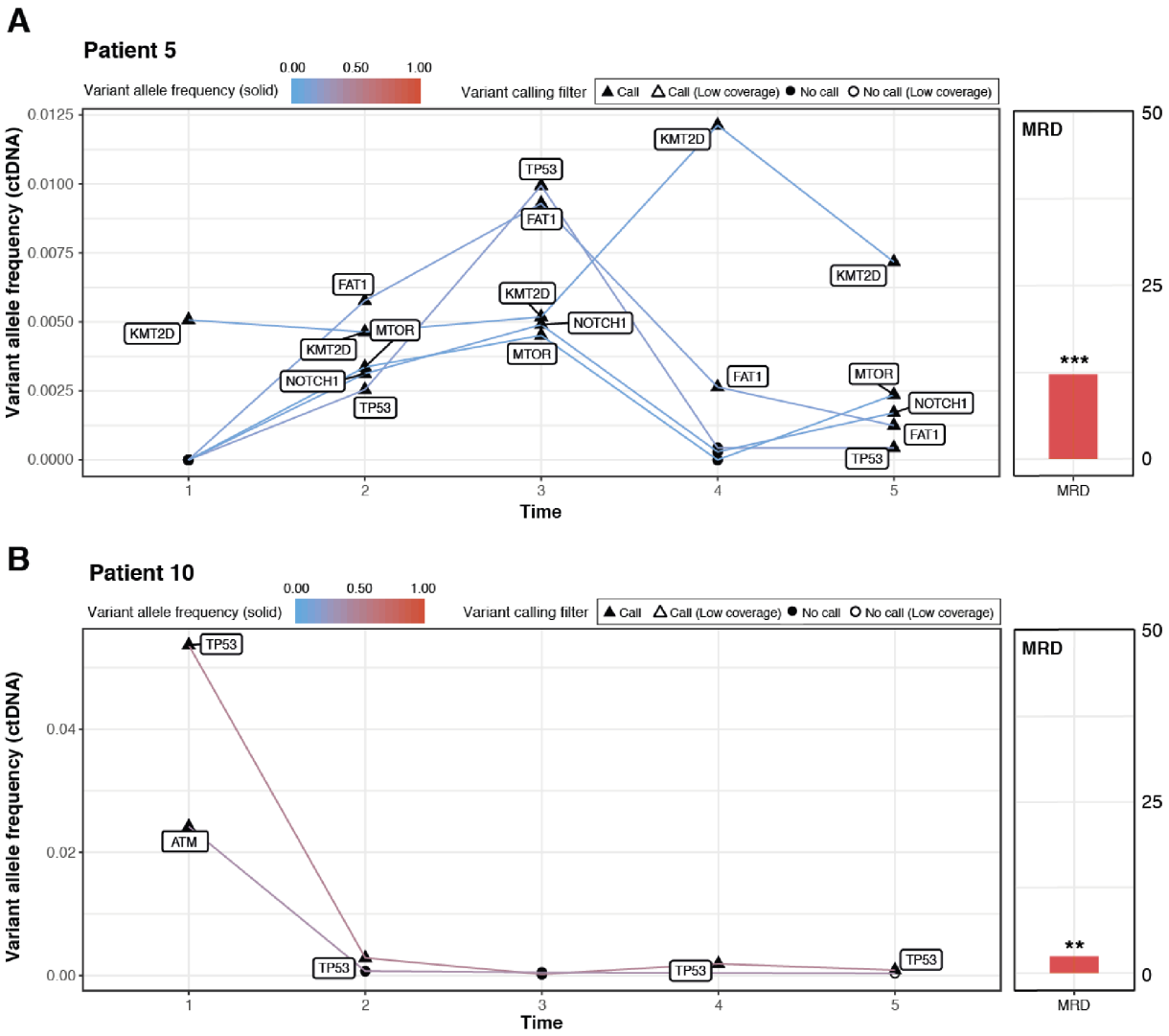

Abbildung 17: MRD-positive Patienten

Die beiden Patienten 5 und 10 wurden als MRD positiv identifiziert. Dargestellt ist die longitudinale Messung der einzelnen Mutationen in den beiden Patienten. Die Linien verbinden die identischen Mutationen zu den verschiedenen Zeitpunkten. Die Farbe der Linien repräsentiert die VAF im soliden Tumor und die Formen der Datenpunkte zeigen an ob die Mutation nachweisbar war. Variante detektiert (schwarzes Dreieck = *call*), Variante detektiert mit geringer Abdeckung (leeres Dreieick = *call with low coverage*), die Treibermutation wurde nicht detektiert (schwarzer Kreis = *no call*) oder die Abdeckung war zu gering für die Detektion der Treibermutation (leerer Kreis = *no call with low coverage*). A) Patient 5: Untersucht wurden die Treibermutationen in den Genen *TP53*, *KMT2D*, *NOTCH1*, *FAT1* im Verlauf der Therapie und der MRD-Wert bei der ersten Nachuntersuchung (t5) im Anschluss an die Behandlung. B) Patient 10: Es wurden die Treibermutationen in den Genen *TP53* und ATM sowie der MRD-Wert beim ersten Follow-up (T5) untersucht. ** für den p-Wert < 0,01 und *** für den p-Wert < 0,001. Die Abbildung entstammt dem Manuskript „*Dynamics of cell-free tumour DNA correlate with treatment response of head and neck cancer patients receiving radiochemotherapy*".

3.1.6 Abschließende Diskussion zu Kopf-Hals Tumoren

In den beiden oben beschriebenen Studien zeigen wir sowohl die Dynamik der gesamten cfDNA, sowie der Tumor-spezifischen ctDNA und cvDNA im Zusammenhang mit ausgewählten klinischen Parametern bei Patienten mit einem lokal fortgeschrittenen *HNSCC*. Hiermit sollte die *Liquid Biopsy* als dynamischer

Marker für die Therapieüberwachung und zur Erkennung von molekularen Resterkrankungen untersucht werden. Darüber hinaus untersuchten wir mehrere klinische Einflussgrößen, die eine dynamische Schwankung der cfDNA im Rahmen der Radiochemotherapie zu Folge hatte. Im Ergebnis konnten wir klinische Anwendungsfelder der ctDNA bei Patienten mit lokal fortgeschrittenem *HNSCC* unter RCTX identifizieren, die in der Zukunft von Bedeutung sein könnten.

In einem ersten Schritt identifizierten wir klinische Merkmale wie Fieber, die Gabe von Antiobiotika oder G-CSF, die einen signifikanten Anstieg der Gesamtmenge der cfDNA zur Folge hatten. Es zeigte sich, dass die Kategorisierung dieser Parameter in *baseline*, *moderate inflammation* und *manifest infection* die eindeutige Unterscheidung zwischen einer nebenwirkungsbedingten Inflammation und Infektion erlaubt.

Für die Anwendung der ctDNA und cvDNA bei Patienten mit einem fortgeschrittenen Kopf-Hals-Tumor konnten wir drei Beobachtungen machen: Die ctDNA kann als Surrogatmarker für die Tumorlast angesehen werden, da ihr Level eng mit dem Gesamttumorvolumen korreliert, wie es bereits zuvor in anderen Kohorten und im Tiermodell gezeigt werden konnte (25, 98, 99). Darüber hinaus beobachteten wir einen zeit- und dosisabhängigen Rückgang der ctDNA im Plasma, der mit dem initialen Behandlungserfolg der RCTX korrespondiert. Zudem haben wir die Verwendung der cvDNA als Biomarker für die Diagnose von *HNSCCs* und zur Kontrolle des Therapieansprechens gezeigt. Genauso wie bei der zellfreien Tumor DNA beobachteten wir eine dynamische Abnahme der cvDNA im Verlauf der Behandlung. Im Gegensatz zur ctDNA ist die Messungen der cvDNA deutlich empfindlicher. Das komplette Verschwinden der cvDNA im Anschluss an die Therapie deuten wir als Hinweis darauf, dass nur Tumorzellen Träger des Virusgenoms sind. Daher hoffen wir, dass die Überwachung der dynamischen Veränderungen der ctDNA und cvDNA ein neuer Weg sein könnte, um das laufende Behandlungsschema zu beobachten und gegebenenfalls anzupassen. Des Weiteren schlagen wir vor, cvDNA als blutbasierten Marker für die Früherkennung von *HNSCC* zu verwenden, ähnlich wie bei der Detektion des Epstein-Barr-Virus beim Nasopharynxkarzinom (100, 101). Darüber hinaus könnte der eindeutige Nachweis von HPV DNA im Plasma nach der Behandlung ein Marker für die Rezidiverkennung sein (102-104).

Als dritten Punkt beobachteten wir eine Korrelation zwischen dem Vorhandensein einer molekularen Resterkrankung im Anschluss an die Therapie und dem

Wiederkehren der Tumorerkrankung. Dies ist ein klarer Hinweis auf das mögliche Potential der MRD als ein Biomarker für Stratifizierung der Patienten in Gruppen mit hohem und niedrigem Rezidivrisiko. Diese Beobachtung wurde bereits bei Mamma-, Bronchial-, Pankreas-, Urothel-, Colon- oder Rektalkarzinomen gemacht (105-110). In diesen Studien war der Nachweis einer minimalen Resterkrankung immer mit einem reduzierten Gesamtüberleben und einer gesteigerten Rezidivrate verbunden. Allerdings konnten wir nicht bei allen Patienten unserer Kohorte, die ein Rezidiv hatten, eine MRD nachweisen.

Eine wesentliche Einschränkung der *Liquid Biopsy* im Rahmen der Tumordiagnostik ist die begrenzte Menge an cfDNA, die aus einer Blutprobe extrahiert wird und der geringe Anteil der ctDNA an der Gesamtmenge. Darüber hinaus zeigen unsere Ergebnisse, dass verschiedene Faktoren während der Therapie den cfDNA-Spiegel beeinflussen können. Mit durchschnittlich 20ng cfDNA pro Probe, das entspricht etwa 6000 Genomäquivalenten, ist die Chance begrenzt anhand nur einer Mutation eine minimale Resterkrankung oder den Behandlungserfolg zu erkennen (111). Diese Limitation kann durch die gezielte Suche nach mehr unabhängigen Mutationen pro Individuum (die verschiedene Gene betreffen) überwunden werden, da es die Wahrscheinlichkeit erhöht, Tumorfragmente mit einer sehr niedrigen Allelfrequenz nachzuweisen (105). Das heißt, dass Potenzial unserer diagnostischen Strategie hängt von der Gesamtzahl der untersuchten Mutationen pro Individuum ab.

Daher sollten in zukünftigen Studien mehr Varianten (*driver* und *passenger*) pro Patient und Zeitpunkt und eine noch höhere Sequenziertiefe zur Anwendung kommen. Auf der anderen Seite bedarf es weiterer grundlegender Untersuchung, die den Ursprung und die Dynamik der zellfreien DNA untersuchen, da sie einen erheblichen Einfluss auf den Anteil der ctDNA an der cfDNA haben können.

3.2 Malignes Melanom

Die Prognose von Patienten mit einem malignen Melanom im Stadium IV ist in der Vergangenheit schlecht gewesen (112). Allerdings hat die Einbeziehung der genetischen Mechanismen, die die Karzinogenese und Immunabwehr dieser Tumoren vorantreiben, zu wirksamen Behandlungsmöglichkeiten geführt. Dazu gehört zum einen die gezielte Inhibition des (RTK)/RAS/MAPKinase-Signalwegs mit *BRAF*- und *MEK*-Inhibitoren und zum anderen die Therapie mit Inhibitoren einzelner

Immuncheckpoints wie dem zytotoxischen T-Lymphozyten-assoziierten Protein 4 (CTLA-4) oder dem programmierten Zelltod Protein 1 (PD-1) bzw. seinem Liganden (PD-L1). Dadurch hat sich das Gesamtüberleben von Patienten im Spätstadium verbessert. Es bedarf aber weiterer Forschung zur Identifikation von Biomarkern für die Unterstützung von Behandlungsentscheidungen und für eine weitere personalisierte Therapie (112).

Zu diesem Zweck haben wir drei retrospektive Studien an Patienten mit einem fortgeschrittenen Malignen Melanom durchgeführt um Mutationen zu identifizieren, die sich für eine gezielte Therapie eignen oder dabei helfen, die Patienten besser als Ansprecher und Nichtansprecher auf eine Immuntherapie zu stratifizieren.

1) Klinische Kohorte von 82 Melanom-Patienten, die vorwiegend mit einer Immuncheckpoint-Therapie behandelt wurden: „*Next-generation sequencing in a real world cohort of 82 advanced melanoma patients identifies distinct mutation pattern in different melanoma subtypes*“
2) Patienten mit einem metastasierten akrolentiginösen- und mukosalen Melanom mit vermehrter Hyperprogression *„MDM2, MDM4 and EGFR Amplifications and Hyperprogression in Metastatic Acral and Mucosal Melanoma“* Forschner et al (113)
3) Inteferon-abhängige Seneszenzinduktion im Mausmodell evaluiert im Hinblick auf genetische Veränderungen der Zellzyklusregulation in einer Kohorte von 42 Patienten mit metastasiertem Malignen Melanom, die entweder mit Anti-PD-1 oder mit einer Kombination aus Anti-CTLA-4 und Anti-PD-1 behandelt wurden: *„Cancer immune control needs senescence induction by interferon-dependent cell cycle regulator pathways in tumours“* (114)

3.2.1 Klinische Kohorte von 82 Patienten mit Malignem Melanom

3.2.1.1 Studiendesign und Patientenkohorte

In dieser Studie wurden 82 Patienten mit einem fortgeschrittenen Melanom untersucht, die mit einem PD-1 Antikörper alleine oder in Kombination mit einem CTLA-4 Antikörper behandelt wurden. Bei der Kohorte handelt es sich um Patienten, die im Rahmen der klinischen Routine durch das Tumorboard der Dermatologie im Jahr 2017 für eine Sequenzierung ausgesucht wurden (Tabelle 3). In der Mehrzahl waren es Patienten mit einem kutanen Melanom (N = 42). Darüber hinaus wurden weitere 14 Patienten mit einem akrolentiginösen und neun mit einem mukosalen Melanom

eingeschlossen. Die kleinste Patientengruppe bildeten die uvealen (N = 8) und okkulten Melanome (N = 9). Das mediane Alter der Patienten lag bei 57 Jahren (Interquartilsspanne 46-67 Jahre) und die Geschlechter waren annährend gleich verteilt mit 37 Frauen (45%) und 45 (55%) Männern.

Tabelle 3: Klinische Charakterisierung der Kohorte

Alter bei der Erstdiagnose – in Jahren	
Median (Interquartilspanne)	57 (46-67)
Geschlecht – Anzahl der Patienten (%)	
Frauen	37 (45)
Männer	45 (55)
Melanom Subtyp – Anzahl der Patienten (%)	
Kutan	42 (51)
Akrolentiginös	14 (17)
Uveal	8 (10)
Mukosal	9 (11)
Okkult	9 (11)
Tumordicke des Primarius – mm	
Median (Interquartilspanne)	3.3 (1.8-5.1)
Tumorstadium z.Z. der Sequenzierung – Anzahl d. Pat. (%)	
Satdium III	5 (6)
Stadium IV	77 (94)
Immuncheckpoint-Therapie	76/82 (93)
Gezielte Therapie	21 (26)
Chemotherapie	4 (5)
Keine Systemtherapie	5 (6)
Ursprung d. sequenzierten Gewebes – Anzahl d. Patienten (%)	
Lymphknoten	19 (23)
Andere Metastasen	57 (70)
Primäres Melanom	6 (7)
Vortherapie des analysierten Gewebes – Anzahl d. Pat. (%)	
Therapienaives Gewebe	52 (63)
Gewebe progredient unter der Immuncheckpoint-Therapie	18 (22)
Gewebe progredient unter der gezielten Therapie	8 (10)
Gewebe progredient unter der Chemotherapie	4 (5)
Median (Interquartilspanne)	33 (9-61)

3.2.1.2 Genetisches Profil der Kohorte

Die Kohorte wurde mit drei verschiedenen Versionen eines Tumorpanels analysiert. 34 Patienten wurden mit der Version ssSCv2, 45 mit der Version ssSCv3 und 3 Patienten mit der Version ssSCv4 untersucht.

Die Panelsequenzierung der 82 Tumorproben von 82 Patienten identifizierte 1.650 somatischen Varianten (SNVs und INDELs) und 2.137 somatische Kopienzahlveränderungen (CNVs), wie z.B. eine Amplifikation oder Deletion eines kompletten Gens. Daraus ergab sich ein Median von 10 SNVs/INDELs pro Patient und

eine mediane Tumorlast (TMB) von 5,82 Mutationen pro Megabase (Spanne: 0-151,75). Für die Identifikation der Treibermutationen (SNVs und CNVs) und die Detektion der Subtyp-spezifischen genetischen Merkmale wurden 275 Gene berücksichtigt. Es handelt sich dabei um die Gene, die in allen drei Versionen des verwendeten Tumorpanels (ssSCv2, v3 und v4) übereinstimmend vorhanden sind. Für die Annotation der Treibermutationen wurde die Internetdatenbank *CancerGenomeInterpreter.org* verwendet (89). Wir identifizierten eine Gesamtzahl von 527 Treibermutationen, 283 SNVs und 244 CNVs, in 149 Genen.

Die Einteilung unserer Kohorte in die drei genomischen Subtypen *BRAF*-, *RAS*-, *NF1*-mutiert und dreifach Wildtyp (*triple-wildtype*) ergab, dass mehr als die Hälfte der Patienten eine Treibermutation in einem der drei Gene trug. Am häufigsten mutiert war die Serin/Threonin-Kinase *BRAF* (28%). Bei dem überwiegenden Teil handelte es sich um die Hotspot-Mutationen V600E/K/R (91%). Zusätzlich hatte ein Patient die *BRAF*-G466E-Treibermutation und ein weiterer zwei gleichzeitige Treibermutationen an den Positionen P367S und K601E (Abbildung 18). Am zweithäufigsten mutiert war die GTPase *NRAS* (24%) mit den Mutationen Q61K/L/R. Bei zwei Patienten konnten wir die seltene Kombination aus gleichzeitig auftretenden Hotspot-Mutationen in dem Gen *BRAF* (V600E) und *NRAS* (Q61K bzw. R) beobachten (Abbildung 18). Treibermutationen in dem Gen *NF1* waren selten mit sechs Prozent. Der Rest der Kohorte, 37 Patienten (45%), wurde als dreifacher Wildtyp klassifiziert.

Alle drei Gene sind elementare Signaltransduktoren des (RTK)/RAS/MAPKinase-Signalweges (im Folgenden RTK/RAS genannt). Neben Treibermutationen in den Genen *BRAF*, *NRAS* und *NF1* fanden wir gehäuft aktivierende Amplifikationen in den Rezeptortyrosinkinasen *ERBB3* und *MET*, sowie in den Signaltransduktoren *KRAS* und *PTPRD* (Abbildung 18). Damit ist der RTK/RAS Signalweg in unserer Kohorte am häufigsten von Treibermutationen betroffen (79%). Die am häufigsten von Deletionen oder Amplifikationen betroffenen Gene waren *CDKN2A* (24%) und *CCND3* (23%), die beide zur Zellzykluskontrolle gehören (Abbildung 18). In 24% der Patienten detektierten wir aktivierende Amplifikationen in dem Gen *MYC*. Die PI3K-Signalkaskade ist der am dritthäufigste mutierte Signalweg (38%) mit Treibermutationen in den Genen *PTEN* (17%) und *RICTOR* (12%). Des Weiteren fanden wir häufiger Treibermutationen im Wnt- und SWI/SNF-Signalweg (*CTNNB1, ARID2, SMARCA4*).

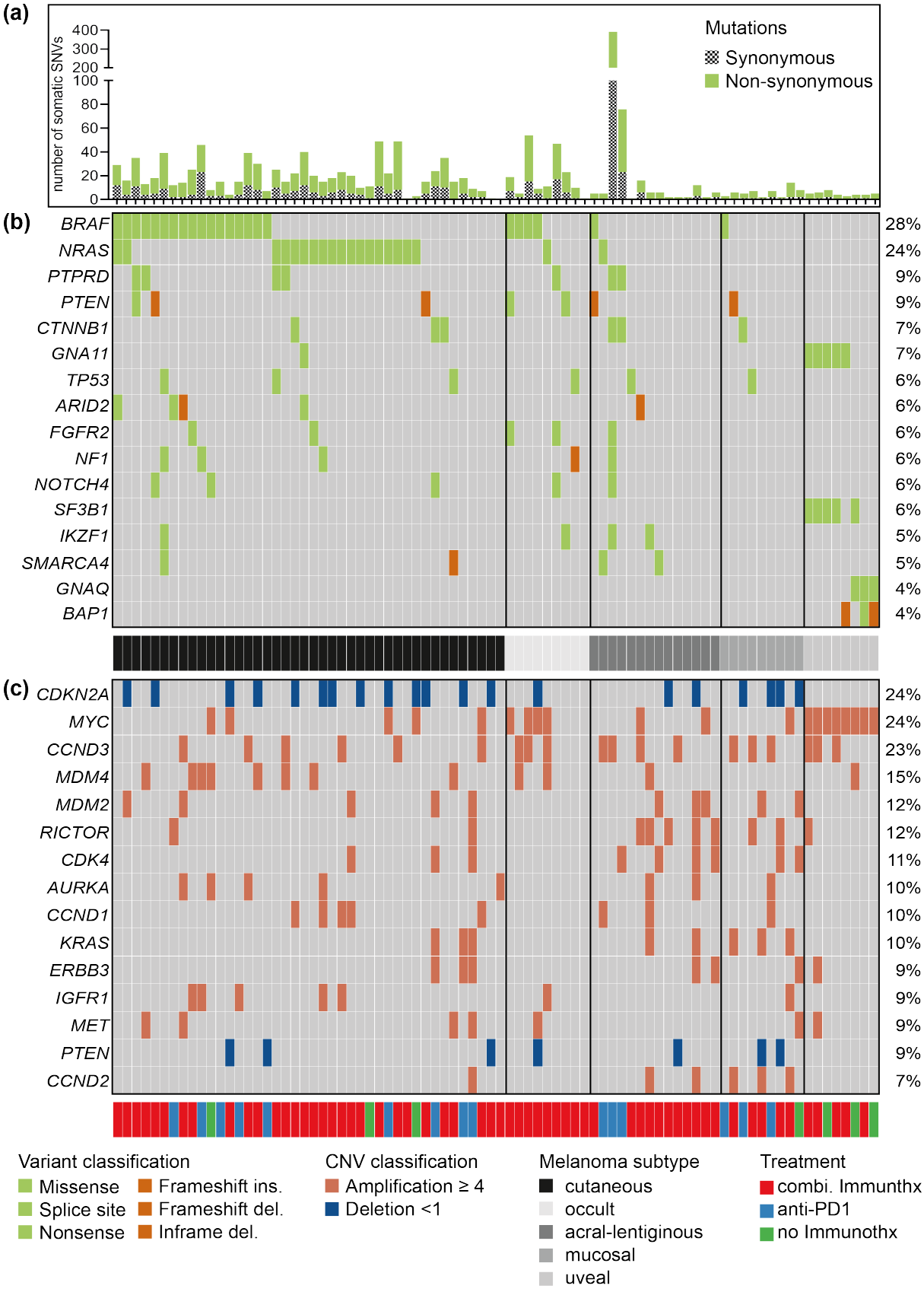

Abbildung 18: *Oncoplot* mit den am häufigsten mutierten Genen (Treibermutationen)

Der *Oncoplot* fasst die Gene zusammen, die am häufigsten von einer Treibermutation betroffen sind. Die Identifikation der Treibermutationen wurde mit dem *Cancer Genome Interpreter* durchgeführt (89). Der *Oncoplot* ist nach den histopathologischen

Subtypen sortiert. Jede Spalte repräsentiert in den Abschnitten a-c den gleichen Patienten. Jede Zeile in den Abschnitten b und c zeigt die Häufigkeit und Art der Treibermutationen für das jeweilige Gen an. Zusätzlich ist die Behandlungsart im unteren Abschnitt angegeben. (a) Das Histogramm illustriert die Anzahl der somatischen Mutationen (synonyme und nicht-synonyme) im kodierenden Bereich jedes einzelnen Patienten. (b) Der Oncoplot listet die 16 Gene auf, in denen am häufigsten eine Treibermutation gefunden wurde. Es handelt sich dabei sowohl um Einzelbasenaustausche (SNVs, *missense*, *splice site*, *nonsense*) als auch kleine Insertionen und Deletionen (INDELs, *frameshift ins.* / *del.*, *inframe del.*). (c) Der Oncoplot listet die 15 Gene auf, in denen am häufigsten eine Treibermutation gefunden wurde. Es handelt sich dabei sowohl um Amplifikationen (≥ 4 Kopien des Gens) als auch Deletionen (< 1 Kopie des Gens). Die Abbildung ist Teil des Manuskripts „*Next-generation sequencing in a real world cohort of 82 advanced melanoma patients identifies distinct mutation pattern in different melanoma subtypes*".

3.2.1.3 Subtyp-spezifische Mutationen der klinischen Kohorte

Die Analyse identifizierte die genetischen Unterschiede der vier histopathologischen Subtypen, sowie die des okkulten Melanoms. In einem ersten Schritt stellten wir große Ähnlichkeiten zwischen dem kutanen und okkulten Melanom fest. In beiden Subtypen beobachteten wir die höchste Anzahl von Mutationen (Median = 7, Bereich = 0-18), was im Vergleich zu den anderen Subtypen in einer signifikant höheren Mutationslast (Median = 9,4, Bereich = 0 - 36,4; $p < 0,003$) resultierte (Abbildung 19). Die Mehrzahl der Patienten mit einem okkulten oder kutanen Melanom können in die drei genomischen Subtypen *BRAF*-, *RAS*- oder *NF1*- mutiert eingeteilt werden. Dagegen weisen die Patienten mit einem akrolentiginösen oder Schleimhautmelanom zu zwei Drittel den dreifach Wildtyp (akrolentiginös = 72%, mukosal = 78%) auf und sind überwiegend von CNVs als Treibermutationen geprägt. Patienten mit einem Schleimhautmelanom haben signifikant mehr somatische CNVs (Median = 177, Bereich 144 - 186; $p < 0,03$) als Patienten mit einem kutanen Melanom (Abbildung 20).

Um die genetischen Unterschiede zwischen den histopathologischen Melanom-Subtypen zu identifizieren, führten wir eine *enrichment* Analyse durch. Sie basiert auf den vorher definierten fünf Subtypen (kutanes, akrolentiginöses, mukosales, uveales und okkultes Melanom) und führt verschiedene Gruppen- und paarweise Vergleiche durch, um angereicherte Mutationen für die jeweiligen Subtypen zu identifizieren. Dabei kategorisiert die Methode in zwei Gruppen, den zu untersuchenden Subtypen und die übrigen Subtypen, bezeichnet als Rest (Abbildung 20).

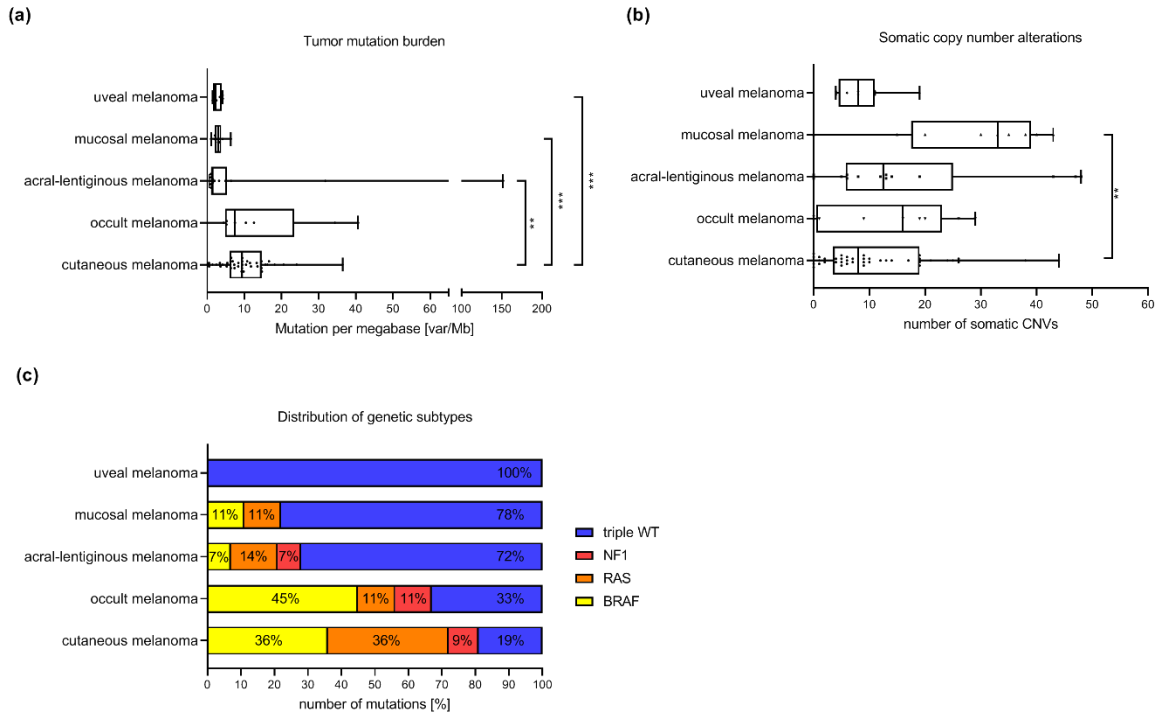

Abbildung 19: Genetische Unterschiede zwischen den histopathologischen Subtypen

Gezeigt werden die Unterschiede der histopathologischen Subtypen in Bezug auf die Tumormutationslast (a), die Anzahl der somatischen Kopienzahlveränderungen (CNVs) und (c) der prozentuale Anteil der genomischen Subtypen (*BRAF*-, *RAS*-, *NF1*-mutiert und *triple wildtype*). Die Abbildung ist Teil des Manuskripts „*Next-generation sequencing in a real world cohort of 82 advanced melanoma patients identifies distinct mutation pattern in different melanoma subtypes*".

Das uveale Melanom zeigte die deutlichsten Unterschiede gegenüber den übrigen Subtypen. Die Analyse identifizierte für die Patienten mit einem uvealen Melanom fünf gehäuft mutierte Gene. Es sind die beiden G-Rezeptor gekoppelten Signalmoleküle *GNA11* und *GNAQ* in Kombination mit dem Spleißfaktor *SF3B1* oder dem deubiquitinierenden Enzym *BAP1*. Zusätzlich konnte bei allen Aderhautmelanompatienten eine *MYC* Amplifikationen festgestellt werden. Im Gegensatz dazu finden sich bei den übrigen Subtypen gehäuft Treibermutationen in den Genen des RTK/RAS-Signalweges und der Zellzykluskontrolle (Abbildung 20). Beim kutanen Melanom sind Hotspot-Mutationen in den Genen *BRAF* und *NRAS* in Kombination mit homozygoten Deletionen des Gens *CDKN2A* angereichert, während beim akrolentiginösen und mokusalen Melanom CNVs dominierten. Die Koamplifikation der Rezeptor-Tyrosinkinasen *KIT* und *PDGFRA* auf Chromosom 4 sowie *CDK4* sind beim akrolentiginösen Melanom angereichert, während das mukosale Melanom eine signifikante Anreicherung von Amplifikation des Gens *CCND2* aufweist. Beim mukosalen Melanom sind Deletionen des Gens *CHEK2* angereichert, einem Mitglied des Fanconi-Anämie-Signalwegs.

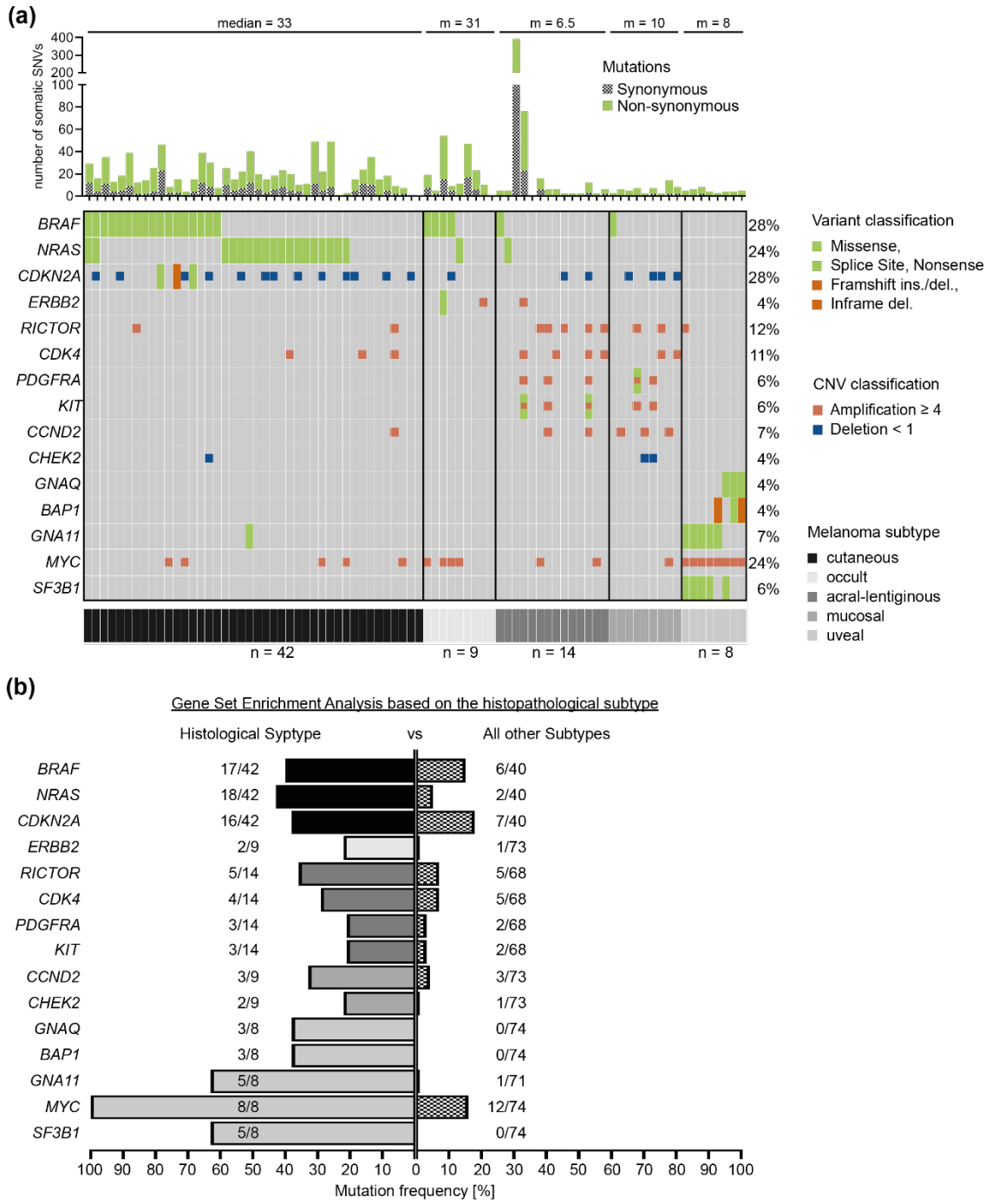

Abbildung 20: Spezifisch mutierte Gene der einzelnen histopathologischen Subtypen

Gezeigt werden die Subtyp-spezifisch mutierten Gene in Form eines *Oncoplots* (a). Es handelt sich ausschließlich um Treibermutationen. Der Oncoplot ist nach den histopathologischen Subtypen sortiert. Jede Spalte repräsentiert einen Patienten. Jede Zeile zeigt die Häufigkeit und Art der Treibermutationen für das jeweilige Gen an. Zusätzlich ist im oberen Bereich ein Histogramm mit der Anzahl der somatischen Mutationen (synonyme und nicht-synonyme) im kodierenden Bereich für jeden einzelnen Patienten zu sehen, sowie die mediane Anzahl der somatischen Mutationen für jeden histopathologischen Subtypen. (b) Gezeigt ist das Ergebnis der Genanreicherung auf der Basis des histopathologischen Subtypen in Form eines Histogramms. Auf der linken Seite ist die Mutationshäufigkeit des Gens pro Subtypen in Prozent angeben, sowie die absolute Anzahl an mutierten und nicht mutierten Patienten. Im Vergleich dazu zeigt die rechte Seite die Mutationsfrequenz und Anzahl für den Rest der Kohorte. Die Abbildung ist Teil des Mansukripts „Next-generation sequencing in a real world cohort of 82 advanced melanoma patients identifies distinct mutation pattern in different melanoma subtypes".

3.2.1.4 Gehäuft mutiert gefundene Gene in der Gruppe der ICB behandelten Patienten

Die Mehrheit der Patientenkohorte (75 von 82), unabhängig vom Subtyp, wurde mit einer Immuncheckpoint-Therapie entweder als kombinierte Immuntherapie mit Ipilimumab und Nivolumab (N = 60) oder mit einem PD-1-Antikörpern alleine (N = 15) behandelt (Abbildung 18). Daher sollte im letzten Schritt untersucht werden, welche Unterschiede sich bei den Patienten in Bezug auf das Therapieansprechen beobachten lassen. Zu diesem Zweck wurden sowohl klinische als auch genetische Parameter untersucht und eine *enrichment* Analyse durchgeführt. Die Patienten wurden gemäß den *Response Evaluation Criteria In Solid Tumors* (RECIST Kriterien) für das Therapieansprechen in drei Gruppen eingeteilt: progressive Erkrankung (*progressive disease*, PD, N = 45), stabile Erkrankung (*stable disease*, SD, N = 12) und partielles Ansprechen (*partial response*, PR, N = 18) (Abbildung 21).

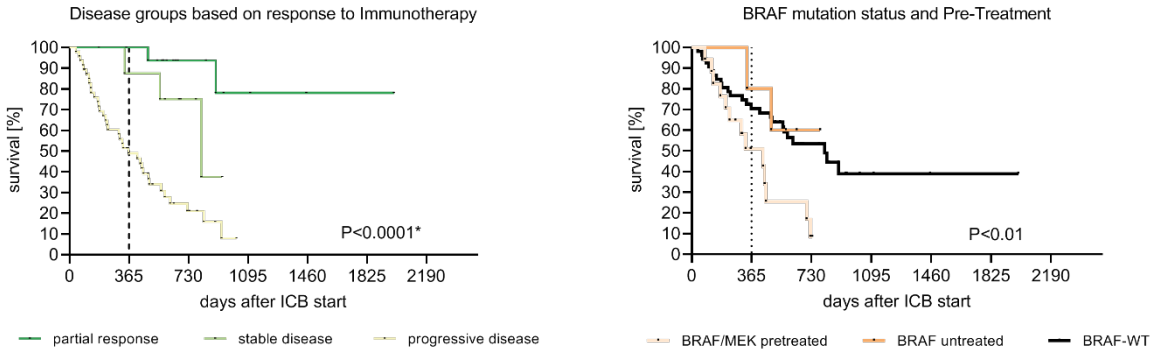

Abbildung 21: Überlebenskurven Immuncheckpoint-Therapie und *BRAF*-Status mit Vortherapie

Gezeigt wird das Überleben in Bezug auf das Therapieansprechen im Rahmen der Immuntherapie und der Einfluss des *BRAF*-Status und die Vortherapie. (links), das Ansprechen auf die Immuncheckpoint-Therapie. (rechts) *BRAF*-Mutationsstatus inklusives der Vortherapie der 75 Patienten die eine Immuncheckpoint-Therapie erhalten haben. Die Daten sind Teil der Arbeit „*Next-generation sequencing in a real world cohort of 82 advanced melanoma patients identifies distinct mutation pattern in different melanoma subtypes*".

Erwartungsgemäß beobachteten wir bei den Patienten mit einem progressiven Krankheitsverlauf die schlechteste einjährige Überlebensrate mit 51% im Vergleich zu 83% bei einem stabilen Verlauf und 100% bei einer partiellen Remission des Tumors. Die *enrichment* Analyse der drei Gruppen in Bezug auf das Therapieansprechen ergab, dass *BRAF* V600-Hotspot-Mutationen und Amplifikationen des endothelialen Wachstumsfaktor-Rezeptors *EGFR* bei den Patienten mit einem progressiven Krankheitsverlauf signifikant angereichert sind (18 von 45, p = 0,01 und 6 von 45, p = 0,04). Interessanterweise hatten die meisten dieser Patienten (16 von 18) vor der

Immuncheckpoint-Therapie eine Behandlung mit einem *BRAF*- und *MEK*-Inhibitor (BRAF/MEKi) erhalten (Abbildung 22). Ein Vergleich der *BRAF*/*MEKi* vorbehandelten und unbehandelten Patienten mit einer *BRAF* Mutation, sowie der *BRAF* Wildtyp Patienten ergab ein signifikant besseres Gesamtüberleben der letzten beiden Gruppen (p = 0,01). Die einjährige Überlebensrate der *BRAF* mutierten aber unbehandelten Patienten betrug 72% im Vergleich zu den behandelten Patienten mit 63%. Für die *BRAF*-WT Patienten lag die Einjahres-Überlebensrate bei 80%. Um den Effekt der *BRAF/MEKi*-Vortherapie auszuschließen, wiederholten wir die *enrichment* Analyse ohne diese Patienten. Dadurch reduzierte sich die Kohorte auf 57 Patienten von denen fünf eine *BRAF* V600-Mutation haben. Bei der erneuten Analyse konnten wir keine Anreicherung eines Genes mit Treibermutation identifizieren.

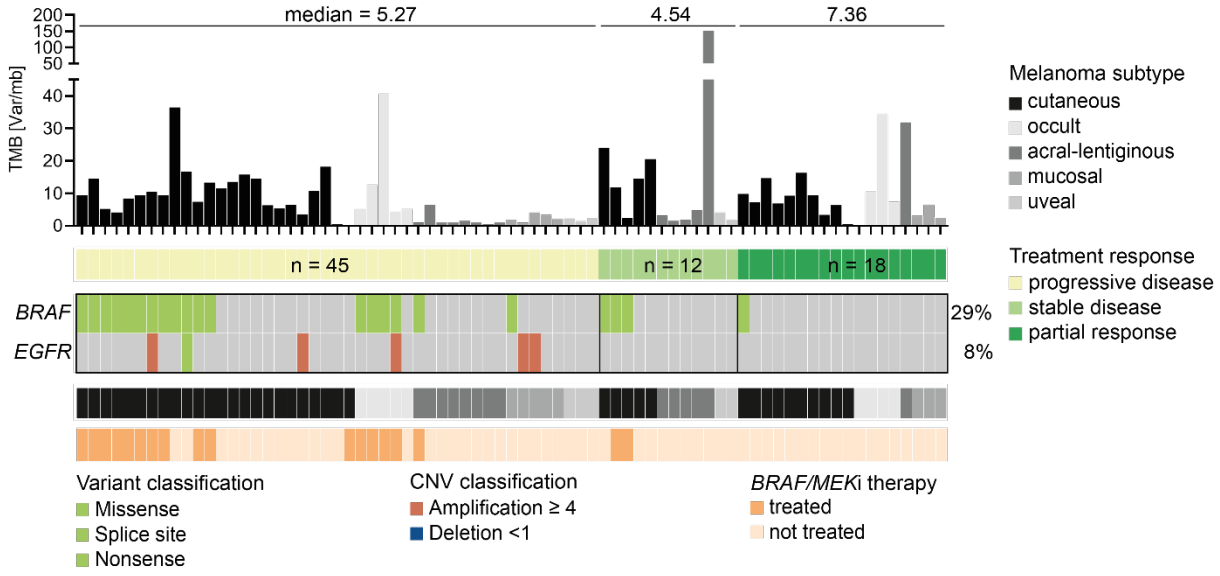

Abbildung 22: Spezifisch mutierte Gene der Therapieversager auf die Immuncheckpoint-Therapie

Der Oncoplot illustriert die Häufigkeit der beiden Gene *BRAF* und *EGFR* in der Gruppe der 75 Patienten die eine Immuncheckpoint-Therapie erhalten haben. Der obere Teil der Abbildung zeigt die Anzahl Tumormutationslast pro Patient und den Median für die drei Gruppen des Therapieansprechens. Der *Oncoplot* ist nach dem Therapieansprechen sortiert. Jede Spalte repräsentiert einen Patienten. Jede Zeile zeigt die Häufigkeit und Art der Treibermutationen für das jeweilige Gen an. Zusätzlich ist der histopathologische Subtyp im *Oncoplot* und dem TMB-Histogramm farblich kodiert. Ob ein Patient vor der Immuncheckpoint-Therapie eine Behandlung mit einem *BRAF/MEK*-Inhibitor erhalten hat ist ebenfalls farblich hinterlegt.

3.2.1.5 Diskussion der klinischen Kohorte

In der Studie „*Next-generation sequencing in a real world cohort of 82 advanced melanoma patients identifies distinct mutation pattern in different melanoma subtypes*“ konnte gezeigt werden, dass sich die histopathologischen Subtypen, sowie das okkulte Melanom genetisch unterscheiden. Darüber hinaus konnten wir potentielle genetische Marker der Resistenz auf die Immuncheckpoint-Blockade identifizieren.

Mit Ausnahme der Patienten mit einem uvealen Melanom waren die übrigen Subtypen durch Treibermutationen in den Genen des (RTK)/RAS/MAPKinase-Signalwegs sowie der Zellzykluskontrolle und dem PI3K-Signalweg geprägt. Wohingegen das Aderhautmelanom dominiert war von *MYC* Amplifikationen, sowie *GNA11* oder *GNAQ* Mutation in Kombination mit den Genen *BAP1* oder *SF3B1*. Die hohe Frequenz von *MYC* Amplifikation ist bereits in vorangegangen Arbeiten beschrieben worden und es ist bekannt, dass eine hohe Expression von *MYC* in Tumoren mit einem erhöhten Risiko für die Entwicklung von Metastasen und einer schlechteren Prognose verbunden ist (115-118). Darüber hinaus fanden wir bei allen Patienten mit einem Aderhautmelanom entweder eine Mutation des Gens *SF3B1* oder *BAP1*. Der Spleißfaktor *SF3B1* ist mit einem erhöhten Risiko für die Metastasierung und die Deubiquitinase *BAP1* mit einer schlechteren Prognose assoziiert (80-82). Diese Beobachtungen erklären vermutlich die Tatsache, dass es sich bei der untersuchten Patientengruppe um metastasierte und weit fortgeschrittene Aderhautmelanome handelt.

Die übrigen drei Subtypen sowie das okkulte Melanom waren, wie bereits erwähnt, durch Treibermutationen in den Genen der Zellzykluskontrolle (*CDKN2A*) und des RTK/RAS/MAPKinase-Signalweges (*BRAF, NRAS, ERRB2*) geprägt. Zusätzlich haben das kutane und okkulte Melanom die höchste Tumormutationslast im Vergleich zu den übrigen Subtypen. Interessanterweise ähneln sie sich auch in Bezug auf die Anzahl der CNVs und bei der Häufigkeit der genomischen Subgruppen *BRAF*-, *RAS*-, *NF1*-mutiert oder dreifach Wildtyp. Zusammengenommen unterstreichen diese Ergebnisse die bereits existierende Vermutung, dass der kutane und okkulte Subtyp ähnlich zu betrachten sind und das okkulte Melanom vermutlich seinen Ursprung in regredierten oder nicht erkannten primären kutanen Melanomen hat (119, 120).

Im Vergleich dazu war die Zahl der somatischen CNVs beim akrolentiginösen und Schleimhautmelanom höher als beim kutanen Melanom. Dieses Ergebnis entspricht dem aktuellen Kenntnisstand (79, 121), wobei eine signifikant höhere Zahl an CNVs nur beim Schleimhautmelanom nachgewiesen werden konnte. Die Treibermutationen in den Genen *RICTOR, CDK4, PDGFRA, KIT* sind spezifisch für das akrolentiginöse Melanom. Das Schleimhautmelanom zeigt die Amplifikation oder Deletion der Gene *CCND2* und *CHEK2*. Damit bestätigt diese Studie die Beobachtung größeren und umfassenderen Studien aus der nahen Vergangenheit (76-78).

Neben der Bestimmung der Subtyp-spezifischen Unterschiede, bildete die Identifikation häufiger Mutation und potentieller genetischer Resistenzen gegenüber der Immuncheckpoint-Therapie einen weiteren Schwerpunkt. So fanden sich gehäuft Treibermutation in den Genen *BRAF* und *EGFR* in der Gruppe der Therapieversager im Rahmen der Immuncheckpoint-Blockade. Mehrere Studien beim nichtkleinzelligen Lungenkarzinom zeigten bereits den Zusammenhang zwischen der Unwirksamkeit der Immuncheckpoint-Therapie und *EGFR* Mutationen in Kombination mit einem niedrigen TMB (122-124). Darüber hinaus konnten mehrere retrospektive Studien zeigen, dass das Ergebnis der Immuncheckpoint-Therapie besser ist, wenn diese Patienten keine vorherige Therapie mit *BRAF*- und *MEK*-Inhibitoren erhalten (125-127).

Die Häufung von Treibermutationen in den Cyclin-abhängigen Kinasen *CDKN2A*, *CDK4*, *CCND1/2/3* und den Genen *MDM2/4* und *TP53* trägt vermutlich zu einer erheblichen Deregulation der Zellzykluskontrolle bei. Deletionen in dem Gen *CDKN2A* scheinen zu einer Resistenz gegenüber der Immuncheckpoint-Therapie zu führen und verschlechtern in Kombination mit der Deregulation von *CDK4* die Prognose beim akrolentiginösen Melanom (128, 129). Daher könnte die Einführung von *CDK4/6*-Hemmern die Behandlungsoptionen erweitern (129-131). Und auch die kombinierte Behandlung mit *MEK*- und *CDK4/6*-Hemmern wäre denkbar (132). Ein weiteres Ziel für eine alternative Behandlung stellen die Treibermutationen in den Genen *ATM*, *CHEK2*, *FANCA*, *FANCC* und *BRCA2* dar, die dem DNA-Reparatursignalweg angehören. Eine Behandlungsmöglichkeit ist die Therapie mit *PARP*-Inhibitoren oder alternativ eine platinbasierte Chemotherapie (133).

Zu den Limitationen der Studie gehört die Tatsache, dass es sich um eine Patientenkohorte handelt, die im klinischen Alltag ohne spezifische Einschlusskriterien gesammelt wurde. Das bedeutet, dass sich alle Patienten in einem fortgeschrittenen Stadium der Erkrankung befanden inklusive Fernmetastasen und bereits mehrere (mindestens zwei) systemische Therapien erhalten hatten. Allerdings wurde dieser Ansatz auch in anderen Studien gewählt und die Identifikation der signifikanten genetischen Unterschiede zwischen den Subtypen zeigt, dass die Studie bereits bekannte Ergebnisse reproduziert (76-78). Darüber hinaus wurde in den meisten Fällen nicht die DNA des Primärtumors, sondern die der Metastasen sequenziert. Die gefundenen genetischen Veränderungen sind daher vermutlich eher ein Abbild der Prozesse, die zur Metastasierung beigetragen haben. Trotz der Unterschiede

zwischen dem Primarius und den Metastasen [82] könnte ihre genetische Analyse einen aktuellen Einblick in die Tumorprogression und Evolution geben. Eine weitere Einschränkung der Studie ist die mehrmalige Änderung des Tumorpanels im Laufe der Studie. Aus diesem Grund konnten nur die Gene berücksichtigt werden, die in allen drei Versionen vorhanden sind.

In der Zukunft sind dringend prospektive Studien erforderlich, um mehr über potenzielle Resistenzmechanismen der Immuncheckpoint-Blockade zu erfahren und es sollten weitere Anstrengungen unternommen werden, um gezielte Therapien jenseits von *BRAF*-, *MEK*- oder *KIT*-Inhibitoren beim fortgeschrittenen Malignen Melanom einzuführen.

3.2.2 Akrolentiginöses und mukosales Melanom

Bei dem akrolentiginösen und mukosalen Melanom handelt es sich um seltene Subtypen des Melanoms. Im Gegensatz zum kutanen Melanom findet man bei diesen beiden Subtypen deutlich weniger somatische Einzelnukleotidmutationen (SNVs), dafür aber mehr somatische Kopienzahlveränderungen (76). Da diese Tumoren vorwiegend zum dreifach Wildtyp gehören, lassen sie sich nicht mit einer gezielten *BRAF*- und *MEK*-Inhibition behandeln. Alternativ zeigt die Immuncheckpoint-Inhibitor-Therapie bei diesen beiden Subtypen eine Ansprechrate von circa 20-30% (134, 135). Daher ist es dringend notwendig, Strategien zu entwickeln, die eine bessere Stratifikation der Patienten erlaubt.

Das Ziel dieser Studie war es, mögliche Korrelationen zwischen dem Therapieansprechen und klinischen sowie genetischen Markern beim akrolentiginösen und mukosalen Melanom zu finden. Insbesondere der Zusammenhang zwischen Amplifikationen der Gene *MDM2*, *MDM4* oder *EGFR* und dem Auftreten einer Hyperprogression im Rahmen der Immuncheckpoint-Therapie sollte untersucht werden. Darüber hinaus wurde der Einfluss der PD-L1-Expression und weiteren klinischen Parametern evaluiert.

3.2.2.1 Studiendesign und Patientenkohorte

Die Kohorte wurde unter Zuhilfenahme des Melanomregisters (Zeitraum: 2007-2017) rekrutiert. In die Untersuchung eingeschlossen wurden alle Patienten mit einem fortgeschrittenen akrolentiginösen und mukosalen Melanom Stadium IV, die mindestens zwei Zyklen eines Checkpoint-Inhibitoren für inoperable Metastasen

erhalten hatten und deren Therapieansprechen radiologisch nach RECIST validiert wurde.

Für die Identifikation von potentiellen genetischen und klinischen Tumormarkern im Rahmen einer Immuncheckpoint-Inhibitor-Therapie wurden die Patienten hinsichtlich ihres Therapieansprechens und des histopathologischen Subtypen untersucht. Die Patienten wurden in die Subgruppen akrolentiginöses, anorektal-mukosales oder mukosales Melanom unterteilt. Für die Gruppierung hinsichtlich des Therapieansprechens wurde die prozentuale Änderung der Tumorlast bestimmt, ausgehend vom Therapiebeginn bis zur ersten radiologischen Nachuntersuchung. Dies führte zur Einteilung in drei Gruppen:

1. Patienten mit einer stabilen Erkrankung (SD = Remission oder Zunahme bis 20%)
2. Patienten mit einer progressiven Erkrankung (PD, Zunahme der Tumorlast von 20-50%)
3. Patienten mit einer Hyperprogression (*hyper progressive disease,* HPD, Zunahme der Tumorlast > 50%)

Die Abfrage des Krebsregisters identifizierte 51 Patienten. Davon hatten 34 ein akrolentiginöses und 17 ein mukosales Melanom. Acht Patienten hatten ein anorektales Schleimhautmelanom. Zum Zeitpunkt des Therapiestarts lag das mediane Alter der Kohorte bei 71 Jahren (Spanne: 40-87 Jahre). Etwa die Hälfte der Patienten (n = 27) wurde mit Ipilimumab behandelt und 15 Patienten mit einer Anti-PD-1-Therapie. Insgesamt neun Patienten erhielten eine Kombination aus Ipilimumab und Nivolumab.

Die erste Nachuntersuchung erfolgte im Median nach 11 Wochen (Interquartilsabstand: 8-13) und kategorisierte 12 Patienten als SD, 17 als PD und 22 als HPD. Insgesamt waren 37 der 51 Patienten (73%) zum Zeitpunkt der Auswertung bereits verstorben. Das mediane Gesamtüberleben betrug seit Beginn der Diagnose 40 Monate und 19 Monate seit Beginn der Immuntherapie.

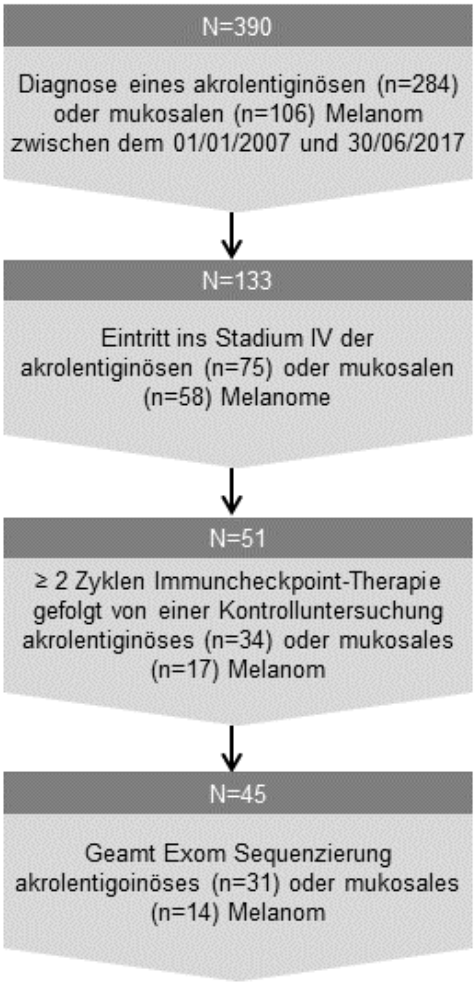

Abbildung 23: Flussdiagramm der Generierung der Kohorte

Die Abbildung zeigt die Auswahl der Patientenkohorte auf der Basis des Melanomregisters. Sie ist angelehnt an die Arbeit von *Forschner et al.* (113).

3.2.2.2 Genetisches Profil der Kohorte

Die Exomsequenzierung von 45 der 51 Patienten resultierte in einer durchschnittlichen Tiefe von 154X (Bereich: 10,36X - 440,1X) für das Tumorgewebe und 170X (Bereich: 15,91X - 467,6X) für das dazugehörige Normalgewebe (Blut). Insgesamt identifizierten wir 8.297 somatische SNVs. Die mediane Tumormutationslast beträgt 2,83 Mutationen/Mb (Bereich: 0,28 - 68,34) und es konnte kein signifikanter Unterschied der medianen TMB zwischen den Patienten mit einem akrolentiginösen oder mukosalen Melanom festgestellt werden. Interessanterweise haben die Schleimhautmelanome ohne den anorektalen Subtyp im Vergleich zu akrolentiginösen Melanomen einen signifikant höheren TMB-Wert.

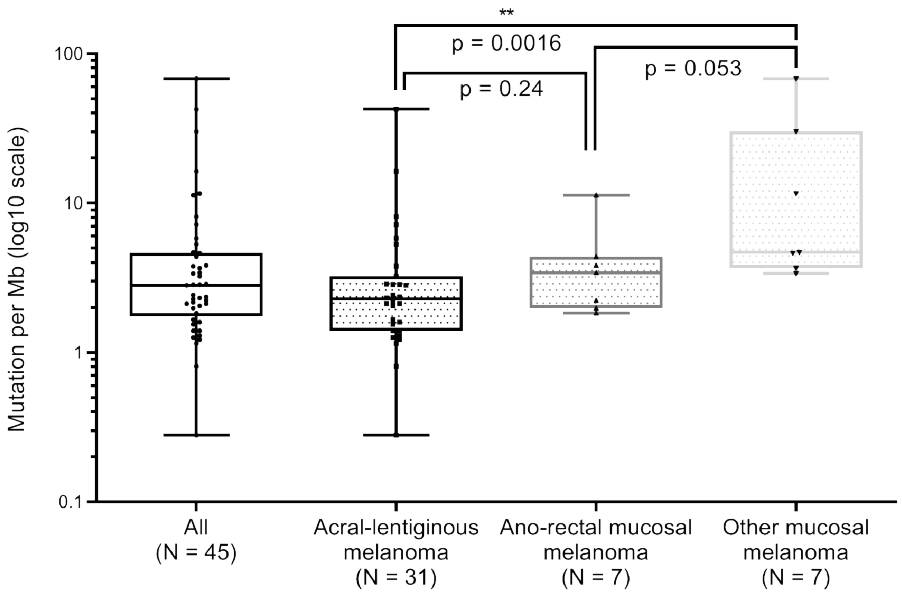

Abbildung 24: Tumormutationslast

Das Diagramm zeigt die Tumormutationslast (TMB) der Gesamtkohorte und den Vergleich der einzelnen Subtypen als Box-Plots. Im Box-Plot werden der Median, das obere und untere Quartil darstellt. Die Box-Whisker markieren die minimal und maximal beobachtete TMB. Verglichen wurden die TMB des akrolentiginösen und mukosalen Melanoms, sowie die des anorektalen Schleimhautmelanoms. Die Daten entstammen der Arbeit von Forschner et al. (113) und die Abbildung ist der Arbeit teilweise entnommen.

Die drei am häufigsten mutierten Gene mit einer Treibermutation sind das Tumorsuppressorgen *NF1*, das Onkogen *NRAS* mit jeweils 18% und das Onkogen *KIT* (11%). Insgesamt drei Patienten mit einem akrolentiginösen Melanom haben eine Treibermutation im Onkogen *BRAF*. Die Auswertung der Kopienzahlveränderungen erfolgte mit Hilfe von GISTIC 2.0 (136) und identifizierte 18 Regionen, die häufig amplifiziert und 16 Regionen, die häufig deletiert waren. Zu den amplifizierten Regionen gehören die Bereiche auf den Chromosomen 5p33.1, 12q14.1/15, 4q12 und 1p12, in denen die Gene *TERT*, *CDK4*, *MDM2*, *KIT* und *NRAS* liegen. Deletiert waren die Regionen 15q15, 22q12/13, 1p36, 16q12/22, 5p15 und 2q37 mit den Tumorsuppressorgenen *SPRED1*, *CHEK2* und *NF2*.

Darüber hinaus wurde die Häufigkeit bekannter Onko- und Tumorsuppressorgene für das akrolentiginöse und mukosale Melanom evaluiert und eine Annotation mit dem *CancerGenomeInterpreter.org* durchgeführt (77, 78, 89). Die fünf am häufigsten mutierten Onkogene unserer Kohorte sind *MYC*, *TERT*, *CCND3*, *RICTOR* und *CDK4* und die am häufigsten mutierten Tumorsuppressorgene sind *CDKN2A/B*.

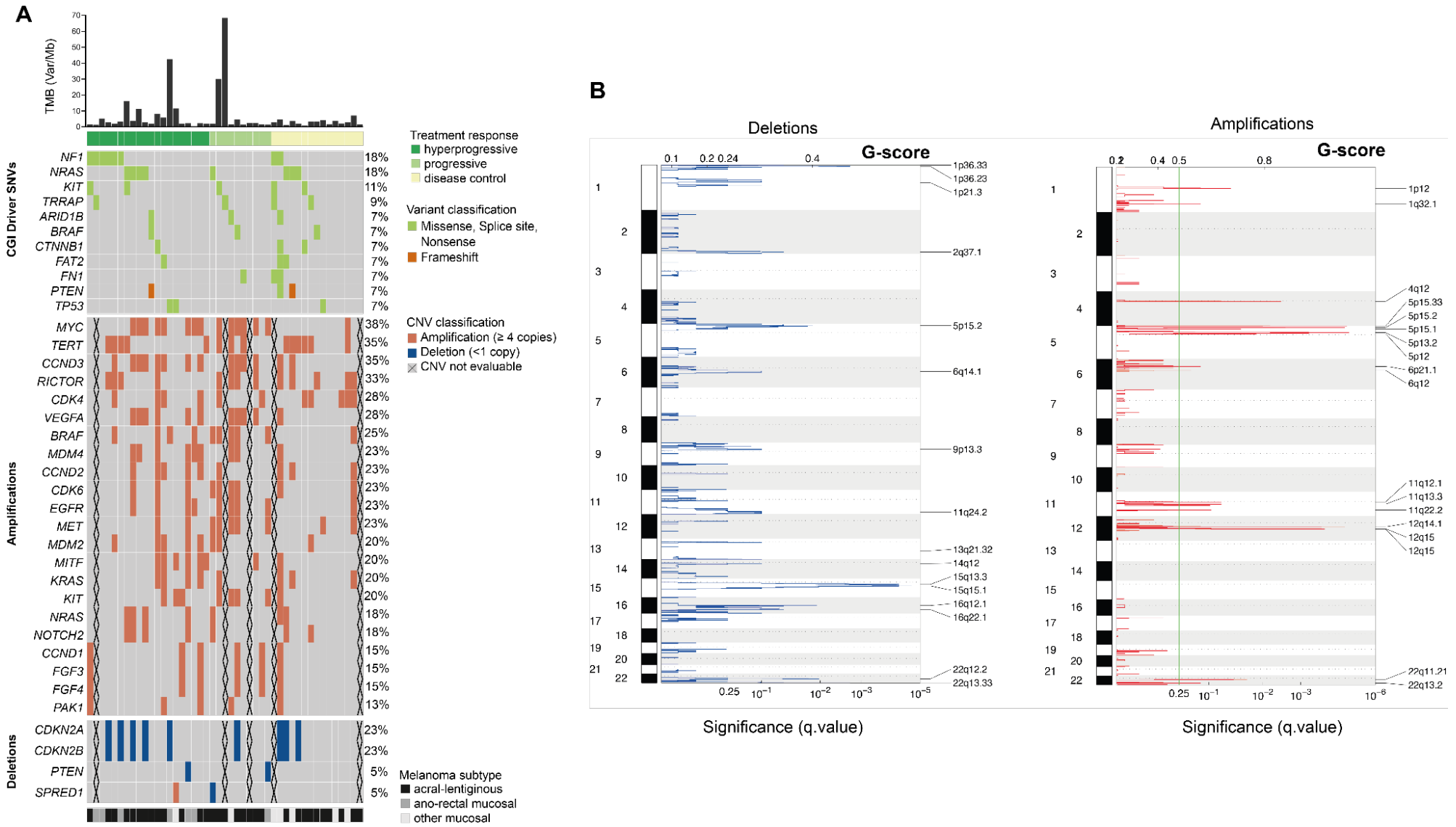
A
TMB (Var/Mb)
CGI Driver SNVs
NF1 18%
NRAS 18%
KIT 11%
TRRAP 9%
ARID1B 7%
BRAF 7%
CTNNB1 7%
FAT2 7%
FN1 7%
PTEN 7%
TP53 7%
Amplifications
MYC 38%
TERT 35%
CCND3 35%
RICTOR 33%
CDK4 28%
VEGFA 28%
BRAF 25%
MDM4 23%
CCND2 23%
CDK6 23%
EGFR 23%
MET 23%
MDM2 20%
MITF 20%
KRAS 20%
KIT 20%
NRAS 18%
NOTCH2 18%
CCND1 15%
FGF3 15%
FGF4 15%
PAK1 13%
Deletions
CDKN2A 23%
CDKN2B 23%
PTEN 5%
SPRED1 5%
Treatment response
hyperprogressive
progressive
disease control
Variant classification
Missense, Splice site, Nonsense
Frameshift
CNV classification
Amplification (≥ 4 copies)
Deletion (<1 copy)
CNV not evaluable
Melanoma subtype
acral-lentiginous
ano-rectal mucosal
other mucosal
B
Deletions
G-score
1p36.33
1p36.23
1p21.3
2q37.1
5p15.2
6q14.1
9p13.3
11q24.2
13q21.32
14q12
15q13.3
15q15.1
16q12.1
16q22.1
22q12.2
22q13.33
Significance (q.value)
Amplifications
G-score
1p12
1q32.1
4q12
5p15.33
5p15.2
5p15.1
5p13.2
5p12
6p21.1
6q12
11q12.1
11q13.3
11q22.2
12q14.1
12q15
12q15
22q11.21
22q13.2
Significance (q.value)

Abbildung 25: Genetisches Profil der Kohorte

Der *Oncoplot* fasst die Gene zusammen, die am häufigsten von einer Treibermutation betroffen sind. Die Identifikation der Treibermutationen wurde mit dem *Cancer Genome Interpreter* durchgeführt (89). Der *Oncoplot* ist nach dem Ansprechen auf die Immuncheckpoint-Inhibitor-Therapie sortiert. Jede Spalte repräsentiert im Abschnitt A den gleichen Patienten. Jede Zeile zeigt die Häufigkeit und Art der Treibermutationen für das jeweilige Gen an. Zusätzlich ist der Subtyp unterhalb des *Oncoplots* farblich markiert. (A) Das Histogramm illustriert die Tumormutationslast (Mutationen pro Megabase) des einzelnen Patienten. Der *Oncoplot* ist zweigeteilt. Im oberen Teil sind die am häufigsten mutierten Gene mit Einzelbasenaustausche und kleineren Insertionen oder Deletionen visualisiert (SNVs, *missense*, *splice site*, *nonsense*; INDELs, *frameshift*). Im unteren Teil finden sich die Gene, die häufig von Amplifikationen (≥ 4 Kopien des Gens) und Deletionen (< 1 Kopie des Gens) betroffen sind. Wenn für den Patienten keine Kopienzahlanalyse durchgeführt werden konnte, ist das durch ein X vermerkt. (B) Es werden die chromosomalen Regionen gezeigt, die mit Hilfe der Software GISTIC 2.0 als signifikant amplifiziert oder deletiert, identifiziert wurden. Die Daten entstammen der Arbeit von *Forschner et al*. (113) und die Abbildung ist der Arbeit teilweise entnommen

3.2.2.3 Klinisches Ansprechen in Korrelation zu den genetischen Markern MDM2, MDM4, EGFR Amp

Patienten mit einem anorektalen Melanom zeigen im Vergleich zu den anderen beiden Subtypen signifikant häufiger einen hyperprogressiven Krankheitsverlauf. In 75% aller anorektalen Melanom-Patienten beobachteten wir eine Hyperprogression, aber nur bei 41% der akrolentiginösen und bei 22% der übrigen Schleimhautmelanome (p=0,012). Darüber hinaus hatten circa 90% der Patienten mit einem progressiven Krankheitsverlauf eine Amplifikation in den Genen *MDM2* (7 von 8), *MDM4* (8 von 9) oder *EGFR* (8 von 9). Eine Hyperprogression beobachteten wir in neun Patienten von denen 66% (6 von 9) eine Amplifikation des Gens *MDM4* haben. Obwohl wir keinen statistisch signifikanten Unterschied zwischen den drei Ansprechgruppen DC, PD und HPD feststellen konnten, gab es einen Trend hin zu einem schlechteren Therapieansprechen bei dem Vorhandensein von Amplifikationen in den Genen *MDM2*, *MDM4* oder *EGFR*. Diese Beobachtung änderte sich auch nicht, wenn die beiden Gruppen, HPD und PD zusammengefasst wurden (Tabelle 4).

Auch die Auswertung der Tumormutationslast (TMB) in Bezug auf das Therapieansprechen zeigte keinen signifikanten Unterschied. Die Patienten mit einem stabilen Krankheitsverlauf im Vergleich zu denen, mit einem progressiven Krankheitsverlauf (PD und HPD zusammen) haben eine mediane Tumormutationslast von 2,4 oder 2,8 Mut/Mb.

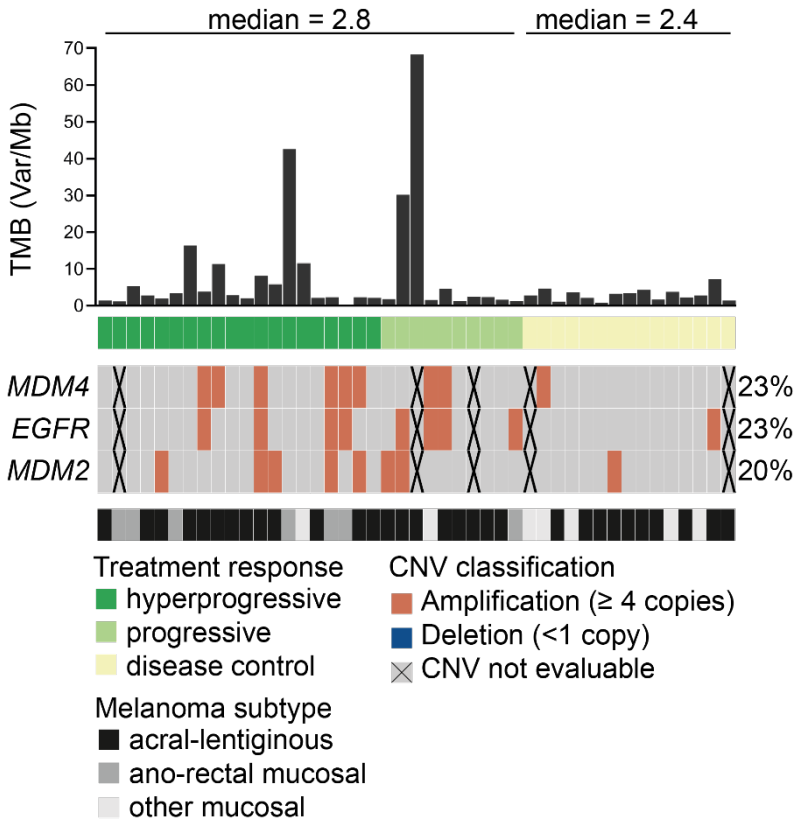

Abbildung 26: Häufigkeit von Amplifikationen in den Genen *MDM2*, *MDM4*, *EGFR*

Der *Oncoplot* zeigt die Häufigkeit von Amplifikationen in den Genen *MDM2*, *MDM4* oder *EGFR*. Der *Oncoplot* ist nach dem Ansprechen auf die Immuncheckpoint-Inhibitor-Therapie sortiert. Jede Spalte repräsentiert den gleichen Patienten. Jede Zeile zeigt die Häufigkeit und Art der Treibermutationen für das jeweilige Gen an. Zusätzlich ist der Subtyp unterhalb des *Oncoplots* angegeben. Das Histogramm oberhalb vom *Oncoplot* zeigt die TMB jedes einzelnen Patienten und den Median für die Patienten mit einem stabilen Krankheitsverlauf im Vergleich zu den Patienten mit einem progressiven Krankheitsverlauf (Hyperprogression und Progression zusammen). Die Daten entstammen der Arbeit von *Forschner et al*. (113) und die Abbildung ist der Arbeit teilweise entnommen.

3.2.2.4 Anorektales Schleimhautmelanom und Lebermetastasen als unabhängige Risikofaktoren

Die Ergebnisse der ersten Nachuntersuchung zeigten, dass die Mehrheit der Patienten einen progressiven Verlauf der Erkrankung hatten (Tabelle 4). Insbesondere die Patienten mit einem anorektalen Melanom sprachen schlecht auf die Immuncheckpoint-Inhibitor-Therapie an. Sieben der acht Patienten (88%) hatten einen progressiven Krankheitsverlauf, wobei sechs eine Hyperprogression entwickelten. Im Vergleich dazu waren es in der Gruppe der akrolentiginösen und den anderen mukosalen Melanomen zusammen nur 16 von 43 Patienten (37%), die eine Hyperprogression entwickelten. Ferner betrug die mediane Überlebenszeit der Patienten mit einem anorektalen Melanom 16 Monate seit der Diagnose bzw. 9,5 Monate seit Beginn der Therapie.

Tabelle 4: Klinische Parameter und Amplifikationen der Gene *MDM2*, *MDM4* oder *EGFR* in Relation zum Therepieansprechen

	Total N=51	**Hyperprogressive Disease N=22**	**Progressive Disease N=12**	**Disease Control N=17**	**p-value**[1]
MDM2 Amplification ≥ 4[2]					
Present	8	5	2	1	0.273
Absent	32	14	6	12	
MDM4 Amplification ≥ 4[2]					
Present	9	6	2	1	0.142
Absent	31	13	6	12	
EGFR Amplification ≥ 4[2]					
Present	9	4	4	1	0.534
Absent	31	15	4	12	
PD-L1 Score[3]					
< 1%	11	7	2	2	0.190
≥ 1%	35	15	6	14	
Melanoma Type					
Other mucosal	9	2	1	6	**0.012***
Acral	34	14	10	10	
Anorectal	8	6	1	1	
Liver metastases					
Present	18	10	3	5	0.319
Absent	33	12	9	12	
	Total N=51	**Hyperprogressive Disease N=22**	**Progressive Disease N=12**	**Disease Control N=17**	**p-value**[1]
MDM2 Amplification ≥ 4[2]					
Present	8	1	7	0	0.721
Absent	32	5	21	6	
MDM4 Amplification ≥ 4[2]					
Present	9	2	5	2	1.0
Absent	31	4	23	4	
EGFR Amplification ≥ 4[2]					
Present	9	3	5	1	0.303
Absent	31	3	23	5	
PD-L1 Score[3]					
< 1%	11	5	6	0	**0.004***
≥ 1%	35	3	23	9	
Liver metastases					
Present	18	4	12	2	0.316
Absent	33	4	22	7	

* significant, [1] Exact Chi-Square Test for Trend (Monte Carlo Simulation), [2] only cases where tissue was available and CNV were evaluable could be considered, therefore 11 cases are missing, [3] only cases where tissue was available could be considered, therefore 6 cases are missing

Die univariate Überlebensanalyse identifizierte den Subtyp des anorektalen Melanoms und das Vorhandensein von Lebermetastasen, sowie das Auftreten einer Hyperprogression als signifikant negative Einflussfaktoren für das Überleben. Die Analyse der Cox-Regressionen-Analyse ergab, dass sowohl Lebermetastasen zu Beginn der Therapie ((HR) 2,073; 95 % Konfidenzintervall (CI) 1,05-4,08)) als auch der Subytp des anorektalen Melanoms ((HR 7,923; 95 % Konfidenzintervall 2,22-28,38)) unabhängige negative Einflussfaktoren auf das Überleben sind (Abbildung 27).

Patienten mit Amplifikation der Gene *MDM2*, *MDM4* oder *EGFR* hatten keine schlechtere Überlebensrate als Patienten ohne diese Amplifikation (Abbildung 27).

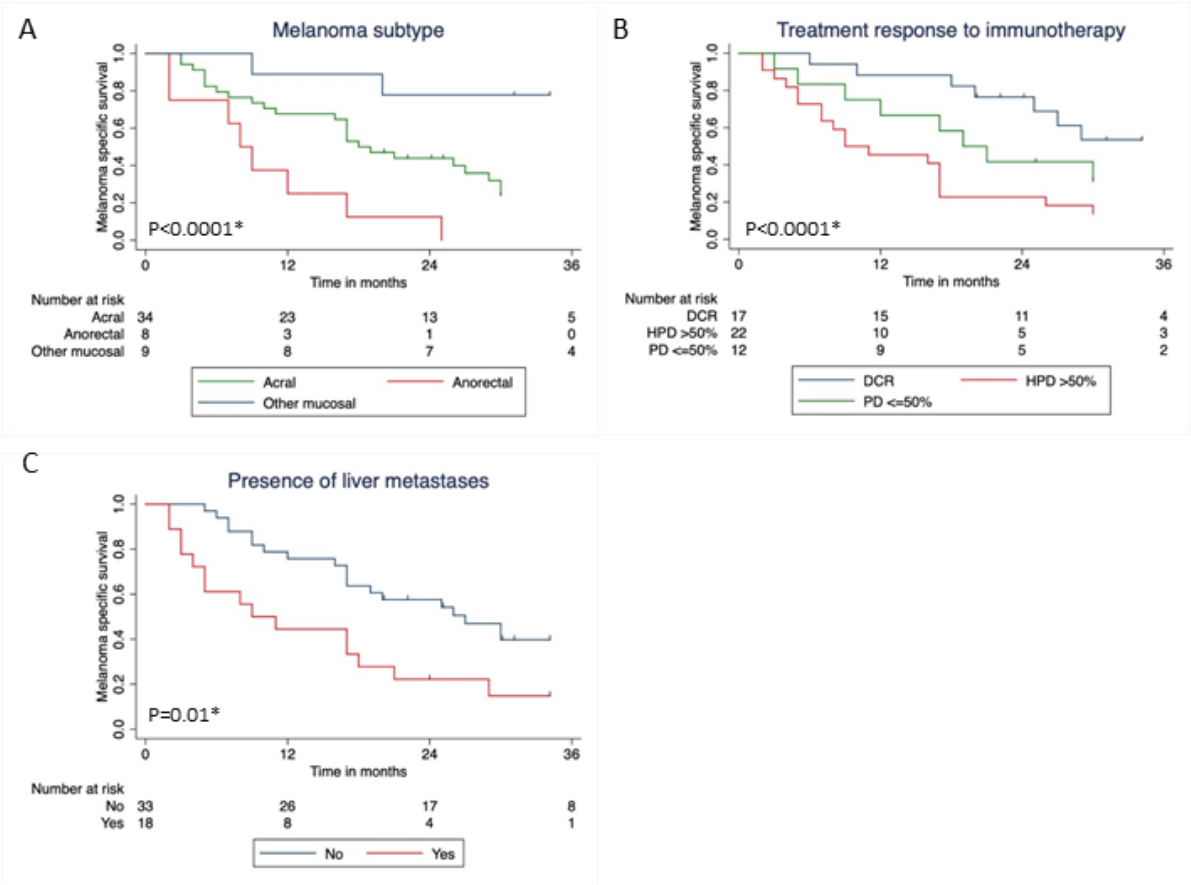

Abbildung 27: Kaplan-Meier-Kurven Diagramm

Gezeigt wird das Überleben in Bezug auf den Melanomsubtypen (A), das Ansprechen auf die Immuncheckpoint-Therapie (B) und das Vorhandensein von Lebermetastasen zum Therapiebeginn der Immuncheckpoint-Inhibitor-Therapie (C). Die Daten entstammen der Arbeit von *Forschner et al.* (113) und die Abbildung ist der Arbeit teilweise entnommen.

3.2.2.5 Diskussion

Die Analyse verschiedener Tumorentitäten hat die Vermutung nahegelegt, dass Amplifikationen in den Genen *MDM2/4* und *EGFR* in Verbindung mit der Hyperprogression im Rahmen einer Immuncheckpoint-Inhibitor-Therapie stehen (137). Die Studie *„MDM2, MDM4 and EGFR Amplifications and Hyperprogression in Metastatic Acral and Mucosal Melanoma“* untersuchte daher das Auftreten einer Hyperprogression von metastasiertem akrolentiginösen- und Schleimhautmelanom in Bezug auf Amplifikationen der Gene *MDM2/4*- oder *EGFR*. Weitere klinische Parameter, wie die PD-L1-Expression, das Vorhandensein von Lebermetastasen zum Therapiestart oder die anorektale Lokalisation des Schleimhautmelanoms und ihr Einfluss auf den Therapieverlauf wurden auch analysiert.

Zusammengefasst, stellte sich in der Studie heraus das der anorektale Subtyp und das Vorhandensein von Lebermetasen zu Therapiebeginn als individuelle Risikofaktoren angesehen werden können, die einen negativen Einfluss auf die Gesamtüberlebenszeit der Patienten haben. Und Amplifikationen in den Genen *MDM2/4* oder *EGFR* sind häufiger in den Tumoren der Patienten mit einer Hyperprogression zu finden als den Patienten mit einem stabilen Krankheitsverlauf.

Der genaue Mechanismus, wie die Gene *MDM2/4* und *EGFR* Einfluss von auf die Immuncheckpoint-Blockade nehmen, ist nicht bekannt. Die Aktivierung von *EGFR* scheint mit einer Hochregulierung von CTLA-1, PD-1 und PD-L1 verbunden sein und die Gene *MDM2* und *MDM4* hemmen den Tumorsuppressor p53 (138, 139). Beide Mechanismen könnten zu einer Resistenz gegenüber der Immuncheck-Blockade beitragen und mit der Entwicklung eines hyperprogressiven Krankheitsverlaufes assoziiert sein (140, 141). Ein statistisch signifikanter Zusammenhang zwischen starken Amplifikationen (≥4 Kopien) von *MDM2*, *MDM4* oder *EGFR* und dem Auftreten einer Hyperprogression im Rahmen der Immuncheckpoint-Therapie konnte nicht festgestellt werden. Dafür zeigte sich aber der Trend, dass Amplifikation eines der drei Gene seltener bei Patienten mit einem stabilen Krankheitsverlauf auftreten im Vergleich zu den Patienten mit einem progressiven Krankheitsverlauf. Allerdings fanden sich auch in drei Patienten mit einem stabilen Krankheitsverlauf Amplifikationen in *MDM2*, *MDM4* oder *EGFR*. Daher sollte nach dem derzeitigen Wissensstand das Vorhandensein einer dieser Amplifikation nicht als Ausschlusskriterium für eine Immuncheckpoint-Inhibitor-Therapie angesehen werden.

Dass der überwiegende Teil der Patienten einen progredienten Krankheitsverlauf aufwies, könnte auch mit der insgesamt niedrigen Tumormutationslast der Kohorte (Median = 2,8 Mut/Mb) zusammenhängen. Die niedrige TMB der Kohorte reproduziert die Ergebnisse anderer Studien, denen zufolge das mukosale und akrolentiginöse Melanom eine signifikant niedrigere TMB als das kutane Melanom hat (76, 142). Retrospektive Analysen ergaben auch, dass die Ansprechraten bei Patienten mit einem mukosalen oder akrolentiginösen Melanom, die mit einer Immuncheckpoint-Therapie behandelt wurden, bei 23% bis 37% lagen (134, 135, 142, 143).

Der Subtyp des anorektalen Schleimhautmelanoms war sowohl mit einem signifikant erhöhten Risiko für eine Hyperprogression als auch mit einem schlechteren Gesamtüberleben assoziiert. Ein weiterer unabhängiger Risikofaktor für ein

schlechteres Gesamtüberleben, war das Vorhandensein von Lebermetastasen zu Therapiebeginn. Die meisten Patienten mit anorektalem Schleimhautmelanom (75%) entwickelten nach dem Start der Therapie eine Hyperprogression. Ebenfalls konnte man bei diesen Patienten eine signifikant geringere PD-L1-Expression im Vergleich zu den anderen Patienten feststellen. Möglicherweise bedeutet das, dass dieser Subtyp weniger immunogen ist und daher schlechter auf die Immuncheckpoint-Therapie anspricht (142). Ob die Hyperprogression durch eine Immuntherapie oder einfach durch den natürlichen Krankheitsverlauf ausgelöst wurde, kann nicht geklärt werden.

Der zweite unabhängige Risikofaktor für eine signifikant schlechtere Überlebensrate ist eine Lebermetastasierung zu Therapiebeginn. Diese Feststellung wurde bereits in anderen Kohorten im Rahmen der Therapie mit Pembrolizumab und einer Kombination aus Ipilimumab oder Nivolumab gemacht (144-146). Möglicherweise ist dies auf eine geringere Dichte der zytotoxischen CD8 T-Zellen in den Lebermetastasen und auch in den übrigen Metastasen in diesen Patienten zurückzuführen (144).

Eine der der Stärken der Studie ist die systematische Abfrage des Melanomregisters, sodass alle Patienten nach eindeutigen Kriterien in die Studie eingeschlossen werden konnten. Durch den retrospektiven Charakter konnte jedoch die Hyperprogression nicht wie zuvor definiert nach zwei Monaten bestimmt werden(147). Das Therapieansprechen wurde stattdessen im Rahmen der normalen klinischen Routine nach 12 Wochen evaluiert. Dennoch konnte auch in diesem Zeitraum eine Hyperprogression durch die Zunahme der Tumormasse von > 50% identifiziert werden. Darüber hinaus wurden nur 18% der Patienten mit einer Kombination aus Ipilimumab und Nivolumab behandelt. Der Grund ist der abgefragte Zeitraum 2007–2017, der nötig war, um eine ausreichend große Anzahl an Patienten mit den seltenen Subtypen des akrolentiginösen und mukosalen Melanoms zu rekrutieren. In Deutschland war die Monotherapie mit Ipilimumab seit 2011 zugelassen und die Kombinationstherapie aus Ipilimumab und Nivolumab erst seit 2016. Da die Kombination mit Ipilimumab und Nivolumab der Monotherapie mit Ipilimumab oder Nivolumab überlegen ist (137), sollte geprüft werden, ob das schlechtere Ansprechen bei MDM2-, MDM4- oder EGFR-Amplifikation auch bei Patienten zu beobachten ist, die mit einer kombinierten Immuntherapie behandelt werden.

Der Einfluss der Amplifikationen von *MDM2/4* und *EGFR* auf das Therapieansprechen im Rahmen der Immuncheckpoint-Therapie konnte im Rahmen der Studie nicht

vollständig geklärt werden. Allerdings ist auch zu berücksichtigen, dass der begrenzte Stichprobenumfang der Studie keine eindeutigen Schlussfolgerungen aus den negativen Ergebnissen erlaubt.

3.2.3 Seneszenz und Zellzyklus

3.2.3.1 Einleitung

In der Vergangenheit konnte gezeigt werden, dass tumorinfiltrierende zytotoxische T-Lymphozyten, natürliche Killer- und TH1-Zellen in der Tumorabwehr aktiviert werden und somit zur Apoptose und Zytolyse von Tumorzellen führen (148-158). Diese Eliminierung ist aber oft nicht vollständig, sodass einzelne Zellen überleben. Ein weiterer Mechanismus der Tumorkontrolle ist die durch das Immunsystem kontrollierte Arretierung der Tumorzellen, im Folgenden Tumorseneszenz genannt (149, 159-165). Die fehlende Induktion der Tumorseneszenz ist eine häufige Ursache von Therapieresistenzen bei Malignomen (151, 155, 164, 166-172). Beim Melanom zeigte sich eine Korrelation zwischen progredientem Krankheitsverlauf bzw. Therapieresistenz unter Immuncheckpoint-Blockade und funktionellen Verlusten des IFN-JAK1-STAT1-Signalwegs (159, 171, 173-177). Insbesondere die kombinierte Wirkung von Interferon gamma (IFN-γ) und des Tumornekrosefaktors (TNF) kann einen stabilen Seneszenz-ähnlichen Wachstumsstopp in Krebszellen induzieren, der als Zytokin-induzierte Seneszenz (CIS) bezeichnet wird (178). Die IFN-JAK1-STAT1 Signalkaskade aktiviert zwei Schlüsselmoleküle der Seneszenz (162, 178, 179) p16Ink4a und p21Cip1. Daher haben wir in dieser Studie die IFN-abhängige Induktion der Zellzyklusregulation über den p16Ink4a-CDK4/6-Rb1- und MDM-p53-p21Cip1-Signalweg untersucht. So sollte getestet werden, ob das Immunsystem die Arretierung derjenigen Krebszellen kontrolliert, die der immuninduzierten Zytotoxizität entgehen.

3.2.3.2 Patientenkohorte

In die Studie wurden 42 Patienten mit einem metastasierten Melanom eingeschlossen, die entweder mit Anti-PD-1 oder mit einer Kombination aus Anti-CTLA-4 und Anti-PD-1 behandelt wurden. Als *non-responder* wurden die Patienten definiert, die innerhalb von drei Monaten nach Beginn der Therapie einen Progress zeigten, wohingegen die *responder* über mehr als ein Jahr eine partielle (> 30%) oder vollständige Tumorregression zeigten. Insgesamt haben 30 Patienten nicht auf die Immuncheckpoint-Inhibitor-Therapie angesprochen (*Non-Responder*) und 12

angesprochen (*Responder*). Das mediane Alter der *non-responder* beträgt 62 Jahre (Spanne: 22-89 Jahre) und das der *responder* 57 Jahre (Spanne: 27-75 Jahre).

3.2.3.3 Genetisches Profil der Kohorte

Die in-vitro und in-vivo Analysen der *RIP1-Tag2* (RT2) Inselzellkarzinom- und λ-Myc Lymphom-Zelllinie zeigten, dass es eine IFN-/STAT1-abhängige Aktivierung der Seneszenz induzierenden Zellzyklusregulatoren p16Ink4a/p19Arf (*CDKN2A*) und p21Cip1 (*CDKN1A*) gibt (114). Im RT2-Tumormodell führte die Immuncheckpoint-Inhibitor-Therapie zu einer *Stat1*-abhängigen Aktivierung von *CDKN2A*. Das gleiche Ergebnis zeigte sich auch im λ-Myc Lymphommodell für die Aktivierung von *CDKN1A*. In beiden Fällen hatte die Aktivierung von *CDKN2A* bzw. *CDKN1A* eine stabile Seneszenz im Tumor zur Folge, die unabhängig von der Therapie induzierten Apoptose des Tumors ist (Abbildung 28).

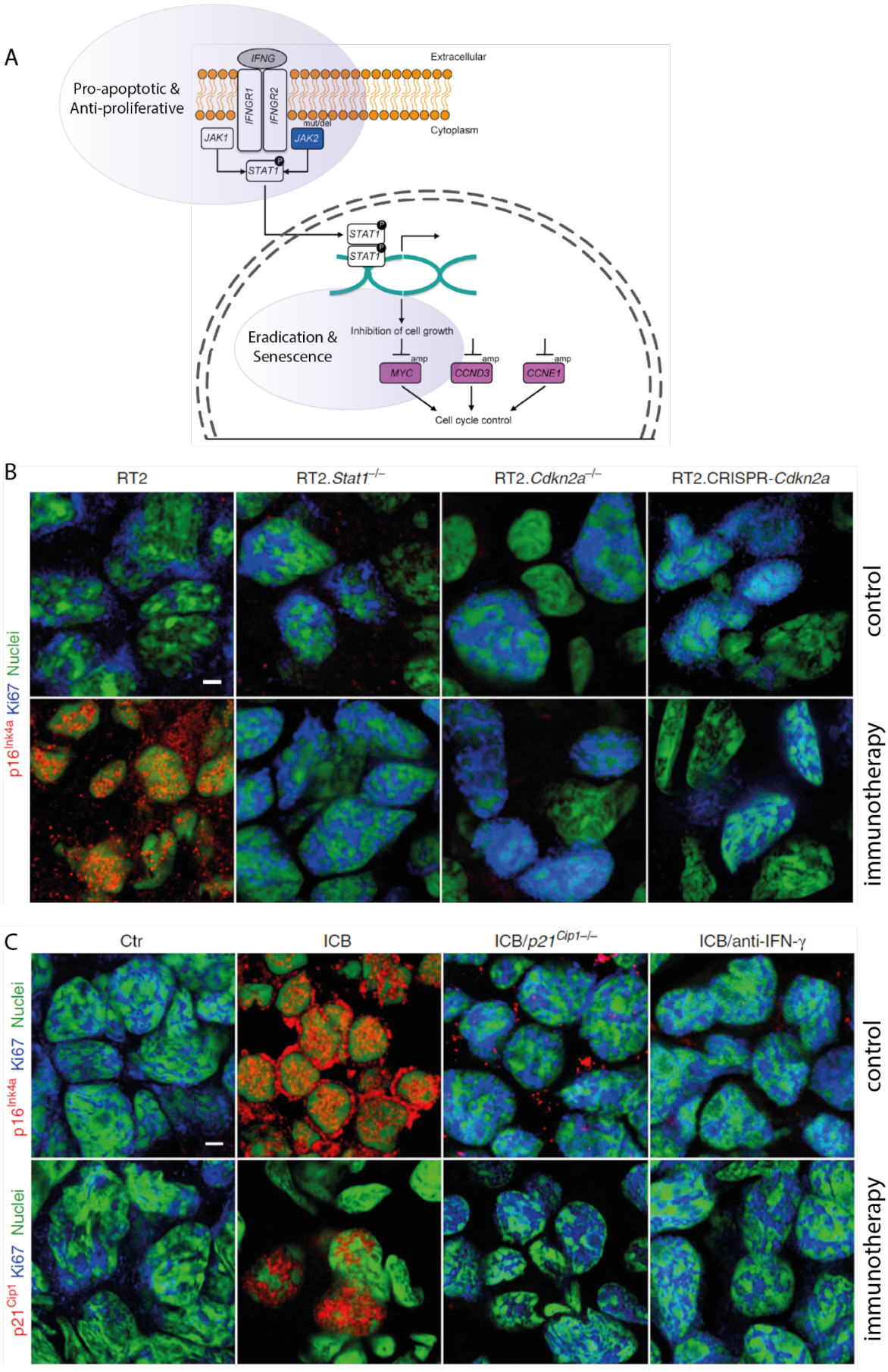

Abbildung 28: Interferon/Satin1 abhängige Kontrolle der Zellzyklusregulation

(A) Dargestellt ist der JAK/STAT Signalweg ausgehend vom Interferonrezeptor. (B) Untersucht wurden Tumorzellen von RIP-Tag2 Mäusen. Das T-antigen wird durch den Ratteninsulinpromotor (RIP) kontrolliert und führt zur Bildung von pankreatischen Inselzelltumoren. Im Mausmodell wurden der Stat1-positive (RT2) oder Stat1-negative RT2-Tumor (RT2.Stat1-/-) erzeugt sowie Tumoren, in denen das Gen *Cdkn2a* ausgeschaltet ist (RT2.Cdkn2a-/-, RT2.CRISPR-Cdkn2a). Zu sehen ist die Dreifachfärbung der Tumorzellen für die Seneszenzmarker p16Ink4a (rot), den Proliferationsmarker Ki67 (blau) und den Nukleus (grün). Die Zellen wurden entweder mit einer Kontrolle (*isotype control mAbs* = *control*) oder einer kombinierten Immuncheckpoint-Therapie (anti-PD-L1 und anti-LAG3 = *immunotherapy*) behandelt. (C) Untersucht wurden im Mausmodell Tumoren, die durch die Aktivierung des humanen Onkogenes *MYC* B-Zell-Lymphome erzeugen. Das humane Onkogenes *MYC* steht unter der Kontrolle des Immunglobulin *λ-Enhancer*. Es wurden neben den *λ-MYC*-Mäusen auch Mäuse generiert, bei denen das Gen *Cdkn1a* ausgeschaltet werden kann (λ-MYC.p21Cip1-/-). Zu sehen ist die Dreifachfärbung für die Seneszenzmarker p16Ink4a (rot, oben), oder p21 (rot, unten) und den Proliferationsmarker Ki67 (blau) sowie den Nukleus (grün). Behandelt wurden die Mäuse gar nicht (*Ctrl*) oder mit einer Kombination aus anti-CTLA4 und anti-PD-1 (*ICB*) bzw. *ICB* und Interferon-γ (ICB/anti-IFN-γ). Die Abbildung basiert auf den Daten und Abbildungen der Arbeit von *Brenner et al*. (114).

Im nächsten Schritt sollte geprüft werden, ob die in-vivo identifizierten Gene, die eine IFN-vermittelte Tumorseneszens auslösen können, ebenfalls bei Patienten mit einem fortgeschrittenen Melanom eine Rolle spielen. Zu diesem Zweck wurden die 42 Patienten mit drei Versionen eines spezifischen Tumorpanels (ssSCv2, v3, v4) sequenziert und die Unterschiede zwischen der Gruppe der *responder* und *non-responder* verglichen. Die Tumorproben wurden mit einer durchschnittlichen Sequenzierungstiefe von 511X und die normalen Normalproben (Blut) mit 521X analysiert.

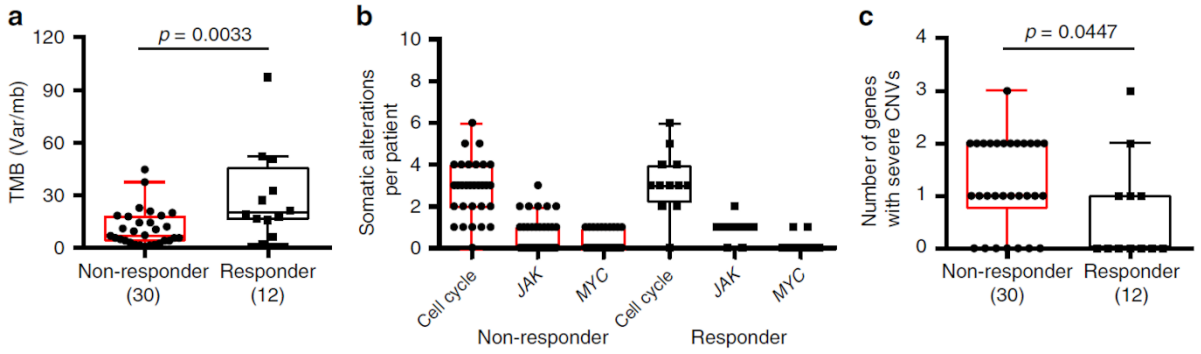

Abbildung 29: Tumormutationslast und genetische Veränderungen im Zellzyklus

Die Abbildung zeigt den Vergleich zwischen den *respondern* und *non-respondern* auf die Immuncheckpoint-Inhibitor-Therapie hinsichtlich ihrer Mutationslast und der Anzahl der genetischen Veränderungen im Zellzyklus. (a) Das Box-Plot Diagramm zeigt den Vergleich zischen der Tumormutationslast (Mutationen pro Megabase) bei *respondern* und *non-respondern* auf die Immuncheckpoint-Therapie. (b) Gezeigt wird die Anzahl an Mutationen pro Patient in den Genen *CCND1/2/3*, *CDKN2A/B/C*, *CDK4/6*, *CCNE1*, *CDKN1A/B*, *RB1*, *TP53*, *MDM2/4* sowie *JAK1,2,3* und *MYC*. (c) Das Box-Plot Diagramm zeigt die mediane Anzahl an mutierten Genen pro Patient in der Gruppe der *non-responder* und *responder*. Darüber hinaus wird der Vergleich der medianen Anzahl an mutierten Genen pro Patient gezeigt (Mann-Whitney-U-Test). Für die Bestimmung der Anzahl an mutierten Genen wurden nur homozygote oder *loss of function* Mutationen, sowie Amplifikationen mit einer Kopienzahl von >3 Kopien berücksichtigt. Die Abbildung basiert auf den Daten und Abbildungen der Arbeit von *Brenner et al*. (114).

Im Einklang mit bereits publizierten Daten konnte bei der Patientengruppe der *responder* eine signifikant höhere Tumormutationslast im Vergleich zu den *non-responder* festgestellt werden (Quelle 8, 10, 46) (Abbildung 29a). Um den Einfluss der Zytokin-induzierten Seneszenz beim fortgeschrittenen Melanom zu ergründen, wurde die Analyse auf 19 Gene konzentriert. Es handelt sich dabei um die Gene der Zellzykluskontrolle (*CCND1/2/3*; *CDKN2A/B/C*, *CDK4/6*, *CCNE1*, *CDKN1A/B*, *RB1*, *TP53*, *MDM2/4*) sowie die Januskinasen (*JAK1,2,3*) und *MYC*. Die Häufigkeit, mit der die oben genannten Gene und Signalwege von einer somatischen Veränderung betroffen sind (sowohl SNVs als auch CNVs) ist in den beiden Gruppen annährend identisch. Sowohl in der Gruppe der *non-responder* als auch *responder* wurden im Median drei mutierte Gene der Zellzykluskontrolle und eine Januskinase pro Patient detektiert (Abbildung 29b). Da im Zell- bzw. Tiermodell der Komplettverlust von *CDKN2A* und *CDKN1A* untersucht wurde, reduzierten wir im nächsten Schritt den Vergleich auf starke Amplifikation (>3 Kopien) und vollständig inaktivierende Mutationen (homozygote Deletionen oder Verlust der Heterozygotie (LOH)). Die gezielte Analyse schwerer Kopienzahlveränderungen ergab einen signifikanten Unterschied zwischen den beiden Gruppen (Abbildung 29c). Die Melanome der *non-responder* wiesen im Vergleich zu den *responder* signifikant mehr vollständig inaktivierende Mutationen in den Seneszenz-induzierenden Genen *CDKN2A*, *TP53* und *JAK2* sowie gleichzeitig starke Amplifikation in den Genen *CCND1/3*, *CDK4/6*, *CCNE1*, *MDM2/4*, *MYC* die die Zellzyklusprogression fördern auf (Abbildung 30).

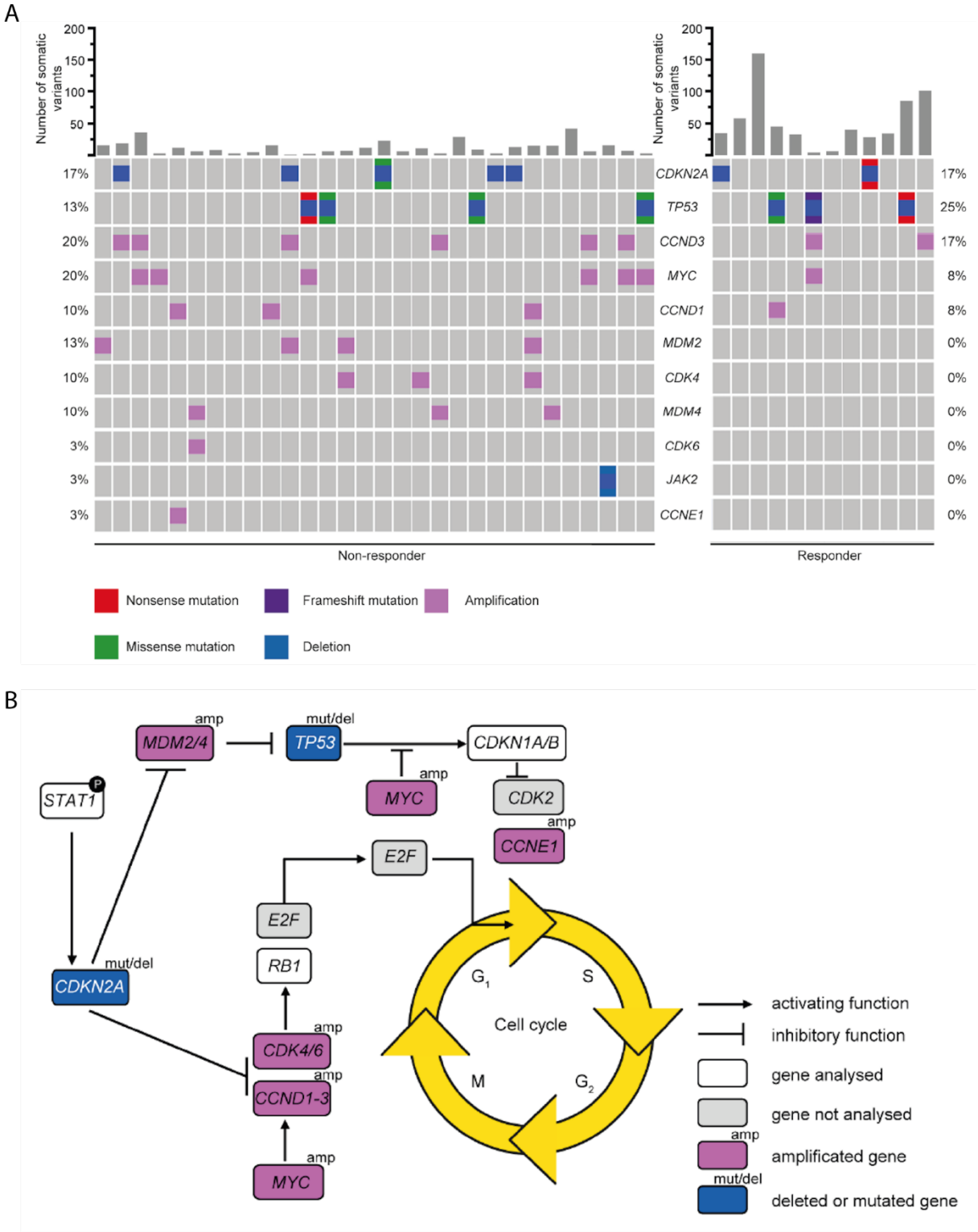

Abbildung 30: Mutationen in den Genen der Zellzykluskontrolle und des JAK/STAT Signalweges

(A) Der Oncoplot zeigt alle schweren Mutationen (homozygote Deletion, Verlust der Heterozygotie oder >3 Kopien) in den Genen der Zellzykluskontrolle und des JAK/STAT-Signalweges. Der *Oncoplot* ist zweigeteilt in die Gruppe der *responder* und *non-responder*. Jede Spalte repräsentiert den gleichen Patienten. Jede Zeile zeigt die Häufigkeit und Art der Treibermutationen für das jeweilige Gen an. Das Histogramm oberhalb vom Oncoplot zeigt die Anzahl an kodieren Mutationen pro Patient. (B) Schematische Darstellung der untersuchten Gene und ihre Funktion in der Regulation der Zellzykluskontrolle. Die Abbildung basiert auf den Daten und Abbildungen der Arbeit von *Brenner et al.* (114).

3.2.3.4 Diskussion

Das primäre Ziel jeder Tumortherapie ist die Reduktion bzw. eine komplette Zerstörung aller malignen Zellen. Allerdings ist dieser Prozess häufig unvollständig, sodass es zu einem späteren Zeitpunkt zur Bildung von Metastasen kommen kann (149, 162, 180-182). Die Daten der Studie *„Cancer immune control needs senescence induction by interferon-dependent cell cycle regulator pathways in tumours“* zeigen, dass es im Rahmen der Immuncheckpoint-Inhibitor-Therapie eine IFN-/STAT1-abhängige Aktivierung von p16Ink4a/p19Arf und p21Cip1 gibt, die zur Tumorseneszenz führt. Die Daten legen nahe, dass therapieresistente Metastasen bzw. Tumorzellen, die dem Therapie-induzierten Zelltod entkommen, in einem Stadium der Seneszenz gehalten werden. Dieses Konzept wird durch aktuelle klinische Daten unterstützt, in denen sich Melanom Metastasen während der Immuncheckpoint-Inhibitor-Therapie zurückbilden aber wieder wachsen, wenn es zu Mutationen im IFN-Signalweg kommt (174). Diese und weitere Beobachtungen deuten darauf hin, dass neben der Tumorzytotoxizität auch die IFN-abhängige Aktivierung der Tumorseneszenz für eine erfolgreiche Hemmung des Tumors im Rahmen der Immuncheckpoint-Inhibitor-Therapie nötig ist (161, 162, 178, 183, 184).

Tumorseneszenz im Anschluss an eine Therapie ist bekannt. Welche Rolle sie bei der Entwicklung von Metastasen und der Reaktion auf Chemo- und Immuncheckpoint-Inhibitor-Therapie spielt, ist nicht geklärt (185-188). Im Mausexperiment beförderte ein Komplettverlust von *CDKN2A* die Entstehung von Metastasen, allerdings nicht beim Menschen (73, 74, 189, 190). Die Beobachtung, dass mehr als die Hälfte der Therapieversager einen Defekt im IFN-abhängigen Seneszenz-Signalweg aufweisen, könnte eine mögliche Erklärung sein. Beim Menschen könnte der bi-allelische Verlust von *CDKN2A* möglicherweise durch die IFN-vermittelte Aktivierung des *MDM2*-p53-p21Cip1-Signalweges kompensiert werden (182). In Übereinstimmung mit dieser Vermutung fanden sich gehäuft starke Amplifikationen der Gene *MDM2* und *MDM4* (26%) sowie *CDK4/6* (13%) in den Tumorbiopsien der Patienten, die nicht auf eine Immuncheckpoint-Inhibitor-Therapie angesprochen haben. Diese Amplifikationen waren in der Gruppe der *responder* deutlich seltener oder abwesend.

Da sowohl p16Ink4a als auch p21Cip1 die Tumorseneszenz durch die Hemmung von *CDK4/6* induzieren, ist die Kombination aus einer Immuncheckpoint-Blockade zusammen mit *CDK4/6*-Inhibitoren möglicherweise eine vielversprechende Strategie.

Mit Hilfe dieser Therapie könnten Metastasen mit Defekten im Seneszenzmechanismus dazu gebracht werden, wieder auf die Immuncheckpoint-Therapie zu reagieren.

3.2.4 Abschließende Diskussion zum Malignen Melanom

Die Immuncheckpoint-Blockade gehört heute zum leitliniengerechten Standard bei der Behandlung des fortgeschrittenen Malignen Melanoms. Aber 40%-50% der Patienten weisen dennoch eine primäre Therapieresistenz auf (174, 191-196). Es ist daher von großer Bedeutung die Mechanismen zu identifizieren, die dem Ansprechen und Nichtansprechen auf die Immuncheckpoint-Inhibitor-Therapie zu Grunde liegen. In den drei oben beschriebenen Studien wurde der Versuch unternommen, das Maligne Melanom genetisch umfassend zu charakterisieren und solche Mechanismen zu beschreiben. Es sollten sowohl klinische wie auch genetische Marker definiert werden, die bei der Therapieentscheidung helfen können.

Mit Hilfe der Tumorpanel- bzw. Exomsequenzierung war es möglich eine genetische Landkarte der drei Kohorten zu erzeugen. In der Kohorte der 82 Patienten aus dem klinischen Alltag identifizierte die genetische Analyse Subtyp-spezifische Gene und Treibermutationen sowie potentielle Resistenzgene der Immuncheckpoint-Inhibitor-Therapie. Darüber hinaus konnten genetische Gemeinsamkeiten zwischen dem kutanen und okkulten Melanom beobachtet werden und weitere Treibermutation als potentielle therapeutische Ziele identifiziert werden.

Die umfassende genetische Charakterisierung der beiden seltenen Subtypen - das akrolentiginöse und mukosale Schleimhautmelanom - in Kombination mit klinischen Parametern konnte dazu beitragen Risikofaktoren zu bestimmen, die zu einem besseren Verständnis beitragen, warum diese Patienten schlechter auf die Immuncheckpoint-Inhibitor-Therapie ansprechen. Insbesondere das Phänomen der Hyperprogression wurde hier untersucht. Interessanterweise zeichnete sich hier der anorektale Subtyp des Schleimhaumelanoms als unabhängiger Risikofaktor für eine Hyperprogression und ein reduziertes Gesamtüberleben. Amplifikationen in den Genen *MDM2/4* oder *EGFR* sind bereits beschriebene genetische Marker, die im Zusammenhang einer Hyperprogression beschrieben wurden. Und auch in dieser Kohorte war ein Trend für ein schlechteres Therapieansprechen zu beobachten. Zusätzlich fanden sich in der Gruppe der Patienten mit einem progressiven Krankheitsverlauf gehäuft Amplifikationen in dem Onkogen *MYC*. Es kontrolliert die

Expression zahlreicher andere Gene und spielt eine wesentliche Rolle bei der Regulation der Zellzykluskontrolle. Die Regulation der Zellzykluskontrolle und ihr Einfluss im Rahmen der Immuncheckpoint-Inhibitor-Therapie standen im Mittelpunkt der dritten Forschungsarbeit zum Malignen Melanom. Die in-vitro und in-vivo Experimente identifizierten die Immuncheckpoint-Inhibitor-Therapie induzierte Tumorseneszenz als zweiten Mechanismus neben der Tumoreradikation. Der Einfluss der IFN/STAT1 Signaltransduktion auf die Tumorseneszenz durch den p16Ink4a-*CDK4/6-Rb1*- und *MDM*-p53-p21Cip1-Signalweg kristallisiert sich als Hauptmechanismus heraus. Dieser Zusammenhang bestätigte sich auch bei der genetischen Analyse einer Kohorte von Patienten mit einem Malignen Melanom, zusammengesetzt aus Therapieversagern und Ansprechern. Häufig fanden sich funktionell relevante Mutationen in den Genen, die durch den IFN/STAT1 Signalweg reguliert werden und Seneszenz induzieren.

In der Zukunft sind dringend größere prospektive Studien erforderlich, um mehr über potenzielle Resistenzmechanismen der Immuncheckpoint-Blockade zu erfahren und es sollten weitere Anstrengungen unternommen werden, um gezielte Therapien jenseits von *BRAF*-, *MEK*- oder *KIT*-Inhibitoren beim fortgeschrittenen Malignen Melanom einzuführen.

Literaturverzeichnis

1. Bray F, Ferlay J, Soerjomataram I, Siegel RL, Torre LA, Jemal A. Global cancer statistics 2018: GLOBOCAN estimates of incidence and mortality worldwide for 36 cancers in 185 countries. CA Cancer J Clin. 2018;68(6):394-424.
2. Hanahan D, Weinberg RA. Hallmarks of cancer: the next generation. Cell. 2011;144(5):646-74.
3. Hanahan D, Weinberg RA. The hallmarks of cancer. Cell. 2000;100(1):57-70.
4. Rous P. A Sarcoma of the Fowl Transmissible by an Agent Separable from the Tumor Cells. J Exp Med. 1911;13(4):397-411.
5. Weinberg RA, Weinberg RA. The Biology of Cancer: CRC Press; 2013.
6. Knudson AG, Jr. Mutation and cancer: statistical study of retinoblastoma. Proc Natl Acad Sci U S A. 1971;68(4):820-3.
7. Vogelstein B, Papadopoulos N, Velculescu VE, Zhou S, Diaz LA, Jr., Kinzler KW. Cancer genome landscapes. Science. 2013;339(6127):1546-58.
8. Consortium ITP-CAoWG. Pan-cancer analysis of whole genomes. Nature. 2020;578(7793):82-93.
9. Bailey MH, Tokheim C, Porta-Pardo E, Sengupta S, Bertrand D, Weerasinghe A, et al. Comprehensive Characterization of Cancer Driver Genes and Mutations. Cell. 2018;174(4):1034-5.
10. Sanchez-Vega F, Mina M, Armenia J, Chatila WK, Luna A, La KC, et al. Oncogenic Signaling Pathways in The Cancer Genome Atlas. Cell. 2018;173(2):321-37 e10.
11. Knijnenburg TA, Wang L, Zimmermann MT, Chambwe N, Gao GF, Cherniack AD, et al. Genomic and Molecular Landscape of DNA Damage Repair Deficiency across The Cancer Genome Atlas. Cell Rep. 2018;23(1):239-54 e6.
12. Ge Z, Leighton JS, Wang Y, Peng X, Chen Z, Chen H, et al. Integrated Genomic Analysis of the Ubiquitin Pathway across Cancer Types. Cell Rep. 2018;23(1):213-26 e3.
13. Seiler M, Peng S, Agrawal AA, Palacino J, Teng T, Zhu P, et al. Somatic Mutational Landscape of Splicing Factor Genes and Their Functional Consequences across 33 Cancer Types. Cell Rep. 2018;23(1):282-96 e4.
14. Garraway LA, Lander ES. Lessons from the cancer genome. Cell. 2013;153(1):17-37.
15. Vogelstein B, Kinzler KW. The Path to Cancer --Three Strikes and You're Out. N Engl J Med. 2015;373(20):1895-8.
16. Faraji F, Schubert A, Kagohara L, Tan M, Xu Y, Zaidi M, et al. The Genome-Wide Molecular Landscape of HPV-Driven and HPV-Negative Head and Neck Squamous Cell Carcinoma. 2018. p. 293-325.
17. Metzker ML. Sequencing technologies - the next generation. Nat Rev Genet. 2010;11(1):31-46.
18. Goodwin S, McPherson JD, McCombie WR. Coming of age: ten years of next-generation sequencing technologies. Nat Rev Genet. 2016;17(6):333-51.
19. Liu L, Li Y, Li S, Hu N, He Y, Pong R, et al. Comparison of next-generation sequencing systems. J Biomed Biotechnol. 2012;2012:251364.
20. Fedurco M, Romieu A, Williams S, Lawrence I, Turcatti G. BTA, a novel reagent for DNA attachment on glass and efficient generation of solid-phase amplified DNA colonies. Nucleic Acids Res. 2006;34(3):e22.
21. Pantel K, Alix-Panabieres C. Circulating tumour cells in cancer patients: challenges and perspectives. Trends Mol Med. 2010;16(9):398-406.
22. Siravegna G, Marsoni S, Siena S, Bardelli A. Integrating liquid biopsies into the management of cancer. Nat Rev Clin Oncol. 2017;14(9):531-48.
23. Wan JCM, Massie C, Garcia-Corbacho J, Mouliere F, Brenton JD, Caldas C, et al. Liquid biopsies come of age: towards implementation of circulating tumour DNA. Nat Rev Cancer. 2017;17(4):223-38.

24. Reckamp KL, Melnikova VO, Karlovich C, Sequist LV, Camidge DR, Wakelee H, et al. A Highly Sensitive and Quantitative Test Platform for Detection of NSCLC EGFR Mutations in Urine and Plasma. J Thorac Oncol. 2016;11(10):1690-700.
25. Wang Y, Springer S, Mulvey CL, Silliman N, Schaefer J, Sausen M, et al. Detection of somatic mutations and HPV in the saliva and plasma of patients with head and neck squamous cell carcinomas. Sci Transl Med. 2015;7(293):293ra104.
26. Kimura H, Fujiwara Y, Sone T, Kunitoh H, Tamura T, Kasahara K, et al. EGFR mutation status in tumour-derived DNA from pleural effusion fluid is a practical basis for predicting the response to gefitinib. Br J Cancer. 2006;95(10):1390-5.
27. De Mattos-Arruda L, Mayor R, Ng CKY, Weigelt B, Martinez-Ricarte F, Torrejon D, et al. Cerebrospinal fluid-derived circulating tumour DNA better represents the genomic alterations of brain tumours than plasma. Nat Commun. 2015;6:8839.
28. Mandel P, Metais P. [Not Available]. C R Seances Soc Biol Fil. 1948;142(3-4):241-3.
29. Koffler D, Agnello V, Winchester R, Kunkel HG. The occurrence of single-stranded DNA in the serum of patients with systemic lupus erythematosus and other diseases. J Clin Invest. 1973;52(1):198-204.
30. Leon SA, Shapiro B, Sklaroff DM, Yaros MJ. Free DNA in the serum of cancer patients and the effect of therapy. Cancer Res. 1977;37(3):646-50.
31. Rodrigues Filho EM, Simon D, Ikuta N, Klovan C, Dannebrock FA, Oliveira de Oliveira C, et al. Elevated cell-free plasma DNA level as an independent predictor of mortality in patients with severe traumatic brain injury. J Neurotrauma. 2014;31(19):1639-46.
32. Tsai NW, Lin TK, Chen SD, Chang WN, Wang HC, Yang TM, et al. The value of serial plasma nuclear and mitochondrial DNA levels in patients with acute ischemic stroke. Clin Chim Acta. 2011;412(5-6):476-9.
33. Breitbach S, Sterzing B, Magallanes C, Tug S, Simon P. Direct measurement of cell-free DNA from serially collected capillary plasma during incremental exercise. J Appl Physiol (1985). 2014;117(2):119-30.
34. De Vlaminck I, Valantine HA, Snyder TM, Strehl C, Cohen G, Luikart H, et al. Circulating cell-free DNA enables noninvasive diagnosis of heart transplant rejection. Sci Transl Med. 2014;6(241):241ra77.
35. De Vlaminck I, Martin L, Kertesz M, Patel K, Kowarsky M, Strehl C, et al. Noninvasive monitoring of infection and rejection after lung transplantation. Proc Natl Acad Sci U S A. 2015;112(43):13336-41.
36. Lo YM, Corbetta N, Chamberlain PF, Rai V, Sargent IL, Redman CW, et al. Presence of fetal DNA in maternal plasma and serum. Lancet. 1997;350(9076):485-7.
37. Crowley E, Di Nicolantonio F, Loupakis F, Bardelli A. Liquid biopsy: monitoring cancer-genetics in the blood. Nat Rev Clin Oncol. 2013;10(8):472-84.
38. Lo YM, Zhang J, Leung TN, Lau TK, Chang AM, Hjelm NM. Rapid clearance of fetal DNA from maternal plasma. Am J Hum Genet. 1999;64(1):218-24.
39. El Messaoudi S, Rolet F, Mouliere F, Thierry AR. Circulating cell free DNA: Preanalytical considerations. Clin Chim Acta. 2013;424:222-30.
40. Heitzer E, Auer M, Hoffmann EM, Pichler M, Gasch C, Ulz P, et al. Establishment of tumor-specific copy number alterations from plasma DNA of patients with cancer. Int J Cancer. 2013;133(2):346-56.
41. Diehl F, Li M, Dressman D, He Y, Shen D, Szabo S, et al. Detection and quantification of mutations in the plasma of patients with colorectal tumors. Proc Natl Acad Sci U S A. 2005;102(45):16368-73.
42. Lo YM, Chan KC, Sun H, Chen EZ, Jiang P, Lun FM, et al. Maternal plasma DNA sequencing reveals the genome-wide genetic and mutational profile of the fetus. Sci Transl Med. 2010;2(61):61ra91.
43. Tinhofer I, Staudte S. Circulating tumor cells as biomarkers in head and neck cancer: recent advances and future outlook. Expert Rev Mol Diagn. 2018;18(10):897-906.

44. Vogelstein B, Kinzler KW. Digital PCR. Proc Natl Acad Sci U S A. 1999;96(16):9236-41.
45. Dressman D, Yan H, Traverso G, Kinzler KW, Vogelstein B. Transforming single DNA molecules into fluorescent magnetic particles for detection and enumeration of genetic variations. Proc Natl Acad Sci U S A. 2003;100(15):8817-22.
46. Koeppel F, Blanchard S, Jovelet C, Genin B, Marcaillou C, Martin E, et al. Whole exome sequencing for determination of tumor mutation load in liquid biopsy from advanced cancer patients. PLoS One. 2017;12(11):e0188174.
47. Newman AM, Lovejoy AF, Klass DM, Kurtz DM, Chabon JJ, Scherer F, et al. Integrated digital error suppression for improved detection of circulating tumor DNA. Nat Biotechnol. 2016;34(5):547-55.
48. Forshew T, Murtaza M, Parkinson C, Gale D, Tsui DW, Kaper F, et al. Noninvasive identification and monitoring of cancer mutations by targeted deep sequencing of plasma DNA. Sci Transl Med. 2012;4(136):136ra68.
49. Phallen J, Sausen M, Adleff V, Leal A, Hruban C, White J, et al. Direct detection of early-stage cancers using circulating tumor DNA. Sci Transl Med. 2017;9(403).
50. Leary RJ, Sausen M, Kinde I, Papadopoulos N, Carpten JD, Craig D, et al. Detection of chromosomal alterations in the circulation of cancer patients with whole-genome sequencing. Sci Transl Med. 2012;4(162):162ra54.
51. Heitzer E, Ulz P, Belic J, Gutschi S, Quehenberger F, Fischereder K, et al. Tumor-associated copy number changes in the circulation of patients with prostate cancer identified through whole-genome sequencing. Genome Med. 2013;5(4):30.
52. Belic J, Koch M, Ulz P, Auer M, Gerhalter T, Mohan S, et al. Rapid Identification of Plasma DNA Samples with Increased ctDNA Levels by a Modified FAST-SeqS Approach. Clin Chem. 2015;61(6):838-49.
53. Bettegowda C, Sausen M, Leary RJ, Kinde I, Wang Y, Agrawal N, et al. Detection of circulating tumor DNA in early- and late-stage human malignancies. Sci Transl Med. 2014;6(224):224ra24.
54. Heitzer E, Haque IS, Roberts CES, Speicher MR. Current and future perspectives of liquid biopsies in genomics-driven oncology. Nat Rev Genet. 2019;20(2):71-88.
55. Murtaza M, Dawson SJ, Pogrebniak K, Rueda OM, Provenzano E, Grant J, et al. Multifocal clonal evolution characterized using circulating tumour DNA in a case of metastatic breast cancer. Nat Commun. 2015;6:8760.
56. Mendelsohn J, Gray, J. W., Howley, P. M., Israel, M. A., & Thompson, C. B. The molecular basis of cancer: Fourth Edition2014. 863 p.
57. Leemans CR, Snijders PJF, Brakenhoff RH. The molecular landscape of head and neck cancer. Nat Rev Cancer. 2018;18(5):269-82.
58. Leemans CR, Braakhuis BJ, Brakenhoff RH. The molecular biology of head and neck cancer. Nat Rev Cancer. 2011;11(1):9-22.
59. Ang KK, Harris J, Wheeler R, Weber R, Rosenthal DI, Nguyen-Tan PF, et al. Human papillomavirus and survival of patients with oropharyngeal cancer. N Engl J Med. 2010;363(1):24-35.
60. O'Sullivan B, Huang SH, Su J, Garden AS, Sturgis EM, Dahlstrom K, et al. Development and validation of a staging system for HPV-related oropharyngeal cancer by the International Collaboration on Oropharyngeal cancer Network for Staging (ICON-S): a multicentre cohort study. Lancet Oncol. 2016;17(4):440-51.
61. Brouns E, Baart J, Karagozoglu K, Aartman I, Bloemena E, van der Waal I. Malignant transformation of oral leukoplakia in a well-defined cohort of 144 patients. Oral Dis. 2014;20(3):e19-24.
62. Roesch-Ely M, Nees M, Karsai S, Ruess A, Bogumil R, Warnken U, et al. Proteomic analysis reveals successive aberrations in protein expression from healthy mucosa to invasive head and neck cancer. Oncogene. 2007;26(1):54-64.
63. Califano J, van der Riet P, Westra W, Nawroz H, Clayman G, Piantadosi S, et al. Genetic progression model for head and neck cancer: implications for field cancerization. Cancer Res. 1996;56(11):2488-92.

64. Cancer Genome Atlas N. Comprehensive genomic characterization of head and neck squamous cell carcinomas. Nature. 2015;517(7536):576-82.
65. Gross AM, Orosco RK, Shen JP, Egloff AM, Carter H, Hofree M, et al. Multi-tiered genomic analysis of head and neck cancer ties TP53 mutation to 3p loss. Nat Genet. 2014;46(9):939-43.
66. Hayes DN, Van Waes C, Seiwert TY. Genetic Landscape of Human Papillomavirus-Associated Head and Neck Cancer and Comparison to Tobacco-Related Tumors. J Clin Oncol. 2015;33(29):3227-34.
67. Shain AH, Bastian BC. From melanocytes to melanomas. Nat Rev Cancer. 2016;16(6):345-58.
68. Mort RL, Jackson IJ, Patton EE. The melanocyte lineage in development and disease. Development. 2015;142(7):1387.
69. Plewig G, Ruzicka T, Kaufmann R, Hertl M. Braun-Falco's Dermatologie, Venerologie und Allergologie: Springer Berlin Heidelberg; 2018.
70. Bastian BC. The molecular pathology of melanoma: an integrated taxonomy of melanocytic neoplasia. Annu Rev Pathol. 2014;9:239-71.
71. Rabbie R, Ferguson P, Molina-Aguilar C, Adams DJ, Robles-Espinoza CD. Melanoma subtypes: genomic profiles, prognostic molecular markers and therapeutic possibilities. J Pathol. 2019;247(5):539-51.
72. Shain AH, Yeh I, Kovalyshyn I, Sriharan A, Talevich E, Gagnon A, et al. The Genetic Evolution of Melanoma from Precursor Lesions. N Engl J Med. 2015;373(20):1926-36.
73. Shain AH, Joseph NM, Yu R, Benhamida J, Liu S, Prow T, et al. Genomic and Transcriptomic Analysis Reveals Incremental Disruption of Key Signaling Pathways during Melanoma Evolution. Cancer Cell. 2018;34(1):45-55 e4.
74. Zeng H, Jorapur A, Shain AH, Lang UE, Torres R, Zhang Y, et al. Bi-allelic Loss of CDKN2A Initiates Melanoma Invasion via BRN2 Activation. Cancer Cell. 2018;34(1):56-68 e9.
75. Cancer Genome Atlas N. Genomic Classification of Cutaneous Melanoma. Cell. 2015;161(7):1681-96.
76. Hayward NK, Wilmott JS, Waddell N, Johansson PA, Field MA, Nones K, et al. Whole-genome landscapes of major melanoma subtypes. Nature. 2017;545(7653):175-80.
77. Liang WS, Hendricks W, Kiefer J, Schmidt J, Sekar S, Carpten J, et al. Integrated genomic analyses reveal frequent TERT aberrations in acral melanoma. Genome Res. 2017;27(4):524-32.
78. Newell F, Kong Y, Wilmott JS, Johansson PA, Ferguson PM, Cui C, et al. Whole-genome landscape of mucosal melanoma reveals diverse drivers and therapeutic targets. Nat Commun. 2019;10(1):3163.
79. Furney SJ, Turajlic S, Stamp G, Nohadani M, Carlisle A, Thomas JM, et al. Genome sequencing of mucosal melanomas reveals that they are driven by distinct mechanisms from cutaneous melanoma. J Pathol. 2013;230(3):261-9.
80. Bakhoum MF, Esmaeli B. Molecular Characteristics of Uveal Melanoma: Insights from the Cancer Genome Atlas (TCGA) Project. Cancers (Basel). 2019;11(8).
81. Park JJ, Diefenbach RJ, Joshua AM, Kefford RF, Carlino MS, Rizos H. Oncogenic signaling in uveal melanoma. Pigment Cell Melanoma Res. 2018;31(6):661-72.
82. Robertson AG, Shih J, Yau C, Gibb EA, Oba J, Mungall KL, et al. Integrative Analysis Identifies Four Molecular and Clinical Subsets in Uveal Melanoma. Cancer Cell. 2017;32(2):204-20 e15.
83. Szalai E, Wells JR, Ward L, Grossniklaus HE. Uveal Melanoma Nuclear BRCA1-Associated Protein-1 Immunoreactivity Is an Indicator of Metastasis. Ophthalmology. 2018;125(2):203-9.
84. Chow LQM. Head and Neck Cancer. N Engl J Med. 2020;382(1):60-72.
85. Pignon JP, le Maitre A, Maillard E, Bourhis J, Group M-NC. Meta-analysis of chemotherapy in head and neck cancer (MACH-NC): an update on 93 randomised trials and 17,346 patients. Radiother Oncol. 2009;92(1):4-14.
86. Budach V, Stromberger C, Poettgen C, Baumann M, Budach W, Grabenbauer G, et al. Hyperfractionated accelerated radiation therapy (HART) of 70.6 Gy with concurrent 5-FU/Mitomycin C is superior to HART of 77.6 Gy alone in locally advanced head and neck cancer: long-term results of the ARO 95-06 randomized phase III trial. Int J Radiat Oncol Biol Phys. 2015;91(5):916-24.

87. Linge A, Lohaus F, Lock S, Nowak A, Gudziol V, Valentini C, et al. HPV status, cancer stem cell marker expression, hypoxia gene signatures and tumour volume identify good prognosis subgroups in patients with HNSCC after primary radiochemotherapy: A multicentre retrospective study of the German Cancer Consortium Radiation Oncology Group (DKTK-ROG). Radiother Oncol. 2016;121(3):364-73.
88. Eder T, Hess AK, Konschak R, Stromberger C, Johrens K, Fleischer V, et al. Interference of tumour mutational burden with outcome of patients with head and neck cancer treated with definitive chemoradiation: a multicentre retrospective study of the German Cancer Consortium Radiation Oncology Group. Eur J Cancer. 2019;116:67-76.
89. Tamborero D, Rubio-Perez C, Deu-Pons J, Schroeder MP, Vivancos A, Rovira A, et al. Cancer Genome Interpreter annotates the biological and clinical relevance of tumor alterations. Genome Med. 2018;10(1):25.
90. Trotti A. Toxicity in head and neck cancer: a review of trends and issues. Int J Radiat Oncol Biol Phys. 2000;47(1):1-12.
91. Volanakis JE. Human C-reactive protein: expression, structure, and function. Mol Immunol. 2001;38(2-3):189-97.
92. Aird WC. The hematologic system as a marker of organ dysfunction in sepsis. Mayo Clin Proc. 2003;78(7):869-81.
93. Schwarzenbach H, Hoon DS, Pantel K. Cell-free nucleic acids as biomarkers in cancer patients. Nat Rev Cancer. 2011;11(6):426-37.
94. Aucamp J, Bronkhorst AJ, Badenhorst CPS, Pretorius PJ. The diverse origins of circulating cell-free DNA in the human body: a critical re-evaluation of the literature. Biol Rev Camb Philos Soc. 2018;93(3):1649-83.
95. Zwirner K, Hilke FJ, Demidov G, Ossowski S, Gani C, Riess O, et al. Circulating cell-free DNA: A potential biomarker to differentiate inflammation and infection during radiochemotherapy. Radiother Oncol. 2018;129(3):575-81.
96. Cox JD, Stetz J, Pajak TF. Toxicity criteria of the Radiation Therapy Oncology Group (RTOG) and the European Organization for Research and Treatment of Cancer (EORTC). Int J Radiat Oncol Biol Phys. 1995;31(5):1341-6.
97. Braakhuis BJ, Brakenhoff RH, Leemans CR. Treatment choice for locally advanced head and neck cancers on the basis of risk factors: biological risk factors. Ann Oncol. 2012;23 Suppl 10:x173-7.
98. Muhanna N, Di Grappa MA, Chan HHL, Khan T, Jin CS, Zheng Y, et al. Cell-Free DNA Kinetics in a Pre-Clinical Model of Head and Neck Cancer. Sci Rep. 2017;7(1):16723.
99. Ahn SM, Chan JY, Zhang Z, Wang H, Khan Z, Bishop JA, et al. Saliva and plasma quantitative polymerase chain reaction-based detection and surveillance of human papillomavirus-related head and neck cancer. JAMA Otolaryngol Head Neck Surg. 2014;140(9):846-54.
100. Chan KC, Hung EC, Woo JK, Chan PK, Leung SF, Lai FP, et al. Early detection of nasopharyngeal carcinoma by plasma Epstein-Barr virus DNA analysis in a surveillance program. Cancer. 2013;119(10):1838-44.
101. Wang WY, Twu CW, Chen HH, Jiang RS, Wu CT, Liang KL, et al. Long-term survival analysis of nasopharyngeal carcinoma by plasma Epstein-Barr virus DNA levels. Cancer. 2013;119(5):963-70.
102. Lin JC, Wang WY, Chen KY, Wei YH, Liang WM, Jan JS, et al. Quantification of plasma Epstein-Barr virus DNA in patients with advanced nasopharyngeal carcinoma. N Engl J Med. 2004;350(24):2461-70.
103. Lo YM, Leung SF, Chan LY, Chan AT, Lo KW, Johnson PJ, et al. Kinetics of plasma Epstein-Barr virus DNA during radiation therapy for nasopharyngeal carcinoma. Cancer Res. 2000;60(9):2351-5.
104. Lo YM, Chan LY, Lo KW, Leung SF, Zhang J, Chan AT, et al. Quantitative analysis of cell-free Epstein-Barr virus DNA in plasma of patients with nasopharyngeal carcinoma. Cancer Res. 1999;59(6):1188-91.
105. Chaudhuri AA, Chabon JJ, Lovejoy AF, Newman AM, Stehr H, Azad TD, et al. Early Detection of Molecular Residual Disease in Localized Lung Cancer by Circulating Tumor DNA Profiling. Cancer Discov. 2017;7(12):1394-403.

106. Tie J, Cohen JD, Wang Y, Li L, Christie M, Simons K, et al. Serial circulating tumour DNA analysis during multimodality treatment of locally advanced rectal cancer: a prospective biomarker study. Gut. 2019;68(4):663-71.
107. Christensen E, Birkenkamp-Demtroder K, Sethi H, Shchegrova S, Salari R, Nordentoft I, et al. Early Detection of Metastatic Relapse and Monitoring of Therapeutic Efficacy by Ultra-Deep Sequencing of Plasma Cell-Free DNA in Patients With Urothelial Bladder Carcinoma. J Clin Oncol. 2019;37(18):1547-57.
108. Garcia-Murillas I, Schiavon G, Weigelt B, Ng C, Hrebien S, Cutts RJ, et al. Mutation tracking in circulating tumor DNA predicts relapse in early breast cancer. Sci Transl Med. 2015;7(302):302ra133.
109. Sausen M, Phallen J, Adleff V, Jones S, Leary RJ, Barrett MT, et al. Clinical implications of genomic alterations in the tumour and circulation of pancreatic cancer patients. Nat Commun. 2015;6:7686.
110. Khakoo S, Carter PD, Brown G, Valeri N, Picchia S, Bali MA, et al. MRI Tumor Regression Grade and Circulating Tumor DNA as Complementary Tools to Assess Response and Guide Therapy Adaptation in Rectal Cancer. Clin Cancer Res. 2020;26(1):183-92.
111. Chin RI, Chen K, Usmani A, Chua C, Harris PK, Binkley MS, et al. Detection of Solid Tumor Molecular Residual Disease (MRD) Using Circulating Tumor DNA (ctDNA). Mol Diagn Ther. 2019;23(3):311-31.
112. Rozeman EA, Dekker TJA, Haanen J, Blank CU. Advanced Melanoma: Current Treatment Options, Biomarkers, and Future Perspectives. Am J Clin Dermatol. 2018;19(3):303-17.
113. Forschner A, Hilke FJ, Bonzheim I, Gschwind A, Demidov G, Amaral T, et al. MDM2, MDM4 and EGFR Amplifications and Hyperprogression in Metastatic Acral and Mucosal Melanoma. Cancers (Basel). 2020;12(3).
114. Brenner E, Schorg BF, Ahmetlic F, Wieder T, Hilke FJ, Simon N, et al. Cancer immune control needs senescence induction by interferon-dependent cell cycle regulator pathways in tumours. Nat Commun. 2020;11(1):1335.
115. Parrella P, Caballero OL, Sidransky D, Merbs SL. Detection of c-myc amplification in uveal melanoma by fluorescent in situ hybridization. Invest Ophthalmol Vis Sci. 2001;42(8):1679-84.
116. Lin X, Sun R, Zhao X, Zhu D, Zhao X, Gu Q, et al. C-myc overexpression drives melanoma metastasis by promoting vasculogenic mimicry via c-myc/snail/Bax signaling. J Mol Med (Berl). 2017;95(1):53-67.
117. Wolfer A, Ramaswamy S. MYC and metastasis. Cancer Res. 2011;71(6):2034-7.
118. McCarthy C, Kalirai H, Lake SL, Dodson A, Damato BE, Coupland SE. Insights into genetic alterations of liver metastases from uveal melanoma. Pigment Cell Melanoma Res. 2016;29(1):60-7.
119. Egberts F, Bergner I, Kruger S, Haag J, Behrens HM, Hauschild A, et al. Metastatic melanoma of unknown primary resembles the genotype of cutaneous melanomas. Ann Oncol. 2014;25(1):246-50.
120. Heppt MV, Tietze JK, Reinholz M, Rahimi F, Jung A, Kirchner T, et al. Disease kinetics but not disease burden is relevant for survival in melanoma of unknown primary tumor. Discov Med. 2015;20(110):231-7.
121. Curtin JA, Fridlyand J, Kageshita T, Patel HN, Busam KJ, Kutzner H, et al. Distinct sets of genetic alterations in melanoma. N Engl J Med. 2005;353(20):2135-47.
122. Fruh M, Peters S. EGFR mutation subtype impacts efficacy of immune checkpoint inhibitors in non-small-cell lung cancer. Ann Oncol. 2019;30(8):1190-2.
123. Lee CK, Man J, Lord S, Links M, Gebski V, Mok T, et al. Checkpoint Inhibitors in Metastatic EGFR-Mutated Non-Small Cell Lung Cancer-A Meta-Analysis. J Thorac Oncol. 2017;12(2):403-7.
124. Ozaki Y, Muto S, Takagi H, Watanabe M, Inoue T, Fukuhara M, et al. Tumor mutation burden and immunological, genomic, and clinicopathological factors as biomarkers for checkpoint inhibitor treatment of patients with non-small-cell lung cancer. Cancer Immunol Immunother. 2020;69(1):127-34.

125. Johnson DB, Pectasides E, Feld E, Ye F, Zhao S, Johnpulle R, et al. Sequencing Treatment in BRAFV600 Mutant Melanoma: Anti-PD-1 Before and After BRAF Inhibition. J Immunother. 2017;40(1):31-5.
126. Moser JC, Chen D, Hu-Lieskovan S, Grossmann KF, Patel S, Colonna SV, et al. Real-world survival of patients with advanced BRAF V600 mutated melanoma treated with front-line BRAF/MEK inhibitors, anti-PD-1 antibodies, or nivolumab/ipilimumab. Cancer Med. 2019;8(18):7637-43.
127. Schilling B, Martens A, Geukes Foppen MH, Gebhardt C, Hassel JC, Rozeman EA, et al. First-line therapy-stratified survival in BRAF-mutant melanoma: a retrospective multicenter analysis. Cancer Immunol Immunother. 2019;68(5):765-72.
128. Horn S, Leonardelli S, Sucker A, Schadendorf D, Griewank KG, Paschen A. Tumor CDKN2A-Associated JAK2 Loss and Susceptibility to Immunotherapy Resistance. J Natl Cancer Inst. 2018;110(6):677-81.
129. Kong Y, Sheng X, Wu X, Yan J, Ma M, Yu J, et al. Frequent Genetic Aberrations in the CDK4 Pathway in Acral Melanoma Indicate the Potential for CDK4/6 Inhibitors in Targeted Therapy. Clin Cancer Res. 2017;23(22):6946-57.
130. Tang B, Sheng X, Kong Y, Chi Z, Si L, Cui C, et al. Palbociclib for treatment of metastatic melanoma with copy number variations of CDK4 pathway: case report. Chin Clin Oncol. 2018;7(6):62.
131. Young RJ, Waldeck K, Martin C, Foo JH, Cameron DP, Kirby L, et al. Loss of CDKN2A expression is a frequent event in primary invasive melanoma and correlates with sensitivity to the CDK4/6 inhibitor PD0332991 in melanoma cell lines. Pigment Cell Melanoma Res. 2014;27(4):590-600.
132. Posch C, Sanlorenzo M, Ma J, Kim ST, Zekhtser M, Ortiz-Urda S. MEK/CDK4,6 co-targeting is effective in a subset of NRAS, BRAF and 'wild type' melanomas. Oncotarget. 2018;9(79):34990-5.
133. Mateo J, Lord CJ, Serra V, Tutt A, Balmana J, Castroviejo-Bermejo M, et al. A decade of clinical development of PARP inhibitors in perspective. Ann Oncol. 2019;30(9):1437-47.
134. D'Angelo SP, Larkin J, Sosman JA, Lebbe C, Brady B, Neyns B, et al. Efficacy and Safety of Nivolumab Alone or in Combination With Ipilimumab in Patients With Mucosal Melanoma: A Pooled Analysis. J Clin Oncol. 2017;35(2):226-35.
135. Shoushtari AN, Munhoz RR, Kuk D, Ott PA, Johnson DB, Tsai KK, et al. The efficacy of anti-PD-1 agents in acral and mucosal melanoma. Cancer. 2016;122(21):3354-62.
136. Mermel CH, Schumacher SE, Hill B, Meyerson ML, Beroukhim R, Getz G. GISTIC2.0 facilitates sensitive and confident localization of the targets of focal somatic copy-number alteration in human cancers. Genome Biol. 2011;12(4):R41.
137. Kato S, Goodman A, Walavalkar V, Barkauskas DA, Sharabi A, Kurzrock R. Hyperprogressors after Immunotherapy: Analysis of Genomic Alterations Associated with Accelerated Growth Rate. Clin Cancer Res. 2017;23(15):4242-50.
138. Wade M, Li YC, Wahl GM. MDM2, MDMX and p53 in oncogenesis and cancer therapy. Nat Rev Cancer. 2013;13(2):83-96.
139. Akbay EA, Koyama S, Carretero J, Altabef A, Tchaicha JH, Christensen CL, et al. Activation of the PD-1 pathway contributes to immune escape in EGFR-driven lung tumors. Cancer Discov. 2013;3(12):1355-63.
140. Kato S, Goodman AM, Walavalkar V, Barkauskas DA, Sharabi A, Kurzrock R. Hyper-progressors after Immunotherapy: Analysis of Genomic Alterations Associated with Accelerated Growth Rate. Clin Cancer Res. 2017.
141. Forschner A, Niessner H, Moller Y, Horak P, Frohlich M, Warsow G, et al. Genomics of Immunotherapy-Associated Hyperprogressors-Letter. Clin Cancer Res. 2017;23(20):6374-5.
142. Dodds TJ, Wilmott JS, Jackett LA, Lo SN, Long GV, Thompson JF, et al. Primary anorectal melanoma: clinical, immunohistology and DNA analysis of 43 cases. Pathology. 2019;51(1):39-45.
143. Postow MA, Luke JJ, Bluth MJ, Ramaiya N, Panageas KS, Lawrence DP, et al. Ipilimumab for patients with advanced mucosal melanoma. Oncologist. 2013;18(6):726-32.
144. Tumeh PC, Hellmann MD, Hamid O, Tsai KK, Loo KL, Gubens MA, et al. Liver Metastasis and Treatment Outcome with Anti-PD-1 Monoclonal Antibody in Patients with Melanoma and NSCLC. Cancer Immunol Res. 2017;5(5):417-24.

145. Forschner A, Battke F, Hadaschik D, Schulze M, Weissgraeber S, Han CT, et al. Tumor mutation burden and circulating tumor DNA in combined CTLA-4 and PD-1 antibody therapy in metastatic melanoma - results of a prospective biomarker study. J Immunother Cancer. 2019;7(1):180.
146. Pires da Silva I, Lo S, Quek C, Gonzalez M, Carlino MS, Long GV, et al. Site-specific response patterns, pseudoprogression, and acquired resistance in patients with melanoma treated with ipilimumab combined with anti-PD-1 therapy. Cancer. 2020;126(1):86-97.
147. Champiat S, Dercle L, Ammari S, Massard C, Hollebecque A, Postel-Vinay S, et al. Hyperprogressive Disease Is a New Pattern of Progression in Cancer Patients Treated by Anti-PD-1/PD-L1. Clinical cancer research : an official journal of the American Association for Cancer Research. 2017;23(8):1920-8.
148. Leach DR, Krummel MF, Allison JP. Enhancement of antitumor immunity by CTLA-4 blockade. Science. 1996;271(5256):1734-6.
149. Koebel CM, Vermi W, Swann JB, Zerafa N, Rodig SJ, Old LJ, et al. Adaptive immunity maintains occult cancer in an equilibrium state. Nature. 2007;450(7171):903-7.
150. Okazaki T, Chikuma S, Iwai Y, Fagarasan S, Honjo T. A rheostat for immune responses: the unique properties of PD-1 and their advantages for clinical application. Nat Immunol. 2013;14(12):1212-8.
151. Tumeh PC, Harview CL, Yearley JH, Shintaku IP, Taylor EJ, Robert L, et al. PD-1 blockade induces responses by inhibiting adaptive immune resistance. Nature. 2014;515(7528):568-71.
152. Twyman-Saint Victor C, Rech AJ, Maity A, Rengan R, Pauken KE, Stelekati E, et al. Radiation and dual checkpoint blockade activate non-redundant immune mechanisms in cancer. Nature. 2015;520(7547):373-7.
153. Topalian SL, Drake CG, Pardoll DM. Immune checkpoint blockade: a common denominator approach to cancer therapy. Cancer Cell. 2015;27(4):450-61.
154. Kroemer G, Senovilla L, Galluzzi L, Andre F, Zitvogel L. Natural and therapy-induced immunosurveillance in breast cancer. Nat Med. 2015;21(10):1128-38.
155. Blank CU, Haanen JB, Ribas A, Schumacher TN. CANCER IMMUNOLOGY. The "cancer immunogram". Science. 2016;352(6286):658-60.
156. Tran E, Robbins PF, Rosenberg SA. 'Final common pathway' of human cancer immunotherapy: targeting random somatic mutations. Nat Immunol. 2017;18(3):255-62.
157. Ribas A, Wolchok JD. Cancer immunotherapy using checkpoint blockade. Science. 2018;359(6382):1350-5.
158. Pommier A, Anaparthy N, Memos N, Kelley ZL, Gouronnec A, Yan R, et al. Unresolved endoplasmic reticulum stress engenders immune-resistant, latent pancreatic cancer metastases. Science. 2018;360(6394).
159. Galon J, Costes A, Sanchez-Cabo F, Kirilovsky A, Mlecnik B, Lagorce-Pages C, et al. Type, density, and location of immune cells within human colorectal tumors predict clinical outcome. Science. 2006;313(5795):1960-4.
160. Rocken M. Early tumor dissemination, but late metastasis: insights into tumor dormancy. J Clin Invest. 2010;120(6):1800-3.
161. Sosa MS, Bragado P, Aguirre-Ghiso JA. Mechanisms of disseminated cancer cell dormancy: an awakening field. Nat Rev Cancer. 2014;14(9):611-22.
162. Perez-Mancera PA, Young AR, Narita M. Inside and out: the activities of senescence in cancer. Nat Rev Cancer. 2014;14(8):547-58.
163. Pollard JW. Defining Metastatic Cell Latency. N Engl J Med. 2016;375(3):280-2.
164. Massague J, Obenauf AC. Metastatic colonization by circulating tumour cells. Nature. 2016;529(7586):298-306.
165. Aguirre-Ghiso JA. How dormant cancer persists and reawakens. Science. 2018;361(6409):1314-5.
166. Schreiber RD, Old LJ, Smyth MJ. Cancer immunoediting: integrating immunity's roles in cancer suppression and promotion. Science. 2011;331(6024):1565-70.

167. Landsberg J, Kohlmeyer J, Renn M, Bald T, Rogava M, Cron M, et al. Melanomas resist T-cell therapy through inflammation-induced reversible dedifferentiation. Nature. 2012;490(7420):412-6.
168. Baumeister SH, Freeman GJ, Dranoff G, Sharpe AH. Coinhibitory Pathways in Immunotherapy for Cancer. Annu Rev Immunol. 2016;34:539-73.
169. Patel SJ, Sanjana NE, Kishton RJ, Eidizadeh A, Vodnala SK, Cam M, et al. Identification of essential genes for cancer immunotherapy. Nature. 2017;548(7669):537-42.
170. Pan D, Kobayashi A, Jiang P, Ferrari de Andrade L, Tay RE, Luoma AM, et al. A major chromatin regulator determines resistance of tumor cells to T cell-mediated killing. Science. 2018;359(6377):770-5.
171. Ferrari de Andrade L, Tay RE, Pan D, Luoma AM, Ito Y, Badrinath S, et al. Antibody-mediated inhibition of MICA and MICB shedding promotes NK cell-driven tumor immunity. Science. 2018;359(6383):1537-42.
172. Milanovic M, Fan DNY, Belenki D, Dabritz JHM, Zhao Z, Yu Y, et al. Senescence-associated reprogramming promotes cancer stemness. Nature. 2018;553(7686):96-100.
173. Muller-Hermelink N, Braumuller H, Pichler B, Wieder T, Mailhammer R, Schaak K, et al. TNFR1 signaling and IFN-gamma signaling determine whether T cells induce tumor dormancy or promote multistage carcinogenesis. Cancer Cell. 2008;13(6):507-18.
174. Zaretsky JM, Garcia-Diaz A, Shin DS, Escuin-Ordinas H, Hugo W, Hu-Lieskovan S, et al. Mutations Associated with Acquired Resistance to PD-1 Blockade in Melanoma. N Engl J Med. 2016;375(9):819-29.
175. Manguso RT, Pope HW, Zimmer MD, Brown FD, Yates KB, Miller BC, et al. In vivo CRISPR screening identifies Ptpn2 as a cancer immunotherapy target. Nature. 2017;547(7664):413-8.
176. Kammertoens T, Friese C, Arina A, Idel C, Briesemeister D, Rothe M, et al. Tumour ischaemia by interferon-gamma resembles physiological blood vessel regression. Nature. 2017;545(7652):98-102.
177. Ayers M, Lunceford J, Nebozhyn M, Murphy E, Loboda A, Kaufman DR, et al. IFN-gamma-related mRNA profile predicts clinical response to PD-1 blockade. J Clin Invest. 2017;127(8):2930-40.
178. Braumuller H, Wieder T, Brenner E, Assmann S, Hahn M, Alkhaled M, et al. T-helper-1-cell cytokines drive cancer into senescence. Nature. 2013;494(7437):361-5.
179. Sun R, Gao B. Negative regulation of liver regeneration by innate immunity (natural killer cells/interferon-gamma). Gastroenterology. 2004;127(5):1525-39.
180. Kroemer G, Galluzzi L, Kepp O, Zitvogel L. Immunogenic cell death in cancer therapy. Annu Rev Immunol. 2013;31:51-72.
181. Pitt JM, Vetizou M, Daillere R, Roberti MP, Yamazaki T, Routy B, et al. Resistance Mechanisms to Immune-Checkpoint Blockade in Cancer: Tumor-Intrinsic and -Extrinsic Factors. Immunity. 2016;44(6):1255-69.
182. Willimsky G, Blankenstein T. Sporadic immunogenic tumours avoid destruction by inducing T-cell tolerance. Nature. 2005;437(7055):141-6.
183. Campisi J. Aging, cellular senescence, and cancer. Annu Rev Physiol. 2013;75:685-705.
184. Serrano M, Lin AW, McCurrach ME, Beach D, Lowe SW. Oncogenic ras provokes premature cell senescence associated with accumulation of p53 and p16INK4a. Cell. 1997;88(5):593-602.
185. Demaria M, O'Leary MN, Chang J, Shao L, Liu S, Alimirah F, et al. Cellular Senescence Promotes Adverse Effects of Chemotherapy and Cancer Relapse. Cancer Discov. 2017;7(2):165-76.
186. Lee S, Schmitt CA. The dynamic nature of senescence in cancer. Nat Cell Biol. 2019;21(1):94-101.
187. Diaz LA, Jr., Le DT. PD-1 Blockade in Tumors with Mismatch-Repair Deficiency. N Engl J Med. 2015;373(20):1979.
188. Topalian SL, Hodi FS, Brahmer JR, Gettinger SN, Smith DC, McDermott DF, et al. Safety, activity, and immune correlates of anti-PD-1 antibody in cancer. N Engl J Med. 2012;366(26):2443-54.
189. Damsky W, Micevic G, Meeth K, Muthusamy V, Curley DP, Santhanakrishnan M, et al. mTORC1 activation blocks BrafV600E-induced growth arrest but is insufficient for melanoma formation. Cancer Cell. 2015;27(1):41-56.

190. Dhomen N, Reis-Filho JS, da Rocha Dias S, Hayward R, Savage K, Delmas V, et al. Oncogenic Braf induces melanocyte senescence and melanoma in mice. Cancer Cell. 2009;15(4):294-303.
191. Liu D, Jenkins RW, Sullivan RJ. Mechanisms of Resistance to Immune Checkpoint Blockade. Am J Clin Dermatol. 2019;20(1):41-54.
192. O'Donnell JS, Long GV, Scolyer RA, Teng MW, Smyth MJ. Resistance to PD1/PDL1 checkpoint inhibition. Cancer Treat Rev. 2017;52:71-81.
193. Johnson DB, Frampton GM, Rioth MJ, Yusko E, Xu Y, Guo X, et al. Targeted Next Generation Sequencing Identifies Markers of Response to PD-1 Blockade. Cancer Immunol Res. 2016;4(11):959-67.
194. Hugo W, Zaretsky JM, Sun L, Song C, Moreno BH, Hu-Lieskovan S, et al. Genomic and Transcriptomic Features of Response to Anti-PD-1 Therapy in Metastatic Melanoma. Cell. 2017;168(3):542.
195. Shin DS, Zaretsky JM, Escuin-Ordinas H, Garcia-Diaz A, Hu-Lieskovan S, Kalbasi A, et al. Primary Resistance to PD-1 Blockade Mediated by JAK1/2 Mutations. Cancer Discov. 2017;7(2):188-201.
196. Snyder A, Makarov V, Merghoub T, Yuan J, Zaretsky JM, Desrichard A, et al. Genetic basis for clinical response to CTLA-4 blockade in melanoma. N Engl J Med. 2014;371(23):2189-99.

Danksagung

Ich danke Olaf Rieß für die Möglichkeit meine wissenschaftlichen Fähigkeiten im Rahmen der Promotion unter Beweis zu stellen. Danke für das Vertrauen, die Unterstützung und die immer offene Tür für Fragen und stets gute und anregende Diskussionen.

Mein besonderer Dank gilt Christopher Schroeder für seine außerordentliche Unterstützung und sein Vertrauen in mich. Danke für die fantastische Zusammenarbeit und die langen und konspirativen Unterhaltungen in den Abendstunden im Flur der Klinik.

Darüber hinaus gilt mein Dank dem gesamten Diagnostikteam nter der Leitung von Tobias Haack sowie der Bioinformatik unter der Leitung von Stephan Ossowski. Ganz besonders bedanken möchte ich mich bei Beate Kootz, für ihre Geduld und Hilfe im Labor. Ferner danke ich meinen Koautoren aus der Universitäts-Hautklinik Tübingen, Universitätsklinik für Radioonkologie Tübingen und dem Institut für Pathologie und Neuropathologie Tübingen.

Ich danke meiner Familie für Ihre Hilfe und Unterstützung.

Anhang

a) Akzeptierte Publikationen

Kerstin Zwirner, **Franz J Hilke**, German Demidov, Stephan Ossowski, Cihan Gani, Olaf Rieß, Daniel Zips, Stefan Welz, Christopher Schroeder. *"Circulating Cell-Free DNA: A Potential Biomarker to Differentiate Inflammation and Infection During Radiochemotherapy"*, Radiother Oncol, 129 (3), 575-581 Dec 2018

Andrea Forschner, **Franz-Joachim Hilke**, Irina Bonzheim, Axel Gschwind, German Demidov, Teresa Amaral, Stephan Ossowski, Olaf Riess, Christopher Schroeder, Peter Martus, Bernhard Klumpp, Irene Gonzalez-Menendez, Claus Garbe, Heike Niessner, Tobias Sinnberg. *"MDM2, MDM4 and EGFR Amplifications and Hyperprogression in Metastatic Acral and Mucosal Melanoma"*, Cancers (Basel), 12 (3) 2020 Feb 26

Ellen Brenner, Barbara F Schörg, Fatima Ahmetlić, Thomas Wieder, **Franz Joachim Hilke**, Nadine Simon, Christopher Schroeder, German Demidov, Tanja Riedel, Birgit Fehrenbacher, Martin Schaller, Andrea Forschner, Thomas Eigentler, Heike Niessner, Tobias Sinnberg, Katharina S Böhm, Nadine Hömberg, Heidi Braumüller, Daniel Dauch, Stefan Zwirner, Lars Zender, Dominik Sonanini, Albert Geishauser, Jürgen Bauer, Martin Eichner, Katja J Jarick, Andreas Beilhack, Saskia Biskup, Dennis Döcker, Dirk Schadendorf, Leticia Quintanilla-Martinez, Bernd J Pichler, Manfred Kneilling, Ralph Mocikat, Martin Röcken. *"Cancer Immune Control Needs Senescence Induction by Interferon-Dependent Cell Cycle Regulator Pathways in Tumours"*, Nat Commun, 11 (1), 1335 2020 Mar 12

b) Eingereichte Manuskripte

Franz J. Hilke*, Francesc Muyas*, Jakob Admard, Beate Kootz, Dominik Nann, Stefan Welz, Olaf Rieß, Daniel Zips, Stephan Ossowski, Christopher Schroeder, Kerstin Clasen. "*Dynamics of cell-free tumour DNA correlate with treatment response of head and neck cancer patients receiving radiochemotherapy"*, Radiother Oncol (major revision)

c) Noch nicht eingereichte Manuskripte

Franz J. Hilke, T. Sinnberg, A. Gschwind, H. Niessner, G. Demidov, T. Amaral, S. Ossowski, I. Bonzheim, O. Riess, C. Garbe, C. Schroeder, A. Forschner. *"Next-generation sequencing in a real world cohort of 82 advanced melanoma patients identifies distinct mutation pattern in different melanoma subtypes"*

Radiotherapy and Oncology xxx (2018) xxx–xxx

Contents lists available at ScienceDirect

Radiotherapy and Oncology

journal homepage: www.thegreenjournal.com

Original article

Circulating cell-free DNA: A potential biomarker to differentiate inflammation and infection during radiochemotherapy

Kerstin Zwirner [a,*], Franz J. Hilke [b], German Demidov [b], Stephan Ossowski [b,c], Cihan Gani [a,d], Olaf Rieß [b], Daniel Zips [a,d], Stefan Welz [a,d], Christopher Schroeder [b]

[a] Department of Radiation Oncology, Medical Faculty and University Hospital, Eberhard Karls University; [b] Institute of Medical Genetics and Applied Genomics, Medical Faculty and University Hospital, Eberhard Karls University, Tübingen, Germany; [c] Centre for Genomic Regulation (CRG), The Barcelona Institute of Science and Technology, Spain; [d] German Cancer Consortium (DKTK), German Cancer Research Center (DKFZ) partner site Tübingen, Germany

ARTICLE INFO

Article history:
Received 8 May 2018
Received in revised form 11 June 2018
Accepted 18 July 2018
Available online xxxx

Keywords:
Cell-free nucleic acids
Liquid biopsy
Radiotherapy
Toxicity
Infection
Granulocyte colony-stimulating factor

ABSTRACT

Background and purpose: Radiochemotherapy is a standard treatment option for patients with head and neck cancer (HNSCC). During radiation, local toxicities are common and need to be differentiated from infections. As levels of circulating cell-free DNA (cfDNA) are known to be elevated during infections, cfDNA might complement clinical parameters. The aim of the study was to investigate the dynamics of cfDNA during radiochemotherapy.

Material and methods: In total, 78 blood samples of 20 patients with HNSCC were analysed in this prospective biomarker study. Blood samples were taken before and during treatment. CfDNA levels were quantified fluorometrically and results were compared to laboratory and clinical parameters.

Results: Elevated cfDNA levels were associated with the pre-treatment volumes of lymph node metastases ($p = 0.0002$), gastrostomy tube placement (20.23 ng/ml vs. 9.04 ng/ml (median), $p = 0.025$), the application of antibiotics (16.47 ng/ml vs. 9.04 ng/ml, $p = 0.006$) and manifest infections (16.81 ng/ml vs. 9.04 ng/ml, $p = 0.010$). Furthermore, a significant difference between moderate inflammation (radiation-induced toxicity RTOG grade 2–3) and manifest infections could be observed (8.97 ng/ml vs. 16.81 ng/ml, $p = 0.014$), allowing for a more pronounced differentiation than by CRP levels ($p = 0.119$). There might be an association between the application of G-CSF and elevated cfDNA levels.

Conclusion: CfDNA levels are correlated with infections during radiochemotherapy and could represent an informative complemental biomarker to drive therapeutic decision-making.

Estimated levels of circulating cell-free tumour DNA (ctDNA) in plasma should be interpreted cautiously when monitoring tumour outcome by next-generation-sequencing, as confounders like infections or drug application might influence the fraction of ctDNA in total cfDNA.

© 2018 Elsevier B.V. All rights reserved. Radiotherapy and Oncology xxx (2018) xxx–xxx

In locally advanced head and neck squamous cell carcinomas (HNSCC), the standard of care implies primary radiotherapy and concomitant chemotherapy [1]. Especially if concomitant chemotherapy is applied, differentiation between radiation-induced toxicity like dermatitis and mucositis – in terms of inflammation – and manifestation of serious (e.g. bacterial) infections is crucial. Clinical visitations of the patients do not always allow differentiation of inflammation versus early infection, although this distinction is essential to assess the need for administration of antibiotic drugs or the applicability of chemotherapy.

An established parameter addressing inflammation and infection is the C-reactive protein (CRP), which is an acute-phase reactant. However, a wide range of conditions can cause elevated CRP levels [2]. Furthermore, alterations of the white blood cell count are commonly used as markers of inflammatory response. Hereby, leucocytosis as well as leucopenia might be associated with infection or sepsis [3]. Yet, additional biomarkers would be valuable to improve the differentiation of toxicity and severe infections in radiation oncology and to drive therapeutic decision-making.

In cancer patients, tumour derived DNA fragments with distinct somatic mutations are shed into the blood. Therefore, the fraction of circulating cell-free tumour DNA (ctDNA) in plasma might support therapy surveillance in terms of 'liquid biopsies' as a non-invasive approach [4,5]. Furthermore, a simple blood sample might perspectively facilitate early tumour detection [6], monitoring of response and the detection of resistance mutations due to selective pressure during the course of therapy in multiple kinds of cancer

* Corresponding author at: Department of Radiation Oncology, Medical Faculty and University Hospital, Eberhard Karls University of Tübingen, Hoppe-Seyler-Straße 3, D-72076 Tübingen, Germany.
E-mail address: Kerstin.Zwirner@med.uni-tuebingen.de (K. Zwirner).

https://doi.org/10.1016/j.radonc.2018.07.016
0167-8140/© 2018 Elsevier B.V. All rights reserved.

Please cite this article in press as: Zwirner K et al. Circulating cell-free DNA: A potential biomarker to differentiate inflammation and infection during radiochemotherapy. Radiother Oncol (2018), https://doi.org/10.1016/j.radonc.2018.07.016

[7]. However, the amount of ctDNA as subset of total cell-free DNA (cfDNA) varies owing to tumour characteristics like size, state and organ of origin and often constitutes a relatively small portion of the total cfDNA in solid tumours and limited disease [4,7–11]. Thus, in most oncologic patients – except of distinct advanced metastatic diseases – the major fraction of cfDNA stems from normal cells [12–14]. CfDNA fragments are mainly released by apoptosis, necrosis or secretion. Thus, cfDNA levels are increased in inflammatory states, trauma, stroke and sepsis [8]. A review by Frank M.O. (2016) suggests an ascent of cfDNA levels due to various clinical conditions: lowest cfDNA levels were measured in chronic inflammation (diabetes mellitus type 2, epilepsy, coronary artery disease, elderly patients), elevated levels in acute inflammation (second degree burns, severe trauma, myocardial infarction) and highest cfDNA levels were found in severe infections (bacteria-related sepsis, hanta virus infection) [15].

The purpose of this study was to investigate if the total amount of cfDNA levels of HNSCC patients, before and during radiochemotherapy, could be an additional biomarker for monitoring inflammation (moderate toxicity) and severe infections.

Materials and methods

This pilot biomarker study investigated 20 patients with locally advanced HNSCC receiving primary radiochemotherapy. All patients declared their informed consent and the study was approved by the local ethics committee (577/2014BO2).

Therapy

Radiotherapy was applied five to six times per week with a cumulative dose of 70–77 Gy. All patients were treated with concomitant chemotherapy and received a percutaneous endoscopic gastrostomy (PEG) before therapy or during the first weeks of treatment for supportive care.

Blood samples

Blood samples for cfDNA measurement were collected prior to therapy (t1 at day −15 to 0) and three times during radiochemotherapy: t2 at the beginning of treatment (day 4–7), t3 during the third week of therapy (day 20–23) and t4 at the end of irradiation (day 37–40). The time line is presented in Fig. 1. Additionally, corresponding routine laboratory values (CRP and leucocytes) were investigated.

cfDNA

We collected peripheral blood samples in EDTA tubes (Sarstedt, Nümbrecht, Germany) to analyse cfDNA. The cfDNA samples were processed within two hours of collection and centrifuged twice for ten minutes for plasma isolation and reliable separation of residual blood cells. After storage at −20 °C, cfDNA was extracted by QIAmp Circulating Nucleic Acid Kit (Qiagen, Hilden, Germany), quantified by Qubit fluorescence method (Thermo Fischer Scientific, Waltham, USA) following the manufacturer's instructions and normalised by plasma volume. The modified FAST-SeqS method (mFAST-SeqS) [16] was used to estimate the fraction of ctDNA in the plasma samples (t1 and t4).

Clinical parameters

Based on clinical reports, we documented the date of gastrostomy placement, application of antibiotics, inpatient and outpatient treatments, toxicity according to the Radiation Therapy Oncology Group (RTOG) grading and clinically manifest infections. As all patients received a PEG placement, mostly accompanied with inpatient status and prophylactic antibiotic treatment, this constellation was evaluated separately if gastrostomy applied within three days before cfDNA sampling. All other cfDNA measurements were done separately from the gastrostomy. Gross tumour volumes (GTVs) of the primary tumours as well as the volumes of the lymph node metastases were extracted from the computed tomography-based delineations for treatment planning. Human papillomavirus (HPV) status was assessed by PCR-based assays or p16 immunohistochemical staining in 19 patients. In one patient the data was missing.

Definition baseline – moderate inflammation – manifest infection

The baseline was defined by cancer diagnosis (chronic inflammation). Therefore, all samples that were collected without correlating significant toxicity (≤RTOG grade 1) or manifest infection were defined as baseline. Moderate inflammation was defined by mucosal or dermal toxicity RTOG grade 2 or 3. Manifest infection was defined in two ways. At first, a strict definition was used. The infection had to be clinically manifest by symptoms (e.g. fever) *and* complemented by at least one of the following criteria: microbiologically confirmed infection *or* application of antibiotics for infection. For the second, a relaxed definition of infection was used. We also included four measurements linked to oral swelling after dental management (extractions), thrombophlebitis after chemotherapy (requiring local treatment), local PEG infection (candida species), and – in one case – abnormal severe local toxicity of bleeding dermatitis and mucositis (RTOG grade 4), wherefore the radiotherapy had to be paused. These four constellations were excluded from statistical analysis of biomarkers during infection, according to the strict definition, but included in the extended infection definition.

Statistics

Statistics were calculated using R. Since sample sizes were small and we could not rely on normality of random variables,

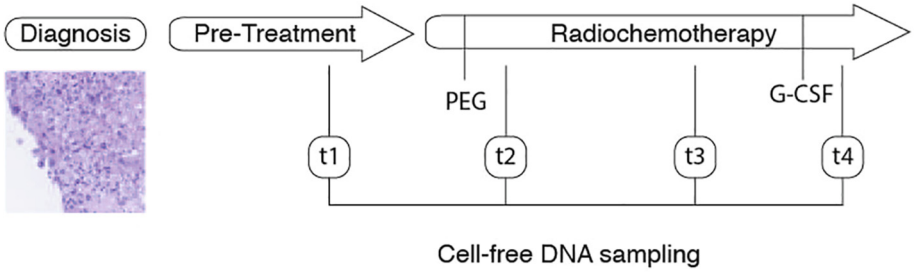

Fig. 1. Timeline of therapy (t1–t4) and measurements of circulating cell-free DNA (cfDNA) and other laboratory values in blood samples. Inclusion criteria implied histologically proven head and neck squamous cell carcinomas (HNSCC). Percutaneous endoscopic gastrostomy (PEG) was mainly performed during the first week of treatment. Four patients received granulocyte-colony stimulating factor (G-CSF) treatment before cfDNA measurement (t4).

Please cite this article in press as: Zwirner K et al. Circulating cell-free DNA: A potential biomarker to differentiate inflammation and infection during radiochemotherapy. Radiother Oncol (2018), https://doi.org/10.1016/j.radonc.2018.07.016

we used the Mann–Whitney U test and the Kruskal–Wallis test. Level of significance was defined as alpha = 0.05. We used the Neumann–Pearson framework and rejected null hypothesis when the level of significance was reached. One-sided alternative was used when the direction of the effect was a priori known. Principal component analysis (PCA) and T-distributed stochastic neighbour embedding (t-SNE) [17] were used for data visualisation. Robust linear regression (M-estimator) from MASS R package was used to investigate cfDNA levels and tumour volumes. Logarithmic scale was chosen to satisfy the assumptions of the linear model. The robust *F*-test (Wald test) was used for estimations of significance of regression coefficients (sfsmisc R package).

Results

Blood samples were taken four times from each of the 20 patients, whereby 78 measurements were suitable for analysis of cfDNA. Two drop-outs were due to procedure delay and failed timing. CtDNA fractions were below the approximate 10% detection limit of mFAST-SeqS (further information is shown in the appendix). Corresponding CRP parameters were available for 49 samples. The relation between cfDNA and CRP levels is shown in the appendix (Fig. A.1A, B).

CfDNA levels varied considerably (range: 2.89–172.90 ng/ml). Two measurements were outstanding: 83.05 ng/ml and 172.90 ng/ml. Clinical data of these two samples suggested a relationship to the application of granulocyte-colony stimulating factor (G-CSF) for neutropenia. G-CSF was injected one and two days before cfDNA measurement for the highest value (172.90 ng/ml) and eight and nine days before the second outstanding measurement (83.05 ng/ml). Two further patients were treated with G-CSF 12 and 13 days before cfDNA measurement, whereby the levels were 21.49 ng/ml and 9.12 ng/ml. The distribution of cfDNA levels that are time-related to G-CSF applications are shown in Table 1 and Fig. 2A, B. As G-CSF could not be ruled out as a confounder, these four measurements were not included in the following analysis. However, analysis of a larger cohort of patients treated with G-CSF is necessary to validate the observed correlation with cfDNA levels ($p = 0.038$).

Next, we investigated the dependences between the measurements of cfDNA/CRP and PEG placement, antibiotic treatment and inpatient status (Table 1 and Fig. 3). CfDNA levels within three days after PEG placement were significantly elevated compared to measurements taken before PEG placement or after a longer interval (t1 and t2 included; Fig. 3A, $p = 0.025$). We observed a similar association between PEG treatment and CRP values (Fig. 3B, $p = 0.026$). Therefore, we conclude that PEG treatment is likely influencing cfDNA and CRP levels and should be considered as a confounder for correlating the biomarkers with inflammation and infection. Hence, we excluded measurements taken within three days of PEG placement in the following analysis.

Using the remaining measurements, cfDNA levels and CRP values were significantly elevated in patients treated with antibiotics (prophylactic treatment excluded) compared to patients without simultaneous antibiotic medication (Fig. 3C, D, $p = 0.006$ and $p = 0.001$). Excluding gastrostomy-associated hospitalisation, no significant relationship between inpatient status and elevated cfDNA levels could be found (Fig. 3E). In contrast, CRP levels showed a significant association with inpatient status (Fig. 3F, $p = 0.031$).

Furthermore, we investigated relations of cfDNA, CRP and leucocyte values with chronic inflammation (baseline: RTOG grade 0–1), moderate inflammation (dermal or mucosal toxicity RTOG grade 2–3) and manifest, severe infection (Table 1 and Fig. 4). CRP values were found to be significantly different between baseline and toxicity (Fig. 4B, $p = 0.029$), whereas cfDNA levels did not show a significant association (Fig. 4A, $p = 0.850$).

Table 1
Measurements of circulating cell-free DNA (cfDNA), C-reactive protein (CRP) and leucocytes in regard to diverse clinical parameters.

G-CSF application	Yes	No	*p*-Value
cfDNA (*median, ng/ml*)	52.27	9.93	0.038
Received PEG within 3 days (t1 and t2)	Yes	No	*p*-Value
cfDNA (*median, ng/ml*)	20.23	9.04	0.025
CRP (*median, mg/dl*)	2.50	0.28	0.026
Antibiotic treatment	Yes	No	*p*-Value
cfDNA (*median, ng/ml*)	16.47	9.04	0.006
CRP (*median, mg/dl*)	9.36	0.85	0.001
Hospitalisation	Inpatient	Outpatient	*p*-Value
cfDNA (*median, ng/ml*)	13.86	9.04	0.133
CRP (*median, mg/dl*)	4.48	0.86	0.031
Ascending inflammation	Baseline	Moderate inflammation	Severe infection (strict)
cfDNA (*median, ng/ml*)	9.04	8.97	16.81
CRP (*median, mg/dl*)	0.48	1.54	8.67
leucocytes (*median, 1/μl*)	7660	3965	8595

Abbreviations: G-CSF – granulocyte-colony stimulating factor; cfDNA – cell-free DNA; PEG – percutaneous endoscopic gastrostomy; t – time of sampling; CRP – C-reactive protein.

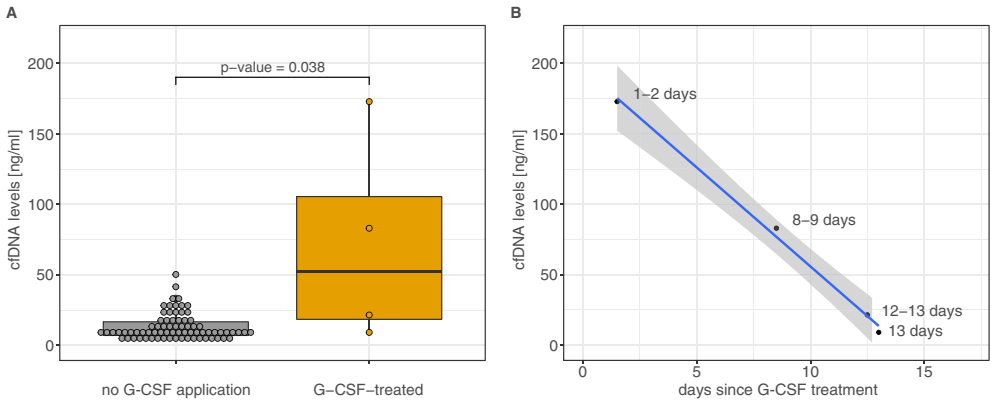

Fig. 2. Effect of granulocyte-colony stimulating factor (G-CSF) on circulating cell-free DNA (cfDNA) levels. (A) cfDNA levels without prior G-CSF treatment compared to measurements after G-CSF application; (B) cfDNA levels and corresponding time interval (days) since G-CSF application.

Please cite this article in press as: Zwirner K et al. Circulating cell-free DNA: A potential biomarker to differentiate inflammation and infection during radiochemotherapy. Radiother Oncol (2018), https://doi.org/10.1016/j.radonc.2018.07.016

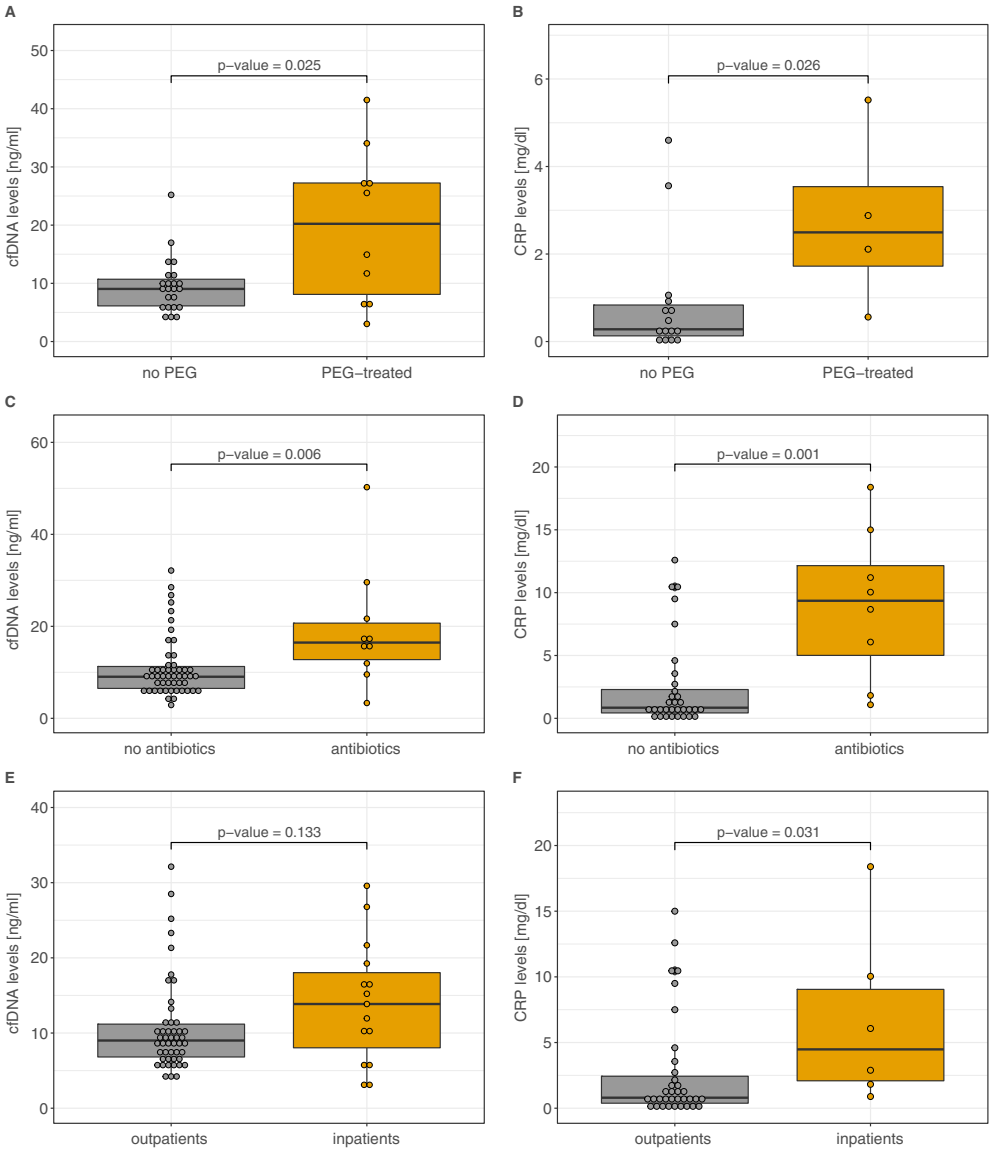

Fig. 3. Relation of biomarkers with other clinical conditions. Samples associated with granulocyte-colony stimulating factor (G-CSF) treatment were excluded. (A) circulating cell-free DNA (cfDNA) measurements in relation to percutaneous endoscopic gastrostomy (PEG) within three days before sampling (t1, t2); (B) C-reactive protein (CRP) values related to PEG placement (t1, t2); (C) cfDNA values of patients not treated with antibiotics vs. contemporaneous antibiotic treatment; (D) CRP levels and corresponding antibiotic treatment; (E) cfDNA measurements in relation to hospitalisation: inpatient vs. outpatient status; (F) CRP values related to hospitalisation.

However, both parameters supported a significant differentiation of baseline and manifest infections by strict definition (CRP: $p = 0.0002$; cfDNA levels: $p = 0.010$). Regarding the distinction between toxicity and severe infection (strict definition), cfDNA showed significantly elevated levels associated with infections ($p = 0.014$), whereas CRP values showed a wide variation for the moderate inflammation group, resulting in a non-significant difference to manifest infections ($p = 0.119$). Using the extended definition of infections changed the results only slightly. All dependences remained similar or increased. Specifically, the cfDNA-based differentiation of baseline and infection as well as toxicity and infection improved (Fig. A. 2A, B). The white blood cell count was found to be significantly different between baseline and toxicity, as lower leucocyte levels correlated with toxicity (Fig. 4C, $p = 0.006$). During manifest infections, levels of white blood cell count were wide spread and included both, leucopenia and leucocytosis.

PCA (Fig. A. 3 and 4 [18]) and t-SNE (Fig. 4D), using cfDNA, CRP and leucocyte levels, show strong clustering of baseline, moderate inflammation and manifest infection groups, indicating that the combined use of biomarkers within a classifier would lead to more accurate differentiation between clinical conditions than with each biomarker alone.

In addition, we correlated the pre-therapeutic cfDNA levels of 18 patients with the corresponding primary tumour volumes, the volumes of the lymph node metastases and the total tumour burden (GTV of the primary tumour + lymph node metastases). Two patients were excluded due to inflammatory conditions at t1. Some patients had comparably small primary tumour volumes but extended lymph node metastases and vice versa. GTV volumes of the primary tumours varied considerably (range 2.2–146.7 ccm^3) but did not show a significant association with cfDNA levels (Fig. 5A, $p = 0.159$). In contrast, volumes of the lymph node metastases (range 1.0–192.8 ccm^3) showed a strong association with cfDNA levels (Fig. 5B, $p = 0.0002$), as extended lymph node metastases correlated with higher cfDNA measurements. The same association was found regarding bigger total tumour burden and elevated cfDNA levels (Fig. 5C, $p = 0.0005$).

Please cite this article in press as: Zwirner K et al. Circulating cell-free DNA: A potential biomarker to differentiate inflammation and infection during radiochemotherapy. Radiother Oncol (2018), https://doi.org/10.1016/j.radonc.2018.07.016

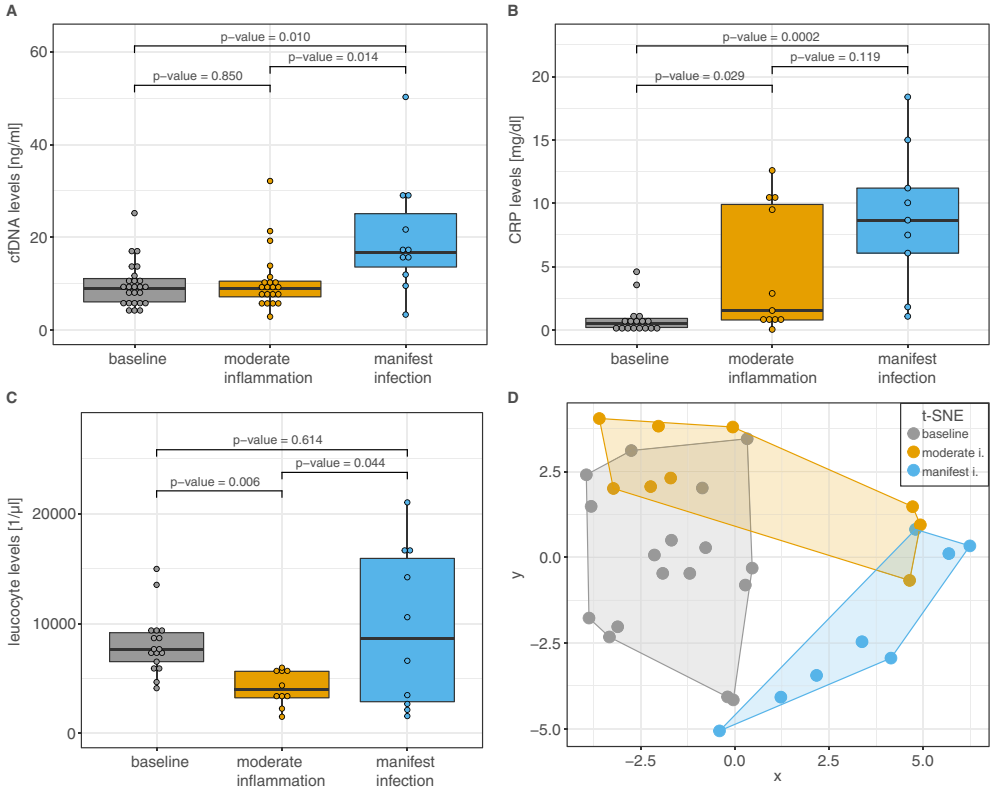

Fig. 4. Differentiation of baseline (chronic inflammation), moderate inflammation (toxicity RTOG grade 2 and 3) and severe infections by (A) circulating cell-free DNA (cfDNA) levels, (B) C-reactive protein (CRP) levels, and (C) white blood cell count. (D) tSNE (unsupervised stochastic nonlinear dimensionality reduction technique) using levels of CRP, cfDNA and leucocytes per patient. Granulocyte-colony stimulating factor (G-CSF) or percutaneous endoscopic gastrostomy (PEG) associated samples were excluded.

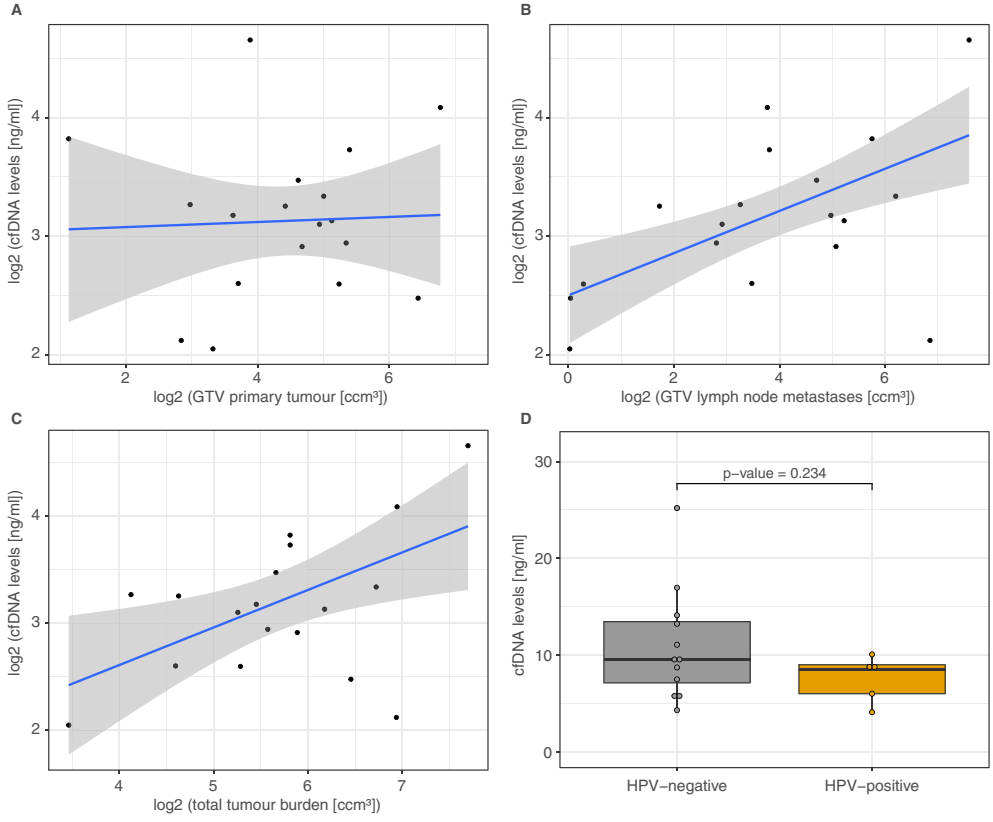

Fig. 5. Association of circulating cell-free DNA (cfDNA) levels with (A) gross tumour volumes (GTVs) of the primary tumours, (B) GTVs of the lymph node metastases, and (C) total tumour burden (primary tumour + lymph node metastases) using a linear regression model and data in log2 scale (the grey area indicates the 95% confidence interval). (D) CfDNA levels in relation to human papilloma virus infection.

Please cite this article in press as: Zwirner K et al. Circulating cell-free DNA: A potential biomarker to differentiate inflammation and infection during radiochemotherapy. Radiother Oncol (2018), https://doi.org/10.1016/j.radonc.2018.07.016

Five patients had HPV-associated tumours. We did not find a significant correlation between the HPV status of the patients and the cfDNA levels at t1 (inflammatory states were excluded; Fig. 5D, $p = 0.234$).

Discussion

The fraction of ctDNA in our plasma samples was shown to be low and we assume that the majority of measured cfDNA originates from non-cancerous cells, which is in line with previous literature [10,11].

Several clinical research studies have reported an influence of inflammation and infection on cfDNA levels [19–22]. Therefore, we investigated the correlation of cfDNA levels with inflammation and infection related parameters over the period of radiochemotherapy.

CfDNA and CRP measurements were significantly increased shortly after PEG placement and during antibiotic treatment for infection, which is in line with the reported influence of severe infections or inflammatory states on these parameters. CRP levels showed a significant association with inpatient status, while cfDNA showed slight, but not significantly elevated levels. This difference might be explained by the observation, that CRP values are also elevated by radiation-induced toxicity, whereas cfDNA levels were not affected by toxicity. Common reasons for hospitalisation imply either supportive care (toxicity support, parenteral nutrition, infusions or pain medication) or infection treatment. As CRP seems to reflect both states, it might be more clearly related to hospitalisation than cfDNA levels.

Based on a recent review [15] suggesting a potential gradient of cfDNA following the severity of inflammation, we defined three levels of inflammation with regard to radiotherapy: chronic inflammation (baseline), moderate acute inflammation (toxicity RTOG grade 2 and 3) and manifest, severe infection. Especially, the differentiation between toxicity-related inflammation and severe infection is of relevance for clinical decision-making. Therefore, additional biomarkers addressing this issue would be valuable. In our cohort, no difference of cfDNA levels between baseline and toxicity was observed, whereas a strong distinction was found between toxicity and manifest infection. These findings were robust to both, strict and extended criteria of clinical infection.

In contrast, CRP levels seem to be more sensitive to differentiate baseline and moderate inflammation, whereas distinction between toxicity and infection was not as strong as by cfDNA. One could speculate that CRP reacts more sensitive to toxicity than cfDNA levels, and therefore the differentiation of infections (and isochronal toxicity) might be less specific than by cfDNA levels. This would be in line with the findings of Moreira et al. (2010), who report on cfDNA as a valuable marker for the severity of infection, as levels increased proportional to the systemic reaction on infection [23]. The diagnostic efficiency as an infection marker was found to be superior to CRP levels.

However, the limitation of our findings is the smaller number of related CRP measurements compared to the cfDNA samples, which might influence significance levels.

Additionally, the white blood cell count was correlated with toxicity and infections, but appears to have a different dynamic than cfDNA and CRP, as leucopenia is a common side effect of chemotherapy [24]. Lowest levels were observed when patients presented with toxicity and had received chemotherapy. Manifest infections could be associated with both, leucopenia or leucocytosis, which is consistent with common sepsis criteria.

CRP, white blood cell count and cfDNA individually represent a valuable biomarker of inflammation and infection monitoring. Moreover, we found that these biomarkers complement each other due to slightly different trajectories in response to side effects of treatment or infections, as demonstrated by PCA and t-SNE analysis. Hence, combining cfDNA, CRP and leucocyte levels in a classification model has the potential to improve distinction between baseline, toxicity and manifest infection states.

Limitations of our study are the relatively small cohort size, the limited number of samples and multiple confounding factors affecting cfDNA levels. Therefore, further studies on this issue are required.

Interestingly, extended volumes of lymph node metastases correlated significantly with elevated pre-therapeutic cfDNA levels while the volume of primary tumours did not show an association. The total tumour burden (GTV of the primary tumour + GTV of the lymph node metastases) correlated with cfDNA levels as well, which is likely explained by the strong effect of the lymph node metastases' volumes. As the ctDNA fractions of our samples were below the detection limit of mFAST-SeqS, the majority of cfDNA likely originated from normal cells. Therefore, the content of tumour DNA is not sufficient to explain associations with lymph node metastases volumes. Relatively small primary tumours with big lymph node metastases might behave differently from bigger primary tumours with only small lymph node metastases. The different associations of metastatic lymph node volumes and the primary tumour volumes with cfDNA levels could therefore reflect the diverse biology of tumours (for example in regards of vascularization, immunogenicity, necrosis, et cetera), while the exact underlying mechanisms are not elucidated, yet.

In case of chemotherapy-induced (febrile) neutropenia, treatment with G-CSF is well established [25]. G-CSF promotes the formation and release of leucocytes (mainly neutrophils) [26,27]. In two cases, we found exceptionally elevated levels of cfDNA that were time-related to the application of G-CSF. Two more patients received G-CSF before cfDNA measurement, showing values within the common range. This might be due to a comparably longer time interval since G-CSF application (12 and 13 days) and pharmacodynamics. G-CSF as a potentially confounding factor of cfDNA levels is an interesting finding and in line with a recent publication that investigated this effect in histone-complexed DNA (hcDNA) levels of healthy volunteers [28]. Blood levels of hcDNA increased significantly after application of G-CSF. Thus, there might be causality between application of G-CSF and elevated cfDNA levels, but further investigation is required to confirm this hypothesis and to elucidate the underlying mechanisms.

Liquid biopsy and the sequencing of ctDNA for monitoring cancer treatment promises to revolutionise clinical practice. Our findings indicate that various confounders like severe infection, PEG placement or drugs influence cfDNA levels during cancer treatment. Therefore, ctDNA/cfDNA ratio-based measures of tumour-load can be biased and dynamics might not accurately predict treatment response. As measuring absolute levels of ctDNA remains technically challenging, confounding factors should be taken into account when interpreting ctDNA/cfDNA dynamics.

Conclusion

Our findings indicate that various factors influence cfDNA levels during cancer treatment. On the one hand, cfDNA might complement CRP, leucocytes and clinical visitations as a valuable biomarker addressing infections. On the other hand, ctDNA dynamics and ratio estimations during treatment monitoring should be interpreted with caution as confounders increasing normal DNA levels need to be considered.

Please cite this article in press as: Zwirner K et al. Circulating cell-free DNA: A potential biomarker to differentiate inflammation and infection during radiochemotherapy. Radiother Oncol (2018), https://doi.org/10.1016/j.radonc.2018.07.016

Funding

This work was supported by the "Stiftung Tumorforschung Kopf-Hals" in Wiesbaden, Germany and K. Zwirner is supported by the intramural Fortüne/PATE Program of the Medical Faculty, Eberhard Karls University of Tübingen (Funding number: 2447-0-0).

Role of funding source

The "Stiftung Tumorforschung Kopf-Hals" supported this project by a grant to finance the material expenses for the genetic analyses. The PATE Program funded the applicant's own position (50%). The study concept was designed independently of our funding sources. The collection, analysis or interpretation of data was not influenced by the funders in any way.

Conflicts of interest

None.

Appendix A. Supplementary data

Supplementary data associated with this article can be found, in the online version, at https://doi.org/10.1016/j.radonc.2018.07.016.

References

[1] Pignon JP, le Maitre A, Maillard E, Bourhis J. Group M-NC. Meta-analysis of chemotherapy in head and neck cancer (MACH-NC): an update on 93 randomised trials and 17,346 patients. Radiother Oncol 2009;92:4–14.
[2] Volanakis JE. Human C-reactive protein: expression, structure, and function. Mol Immunol 2001;38:189–97.
[3] Aird WC. The hematologic system as a marker of organ dysfunction in sepsis. Mayo Clin Proc 2003;78:869–81.
[4] Schmidt H, Kulasinghe A, Kenny L, Punyadeera C. The development of a liquid biopsy for head and neck cancers. Oral Oncol 2016;61:8–11.
[5] Rave-Frank M. Tumour-derived plasma cell-free DNA in patients with head and neck cancer: A short review. Cancer Radiother 2017;21:554–6.
[6] Cohen JD, Li L, Wang Y, Thoburn C, Afsari B, Danilova L, et al. Detection and localization of surgically resectable cancers with a multi-analyte blood test. Science 2018;359:926–30.
[7] Bettegowda C, Sausen M, Leary RJ, Kinde I, Wang Y, Agrawal N, et al. Detection of circulating tumor DNA in early- and late-stage human malignancies. Sci Transl Med 2014;6:224ra24.
[8] Schwarzenbach H, Hoon DS, Pantel K. Cell-free nucleic acids as biomarkers in cancer patients. Nat Rev Cancer 2011;11:426–37.
[9] Cree IA, Uttley L, Buckley Woods H, Kikuchi H, Reiman A, Harnan S, et al. The evidence base for circulating tumour DNA blood-based biomarkers for the early detection of cancer: a systematic mapping review. BMC Cancer 2017;17:697.
[10] Rostami A, Bratman SV. Utilizing circulating tumour DNA in radiation oncology. Radiother Oncol 2017;124:357–64.
[11] Heitzer E, Ulz P, Geigl JB. Circulating tumor DNA as a liquid biopsy for cancer. Clin Chem 2015;61:112–23.
[12] Underhill HR, Kitzman JO, Hellwig S, Welker NC, Daza R, Baker DN, et al. Fragment length of circulating tumor DNA. PLoS Genet 2016;12:e1006162.
[13] Husain H, Velculescu VE. Cancer DNA in the circulation: the liquid biopsy. JAMA 2017;318:1272–4.
[14] Newman AM, Bratman SV, To J, Wynne JF, Eclov NCW, Modlin LA, et al. An ultrasensitive method for quantitating circulating tumor DNA with broad patient coverage. Nat Med 2014;20:552–8.
[15] Frank MO. Circulating cell-free DNA differentiates severity of inflammation. Biol Res Nurs 2016;18:477–88.
[16] Belic J, Koch M, Ulz P, Auer M, Gerhalter T, Mohan S, et al. Rapid Identification of Plasma DNA Samples with Increased ctDNA Levels by a modified FAST-SeqS approach. Clin Chem 2015;61:838–49.
[17] van der Maaten L, Hinton G. Visualizing data using t-SNE. J Machine Learning Res 2008;9:2579–605.
[18] Sugiyama M. Local Fisher discriminant analysis for supervised dimensionality reduction. ICML '06 Proceedings of the 23rd international conference on Machine learning; 2006:905–12.
[19] Altrichter J, Zedler S, Kraft R, Faist E, Mitzner SR, Sauer M, et al. Neutrophil-derived circulating free DNA (cf-DNA/NETs), a potential prognostic marker for mortality in patients with severe burn injury. Eur J Trauma Emerg Surg 2010;36:551–7.
[20] Margraf S, Logters T, Reipen J, Altrichter J, Scholz M, Windolf J. Neutrophil-derived circulating free DNA (cf-DNA/NETs): a potential prognostic marker for posttraumatic development of inflammatory second hit and sepsis. Shock 2008;30:352–8.
[21] Huttunen R, Kuparinen T, Jylhava J, Aittoniemi J, Vuento R, Huhtala H, et al. Fatal outcome in bacteremia is characterized by high plasma cell free DNA concentration and apoptotic DNA fragmentation: a prospective cohort study. PLoS One 2011;6:e21700.
[22] Jylhava J, Nevalainen T, Marttila S, Jylha M, Hervonen A, Hurme M. Characterization of the role of distinct plasma cell-free DNA species in age-associated inflammation and frailty. Aging Cell 2013;12:388–97.
[23] Moreira VG, Prieto B, Rodriguez JS, Alvarez FV. Usefulness of cell-free plasma DNA, procalcitonin and C-reactive protein as markers of infection in febrile patients. Ann Clin Biochem 2010;47:253–8.
[24] Lustberg MB. Management of neutropenia in cancer patients. Clin Adv Hematol Oncol 2012;10:825–6.
[25] Aapro MS, Bohlius J, Cameron DA, Dal Lago L, Donnelly JP, Kearney N, et al. 2010 update of EORTC guidelines for the use of granulocyte-colony stimulating factor to reduce the incidence of chemotherapy-induced febrile neutropenia in adult patients with lymphoproliferative disorders and solid tumours. Eur J Cancer 2011;47:8–32.
[26] Dale DC. Colony-stimulating factors for the management of neutropenia in cancer patients. Drugs 2002;62:1–15.
[27] Kraj L, Krawczyk-Lipiec J, Gorniewska J, Orlik G. Efficacy and safety of biosimilar filgrastim in primary and secondary prevention of febrile neutropenia. Biomed Rep 2017;7:143–7.
[28] Schoergenhofer C, Schwameis M, Wohlfarth P, Brostjan C, Abrams ST, Toh CH, et al. Granulocyte colony-stimulating factor (G-CSF) increases histone-complexed DNA plasma levels in healthy volunteers. Clin Exp Med 2017;17:243–9.

Please cite this article in press as: Zwirner K et al. Circulating cell-free DNA: A potential biomarker to differentiate inflammation and infection during radiochemotherapy. Radiother Oncol (2018), https://doi.org/10.1016/j.radonc.2018.07.016

nature COMMUNICATIONS

ARTICLE

https://doi.org/10.1038/s41467-020-14987-6 OPEN

Cancer immune control needs senescence induction by interferon-dependent cell cycle regulator pathways in tumours

Ellen Brenner[1,14], Barbara F. Schörg[2,14], Fatima Ahmetlić[3,4,14], Thomas Wieder[1], Franz Joachim Hilke[5], Nadine Simon[1], Christopher Schroeder[5], German Demidov[5], Tanja Riedel[3], Birgit Fehrenbacher[1], Martin Schaller[1], Andrea Forschner[1], Thomas Eigentler[1], Heike Niessner[1], Tobias Sinnberg[1], Katharina S. Böhm[1], Nadine Hömberg[3,4], Heidi Braumüller[1], Daniel Dauch[6,7], Stefan Zwirner[6], Lars Zender[6,7,8], Dominik Sonanini[2,6], Albert Geishauser[3,4], Jürgen Bauer[1], Martin Eichner[9], Katja J. Jarick[10], Andreas Beilhack[10], Saskia Biskup[8,11], Dennis Döcker[1,11], Dirk Schadendorf[7,12], Leticia Quintanilla-Martinez[8,13], Bernd J. Pichler[2,8], Manfred Kneilling[1,2,8], Ralph Mocikat[3,4] & Martin Röcken[1,7,8]✉

Immune checkpoint blockade (ICB)-based or natural cancer immune responses largely eliminate tumours. Yet, they require additional mechanisms to arrest those cancer cells that are not rejected. Cytokine-induced senescence (CIS) can stably arrest cancer cells, suggesting that interferon-dependent induction of senescence-inducing cell cycle regulators is needed to control those cancer cells that escape from killing. Here we report in two different cancers sensitive to T cell-mediated rejection, that deletion of the senescence-inducing cell cycle regulators $p16^{Ink4a}/p19^{Arf}$ (*Cdkn2a*) or $p21^{Cip1}$ (*Cdkn1a*) in the tumour cells abrogates both the natural and the ICB-induced cancer immune control. Also in humans, melanoma metastases that progressed rapidly during ICB have losses of senescence-inducing genes and amplifications of senescence inhibitors. Metastatic cells also resist CIS. Such genetic and functional alterations are infrequent in metastatic melanomas regressing during ICB. Thus, activation of tumour-intrinsic, senescence-inducing cell cycle regulators is required to stably arrest cancer cells that escape from eradication.

[1] Department of Dermatology, University of Tübingen, 72076 Tübingen, Germany. [2] Department of Preclinical Imaging and Radiopharmacy, Laboratory for Preclinical Imaging and Imaging Technology of the Werner Siemens-Foundation, University of Tübingen, 72076 Tübingen, Germany. [3] Institut für Molekulare Immunologie, Helmholtz-Zentrum München, 81377 Munich, Germany. [4] Eigenständige Forschungseinheit Translationale Molekulare Immunologie, Helmholtz Zentrum München, 81377 Munich, Germany. [5] Institute of Medical Genetics and Applied Genomics, University of Tübingen, 72076 Tübingen, Germany. [6] Department of Medical Oncology and Pneumology, University Hospital Tübingen, 72076 Tübingen, Germany. [7] German Cancer Research Consortium (DKTK), German Cancer Research Center (DKFZ), 69120 Heidelberg, Germany. [8] Cluster of Excellence iFIT (EXC 2180) "Image Guided and Functionally Instructed Tumor Therapies", 72076 Tübingen, Germany. [9] Institute of Clinical Epidemiology and Applied Biometry, University of Tübingen, 72076 Tübingen, Germany. [10] Department of Medicine II, Würzburg University, 97078 Würzburg, Germany. [11] Center for Genomics and Transcriptomics (CeGaT) GmbH and Practice for Human Genetics, 72076 Tübingen, Germany. [12] Department of Dermatology, University Hospital, West German Cancer Centre, University Duisburg-Essen, 45147 Essen, Germany. [13] Institute of Pathology, University of Tübingen, 72076 Tübingen, Germany. [14] These authors contributed equally: Ellen Brenner, Barbara F. Schörg, Fatima Ahmetlić. ✉email: mrocken@med.uni-tuebingen.de

Immune therapy with ICB and natural immune responses reveal that tumour-infiltrating cytotoxic T cells, natural killer cells and T_H1 cells can be activated to cause cancer regression and clearance of tumour cells through cytolysis, apoptosis and by activated macrophages in mice and in humans[1–10]. Nonetheless, cancers are often not completely eliminated, and aggregate or single cancer cells may persist in a controlled state, called tumour dormancy[2,11–17]. The failure of inducing tumour dormancy is a major cause of treatment resistance that may result from inappropriate immune activation, low tumour mutation burden, resistance to lysis or apoptosis, and other mechanisms[4,8,16,18–24]. More recent data associate melanoma progression and treatment resistance of cancers with functional losses of the IFN-JAK1-STAT1 signalling pathway[11,23,25–30]. IFN-γ has multiple effects on cancers. Previously, we have shown that the combined action of IFN-γ and TNF is capable of inducing a stable, senescence-like growth arrest in cancer cells that is called cytokine-induced senescence (CIS)[31]. As the IFN-JAK1-STAT1 signalling cascade activates two key inducers of senescence[14,31,32], $p16^{Ink4a}$ and $p21^{Cip1}$, here we analyse whether cancer immune control requires the IFN-γ-dependent induction of the tumour-intrinsic $p16^{Ink4a}$-CDK4/6-Rb1 and MDM-p53-$p21^{Cip1}$ cell cycle regulation pathways to arrest those cancer cells that escape from cytotoxicity.

Results

Cancer immune control needs *Stat1*-dependent *Cdkn2a* activity. In vitro activation of $p16^{Ink4a}$ and $p21^{Cip1}$ requires IFN-γ signalling in the tumour cells[31,32]. We therefore asked whether in vivo activation of $p16^{Ink4a}$, senescence induction and cancer immune control also require a functioning IFN-γ signalling cascade in the cancer cells. To investigate the role of the IFN-*Stat1*-dependent activation of *Cdkn2a*, what encodes alternatively spliced variants, including the structurally related CDK4 kinase inhibitor isoforms $p16^{Ink4a}$ and $p19^{Arf}$, we analysed the immune control of transplanted cancer cells isolated from RIP-Tag2 mice, where expression of the T antigen under the control of the rat insulin promoter (RIP) leads to pancreatic islet cancers (RT2-cancers)[25]. For this, we implanted either *Stat1*-positive or *Stat1*-negative RT2-cancer cells into syngeneic mice. Most *Stat1*-positive and *Stat1*-negative RT2-cancers (>80%) were rejected. As *Stat1*-positive and *Stat1*-negative RT2-cancers were similarly susceptible to lysis by cytotoxic $CD8^+$ T cells (Supplementary Fig. 1a), we depleted CD8 T cells with mAb before transplanting the cancer cells. Following CD8-depletion the tumours grew in vivo, and treatment was started when tumours reached > 3 mm (Supplementary Fig. 1b). In sham-treated mice cancers reached a critical size within three weeks, and the tumours were analysed (Fig. 1a). The rapidly growing cancers from sham-treated mice had a proliferative $Ki67^+p16^{Ink4a-}$ phenotype (Fig. 1b, c and Fig. 2a) that was negative for phosphorylated heterochromatin protein 1γ (S93) (pHP1γ) in senescence-associated heterochromatin foci (SAHF), H3K9me3 and senescence-associated β-galactosidase (SA-β-gal) (Fig. 2b–d, Supplementary Fig. 2a, b). To determine whether the immune system can control these cancers, we treated mice with a combination of anti-PD-L1 and anti-LAG-3 mAb[33]. In preclinical studies and human trials, dual blockade of LAG-3 and the PD-1/PD-L1 interaction generates a more efficient anti-cancer immunity in mice and in humans than blocking either molecule alone[34]. The *Stat1*-positive RT2-cancers became growth arrested or regressed (Fig. 1a). The residual cancer cells displayed a senescent $p16^{Ink4a+}$, $Ki67^-$ phenotype with an induction of $p21^{Cip1}$ in single cells (Fig. 1b, c and Fig. 2a). RT2-cancers were also positive for pHP1γ, H3K9me3 and SA-β-gal (Fig. 2b–d), and showed no ICB-induced double strand breaks as determined by γH2AX and DNA-PK staining (Supplementary Fig. 3a, b). In contrast, ICB did not arrest *Stat1*-negative RT2-cancers that grew rapidly even when treated with ICB (Fig. 1a). *Stat1*-negative tumour cells were $p16^{Ink4a}$-negative and expressed Ki67 (Fig. 1b, c) but neither pHP1γ, H3K9me3, nor SA-β-gal (Fig. 2b–d). In vitro data confirmed that RT2.*Stat1*$^{-/-}$-cancers were selectively resistant to CIS but susceptible to apoptosis (Fig. 3a).

Immune activation with anti-PD-L1 and anti-LAG-3 requires the presence of PD-L1. *Stat1*-positive and *Stat1*-negative RT2-cancers expressed PD-L1 in the tumour tissue and on more than 10% of the isolated cancer cells (Supplementary Fig. 4a, b), showing that *Stat1*-negative RT2-cancers expressed the target of the anti-PD-L1 mAb. IFN-γ strongly increased PD-L1 and β2-microglobulin expression on RT2-cancer cells but not on RT2.*Stat1*$^{-/-}$-cancer cells; β2-microglobulin$^+$ cells were found in sections of RT2.*Stat1*$^{-/-}$-cancers, showing that IFN-γ-responsive host immune cells infiltrated the tumour microenvironment during ICB (Supplementary Fig. 4a–d).

Stat1 was not required for tumour elimination by $CD8^+$ cells but for the induction of $p16^{Ink4a}$ by IFN-γ-producing immune cells and for an efficient cancer immune control. As $p16^{Ink4a}$ is needed for CIS in RT2-cancer cells[31], we asked whether cancer immune control needs the senescence-inducing cell cycle regulator $p16^{Ink4a}$ in the tumour cells. To address this question, we generated *Cdkn2a*-deficient RT2-cancer cell lines through in vitro and in vivo selection. Comparative genomic hybridisation (CGH) showed the loss of *Cdkn2a* on chromosome 4 (qC4.A) as the only genetic aberration common to all six cell lines (Supplementary Fig. 5a). PCR analysis confirmed the loss of *Cdkn2a* (Supplementary Fig. 5b); PCR also revealed that *Cdkn2a*$^{-/-}$-RT2-cancer cells expressed Tag. RT2.*Cdkn2a*$^{-/-}$-cancer cells also expressed PD-L1 and responded to IFN-γ (Supplementary Fig. 4a, b, d). While the parental RT2-cancer cells were susceptible to CIS and to apoptosis, the *Cdkn2a*-loss mutant cell lines were resistant to CIS but susceptible to apoptosis in vitro (Fig. 3b). To test the role of *Cdkn2a* for tumour immune control in vivo, we injected the tumour cell lines into syngeneic mice and again started treatment with ICB once tumours reached a diameter >3 mm. As we transferred polyclonal *Cdkn2a*-loss mutant cancer cell lines, the tumours grew with slightly different dynamics (Fig. 1a). ICB did not attenuate the growth of *Cdkn2a*-deficient RT2-cancers. Immune histology showed that ICB also failed to induce senescence in *Cdkn2a*-deficient RT2-cancers as they displayed a $Ki67^+p16^{Ink4a-}$, $pHP1\gamma^-$, $H3K9me3^-$, SA-β-gal^- phenotype (Fig. 1b, c and Fig. 2b–d).

To test whether the resistance to ICB specifically resulted from the $p16^{Ink4a}$/$p19^{Arf}$ loss, and to exclude other potential confounders, we generated RT2-cancer cells from another diseased mouse and deleted *p16*^{Ink4a}/*p19*^{Arf} (g*Cdkn2a*) using CRISPR-Cas9[31]. In vitro, RT2-cancer cells transfected with either a control sgGFP or the g*Cdkn2a* construct grew with similar dynamics. Both cell types were sensitive to apoptosis. The CRISPR-Cas9 control cells expressed SA-β-gal when exposed to IFN-γ/TNF and did not restart their exponential growth following IFN-γ/TNF withdrawal, showing that they were susceptible to CIS (Fig. 3c). In contrast, IFN-γ/TNF did not induce SA-β-gal in the RT2.CRISPR-*Cdkn2a*-cancer cells, and the cells restarted exponentially growing after IFN-γ/TNF withdrawal, showing that RT2.CRISPR-*Cdkn2a*-cancer cells were resistant to CIS (Fig. 3c). To specifically analyse *Cdkn2a* in vivo, we injected the cells into the CD8-depleted mice. All CRISPR-Cas9 control cell lines were rejected, revealing that the cells were highly immunogenic. In contrast, 80% of the RT2.CRISPR-*Cdkn2a*-cancer cells grew in syngeneic mice (Supplementary Fig. 5c), demonstrating that natural immune responses required the senescence-inducing *Cdkn2a* gene to control these highly immunogenic cancer cells (Fig. 1a, upper panel). Even enhancement of the immune response with ICB did not arrest

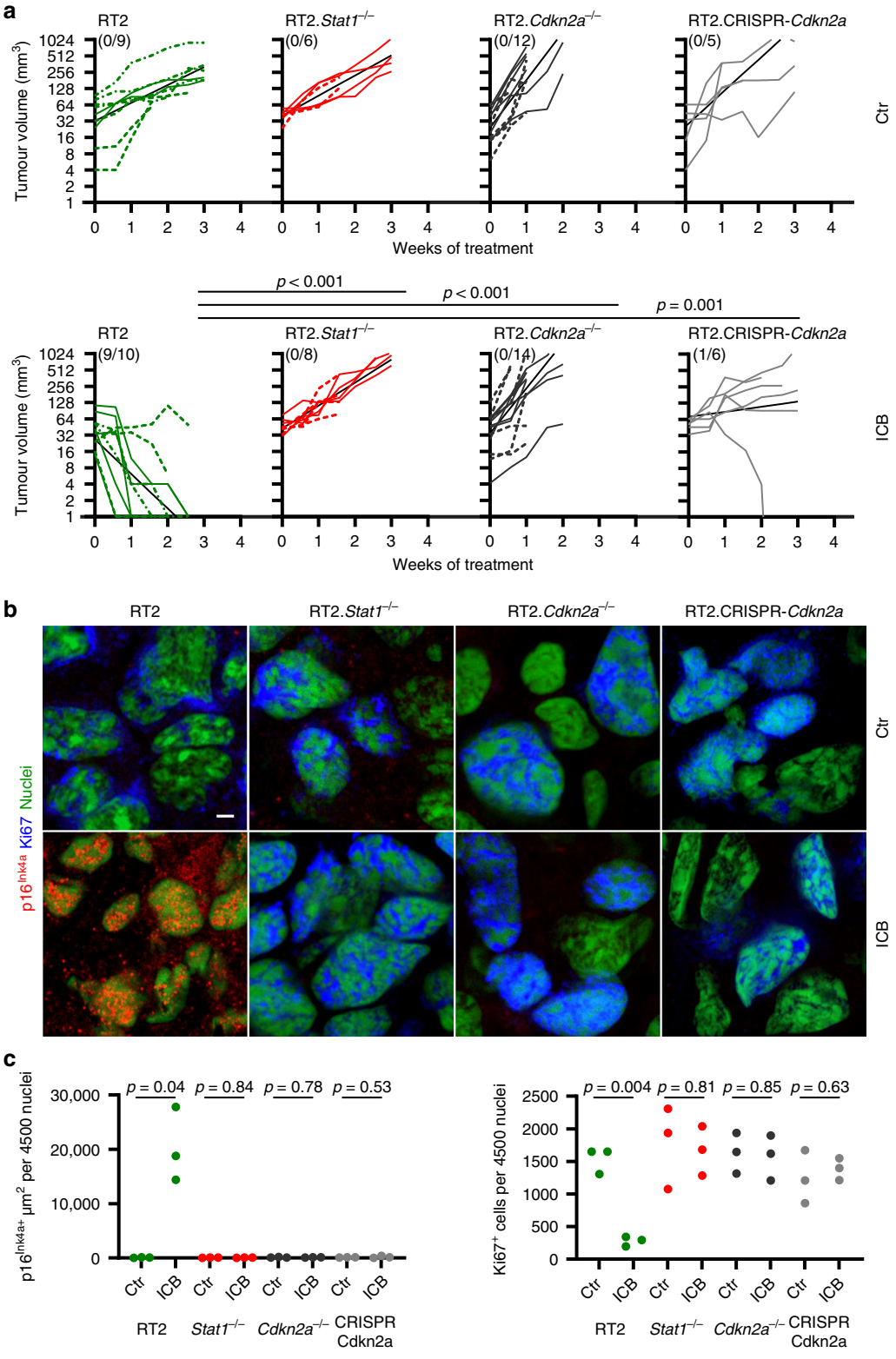

their growth in vivo (Fig. 1a, lower panel). RT2.CRISPR-*Cdkn2a*-cancer cells expressed PD-L1, β2-microglobulin (Supplementary Fig. 4a–d) and Tag. Immune histology revealed that the rapidly growing RT2.CRISPR-*Cdkn2a*-cancer cells had a Ki67^{+}, p16^{Ink4a-}, pHP1γ^{-}, SA-β-gal^{-} proliferative phenotype, but were positive for H3K9me3 (Fig. 1b, c and Fig. 2b–d). Even though H3K9me3 is a marker of senescence, others have shown that CRISPR-Cas9 editing itself may also induce a non-specific H3K9 methylation that persists[35]. Importantly, ICB treatment increased neither H3K9me3, nor DNA-PK, nor γH2AX in RT2.CRISPR-*Cdkn2a*-cancer cells (Fig. 2c, Supplementary Fig. 3a, b).

CGH of 10 different cell lines revealed that the loss of the *p16*^{Ink4a}/*p19*^{Arf}-locus was the only common signature where the RT2.*Cdkn2a*$^{-/-}$- or the RT2.CRISPR-*Cdkn2a*-cancer cells differed from the parental or the CRISPR-Cas9 control cell lines (Supplementary Fig. 5a, b). We analysed a total of seven different

Fig. 1 *Stat1- and Cdkn2a*-dependent immune control of transplanted RT2-cancers and induction of Ki67$^-$p16^{Ink4a+} senescent cancer cells. a Individual follow-up of tumour volumes. CD8-depleted mice were subcutaneously (s.c.) engrafted with 1 × 10^6 RT2-, RT2.*Stat1*$^{-/-}$-, RT2.*Cdkn2a*$^{-/-}$- or RT2.CRISPR-*Cdkn2a*-cancer cells. Treatment with isotype control mAbs (Ctr) or combined immune checkpoint inhibitors (ICB; anti-PD-L1 and anti-LAG-3) once per week was started when tumours were >3 mm in diameter. Cancer size was measured 2 times per week. Number of mice with regressing tumours and the total number of mice is given in parenthesis; RT2 Ctr $N = 9$, ICB $N = 10$, RT2.*Stat1*$^{-/-}$ Ctr $N = 6$, ICB $N = 8$, RT2.*Cdkn2a*$^{-/-}$ Ctr $N = 12$, ICB $N = 14$, RT2.CRISPR-*Cdkn2a* Ctr $N = 5$, ICB $N = 10$. Each cell line was given a different lining. Black lines summarise the results for different treatment groups (as obtained from ANCOVA). *p*-values examine the question whether the treatment effect was different between two genotypes. Mice were killed either when tumours reached the critical diameter of 15–20 mm or ulcerated, or when mice developed signs of wasting. **b** Representative triple-staining for the senescence marker p16^{Ink4a} (red) and the proliferation marker Ki67 (blue) and for nuclei (green) of the s.c. tumour of individual mice treated as described in (**a**). Scale bar 2 µm. **c** Individual data points showing quantification of p16^{Ink4a+} (left) or Ki67$^+$ (right) cells. Each data point represents the total of three tumour slides measurements, tumours of three individual mice (described in **a**) were analysed. In **a** significance was tested by using unequal variances *t*-test, *p*-values examines the treatment effect, comparing the ICB-treated RT2-cancers with each ICB-treated knock-out group.

Cdkn2a-deficient RT2-cancer cell lines in vitro. All were resistant to CIS. Next, we analysed three of them in vivo, all were resistant to ICB. Thus, cytotoxic CD8$^+$ T cells can directly reject *Cdkn2a*-deficient RT2-cancers, but senescence-induction through IFN-γ-mediated activation of the cell cycle regulators p16^{Ink4a}/p19^{Arf} was strictly needed to control those cancer cells that escape from cytotoxicity.

Cancers are frequently rejected by CD8 T cells. In addition, immune clearance of senescent cancer is mediated by IFN-γ-producing T_H1 cells and by IFN-γ-activated type I macrophages[25,31,36–39]. Indeed, the tumours controlled by ICB showed the established features of the T_H1-mediated clearance mechanism, as β2-microglobulin was strongly expressed (Supplementary Fig. 4c, d) and as the tumours were infiltrated by CD3$^+$CD8$^-$ T cells and F4/80$^+$ and MHC class II$^+$ activated macrophages (Supplementary Fig. 6a–c). We detected no CD8$^+$ T cells and no CD49b$^+$ NK cells (Supplementary Fig. 6d), what may be due to the fact that NK cells are primarily found in the spleen[40,41]. As ICB induced a similar immune infiltrate in RT2-cancers and in *Stat1*- and *Cdkn2a*-deficient RT2-cancers (Supplementary Fig. 6a–c), the data strongly suggest that senescence induction in the cancer cells was a prerequisite for tumour cell clearance by T_H1 cells and IFN-γ-activated type I macrophages[25,31,36–39].

Cancer immune therapy and senescence induction require *Stat1*. To determine whether IFN-γ signalling through *Stat1* is also needed for the induction of p16^{Ink4a}, p21^{Cip1}, senescence and the control of endogenous cancers that are destroyed by strong T cell responses, we treated RT2 mice by the combination of anti-PD-L1 and anti-LAG-3 mAbs and adoptive T cell transfer (AT), with T_H1 cells specific for a tumour associated antigen (TAA) in the SV40-Tag protein[31] (Supplementary Fig. 7a). Combining anti-PD-L1/anti-LAG-3 mAbs with AT further enhances the therapeutic effect of ICB and largely eradicates all cancer cells[33]. We started the treatment once RT2 mice had a major cancer load, as documented by magnetic resonance imaging (Supplementary Fig. 7b). This immune therapy strongly decreased the islet size within 4 weeks, and functionally restored the blood glucose control (Fig. 4a–c). It largely destroyed the RT2-cancers but failed to eradicate all cancer cells (Fig. 4b, Supplementary Fig. 8a). Immune histology of residual RT2-cancers showed CD3$^+$ cells, MHC class II$^+$ and F4/80$^+$ cells following ICB/AT treatment but only very few or no Foxp3$^+$ regulatory T cells, CD8$^+$ or CD49b$^+$ cells (Fig. 5a, Supplementary Fig. 8a–c). The RT2-cancers expressed normal levels of Tag mRNA and protein (Fig. 5b, c) and expressed PD-L1 and β2-microglobulin protein (Supplementary Fig. 8d). The RT2-cancer cells showed a senescent phenotype as they expressed p16^{Ink4a}, p21^{Cip1}, H3K9me3, pHP1γ, and SA-β-gal but were Ki67$^-$ (Fig. 4d, e and Fig. 6a–d). Staining for γH2AX and DNA-PK, markers that mainly indicate double strand breaks, remained largely negative, confirming that CIS caused only minor DNA damage (Supplementary Fig. 9). Electron microscopy confirmed the accumulation of SA-β-gal in the cytoplasm of senescent tumour cells (Supplementary Fig. 10a–c). These residual RT2-cancer cells were also functionally senescent. When isolated and cultured for ≥5 passages in vitro they preserved their growth-arrested, SA-β-gal$^+$ phenotype (Fig. 7a–c). RT2-cancer cells with such a senescent phenotype remain growth arrested for at least 3 months, even when transplanted into immune compromised NOD–SCIDIl2rγ$^{-/-}$ mice, demonstrating the absence of cancer initiating cells[31].

Sham-treated RT2-mice, sham-treated *Stat1*$^{-/-}$ RT2 mice or *Stat1*$^{-/-}$ RT2 mice treated with ICB/AT died within 4 weeks, showed large tumours and failed to control their blood glucose levels (Fig. 4a–c). The tumours of these three groups of mice were strongly enriched in Ki67$^+$ RT2-cancer cells that were negative for p16^{Ink4a}, p21^{Cip1}, H3K9me3, pHP1γ, and SA-β-gal (Fig. 4d, e and Fig. 6a–d). The isolated tumour cells also proliferated strongly when cultured in vitro and did not develop a senescent phenotype (Fig. 7a–c). While treatment with ICB/AT did not induce a senescent phenotype and did not attenuate the tumour growth in the RT2.*Stat1*$^{-/-}$ mice, the inflammatory infiltrate was similar to that of cancers in RT2.*Stat*$^{+/+}$ mice (Supplementary Fig. 8a–c). Also three-dimensional imaging and FACS analyses revealed that the adoptively transferred T cells and dendritic cells infiltrated RT2-cancers of *Stat1*$^{-/-}$ or *Stat1*$^{+/+}$ mice with similar dynamics (Supplementary Fig. 11a–e); immune histology confirmed these findings. Islet tumours of RT2 and RT2.*Stat1*$^{-/-}$ mice had both CD3$^+$ T-cells and MHC class II$^+$, F4/80$^+$ macrophages (Fig. 5a and Supplementary Fig. 8a, b). In islet tumours of RT2.*Stat1*$^{-/-}$ mice the T cell infiltrate was variable but there was no detectable size difference between tumour areas that were strongly or poorly infiltrated. At this advanced cancer stage, the combined ICB/AT therapy was superior to either ICB or AT monotherapy that provided intermediate results (Fig. 4a–e and Fig. 6a–d).

Importantly, the tumour cells surviving the combined ICB/AT immune therapy did not result from classical immune evasion mechanisms. In vitro, all RT2-cancer cells, including the RT2.*Stat1*$^{-/-}$-cancer cells were fully susceptible to T cell-mediated killing (Supplementary Fig. 1a) or apoptosis (Fig. 3a). RT2.*Stat1*$^{+/+}$-cancer cells and RT2.*Stat1*$^{-/-}$-cancer cells expressed normal levels of Tag (Fig. 5b, c), the antigen targeted by the immune therapy. RT2.*Stat1*$^{+/+}$-cancers and RT2.*Stat1*$^{-/-}$-cancers had normal baseline levels of PD-L1 and β2-microglobulin, and in RT2.*Stat1*$^{-/-}$-cancers β2-microglobulin was in the tumour microenvironment (Supplementary Fig. 4a–d and Supplementary Fig. 8d). Foxp3 regulatory T cells were not increased inside the tumours (Supplementary Fig. 8b). In consequence, the RT2.*Stat1*$^{-/-}$-cancers differed from RT2.*Stat1*$^{+/+}$-cancers selectively by their resistance to CIS (Fig. 3a).

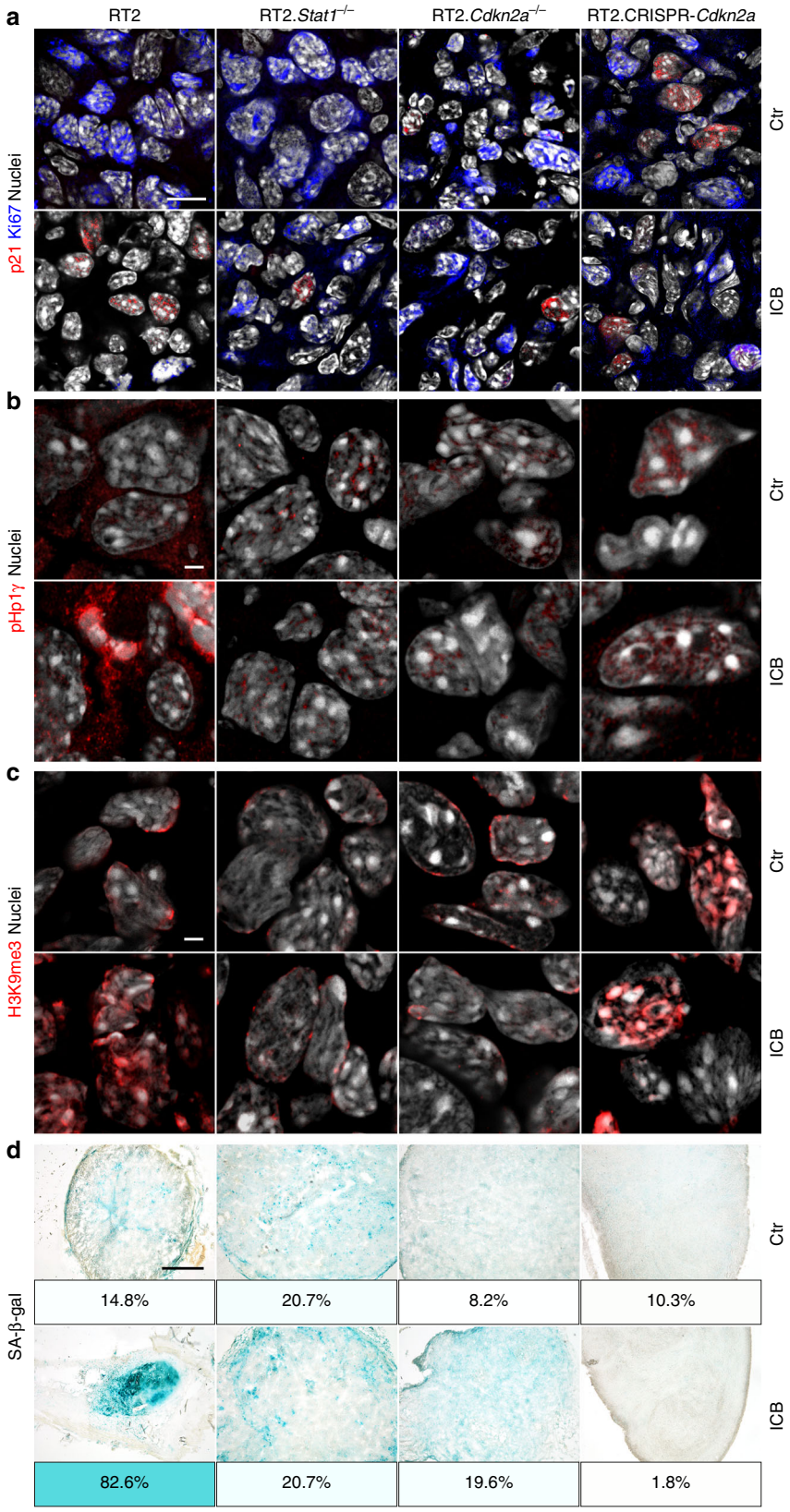

Fig. 2 *Stat1*- and *Cdkn2a*-dependent induction of the senescence markers pHP1γ, H3K9me3, and of SA-β-gal in transplanted RT2-cancers. **a**–**d** Representative microscopic images of s.c. RT2-cancers from either RT2-, RT2.*Stat1*$^{-/-}$-, RT2.*Cdkn2a*$^{-/-}$- or from RT2.CRISPR-*Cdkn2a*-cancer cells. Mice were treated with isotype control mAbs (Ctr) or with immune checkpoint blockade (ICB, anti-PD-L1 and anti-LAG-3). Staining for the senescence marker p21^{Cip1} (red), the proliferation marker Ki67 (blue) and for nuclei (white) (**a**), pHP1γ (red), nuclei (white) (**b**), H3K9me3 (red), nuclei (white) (**c**). SA-β-gal activity at pH5.5 and percentage of SA-β-gal positive tumour cells in each tumour (**d**). The colour evaluation and calculation of the SA-β-gal^{+} cells are described in Supplementary Fig. 2 and Methods (for **d**). Scale bars 10 µm (**a**), 2 µm (**b**, **c**), 1000 µm (**d**). Histology was performed in one to three representative tumours from Fig. 1c.

Even though the ICB/AT combination therapy largely destroyed the tumours, the therapy failed to eradicate all cancer cells. Together the data prove that *Stat1* is needed to activate $p16^{Ink4a}$ in vitro and in vivo and that *Stat1*-mediated activation of *Cdkn2a* is needed to induce senescence in cancer cells. In consequence, cancer immune control required *Stat1*-mediated activation of the cell cycle regulators like $p16^{Ink4a}$ to stably arrest the growth of those cancer cells that are not eliminated by cytotoxicity.

Cancer immune control needs IFN-γ-dependent $p21^{Cip1}$ induction. Following ICB *Stat1*-deficient cancers showed neither increased $p16^{Ink4a}$ nor $p21^{Cip1}$. Thus, besides $p16^{Ink4a}$, cancer immune control may also require $p21^{Cip1}$ activation. SV40-Tag expression impairs p53 activation[42]. As p53 regulates mRNA and protein production of $p21^{Cip1}$, RT2-cancers are inappropriate to carefully investigate the role of $p21^{Cip1}$ for senescence induction in response to ICB. To test the need of senescence-inducing $p21^{Cip1}$ for cancer immune control and to determine whether senescence induction is also needed for tumours other than RT2-cancers, we studied the role of $p21^{Cip1}$ in the immune control of lymphomas. For this, we used λ-*MYC* mice, where a human *MYC* oncogene under the control of the immunoglobulin λ enhancer induces the development of endogenous B-cell lymphomas[43]. This also allows directly investigating the role of $p21^{Cip1}$ in the immune therapy of a naturally developing malignancy. Untreated mice died within <150 days (Fig. 8a) from $Ki67^{+}p16^{Ink4a-}$, $CD20^{low}$ B-cell lymphomas that destroyed lymph nodes and spleen (Fig. 8b, c and Supplementary Fig. 12a). The $Ki67^{+}$ B cells were also negative for $p21^{Cip1}$, pHP1γ, H3K9me3 or SA-β-gal, showing that the tumours had a high proliferative capacity and were not senescent (Fig. 8b, c and Fig. 9a–c). Combined ICB with anti-CTLA-4 and anti-PD-1 mAb protected 18% (Fig. 8a) to 30% (Fig. 8d) of λ-*MYC* mice from lymphomas for at least 200 days. In a long-term experiment, 18% of the λ-*MYC* mice with a combined ICB therapy were still healthy at >250 days (Fig. 8a), a lifetime that has never been achieved by any other therapy in this mouse model. Treatment with either mAb alone did not rescue mice from lymphomas. Lymph nodes from healthy ICB-treated λ-*MYC* mice showed a normal architecture with normal B and T cell areas, expression of PD-L1 and β2-microglobulin, no T cell infiltration, normal $CD20^{+}λ\text{-}MYC^{-}$ B cells, few $CD161^{+}$ cells, no signs of DNA double strand breaks and no destruction (Supplementary Fig. 12a–e). Even though we found no signs of immune destruction in the lymph nodes, depletion of pan-T cells with a mAb abrogated the ICB-mediated protection of λ-*MYC* mice, as all mice died from lymphomas by day 200 (Fig. 8d). Splenic dendritic cells of λ-*MYC* mice express the CTLA-4-targets CD80 and CD86 that are enhanced by IFN-γ[41]. Lymphoma-specific, regulatory T cells are also increased in the spleen. Yet, depletion of regulatory T cells delays lymphoma development and death only for a short time[40].

Nodal B cells from ICB-treated, healthy λ-*MYC* mice were $Ki67^{-}$ but strongly expressed nuclear $p16^{Ink4a}$ and $p21^{Cip1}$ (Fig. 8b, c), pHP1γ, H3K9me3 and SA-β-gal (Fig. 9a–c), displaying a senescent phenotype[24,31]. This suggests that ICB-mediated protection from B-cell lymphomas included mechanisms other than cancer cell killing. To test whether ICB-mediated lymphoma prevention required the senescence-inducing $p21^{Cip1}$, we generated syngeneic λ-*MYC.p21*$^{Cip1-/-}$ mice. While ICB protected 18–30% of λ-*MYC* mice from lymphoma and death (Fig. 8a, d), all ICB-treated λ-*MYC.p21*$^{Cip1-/-}$ mice died from lymphomas between day 100 and 210 (Fig. 8e). Histology revealed lymph node destruction by $Ki67^{+}$, $CD20^{low}$ B cells that were devoid of the senescence markers $p16^{Ink4a}$, $p21^{Cip1}$, pHP1γ, H3K9me3, or SA-β-gal (Fig. 8b, c, Fig. 9a–c and Supplementary Fig. 12a).

ICB-mediated $p21^{Cip1}$ induction and lymphoma prevention required IFN-γ, as mice receiving ICB in the presence of anti-IFN-γ mAb died from $CD20^{low}$ B-cell lymphomas as fast as untreated mice (Fig. 8a). B cells were $Ki67^{+}$ and negative for $p21^{Cip1}$, $p16^{Ink4a}$, pHP1γ, H3K9me3 and SA-β-gal (Fig. 8b, c and Fig. 9a–c), showing that IFN-γ was needed to activate the cell cycle regulators $p16^{Ink4a}$ and $p21^{Cip1}$ that, in turn, were required for senescence-induction in vivo. This proves that the senescence-inducing cell cycle regulator $p21^{Cip1}$ was strictly required to prevent the transition of pre-malignant B cells into B-cell lymphomas in ICB-treated λ-*MYC* mice, and that ICB-mediated $p21^{Cip1}$ activation was IFN-γ-dependent.

Impaired senescence pathways in melanomas resistant to ICB. ICB is an approved standard of care therapy for metastatic melanoma and some other cancers, and efficient in about 40% of patients with metastatic melanoma. Another 40% are non-responder patients that mostly progress rapidly despite ICB therapy[6,8,30,44]. Based on the experimental data, we asked whether cell cycle regulator genes that control senescence induction were also needed for cancer immune control in humans. To address this, we compared the genetic alterations by targeted panel sequencing of 30 melanoma biopsies of consecutive non-responder patients, where metastases progressed within <3 months of ICB with the genetic alterations in melanoma biopsies of 12 responder patients, where metastases regressed during ICB ≥1 year. For each patient we identified the tumour-specific alterations by paired sequencing of tumour and normal tissue. In agreement with published data, the biopsy material of responder patients had a significantly higher tumour mutational burden than that of non-responder patients[8,10,45] (Fig. 10a). We used a panel that includes a total of 678 established cancer-associated genes[46] (Supplementary Data Tables 1–3). To determine whether CIS was needed to protect from tumour progression, we explicitly focussed only on 19 genes of the panel that encode for molecules that are also involved in the IFN-γ-mediated activation of the senescence signalling pathways that we identified in our murine experiments. This panel approach may have missed very rare fusion/translocation alterations of the genes investigated, but it would be difficult to identify such rare fusion/translocation alterations also with an exome-based approach, as the panel allowed the deep sequencing necessary to find the DNA alterations in less than 10% of all cells of the melanoma metastases.

We focused on somatic alterations, namely copy number variants (CNVs) and single nucleotide variants (SNVs) in key cell cycle control genes (*CCND1/2/3*; *CDKN2A/B/C*, *CDK4/6*, *CCNE1*, *CDKN1A/B*, *RB1*, *TP53*, *MDM2/4*), as well as *JAK1,2,3* and *MYC*. Both groups had a similar distribution of genetic aberrations in *JAK1,2,3*, *MYC* and the cell cycle control genes when all somatic alterations (SNVs and CNVs) were included (Fig. 10b). In contrast, comparing especially the number of strong amplification (≥ 3fold amplification) and of fully inactivating mutations (homozygous deletions and loss of heterozygosity (LOH)), we observed significant differences between the two groups. Melanomas of non-responder patients had significantly more fully inactivating mutations of senescence-inducing cell cycle genes (*CDKN2A/B/C*; *CDKN1A/B*; *RB1*; *TP53*; *JAK1/2/3*) or ≥ 3fold amplifications of genes promoting cell cycle progression (*CCND1/2/3*; *CDK4/6*; *CCNE1*; *MDM2/4*; *MYC*) than the biopsy material of melanomas from responder patients (Fig. 10c, Supplementary Fig. 13 and 14a, b).

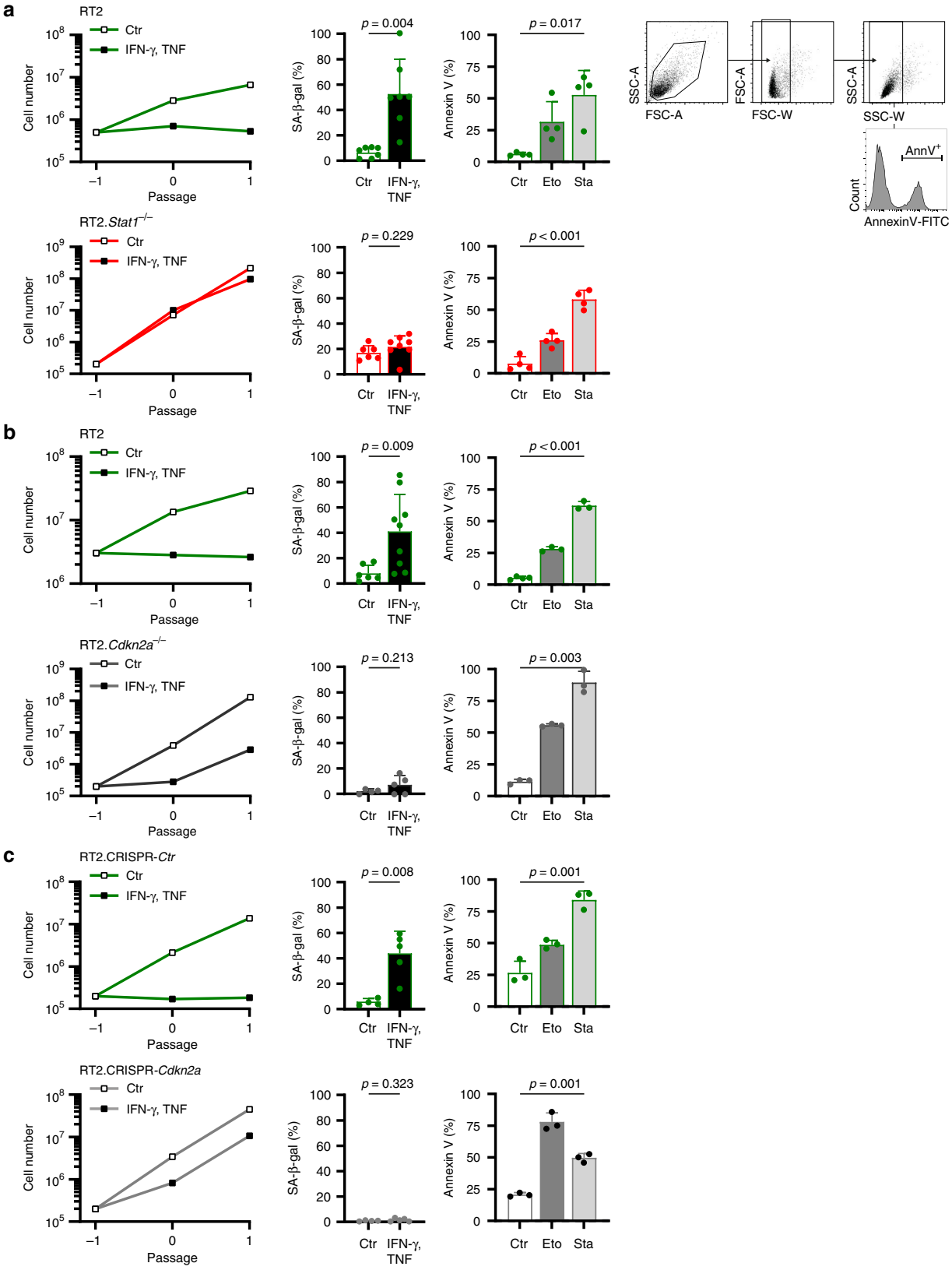

The genetic data were supported by functional analyses in vitro. Melanoma lines that we developed from biopsies of non-responder patients grew with similar dynamics as those derived from biopsies of responder patients and were susceptible to apoptosis (Fig. 10d). Yet, these cell lines were resistant to CIS. In contrast, melanoma lines that we derived from biopsy material of responder patients were susceptible to both, CIS and drug-induced apoptosis. TNF and IFN-γ are established inducers of annexin V and apoptosis in multiple cancer cells including melanoma cell lines[47]. Importantly, they induced senescence only in selected lines, such as those that could be derived from biopsy material of responder patients (Fig. 10e).

Fig. 3 *Stat1*- and *Cdkn2a*-dependent induction of CIS in RT2-cancer cells, but *Stat1*- and *Cdkn2a*-independent induction of apoptosis. a–c Assays were performed with RT2-cancer cells (**a**, **b**), RT2.*Stat1*$^{-/-}$-cancer cells (**a**), *Cdkn2a*-deficient RT2-cancer cells (**b**), or RT2.CRISPR-Ctr- control, or RT2.CRISPR-*Cdkn2a*-cancer cells (**c**). For the senescence growth assay, cells were cultured either with medium (Ctr) or with medium containing 100 ng ml^{-1} IFN-γ and 10 ng ml^{-1} TNF for 96 h, washed and then cultured with medium for another 3–4 days. One representative out of 3 independent experiments was given. SA-β-gal activity was determined after 96 h of culture with medium (Ctr) or with medium containing 100 ng ml^{-1} IFN-γ and 10 ng ml^{-1} TNF, data show the mean with SD, RT2 Ctr $n = 7$, CIS $n = 7$, RT2.*Stat1*$^{-/-}$ Ctr $n = 6$, CIS $n = 8$ (**a**), RT2 Ctr $n = 6$, CIS $n = 9$, RT2.*Cdkn2a*$^{-/-}$ Ctr $n = 4$, CIS $n = 5$ (**b**), RT2.CRISPR-*Ctr* Ctr $n = 4$, CIS $n = 5$, RT2.CRISPR-*Cdkn2a* Ctr $n = 4$, CIS $n = 5$ (**c**). For apoptosis induction, cells were exposed to either medium (Ctr) or etoposide (Eto, 100 μM) or staurosporine (Sta, 0.5 μM) for 24 h and then stained for annexin V. Positive cells were detected by flow cytometry data show the mean with SD (**a** (including gating strategy), **b**, **c**), RT2 $n = 4$, RT2.*Stat1*$^{-/-}$ $n = 4$ (**a**), RT2 Ctr $n = 4$, Eto, Stau $n = 3$, RT2.*Cdkn2a*$^{-/-}$ $n = 3$ (**b**), RT2.CRISPR-*Ctr* and RT2.CRISPR-*Cdkn2a* $n = 3$ (**c**). Significance tested by using unequal variances *t*-test.

Discussion

Our results show that cancer control strictly requires the activation of tumour-intrinsic, senescence-inducing cell cycle regulators by the immune system to stably arrest those cancer cells that escape from eradication, in mice and in humans. Even though elimination of cancer cells is a primary therapeutic goal, cancer cell reduction by cytotoxicity is frequently incomplete and insufficient for permanent cancer control. About 90% of all cancer-related deaths result from metastases arising from reawakened, dormant cancer cells that survive chemo- or immune-therapies[2,48–51], often months to decades after treatment of the primary tumour[15]. The data here unravel that IFN-γ/STAT1-dependent activation of the senescence-inducing cell cycle regulators p16^{Ink4a}/p19^{Arf} and p21^{Cip1} is needed to keep those cells senescent that escape from ICB-induced cell death, and that metastases resistant to immune therapies grow, when senescence-inducing signalling pathways become interrupted. This concept is supported by recent clinical data. Thus, melanoma metastases regress and may even clinically disappear upon ICB therapy, but can restart growing when mutations abrogate the IFN-γ-signalling pathway[26]. Various observations suggest that immune control of cancers requires, in addition to cancer cell killing, IFN-dependent activation of cancer-intrinsic senescence-inducing cell cycle regulators[13,14,31,52,53], to stably arrest those cancer cells that escape from cytotoxicity.

Even though senescence occurs following cancer therapy[54], the role of senescence in the development of metastases and the response to chemo- and immune-therapy has not been resolved[52,53,55]. In mice, loss of *p16^{Ink4a}* promotes the development of melanoma metastases in mice[56] and loss of the *Suv39h1* or *p53* genes in senescent cells may transform these cells in highly aggressive, cancer initiating cells[24]. In contrast, in humans the biallelic loss of *CDKN2A* has only been shown to promote melanoma invasion. Until now, it was not possible to identify specific gene mutations, like the loss of *CDKN2A* that promote the development of melanoma metastases in humans. This has only been demonstrated in mice[56–59]. The missing identification of metastases-promoting genes may be due to the fact that the IFN-γ-mediated activation of the MDM2-p53-p21^{Cip1} senescence pathway can in part compensate the loss of *CDKN2A*[55]. In line with this, we found gene amplifications of *MDM2* and *MDM4* in 26% and of *CDK4/6* in 13% of the melanoma biopsies of patients that did not respond to ICB. These amplifications were absent in melanoma biopsies of patients responding to ICB. More than half of the metastases of non-responder patients had at least one defect in the IFN-dependent senescence-signalling pathway. Both, p16^{Ink4a} and p21^{Cip1} induce senescence by inhibiting CDK4/6, and most genes associated with the resistance of melanoma metastases to ICB were up-stream of CDK4/6. Therefore, combining ICB with CDK4/6 inhibitors is a promising strategy to turn metastases with these types of defects in the senescence pathway from metastases not responding to ICB into metastases responding to ICB.

While senescence is established as a barrier against cancer development[60], and while it is needed to prevent the rapid regrowth of cancers that escape from therapy- or immune-mediated lysis or apoptosis, the exact role of senescence in halting the progression of established cancers is still under debate. Some data suggest that the senescence-associated secretory phenotype (SASP) may even exert harmful effects[54]. Moreover, senescence induction requires subsequent clearance of the residual cancer cells by T_H1 cells and macrophages to protect from cancer progression in a model of hepatocellular carcinoma[36]. In contrast, other data strongly suggest that senescence is a critical barrier that protects better against the progression of cancers than the attempt to clear all cancer cells[61].

It remains open whether senescence in established cancers generally protects against cancer progression or whether this depends on the mode of senescence induction. TNF and IFN-γ are major inducers of apoptosis in cancer cells but some cells escape from TNF- and IFN-γ-induced apoptosis[47]. We have previously shown that TNF and IFN-γ induced senescence in cells escaping from TNF/IFN-γ-mediated apoptosis[31], and here we showed that CIS protected from the regrowth of cancer cells resistant to the elimination by natural or ICB-enhanced cytotoxicity. In RT2-cancers, CIS establishes a stable type of senescence where the SASP does not promote cancer progression for prolonged periods of time, as the senescent RT2-cancer cells remain growth arrested for extended periods of time, even when transplanted into severely immune compromised mice[31]. Importantly, CIS requires the combined action of TNF and IFN-γ, as immune therapies of cancers in the absence of either IFN-γ, of Stat1- or of Tnfr1-signalling strongly accelerate the transformation and growth of cancer cells[19,25].

This is especially relevant in the context of our data showing that melanoma metastases that fail responding to ICB therapies and that grow very fast despite ICB, frequently show functionally relevant gene aberrations in IFN-γ-regulated, cancer-intrinsic senescence-inducing cell cycle regulators. Even though IFN-γ induces a broad spectrum of tumour-protective mechanisms, the data here proved that IFN-γ-dependent senescence induction is a key mechanism required to protect against those cancer cells that escape from cytotoxicity.

Methods

Animals. C3HeB/FeJ mice were purchased from The Jackson Laboratory (Bar Harbor, ME, USA). Syngeneic transgenic TCR2 mice[31,62] express a T cell receptor (TCR) specific for Tag peptide 362-384 on CD4$^+$ T cells, RIP-Tag2 (RT2) mice express the T antigen under control of the rat insulin promotor (RIP) that leads to pancreatic islet cancers (RT2-cancers)[31,62] and double transgenic RT2.*Stat1*$^{-/-}$ mice (backcross of 129S6/SvEv-*Stat1^{tm1Rds}* mice[31]) were provided by Taconic and backcrossed to C3HeB/FeJ. OT-I mice (C57BL/6-Tg(TcraTcrb)1100Mjb/J, and NSG (NOD.*Cg-Prkdc^{scid} Il2rg^{tm1Wjl}*/SzJ) mice were from The Jackson Laboratory. λ-*MYC* mice and double transgenic λ-*MYC.p21*$^{-/-}$ mice (both C57BL/6 background) express a human *MYC* oncogene under the control of the immunoglobulin λ enhancer and develop an endogenous B-cell lymphoma[43]. Mice with C3HeB/FeJ background, OT-I mice and NSG-mice were bred in the animal facility Tübingen. λ-*MYC* and λ-*MYC.p21*$^{-/-}$ mice were bred in the animal facility Munich. All animals were bred under specific pathogen-free conditions. Animal

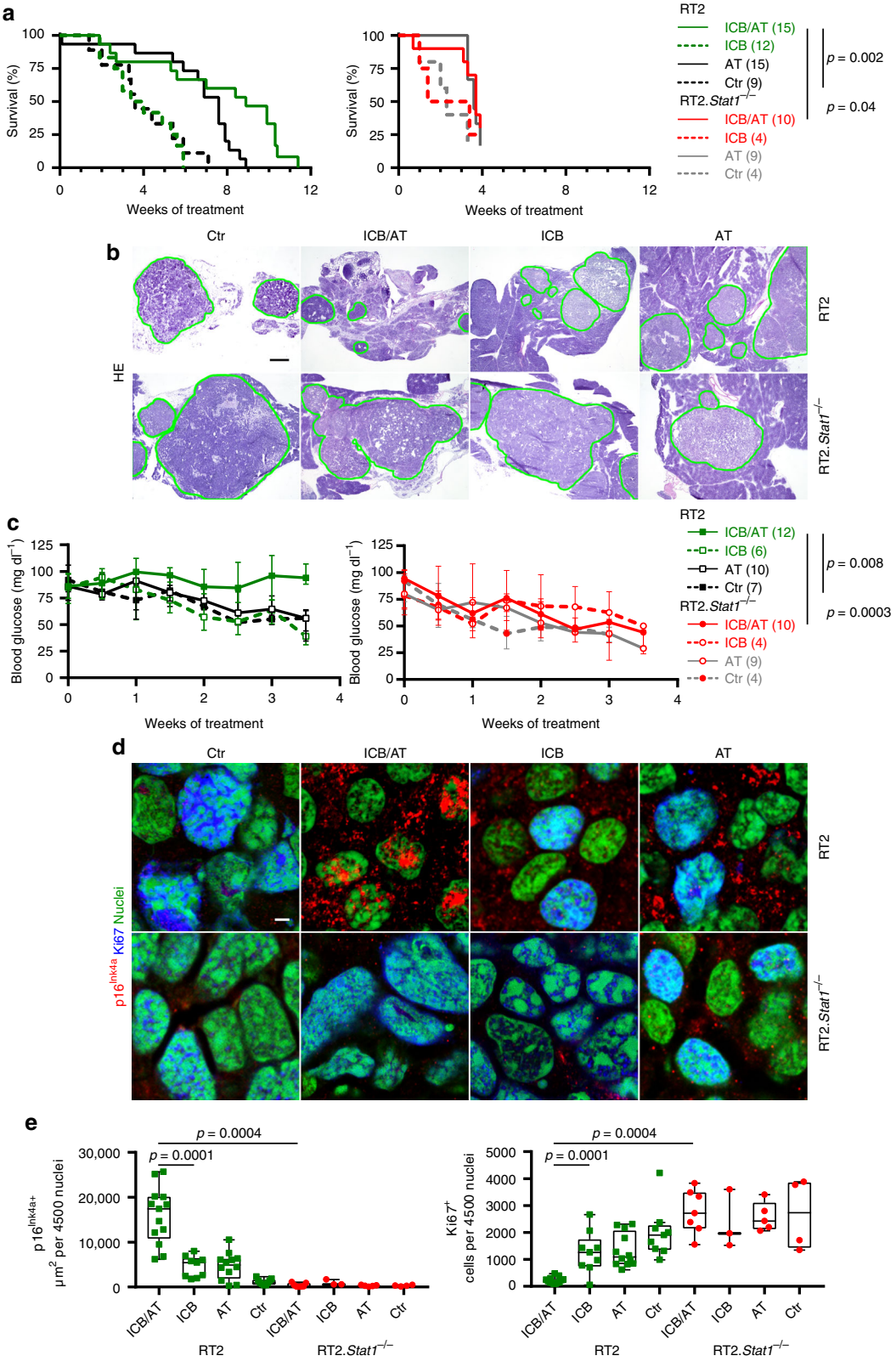

experiments were in accordance with animal welfare regulations and ethical approval was obtained by the local authorities (Regierung von Oberbayern and Regierungspräsidium Tübingen).

Treatment of RT2-cancers in C3HeB/FeJ mice. A total of 1×10^6 cells (in 100 µl NaCl) RT2-, RT2.*Stat1*$^{-/-}$-, RT2.*Cdkn2a*$^{-/-}$- or RT2.CRISPR-*Cdkn2a*-cancer cells were s.c. transplanted, three days after depletion of CD8 cells with 100 µg anti-CD8 mAb[39] (Rm-CD8-2 AK, Core Facility mAb, Helmholtz-Zentrum München). CD8 depletion was repeated every ten days till the tumour lesion became palpable. Once tumours were ≥3 mm, mice were treated with anti-PD-L1 mAb and anti-LAG-3 mAb once per week (initially 500 µg, then 200 µg). Ctr mice received isotype-control mAbs (clone LTF-2 and HRPN, Bio X Cell). Tumour growth was monitored two times per week using a calliper and blood glucose was measured twice a week using an Accu-Check sensor for up to 8 weeks. Cancer size was measured two times per week. Mice were sacrificed after 4 treatment cycles, when the tumour

Fig. 4 *Stat1*-dependent immune control of endogenous RT2-cancers and induction of Ki67$^-$p16^{Ink4a+} senescent cancer cells. a Survival curves of RT2 or RT2.*Stat1*$^{-/-}$ mice treated with either isotype control mAbs (Ctr, RT2 $N = 9$, RT2.*Stat1*$^{-/-}$ $N = 4$), with adoptive transfer of T antigen-specific CD4$^+$ T_H1 cells (AT, RT2 $N = 15$, RT2.*Stat1*$^{-/-}$ $N = 9$), with immune checkpoint inhibitors (ICB, RT2 $N = 12$, RT2.*Stat1*$^{-/-}$ $N = 4$; anti-PD-L1 and anti-LAG-3) or with ICB/AT (RT2 $N = 15$, RT2.*Stat1*$^{-/-}$ $N = 10$). For each AT experiment we generated a non-cytotoxic Tag-specific T_H1 cell line. **b** Cancer size shown by representative hematoxylin and eosin staining of pancreas of RT2 (upper panel) or RT2.*Stat1*$^{-/-}$ mice (lower panel) after four weeks of treatment. Mice were treated as described in **a**. Green lines depict the size of RT2-cancers after treatment. After 4 weeks of treatment ICB/AT-treated mice ($N = 6$) had a two-fold smaller islet size than Ctr ($N = 7$). **c** Time course of blood glucose levels as surrogate marker for the growth of the insulin-producing tumours of RT2 or RT2.*Stat1*$^{-/-}$ mice (median ± interquartile range) treated as described in (**a** Ctr, RT2 $N = 7$, RT2.*Stat1*$^{-/-}$ $N = 4$; AT, RT2 $N = 10$, RT2.*Stat1*$^{-/-}$ $N = 9$; ICB, RT2 $N = 6$, RT2.*Stat1*$^{-/-}$ $N = 4$, ICB/AT, RT2 $N = 12$, RT2.*Stat1*$^{-/-}$ $N = 10$). The mice were sacrificed after 4 weeks of treatment for ex vivo analysis. **d, e** Representative triple-staining for the senescence marker p16^{Ink4a} (red) and the proliferation marker Ki67 (blue) and for nuclei (green) (**d**), **e** showing quantification of p16^{Ink4a+} (left) or Ki67$^+$ (right) cancer cells of individual mice, treated as described in **a**, each data point represents the total of three tumour slides measurements (Ctr, RT2 $N = 9$, RT2.*Stat1*$^{-/-}$ $N = 4$; AT, RT2 $N = 12$, RT2.*Stat1*$^{-/-}$ $N = 5$; ICB, RT2 $N = 9$, RT2.*Stat1*$^{-/-}$ $N = 3$, ICB/AT, RT2 $N = 13$, RT2.*Stat1*$^{-/-}$ $N = 7$), box plots show the median with 25th and 75th interquartile range (IQR), and whiskers indicate 1.5 × IQR. Significance tested by using Log Rank test (**a**, left), Fishers exact test (**a**, right), or two-tailed Mann-Whitney test (**c**, **e**). RT2.*Stat1*$^{-/-}$ mice have been censored after 3.7 weeks of treatment. Scale bars 200 µm (**b**) or 2 µm (**d**). Number of mice is given in parenthesis.

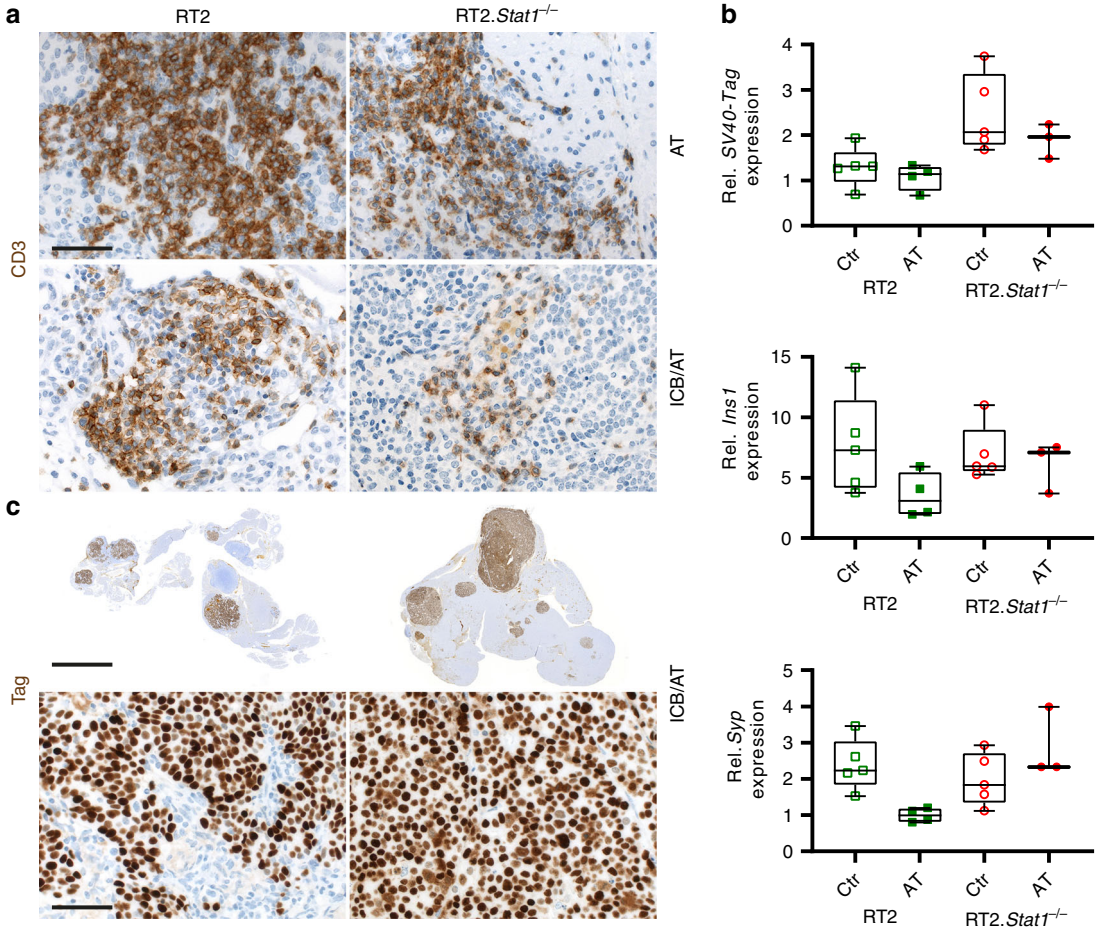

Fig. 5 Infiltration of either RT2 or RT2.*Stat1*$^{-/-}$ cancers by CD3$^+$ T cells, mRNA expression of tumour associated antigens (TAA) and protein expression of the SV40-Tag tumour antigen recognised by the transferred TAA-specific T_H1 cells. a Representative CD3 immune histochemistry images of RT2-cancers from either RT2 or RT2.*Stat1*$^{-/-}$ mice treated with adoptive transfer of T antigen-specific CD4$^+$ T_H1 cells (AT) or immune checkpoint blockade combined with AT (ICB/AT), scale bar 20 µm. **b** Relative expression of *SV40-Tag*, insulin (*Ins1*) or of synaptophysin (*Syp*) in single tumours isolated from RT2 or RT2.*Stat1*$^{-/-}$ mice after control (Ctr) treatment with NaCl or AT. Gene expression was analysed using *Actb* and *Eef1a1* as references. Each point represents one tumour from one mouse (Ctr, RT2 $N = 5$, RT2.*Stat1*$^{-/-}$ $N = 5$; AT, RT2 $N = 4$, RT2.*Stat1*$^{-/-}$ $N = 3$), box plots show the median with 25th and 75th interquartile range (IQR), and whiskers indicate 1.5 × IQR. **c** SV40-Tag immune histochemistry images of RT2-cancers were from either RT2 or RT2.*Stat1*$^{-/-}$ mice after ICB/AT therapy. Scale bar upper panel 400 µm, lower panel 20 µm.

diameter reached >15 mm, or ulcerated or when blood glucose dropped the second time below 30 mg dl^{-1}. Tumours were collected for ex vivo analysis. The tumour volume was calculated as ellipsoid $V = \frac{3}{4}\pi abc$; a, b, c are the semi-major axis $\left(\frac{lenght}{2}\right)$, $\left(\frac{width}{2}\right)$, with the assumption that the tumour height is equal to the short tumour side, defined as width $b = c$.

Treatment of RT2 or RT2.*Stat1*$^{-/-}$ mice. Ten- to eleven-week-old old female RIP-Tag2 (RT2)[31,62] or RT2.*Stat1*$^{-/-}$ mice were irradiated with 2 Gy one day before the first i.p. transfer of 1 × 10^7 tumour antigen-specific T_H1 cells. Tag-specific T_H1 cells were generated from spleen and lymph node cells of TCR2 mice. CD4$^+$ T cells were enriched by positive selection over magnetic microbeads. To generate Tag-T_H1 cells CD4$^+$ T cells were stimulated with Tag

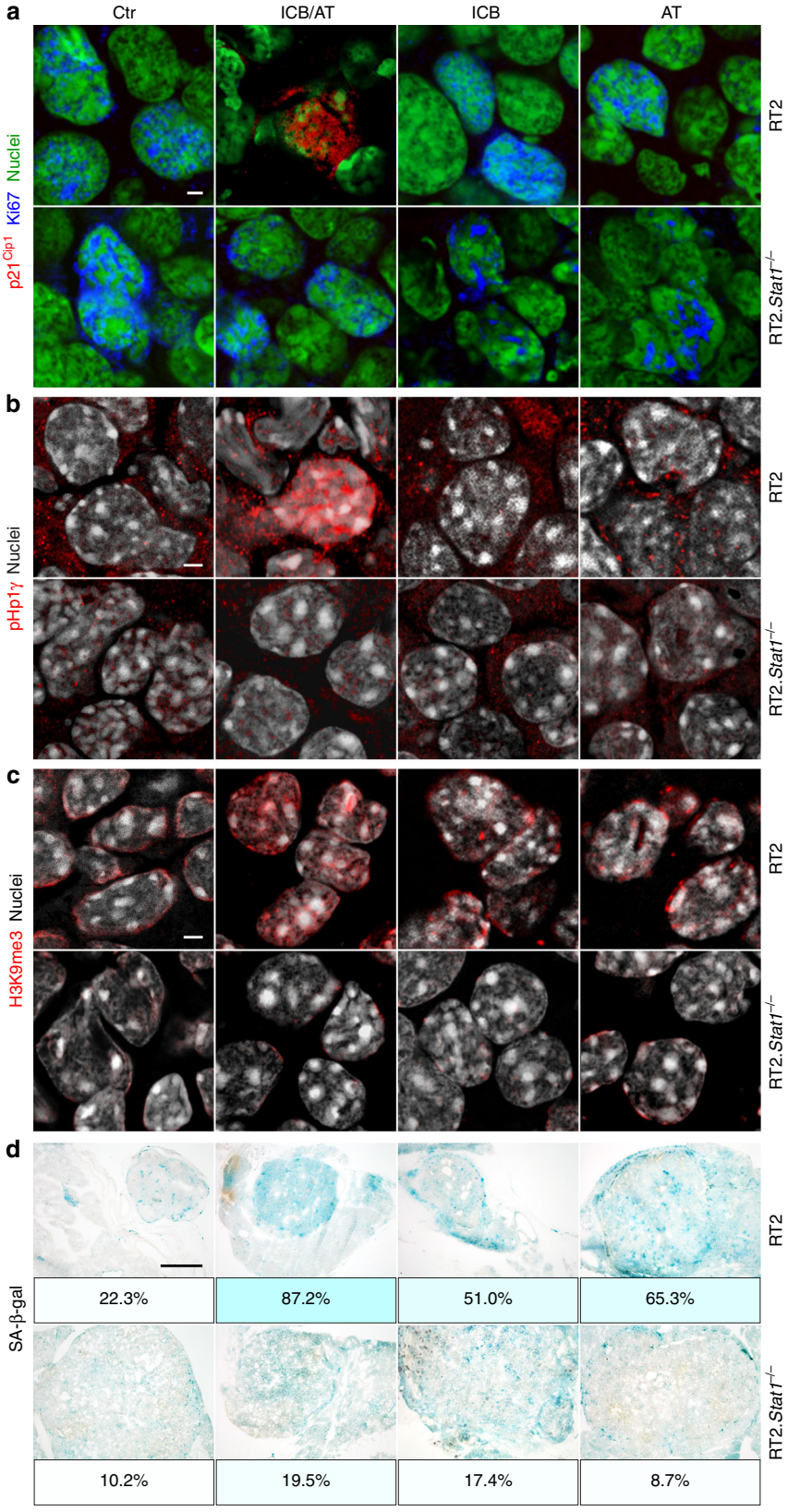

peptide 362–384 (EMC Microcollections), CpG-DNA 1668 (Eurofins MWG Operon) and 11B11 mAb (anti-IL-4; in-house production) and cultured in the presence of irradiated (30 Gy), syngeneic, T-cell-depleted antigen presenting cells (APC)[39]. After 3–4 days, Tag-T_H1 cells were expanded in the presence of 50 U IL-2 (hrIL-2). After cultivation for another 8 days, the Tag-T_H1 cells were used for adoptive transfer[31]. Cell transfer was applied once weekly. Anti-PD-L1 mAb (clone 10F.9G2, Bio X Cell) and anti-LAG-3 mAb (clone C9B7W, Bio X Cell) were i.p. injected twice per week (initially 500 µg each, afterwards 200 µg). Ctr mice received isotype-matched control antibodies (clone LTF-2 and HRPN, Bio X Cell) and PBS. Blood glucose was measured twice per week using the HemoCue Glucose 201+ System (HemoCue). Treatment was ended either after 4 treatment cycles for ex vivo analysis of tumour tissue, or when the blood glucose of the mice dropped twice below 30 mg dl^{-1} or when disease reached evidence; mice had no food restriction.

Fig. 6 *Stat1*-dependent induction of the nuclear senescence markers p21^{Cip1}, HP1γ, H3K9me3, and of SA-β-gal in RT2-cancers by combined ICB/AT therapy. Representative fresh frozen cryostat sections of RT2-cancers from either RT2 or RT2.*Stat1*$^{-/-}$ mice with established cancers were treated with either isotype control mAbs (Ctr), with adoptive transfer of TAA-specific T_H1 cells (AT), with immune checkpoint inhibitors (ICB; anti-PD-L1 and anti-LAG-3), or with ICB/AT. **a** p21^{Cip1} (red), Ki67 (blue), nuclei (green). **b** HP1γ (red), nuclei (white). **c** H3K9me3 (red), nuclei (white). **d** Representative microscopic images of SA-β-gal activity at pH5.5 and percentage of SA-β-gal positive tumour cells in each tumour. The colour evaluation and calculation of the SA-β-gal$^+$ cells are described in Supplementary Fig. 2 and Methods. Scale bars 2 µm (**a**–**c**), 1000 µm (**d**). Histology was performed in one to three representative tumours from Fig. 4e.

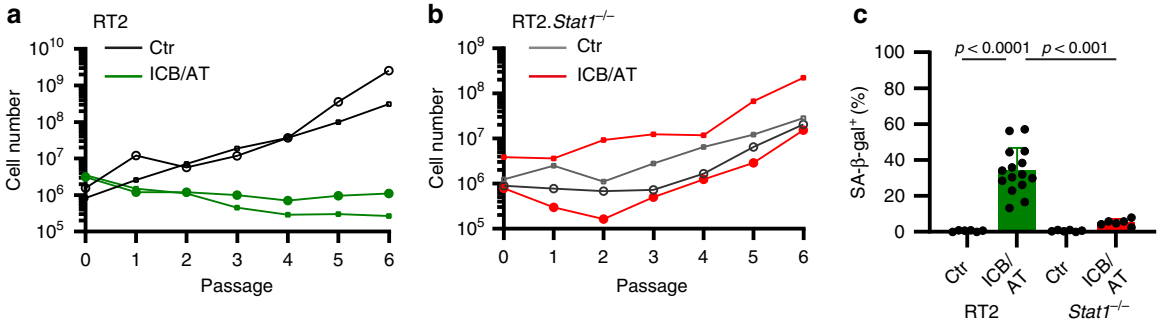

Fig. 7 *Stat1*-dependent induction of senescence in RT2-cancers by combined ICB/AT therapy. a, b Either RT2 mice (**a**) or RT2.*Stat1*$^{-/-}$ mice (**b**) with established cancers were either treated with isotype control mAbs (Ctr) or treated with immune checkpoint blockade (anti-PD-L1 and anti-LAG-3) and adoptive transfer of TAA-specific T_H1 cells (ICB/AT). After four weeks of treatment cells were isolated from the RT2-cancers and cultured in medium. Cells were counted at each passage. **c** After the passage ≥5, we determined the percentage of the SA-β-gal$^+$ cells. Data show the mean with SD; Ctr, RT2 $n = 6$, RT2.*Stat1*$^{-/-}$ $n = 6$; ICB/AT, RT2 $n = 15$, RT2.*Stat1*$^{-/-}$ $n = 6$. Staining for synaptophysin confirmed that the cultured cells were RT2-cancer cells. Significance was tested by using unequal variances *t*-test.

Treatment of λ-*MYC* mice. λ-*MYC* mice and double transgenic λ-*MYC.p21*$^{-/-}$ mice received intraperitoneal (i.p.) injections of 100 µg anti-CTLA-4 mAb (clone UC10-4B9, BioLegend) and 100 µg anti-PD-1 mAb (clone J43, Bio X Cell) (ICB) two to four times every ten days, starting at day 55 after birth. Control mice (Ctr) received no treatment. For IFN-γ neutralisation (ICB/anti-IFN-γ mAb), mice were additionally treated with an initial dose of 500 µg on day 54 and later with 300 µg anti-IFN-γ mAb (clone XMG1.2[25], Core Facility mAb, Helmholtz-Zentrum München) 6 h prior to the anti-CTLA-4/ PD-1 mAbs injection. Administration of 100 µg of the IFN-γ-neutralising mAb was continued at ten day intervals until the mice developed lymphomas. T cells were depleted by i.p. injection of 1 mg anti-pan-T-cell mAb MmTC[63] at day 54. Treatment was repeated every 3 to 4 days using doses of 400 µg. Mice were sacrificed as soon as tumours became clinically visible.

Immunofluorescence staining. Fresh frozen 5 µm serial cryosections of lymph nodes from λ-*MYC* mice, whole pancreas from RT2 and RT2.*Stat1*$^{-/-}$ mice or isolated RT2-, *Stat1*-, or *p16^{Ink4a}*-deficient RT2-cancer cells were fixed with perjodate-lysine-paraformaldehyde. Sections were blocked using donkey serum and stained with primary antibodies using rabbit-anti-p16^{Ink4a} (clone CDKN2A, catalogue number AHP1488, dilution 1:100 Bio-Rad/Serotec), rat-anti-Ki67 (clone SolA15, catalogue number 14-5698-82, dilution 1:100, Thermo Fisher Scientific/ eBioscience), rat-anti-p21^{Cip1} (clone HUGO291, catalogue number, dilution 1:100, Abcam), goat-anti-CD20 (clone M-20, catalogue number sc-7735, dilution 1:50, Santa Cruz), rabbit-anti-CD3 (clone SP7, catalogue number C1597R06, dilution 1:100, DCS), rabbit-anti-pHP1γ phospho S93 (aa 50-150, catalogue number ab45270, dilution 1:50, Abcam), rabbit-anti-H3K9me3 (aa 1-100, catalogue number ab8898, dilution 1:100, Abcam), rat-anti-PD-L1 (clone MIH6, catalogue number ab80276, dilution 1:50, Abcam) to use a mAb that recognises a different PD-L1 epitope than the applied in vivo mAb from clone 10F.9G2, rabbit-anti-beta 2 microglobulin antibody (clone EP2978Y, catalogue number ab75853, dilution 1:50, Abcam), goat-anti-CD3ε (clone M-20, catalogue number sc-1127, dilution 1:20, Santa Cruz), rat-anti-CD8a (clone 53-6.7, catalogue number 14-0081, dilution 1:1000, eBioscience), rat-anti-F4/80 (clone BM8, catalogue number 14-4801-82, dilution 1:50, eBioscience), rat-anti-MHC Class II antigen I Ak,d,b,q,r (ER-TR3) (catalogue number NB100-64961, dilution 1:200 Novusbio), armenian hamster-anti-CD49b (Integrin alpha 2) (catalogue number 14-0491 dilution 1:50, eBioscience), rabbit-anti-gamma H2A.X (phospho S139) (aa 100-200, catalogue number ab2893, dilution 1:200, abcam), goat-anti-DNA PKcs (aa 4078-4128, catalogue number ab168854, dilution 1:500, abcam), rabbit-anti-synaptophysin (aa 41-62, catalogue number NB300-653, dilution 1:200, Novusbio), rabbit-anti-CD161 antibody (clone ERP21236, catalogue number ab234107, dilution 1:100, abcam), rabbit-anti-Foxp3 (aa 43-100, catalogue number NB 100-39002, dilution 1:200, Novusbio). Bound antibodies were visualised using donkey-anti-rabbit-Cy3 (catalogue number 711-166-152, dilution 1:500 Dianova), donkey-anti-rat-Alexa 647 (catalogue number 712-606-153, dilution 1:500 Dianova), donkey-anti-rat-Cy3 (catalogue number 712-166-153, dilution 1:500, Dianova), donkey-anti-goat-Cy3 (catalogue number 705-166-147, dilution 1:500, Dianova) and donkey-anti-rabbit-Alexa 488 catalogue number 711-546-152, dilution 1:500, Dianova). For nuclear staining, Yopro (catalogue number Y 3603, dilution 1:1000, Invitrogen) or DAPI (catalogue number D9542, dilution 1:2000 Sigma) was used. Sections were analysed using a LSM 800 confocal laser scanning microscope (Zeiss Oberkochen). Images were processed with the software ZEN 2.3 (blue edition) and the Image Analysis Module.

Quantification of immunofluorescence. Tumour areas of images derived from three individual stained cryosections per tissue sample were analysed. For quantification of the Ki67 staining, 4500 Yopro stained nuclei were counted for Ki67$^+$ cells (1500 per slide, three serial slides per mouse). For quantification of p16^{Ink4a}, the area (µm^2) of the nuclear p16^{Ink4a} signal derived from 4500 Yopro stained nuclei (1500 per slide three serial slides per mouse) was measured.

Hematoxylin and eosin staining. Hematoxylin and eosin staining of the serial cryosections was performed according to standard procedures.

Immunohistochemistry staining. Immunohistochemistry was performed on an automated immunostainer (Ventana Medical Systems) according to the company's protocols for open procedures with slight modifications. 5 µm sections were stained with rabbit-anti-human/mouse-CD3 (clone SP7, catalogue number CI597C01, dilution 1:50, DCS-diagnostics) and PAB101 (Tag-specific mouse IgG2a mAb; dilution 1:200; in-house production).

SA-β-gal detection. 20 µm serial cryosections were fixed in 2% formaldehyde/ 0.25% glutaraldehyde and washed in PBS/$MgCl_2$. Slides were incubated in X-gal (5-bromo-4-chloro-3-indolyl-beta-D-galactopyranoside) staining solution (1 mg/mL X-Gal, 1 mM $MgCl_2$, 5 mM K3Fe(CN)6, 5 mM K4Fe(CN)6 in PBS, pH 4.0, 5.5, and 7.0) up to 10 h at 37 °C.[64]. The stained slides were rinsed in PBS/$MgCl_2$ and analysed using a Nikon Eclipse 80i microscope; magnification ×4.

SA-β-gal positive percentage quotation with Adobe Photoshop CS6. All images were analysed with the "White Balance Tool" to obtain the same white background, followed by "Quick Mask Mode" to identify only the tumour area. Using this area the arithmetic mean of the blue-green values was obtained by the filter "Blur Average Tool". The "Eye Dropper Tool" was used to identify the red, green and blue (RGB) colour code to get the corresponding colour field (Supplementary Fig. 2a). Afterwards the tumour area was reselected using the previous created "Quick Mask Mode Layer". The pixels outside the tumour area were deleted by inversing the selection. The number of pixels in the histogram correlates with the tumour area. "The Posterize Tool" separated the different tonal values, in

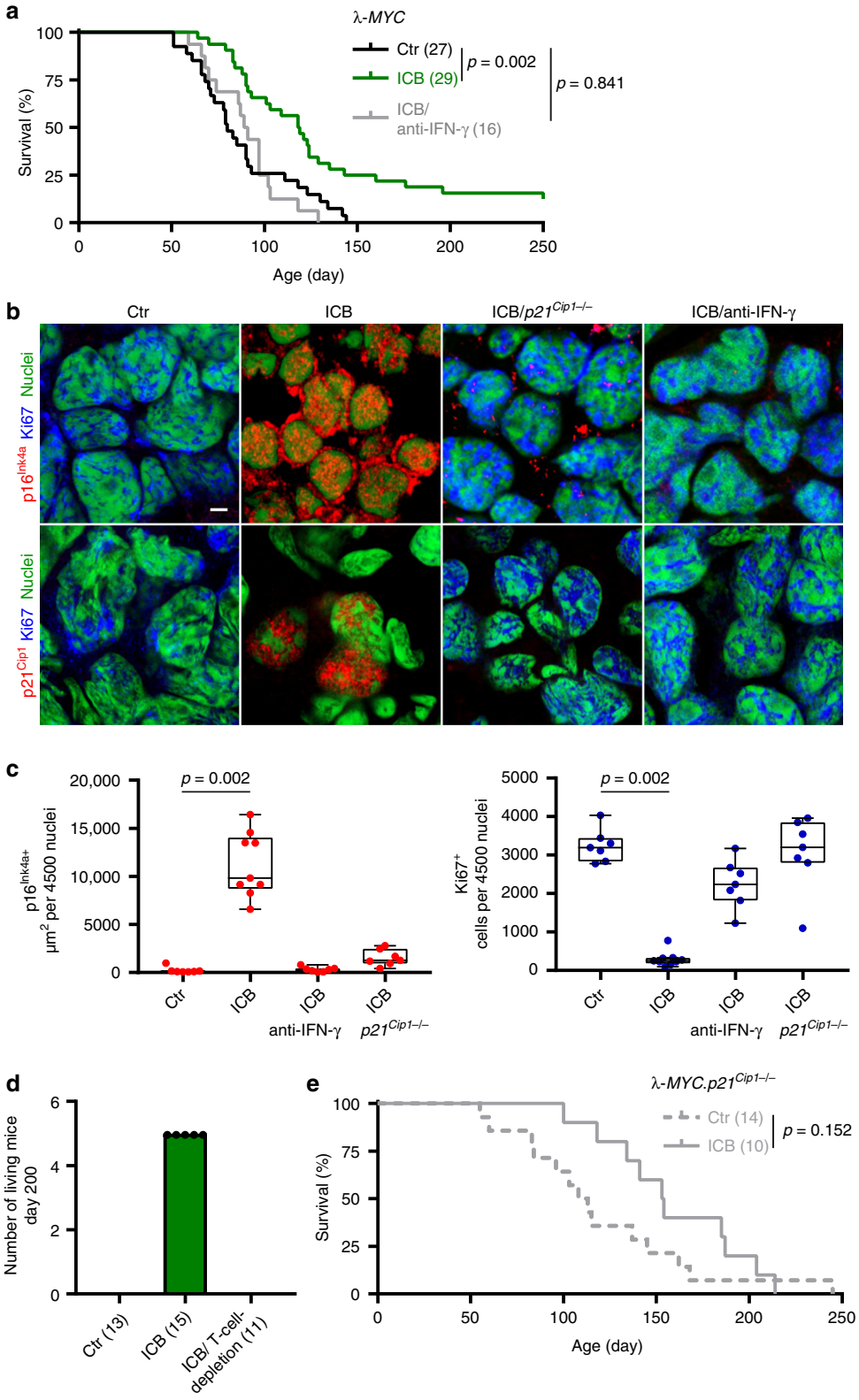

our case blue-green. "The Magic Wand Tool" was used to select and delete the white pixels (Supplementary Fig. 2b). The number of pixels correlates with the area of SA-β-gal stained tumour cells. The SA-β-gal stained tumour cells in Fig. 2d, Fig. 6d and Fig. 9c were calculated and given in percent (blue pixel of total pixels of the tumour area).

SA-β-gal activity for electron microscopy. Small tissue samples (semi-thin 0.5 µm and for electron microscopy ultra-thin 20 nm, respectively) were fixed in fixation solution (0.25% Glutaraldehyde in 2% PFA) and washed in PBS/$MgCl_2$ solution. X-gal staining solution was added for 12 h. Samples were washed in PBS/$MgCl_2$ solution afterwards followed by Karnovsky fixation. Samples were embedded in glycid ether for electron microscopic analysis[64].

Electron microscopy. SA-β-gal stained cryosections were fixed with Karnovsky's fixative for 24 h. Post-fixation was based on 1% osmium tetroxide containing 1.5% K-ferrocyanide in cacodylate buffer. After following the standard methods, blocks were embedded in glycide ether and cut using an ultra-microtome (Ultracut, Reichert, Vienna, Austria). Ultra-thin sections (30 nm) were mounted on copper

Fig. 8 IFN-γ and *p21*^{Cip1}-dependent immune control of λ-*MYC*-induced lymphomas by ICB therapy. a Survival curves of control (Ctr $N = 27$), or immune checkpoint inhibitor (ICB; anti-CTLA-4 and anti-PD-1 $N = 29$) treated λ-*MYC* mice, or of λ-*MYC* mice treated with ICB and anti-IFN-γ ($N = 16$). **b, c** Triple-staining for the senescence marker p16^{Ink4a} (red, upper panel) or p21^{Cip1} (red, lower panel), the proliferation marker Ki67 (blue), and for nuclei (green); scale bar 2 µm; representative pictures from Fig. 8c (**b**). Box plots with individual data points representing p16^{Ink4a+} (**c**, left) or Ki67^{+} nuclei (**c**, right) of B cells from Ctr- ($N = 7$), ICB- ($N = 9$), ICB and anti-IFN-γ-treated λ-*MYC* mice ($N = 7$), or ICB-treated λ-*MYC.p21*$^{Cip1-/-}$ mice ($N = 7$). Lymph nodes were isolated at similar ages. Each point represents triplicates from one mouse, box plot show the median with 25th and 75th interquartile range (IQR), and whiskers indicate 1.5 × IQR. **d** λ-*MYC* mice from the individual treatment groups living at day 200, Ctr $N = 13$, ICB $N = 15$, ICB and T-cell-depletion $N = 11$. **e** Survival curves of either control (Ctr, $N = 14$) or ICB-treated λ-*MYC.p21*$^{Cip1-/-}$ mice ($N = 10$). Significance tested by using Log Rank test (**a**, **e**), two-tailed Mann-Whitney test (**c**).

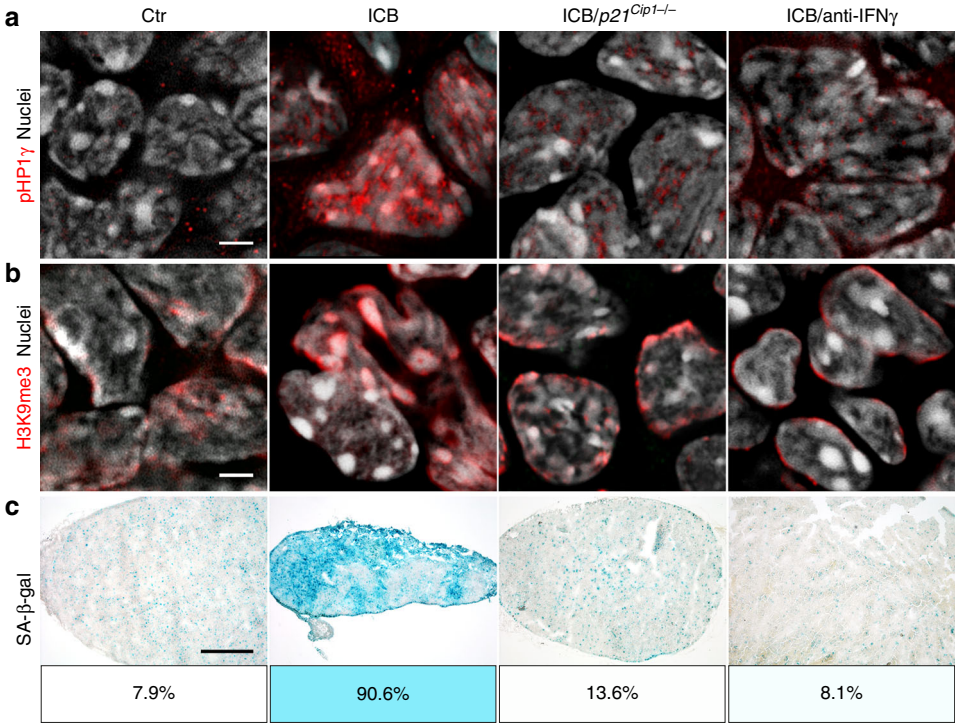

Fig. 9 IFN-γ and *p21*^{Cip1}-dependent senescence induction in B cells of λ-*MYC* mice during ICB. a–c Fresh frozen cryostat sections of representative lymph nodes of λ-*MYC* or λ-*MYC.p21*$^{Cip1-/-}$ mice. λ-*MYC* mice were controls (Ctr) or treated with anti-CTLA-4 and anti-PD-1 mAbs (ICB) or anti-CTLA-4, anti-PD-1 and anti-IFN-γ mAbs (ICB/anti-IFN-γ), or λ-*MYC.p21*$^{Cip1-/-}$ mice were treated with ICB (ICB/*p21*$^{Cip1-/-}$). pHP1γ (red), nuclei (white) (**a**). H3K9me3 (red), nuclei (white) (**b**). Representative microscopic images of SA-β-gal activity at pH5.5 and percentage of SA-β-gal positive tumour cells in each tumour (**c**). The colour evaluation and calculation of the SA-β-gal^{+} cells are described in Supplementary Fig. 2 and Methods. Scale bars 2 µm (**a**, **b**), 1000 µm (**c**). The SA-β-gal data are representative for three individual tumours. Immune fluorescence was performed in one to two representative tumours from Fig. 8c.

grids and analysed using a Zeiss LIBRA 120 transmission electron microscope (Carl Zeiss, Oberkochen, Germany) operating at 120 kV.

Cell culture. Adherent primary murine RT2-cancer cells (described above), B16-F10 melanoma cells (catalogue number CRL-6475, ATCC) and B16-OVA melanoma cells (gift from R. Dutton, Trudeau Institute, New York, USA) were cultured in Dulbecco's Modified Eagle's Medium (DMEM) supplemented with 10% foetal calf serum (FCS), nonessential amino acids, sodium pyruvate, antibiotics, and 50 µM 2-mercaptoethanol at 37 °C and 7.5% CO_2. The murine melanoma cell lines B16 and B16-OVA were cultured in DMEM medium, containing 10% FCS and penicillin/streptomycin (100 U ml^{-1}; all from Biochrom AG), at 37 °C and 5% CO_2. The human patient-derived xenograft (PDX) cell lines were cultured in RPMI-1640 medium supplemented with 10% FCS, nonessential amino acids, sodium pyruvate, antibiotics, and 5 µg ml^{-1} Plasmocin (Invitrogen) to treat infections of clinical samples, at 37 °C and 5.0% CO_2. Cell line supernatants were tested with a mycoplasma detection PCR Venor Ge*M* (Minerva Biolabs GmbH) regularly every 4 weeks.

Generation of primary murine RT2- or RT2.*Stat1*$^{-/-}$-cell lines. RT2-cancers were isolated from the pancreas of female RT2 or RT2.*Stat1*$^{-/-}$ mice by intraductal injection of collagenase (1 mg ml^{-1}, Serva, Heidelberg, Germany)[25,31]. After injection, the pancreata were harvested, digested in collagenase solution at 37 °C for 10 min, and then mechanically disrupted. Whole encapsulated tumours were separated under a dissection microscope (Leica Microsystems) and further processed for immunofluorescence microscopy, immunohistochemistry or gene expression analysis. Alternatively, single tumour cells were obtained by incubation of the tumours in 0.05% trypsin/EDTA solution (Invitrogen) at 37 °C for 10 min. After incubation, RT2-cancer cells were seeded onto tissue culture plates.

Generation of primary *p16*^{Ink4a}-deficient RT2-cell lines. CDKN2a-loss variants on chromosome 4, qC4.A were generated by random selection from CIS- or ICB-resistant RT2-cancer cells.

Generation of CRISPR-mediated deletion of *Cdkn2a* in primary RT2-cell lines. gRNAs targeting Exon 2 (position 120-142 and 125-157) of murine *Cdkn2a* (sequence from Ensembl genome browser 97) were designed using CRISPRdirect[65] (g*Cdkn2a*_1: 5′-gcgtcgtggtggtcgcacagg-3′, g*Cdkn2*a_2: 5′-gacacgctggtggtgctgcac-3′). As a control a previously described gRNA targeting GFP gRNA targeting GFP (sgRNA target site sequence: 5′-gggcgaggagctgttcaccg-3′)[66] was used. The DNA oligos were ordered from Sigma Aldrich. Equimolar amounts of complementary DNA oligos were annealed and phosphorylated in T4 ligation buffer (NEB). The reaction was performed at 37 °C for 30 min, 95 °C for 5 min, followed by a gradual temperature reduction to 25 °C (5 °C/min). The vector pSpCas9(BB)-2A-GFP (pX458; Addgene plasmid ID: 48138) was digested with the *BbsI* restriction enzyme (NEB) and dephosphorylated using Calf Intestinal Alkaline Phosphatase (NEB). The ligation reaction (NEB) was performed overnight. The plasmids were sequenced (Microsynth Seqlab) with a hU6 sequencing primer (LKO.1 5′: gactatcatatgcttaccgt). For transfection, plasmid DNA was generated by using the Qiagen

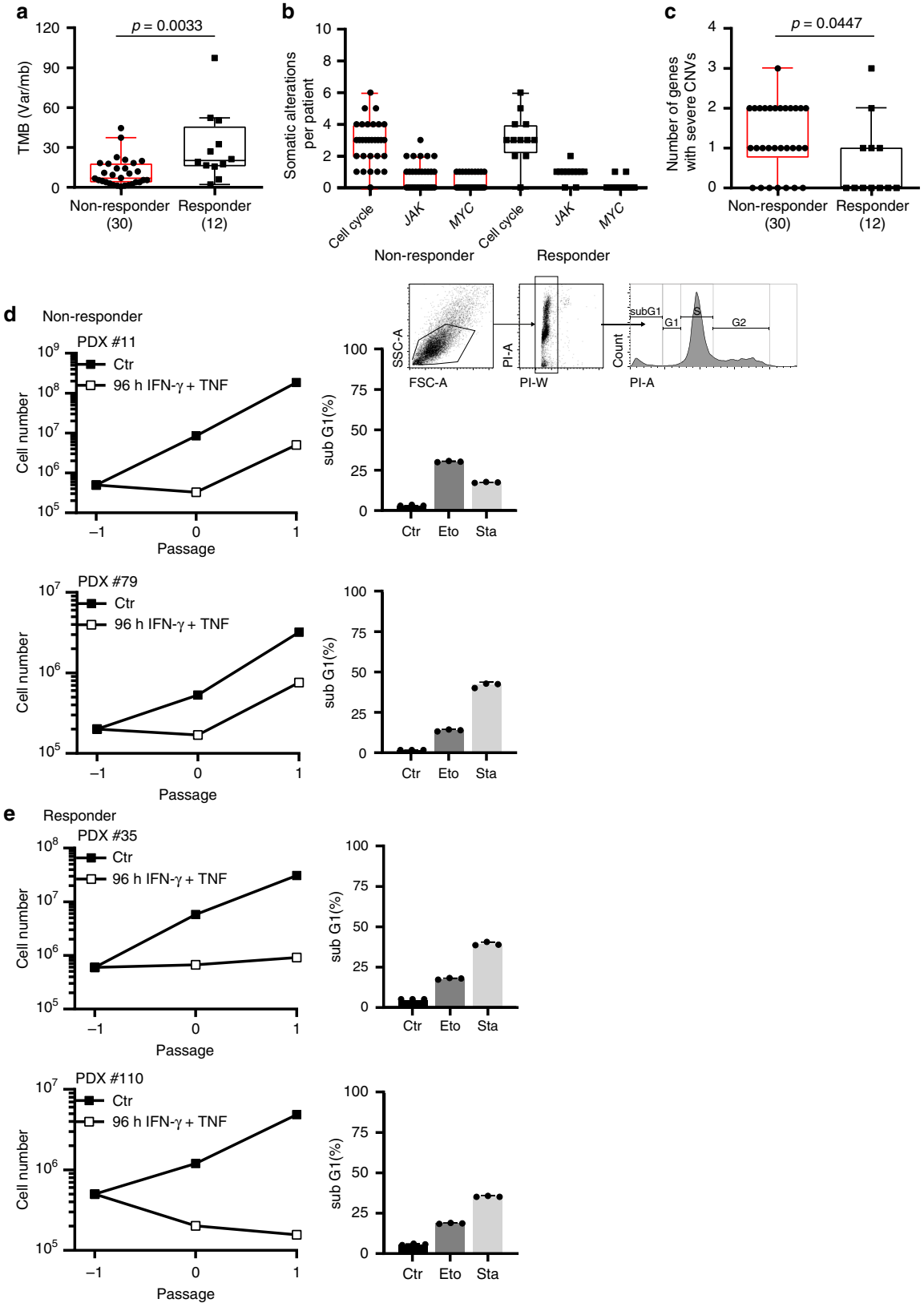

EndoFreeMaxi Kit.[66] The primary RT2-cell lines were transfected using the Quiagene Effectene Transfection Reagent.

Generation of primary human melanoma cell lines. Melanoma tissue was cut into small pieces, digested in HBBS (w/o Ca^{2+} and Mg^{2+}) with 0.05% collagenase, 0.1% hyaluronidase and 0.15% dispase, at 37 °C for 1 h and filtered through a cell strainer (100 µm mesh). The melanoma cell suspension was implanted with Matrigel (Corning Life Sciences) subcutaneously in NSG (NOD.*Cg-Prkdc*^{scid} *Il2rg*^{tm1Wjl}/*SzJ*) mice, patient derived xenografts (PDX). Tumour grafts were harvested when they reached a diameter of 10 to 15 mm, digested as above and the single cells were taken into culture using RPMI1640 with Hepes and L-Glutamine, containing 10% foetal bovine serum, 1% penicillin-streptomycin at 37 °C with 5% CO_2 and 95% humidity. For cryo-preservation cell pellets were resuspended in Biofreeze medium (Biochrom/Merck)

Fig. 10 Loss of senescence-inducing and amplification of senescence-inhibiting cell cycle regulator genes in melanoma metastases of patients resistant to ICB. a–c Sequencing data from metastases of non-responder patients ($N = 30$) versus metastases of responder patients ($N = 12$). In non-responder patients disease progressed within 3 months of ICB therapy. In responder patients metastases regressed ≥1 year of ICB therapy. Tumour mutational burden (TMB, copy number variations) (**a**). Number of tumour-specific alterations in 19 genes of the cell cycle, *JAK* or *MYC* pathway (**b**). Number of genes with homozygous deletions in cycle inhibitors or amplifications ≥ 3fold in cell cycle promoters. Genes analysed: *CDKN2A/B/C, CDKN1A/B, RB1, TP53, JAK1/2/3, CCND1/2/3, CDK4/6, CCNE1, MDM2/4, MYC*. We performed paired panel sequencing of the tumour DNA and of normal DNA to identify tumour-specific alterations. Box plots show the median with 25th and 75th interquartile range (IQR), and whiskers indicate 1.5 × IQR (**c**). **d, e** Growth curves of patient derived melanoma lines from two metastases of non-responder patients (**d**) or from two metastases of responder patients (**e**). Cells were cultured for the senescence assay either with medium (Ctr) or with medium containing 100 ng ml^{-1} IFN-γ and 10 ng ml^{-1} TNF for 96 *h*, washed and then cultured with medium for another 4–6 days. **d, e** Apoptosis assay with melanoma cells derived from two non-responder (**d**, including gating strategy) or two responder patients (**e**) were exposed to either medium (Ctr) or etoposide (Eto, 100 μM) or staurosporine (Sta, 0.5 μM) for 24 h for apoptosis induction and then stained with propidium iodide. SubG$_1$ cells were detected by flow cytometry analysis; data show the geometric mean with geometric SD, $n = 3$. Significance tested by using two-tailed Mann-Whitney test (**a–c**).

and 1 ml per cryotube of the cell suspension was frozen for short-term storage at −80 °C and for long-term storage in liquid nitrogen.

Senescence assay. RT2-, RT2.*Stat1*$^{-/-}$-, RT2.*p16*^{Ink4a}-, RT2-CRISPER-control- or RT-CRISPER-*p16*^{Ink4a}-cancer cells or human melanoma-derived (PDX) cells were cultured with medium containing 100 ng ml^{-1}IFN-γ and 10 ng ml^{-1} TNF or exclusively with medium (Ctr) for 96 h, washed, then cultured with medium for another 3–4 days (till the Ctr cells reach confluence) and counted[31].

SA-β-galactosidase activity assay in vitro. After treatment with IFN-γ and TNF, RT2-cancer cells were fixed for 15 min at room temperature, and then stained for 16 h at 37 °C using the β-galactosidase staining kit (United States Biological)[31]. In addition, cell nuclei were stained with 4′,6-diamidin-2-phenylindole (DAPI; Invitrogen). SA-β-gal-positive and -negative cells were counted using a Zeiss Axiovert 200 microscope equipped with Visiview software and analysed by using ImageJ software (NIH).

Apoptosis assay. For apoptosis assay, cancer cells were exposed to etoposide (Eto, 100 μM, Bristol-Meyers-Squibb, ETOPOPHOS), staurosporine (Sta, 0.5 μM, Bio-Vision) or medium (Ctr) for 24 h and stained for propidium iodide and annexin V. Annexin V-positive and subG1 cells were detected and quantified by flow cytometry. Analysis was performed on a LSRII cytometer (BD Bioscience) and analysed by FlowJo software version 10.

Chromium release assay. CD8$^+$ cytotoxic T cells (CTL) were generated from spleen and lymph node cells of OT I-transgenic mice. CD8$^+$ T cells were enriched by positive selection over magnetic microbeads. To generate CTL cells CD8$^+$ T cells were cultured in the presence of irradiated (30 Gy), syngeneic, T-cell-depleted antigen presenting cells (APC)[39] in the presence of IL-2 (10 U ml^{-1}), IL-12 (5 ng ml^{-1}), and anti-IL-4 Ab (10 μg ml^{-1}).[31] 2.5 × 10^6 target cells were labelled with 250 μCi (9.25 MBq)^{51}NaCr (Hartmann Analytic) at 37 °C for 1.5 h, washed and plated into microtitre round bottom plates at 1 × 10^4 cells per well. CD8$^+$ effector cells were added to target cells in the ratio 40 to 1 and incubated at 37 °C for 4 h. B16-OVA cells were used as positive controls, B16-F10 melanoma cells were used as negative controls. Spontaneous release in the absence of effector cells was <30% of the maximal release induced by 1% Triton X-100. After incubation, 50 μl supernatant per well was mixed with 200 μl scintillation cocktail (Ultima Gold, PerkinElmer) and measured in a liquid scintillation counter (MicroBeta, PerkinElmer).

Patients and specimen collection. Patients with metastatic melanoma were treated with either anti-PD-1 mAb or combined anti-CTLA-4 and anti-PD-1 mAbs. Non-responder patients were 30 patients (43.3% female, 61.5 median age, 22–89 age range) that progressed during the first 3 month of therapy. Responder patients were 12 patients (33.3% female, 56.5 median age, 27–75 age range) that had either a partial (>30%) or complete tumour regression over more than 1 year. Tumour biopsies were compared to healthy tissue from the safety margins as control tissue. Ethical approval was obtained from the Ethics Committee Tübingen. All patients had signed the written informed consent form for research analyses. The study was carried out in accordance with the Declaration of Helsinki and good clinical practice.

Sequencing. All patient samples were analysed using a hybridisation-based custom gene panel. Since the patient samples were collected in clinical routine, three different versions of the panel were used (ssSCv2, ssSCv3 and ssSCv4). The number of target genes was increased from one version to the next starting from 337 genes on ssSCv2, to 678 genes on version ssSCv3 and 693 on the current version ssSCv4. The panels were designed to detect somatic mutations (SNVs), small insertions and deletions (INDELs), copy number alterations (CNAs) and selected structural rearrangements Supplementary Data Tables 1–3 (custom gene panel ssSCv2 ssSCv3 ssSCv4). The library preparation and in solution capture of the target region was performed using the Agilent SureSelectXT and SureSelectXT^{HS} reagent kit (Agilent, Santa Clara, CA). DNA from tumour (FFPE) and matched normal controls (blood) were sequenced in parallel on an Illumina NextSeq500 using 75 bp paired-end reads. The tumour samples were sequenced to an average sequencing depth of coverage of 511x and the normal control samples to 521×, respectively. An in-house developed pipeline, called "megSAP" was used for data analysis [https://github.com/imgag/megSAP, version: 0.1-733-g19bde95 and 0.1-751-g1c381e5]. The sequencing reads were aligned to the human genome reference sequence (GRCh37) using BWA (vers. 0.7.15)[67]. Variants were called using Strelka2 (vers. 2.7.1) and annotated with SNPeff/SnpSift (vers. 4.3i)[68,69]. The overall mutational rate was as calculated using the formula: $\left[\frac{\left(\frac{Somatic-Known-Tumorgenes}{Target\ size}\times Genome\ size\right)+Tumorgenes}{Genome\ size}\right]$. For validity and clinical relevance, an allele fraction of ≥ 5% (i.e. ≥10% affected tumour cell fraction) was required for reported mutations (SNVs, INDELs). Copy number alterations (CNAs) were identified using ClinCNV [https://doi.org/10.1101/837971, https://doi.org/10.1101/837971v1], a method for multi-sample CNV detection using targeted or whole-genome NGS data. The method consists of four steps: (i) quantification of reads per target region, (ii) normalisation by GC-content, library size and median-coverage within a cohort of samples sequenced with the same NGS panel, (iii) calculation of log2-fold changes between tumour and normal sample, (iv) segmentation and CNV calling. Using log2-fold changes ClinCNV estimates statistical models for different copy number states per region (conditioned by tumour sample purity) and reports an likelihood for each statistical model, assuming that the majority of samples are diploid at a focal region. The log-likelihood of the diploid model is subtracted from alternative models, resulting in positive likelihoods for true alternative copy number states. Finally, maximum segments of contiguous regions with positive log-likelihood ratios are identified in an iterative manner. Segments consisting of at least three regions with log-likelihood ratio ≥ 40 and CN state ≤ 1.5 or ≥ 3 are reported as CNVs. Quality control (QC) parameters were collected during all analysis steps[70].

Comparative genomic hybridisation (CGH) array. DNA was isolated from RT2-cancer cells or reference spleen (wildtype male) tissue with the DNeasy Blood & Tissue Kit (Qiagen) according to the manufacturer's instructions. DNA was labelled using the SureTag Complete DNA Labelling Kit (Agilent Technologies) and hybridised on an Agilent Mouse Genome CGH Microarray, 2 × 105 K (Agilent Technologies), and the image was analysed using Feature Extraction 10.5.1.1 and Agilent Genomic Workbench Lite Edition 6.5 with Genome Reference Consortium Mouse Build 38.

Quantitative PCR. RT2-cancer cells were harvested by trypsin digestion and snap frozen in liquid nitrogen. RNA was prepared using the Nucleospin RNA Mini kit (Macherey-Nagel); cells were lysed using Tris(2-carboxyethyl)phosphine (TCEP)-containing RL1 buffer, followed by DNase digestion (Invitrogen). RNA quality was controlled by agarose gel electrophoresis and by OD600 measurements using a photometer (Eppendorf AG). Complementary DNA was prepared using the iScript cDNA synthesis kit (Bio-Rad Laboratories). Quantitative PCR was performed with SybrGreen using a LightCycler 480 (Roche). Gene expression was analysed using qbase software (Biogazelle) based on the delta-delta-CT-method and reference genes were evaluated using geNorm (feature of the q base software, Biogazelle). The following primers were used: *SV40-Tag* sense 5′-tcc act cca caa ttc tgc tct-3′, antisense 5′-ttg ctt ctt atg tta att tgg tac aga-3; *Cdkn2a* sense 5′-ttg ccc atc atc atc acct-3′, antisense 5′-ggg ttt tct tgg tga agt tcg-3′; *Actb* sense 5′-cta agg cca acc gtg aaa ag-3′, antisense 5′ acc aga ggc ata cag gga ca 3′; *Eef1a1* sense 5′ aca cgt aga ttc cgg caa gt 3′, antisense 5′ agg agc cct ttc cca tctc 3′.

Magnetic resonance imaging. Magnetic resonance imaging (MRI) was performed with ten-week-old RT2 mice under 1.5% isoflurane anaesthesia using a 7 T small animal magnetic resonance scanner (ClinScan, Bruker Biospin MRI, Ettlingen, Germany) equipped with quadrature mouse whole-body coil with an inner diameter of 35 mm. For detection of the β-cancers and general anatomic information, a T2-weighted 3D turbo spin-echo-sequence (TE/TR 205/3,000 ms, image matrix of 160 × 256, slice thickness 0.22 mm) was used. Respiration was monitored and used for triggering MRI data acquisition. The acquired MRI data was visualised using Inveon Research Workplace software (Siemens Preclinical Solutions, Knoxville, TN, USA).

Light sheet fluorescence microscopy. Five-week-old RT2 or RT2.*Stat1*$^{-/-}$ mice were treated with TAA-T_H1 cells or NaCl as described. Mice were injected i.v. with 50 µg of Alexa Fluor 700 anti-mouse CD4 mAb clone GK1.5 and Alexa Fluor 647 anti-mouse CD11b mAb clone M1/70 (BioLegend), 48 h after the second treatment. After 2 h, organs were harvested and fixed in 4% paraformaldehyde/PBS solution at 4 °C for 8 h. Tissue was dehydrated at room temperature using increasing concentrations of ethanol (30, 50, 70, 80, 90%) for 2 h each and in 100% ethanol at 4 °C overnight. Tissues were incubated in n-hexane for 2 h and then cleared using two parts benzyl benzoate and one part benzyl alcohol (Sigma-Aldrich) three times for 30 min. Air exposure was strictly avoided during this step. The samples were then visualised and analysed using a custom-built laser scanning light sheet microscope using a high NA 20× magnification and reconstructed using the IMARIS software (Bitplane).

Flow cytometry. Five-week-old RT2 or RT2.*Stat1*$^{-/-}$ mice were irradiated with 2 Gy one day before the first i.p. transfer of 1×10^7 TAA-T_H1 cells or NaCl[25]. 48 h after the second treatment mice were sacrificed. The pancreatic lymph node was separated from the pancreas tissue of each mouse, the pancreas was homogenised via a 200 µm cell strainer in DMEM media containing 20% FCS at 4 °C, erythrocytes were lysed with ACK lysis buffer (Cambrex), and samples were stained for 30 min at 8 °C with fluorochrome-conjugated antibodies (anti-mouse CD4-Pacific Blue, clone GK1.5, catalogue number 100428; anti-mouse CD8a-PE-Cy7, clone 53–6.7, catalogue number 100722; anti-mouse CD45.2-APC-Cy7, clone 104 catalogue number 101224; anti-mouse-CD11c-APC, clone N418, catalogue number 117310; anti-mouse CD11b-Pacific blue, clone M1/70, catalogue number 101224; or corresponding isotype controls (dilution 1:150, BioLegend)). Cells were separated again via a 50 µm cell strainer. Flow cytometry was performed using a FACS Aria and analysed with DIVA software (Becton Dickinson). Alternatively, flow cytometry analyses with T_H1 cells or RT2-cancer cells which have been stained with fluorochrome-conjugated antibodies (anti-mouse-PE-IFN-γ, clone XMG1.2, catalogue number 505807; anti-mouse-PE-TNF-α, clone MP6-XT22, catalogue number 506306; anti-mouse-PE IL-4, clone 11B11, catalogue number 504104; anti-mouse- PE β2-microglobulin, clone A16041A, catalogue number 154503; anti-mouse PE/Cy7 CD274 (B7-H1, PD-L1), clone 10F.9G2, catalogue number 124313 (dilution 1:250, BioLegend)) were performed on a LSRII cytometer (BD Bioscience) and analysed by FlowJo software version 10.

Statistical analysis. The experiments were not randomised. The investigators were not blinded to allocation during the experiments or outcome assessment. No power calculations were used, but sample sizes were selected on the basis of previous experiments; in vitro results were based on three independent experiments to guarantee reproducibility of findings. The statistics software JMP version 12.2.0 (SAS Institute) and GraphPad Prism version 6 (GraphPadSoftware, California, USA) were used for statistical analyses and for the generation of diagrams. To address the question whether the treatment effect was different between two genotypes, the decadic logarithms of tumour volumes were analysed in ANCOVAs, using the nominal factors "mouseID" (nested under "treatment" and "genotype"), "treatment" and "genotype" as well as the combination "treatment" and "genotype"; "time" was used as continuous factor; finally, the combinations of "mouse ID" and "time", "treatment" and "time", "genotype" and time" and the most important combination "treatment" and "genotype" and "time" were used. For purpose of normalisation, decadic logarithms of tumour volume were used in the analyses; zero observations were replaced by half the minimum of positive values before calculating the logarithms. Group comparisons were made with non-parametric, unpaired, two-tailed Mann-Whitney (Wilcoxon) tests or parametric, unpaired, two-tailed t test with Welch's correction for unequal variances. Log-rank test was used for the comparison of survival from λ-*MYC* mice, RT2 mice and tumour latency curves. Because of disparate censoring between RT2 mice and RT2.*Stat1*$^{-/-}$ mice Fisher's exact tests was used to compare the survival (as indicated in the text). N refers to the number of patients, mice or samples and cell lines from different mice, respectively.

Data availability

Primary generated cancer cells are available from the authors. The sequencing data from patient samples have been deposited in the EGA database under the accession code EGAS00001004151. Comparative genome hybridisation array data have been deposited in the NCBI GEO database under the accession code GSE142192. All the other data supporting the findings of this study are available within the article and its supplementary information files and from the corresponding author upon request. Source data for Fig. 1a, c and 3a–c and 4a, c, e and 5b and 7a–c and 8a, c, d, e and 10a–e and Supplementary Figs. 1a and 11c–e are available as a source data file. A reporting summary for this article is available as a Supplementary Information file.

Received: 26 November 2018; Accepted: 7 February 2020;
Published online: 12 March 2020

References

1. Leach, D. R., Krummel, M. F. & Allison, J. P. Enhancement of antitumor immunity by CTLA-4 blockade. *Science* **271**, 1734–1736 (1996).
2. Koebel, C. M. et al. Adaptive immunity maintains occult cancer in an equilibrium state. *Nature* **450**, 903–907 (2007).
3. Okazaki, T., Chikuma, S., Iwai, Y., Fagarasan, S. & Honjo, T. A rheostat for immune responses: the unique properties of PD-1 and their advantages for clinical application. *Nat. Immunol.* **14**, 1212–1218 (2013).
4. Tumeh, P. C. et al. PD-1 blockade induces responses by inhibiting adaptive immune resistance. *Nature* **515**, 568–571 (2014).
5. Twyman-Saint Victor, C. et al. Radiation and dual checkpoint blockade activate non-redundant immune mechanisms in cancer. *Nature* **520**, 373–377 (2015).
6. Topalian, S. L., Drake, C. G. & Pardoll, D. M. Immune checkpoint blockade: a common denominator approach to cancer therapy. *Cancer Cell* **27**, 450–461 (2015).
7. Kroemer, G., Senovilla, L., Galluzzi, L., Andre, F. & Zitvogel, L. Natural and therapy-induced immunosurveillance in breast cancer. *Nat. Med.* **21**, 1128–1138 (2015).
8. Blank, C. U., Haanen, J. B., Ribas, A. & Schumacher, T. N. Cancer immunology. The "cancer immunogram". *Science* **352**, 658–660 (2016).
9. Tran, E., Robbins, P. F. & Rosenberg, S. A. 'Final common pathway' of human cancer immunotherapy: targeting random somatic mutations. *Nat. Immunol.* **18**, 255–262 (2017).
10. Ribas, A. & Wolchok, J. D. Cancer immunotherapy using checkpoint blockade. *Science* **359**, 1350–1355 (2018).
11. Galon, J. et al. Type, density, and location of immune cells within human colorectal tumors predict clinical outcome. *Science* **313**, 1960–1964 (2006).
12. Rocken, M. Early tumor dissemination, but late metastasis: insights into tumor dormancy. *J. Clin. Invest.* **120**, 1800–1803 (2010).
13. Sosa, M. S., Bragado, P. & Aguirre-Ghiso, J. A. Mechanisms of disseminated cancer cell dormancy: an awakening field. *Nat. Rev. Cancer* **14**, 611–622 (2014).
14. Perez-Mancera, P. A., Young, A. R. & Narita, M. Inside and out: the activities of senescence in cancer. *Nat. Rev. Cancer* **14**, 547–558 (2014).
15. Pollard, J. W. Defining metastatic cell latency. *N. Engl. J. Med* **375**, 280–282 (2016).
16. Massague, J. & Obenauf, A. C. Metastatic colonization by circulating tumour cells. *Nature* **529**, 298–306 (2016).
17. Aguirre-Ghiso, J. A. How dormant cancer persists and reawakens. *Science* **361**, 1314–1315 (2018).
18. Schreiber, R. D., Old, L. J. & Smyth, M. J. Cancer immunoediting: integrating immunity's roles in cancer suppression and promotion. *Science* **331**, 1565–1570 (2011).
19. Landsberg, J. et al. Melanomas resist T-cell therapy through inflammation-induced reversible dedifferentiation. *Nature* **490**, 412–416 (2012).
20. Baumeister, S. H., Freeman, G. J., Dranoff, G. & Sharpe, A. H. Coinhibitory Pathways in Immunotherapy for Cancer. *Annu. Rev. Immunol.* **34**, 539–573 (2016).
21. Patel, S. J. et al. Identification of essential genes for cancer immunotherapy. *Nature* **548**, 537–542 (2017).
22. Pan D. et al. A major chromatin regulator determines resistance of tumor cells to T cell-mediated killing. *Science* **359**, 770–775 (2018).
23. Ferrari de Andrade, L. et al. Antibody-mediated inhibition of MICA and MICB shedding promotes NK cell-driven tumor immunity. *Science* **359**, 1537–1542 (2018).
24. Milanovic, M. et al. Senescence-associated reprogramming promotes cancer stemness. *Nature* **553**, 96–100 (2018).
25. Muller-Hermelink, N. et al. TNFR1 signaling and IFN-gamma signaling determine whether T cells induce tumor dormancy or promote multistage carcinogenesis. *Cancer Cell* **13**, 507–518 (2008).
26. Zaretsky, J. M. et al. Mutations Associated with Acquired Resistance to PD-1 Blockade in Melanoma. *N. Engl. J. Med.* **375**, 819–829 (2016).
27. Manguso, R. T. et al. In vivo CRISPR screening identifies Ptpn2 as a cancer immunotherapy target. *Nature* **547**, 413–418 (2017).
28. Kammertoens, T. et al. Tumour ischaemia by interferon-gamma resembles physiological blood vessel regression. *Nature* **545**, 98–102 (2017).

29. Ayers M., et al. IFN-gamma-related mRNA profile predicts clinical response to PD-1 blockade. *J. Clin. Invest.* **127**, 2930–2940 (2017).
30. Wieder T., Eigentler T., Brenner E., Rocken M. Immune checkpoint blockade therapy. *J. Allergy Clin. Immunol.* **142**, 1403–1414 (2018).
31. Braumuller, H. et al. T-helper-1-cell cytokines drive cancer into senescence. *Nature* **494**, 361–365 (2013).
32. Sun, R. & Gao, B. Negative regulation of liver regeneration by innate immunity (natural killer cells/interferon-gamma). *Gastroenterology* **127**, 1525–1539 (2004).
33. Goding, S. R. et al. Restoring immune function of tumor-specific CD4+ T cells during recurrence of melanoma. *J. Immunol.* **190**, 4899–4909 (2013).
34. Nguyen, L. T. & Ohashi, P. S. Clinical blockade of PD1 and LAG3—potential mechanisms of action. *Nat. Rev. Immunol.* **15**, 45–56 (2015).
35. Braun, S. M. G. et al. Rapid and reversible epigenome editing by endogenous chromatin regulators. *Nat. Commun.* **8**, 560 (2017).
36. Kang, T.-W. et al. Senescence surveillance of pre-malignant hepatocytes limits liver cancer development. *Nature* **479**, 547–551 (2011).
37. Speiser, D. E. et al. Self antigens expressed by solid tumors Do not efficiently stimulate naive or activated T cells: implications for immunotherapy. *J. Exp. Med.* **186**, 645–653 (1997).
38. van den Broek, M. E. et al. Decreased tumor surveillance in perforin-deficient mice. *J. Exp. Med.* **184**, 1781–1790 (1996).
39. Egeter, O., Mocikat, R., Ghoreschi, K., Dieckmann, A. & Rocken, M. Eradication of disseminated lymphomas with CpG-DNA activated T helper type 1 cells from nontransgenic mice. *Cancer Res.* **60**, 1515–1520 (2000).
40. Ahmetlic, F. et al. Regulatory T cells in an endogenous mouse lymphoma recognize specific antigen peptides and contribute to immune escape. *Cancer Immunol. Res.* **7**, 600–608 (2019).
41. Naujoks, M. et al. Alterations of costimulatory molecules and instructive cytokines expressed by dendritic cells in the microenvironment of an endogenous mouse lymphoma. *Cancer Immunol. Immunother.* **63**, 491–499 (2014).
42. Casanovas, O., Hager, J. H., Chun, M. G. & Hanahan, D. Incomplete inhibition of the Rb tumor suppressor pathway in the context of inactivated p53 is sufficient for pancreatic islet tumorigenesis. *Oncogene* **24**, 6597–6604 (2005).
43. Kovalchuk, A. L. et al. Burkitt lymphoma in the mouse. *J. Exp. Med* **192**, 1183–1190 (2000).
44. Chen, D. S. & Mellman, I. Elements of cancer immunity and the cancer-immune set point. *Nature* **541**, 321–330 (2017).
45. Cristescu R. et al. Pan-tumor genomic biomarkers for PD-1 checkpoint blockade-based immunotherapy. *Science* **362** (2018).
46. Wang, Z. L. et al. Comprehensive genomic characterization of RNA-binding proteins across human cancers. *Cell Rep.* **22**, 286–298 (2018).
47. Kroemer, G., Galluzzi, L., Kepp, O. & Zitvogel, L. Immunogenic cell death in cancer therapy. *Annu Rev. Immunol.* **31**, 51–72 (2013).
48. Pitt, J. M. et al. Resistance mechanisms to immune-checkpoint blockade in cancer: tumor-intrinsic and -extrinsic factors. *Immunity* **44**, 1255–1269 (2016).
49. Willimsky, G. & Blankenstein, T. Sporadic immunogenic tumours avoid destruction by inducing T-cell tolerance. *Nature* **437**, 141–146 (2005).
50. Le, D. T. et al. PD-1 blockade in tumors with mismatch-repair deficiency. *N. Engl. J. Med.* **372**, 2509–2520 (2015).
51. Topalian, S. L. et al. Safety, activity, and immune correlates of anti-PD-1 antibody in cancer. *N. Engl. J. Med.* **366**, 2443–2454 (2012).
52. Campisi, J. Aging, cellular senescence, and cancer. *Annu. Rev. Physiol.* **75**, 685–705 (2013).
53. Serrano, M., Lin, A. W., McCurrach, M. E., Beach, D. & Lowe, S. W. Oncogenic ras provokes premature cell senescence associated with accumulation of p53 and p16INK4a. *Cell* **88**, 593–602 (1997).
54. Demaria, M. et al. Cellular senescence promotes adverse effects of chemotherapy and cancer relapse. *Cancer Disco.* **7**, 165–176 (2017).
55. Lee, S. & Schmitt, C. A. The dynamic nature of senescence in cancer. *Nat. Cell Biol.* **21**, 94–101 (2019).
56. Krimpenfort, P., Quon, K. C., Mooi, W. J., Loonstra, A. & Berns, A. Loss of p16Ink4a confers susceptibility to metastatic melanoma in mice. *Nature* **413**, 83–86 (2001).
57. Damsky, W. et al. mTORC1 activation blocks BrafV600E-induced growth arrest but is insufficient for melanoma formation. *Cancer Cell* **27**, 41–56 (2015).
58. Zeng, H. et al. Bi-allelic loss of CDKN2A initiates melanoma invasion via BRN2 activation. *Cancer Cell* **34**, 56–68.e59 (2018).
59. Shain, A. H. et al. Genomic and transcriptomic analysis reveals incremental disruption of key signaling pathways during melanoma evolution. *Cancer Cell* **34**, 45–55.e44 (2018).
60. Mooi, W. J. & Peeper, D. S. Oncogene-induced cell senescence—halting on the road to cancer. *N. Engl. J. Med.* **355**, 1037–1046 (2006).
61. Pencik, J. et al. STAT3 regulated ARF expression suppresses prostate cancer metastasis. *Nat. Commun.* **6**, 7736 (2015).
62. Forster, I., Hirose, R., Arbeit, J. M., Clausen, B. E. & Hanahan, D. Limited capacity for tolerization of CD4+ T cells specific for a pancreatic beta cell neo-antigen. *Immunity* **2**, 573–585 (1995).
63. Homberg, N. et al. CD40-independent natural killer-cell help promotes dendritic cell vaccine-induced T-cell immunity against endogenous B-cell lymphoma. *Int J. Cancer* **135**, 2825–2833 (2014).
64. Feil, S. et al. Transdifferentiation of vascular smooth muscle cells to macrophage-like cells during atherogenesis. *Circ. Res.* **115**, 662–667 (2014).
65. Naito, Y., Hino, K., Bono, H. & Ui-Tei, K. CRISPRdirect: software for designing CRISPR/Cas guide RNA with reduced off-target sites. *Bioinformatics* **31**, 1120–1123 (2015).
66. Xue, W. et al. CRISPR-mediated direct mutation of cancer genes in the mouse liver. *Nature* **514**, 380–384 (2014).
67. Li, H. & Durbin, R. Fast and accurate short read alignment with Burrows-Wheeler transform. *Bioinformatics* **25**, 1754–1760 (2009).
68. Kim, S. et al. Strelka2: fast and accurate calling of germline and somatic variants. *Nat. Methods* **15**, 591–594 (2018).
69. Cingolani, P. et al. A program for annotating and predicting the effects of single nucleotide polymorphisms, SnpEff: SNPs in the genome of Drosophila melanogaster strain w1118; iso-2; iso-3. *Fly. (Austin)* **6**, 80–92 (2012).
70. Schroeder, C. M. et al. A comprehensive quality control workflow for paired tumor-normal NGS experiments. *Bioinformatics* **33**, 1721–1722 (2017).

Acknowledgements

The excellent technical assistance of S. Weidemann, V. Galinat, E. Müller-Hermelink, A. Odon, R. Nordin, S. Riel and T. Schneider, C. Grimmel is gratefully acknowledged. The authors thank H.G. Rammensee, O. Rieß, K. Ghoreschi, J. Brück, B. Bauer, M. Rentschler for helpful discussions, and T. Haug for technical support in the chromium release assay. Furthermore, the authors thank M. Hagemann, F. Liebel, J. Teutsch and M. Möschter for help in animal experiments. S. Kaesler for providing B16-OVA cells. This work is part of the doctoral thesis of E.B., B.F.S., F.A., T.R., F.J.H., G.D. and N.S. Wilhelm Sander-Stiftung (2012.056.3), Deutsche Krebshilfe (application numbers 109037, 110662, 110664, 70112332 and 70112337), Werner Reichenbach Stiftung and the Deutsche Forschungsgemeinschaft (SFB 685, SFB TRR 156/2, RO 764/14-1; RO 764/15-1, SFB 773, Wi 1279/4-1). Cluster of Excellence iFIT (EXC 2180) "Image-Guided and Functionally Instructed Tumor Therapies", University of Tübingen, Germany, funded by the Deutsche Forschungsgemeinschaft (DFG, German Research Foundation) under Germany's Excellence Strategy - EXC 2180 – 390900677.

Author contributions

M.R. developed the concept, together with E.B., T.W., and with R.M., F.A., T.R. (Fig. 8) and M.K., B.F.S. (Fig. 4) M.R. planned and designed the experiments. E.B. performed or experimentally supported most experiments and analysed most data with the help of T.W. or B.F. (except Fig. 8a, c, d, e; Fig. 10a–c; Supplementary Fig. 7b and Supplementary Fig. 13a); B.F.S. and D.So. performed the experiments Fig. 4a–c. F.A., T.R., N.H., and A. G. performed the experiments Fig. 8a, d, e. F.J.H., C.S., and G.D. did the genomic analysis of melanoma patients, initiated by S.B. and D.D. B.F. and M.Scha. established and carried out fluorescence and electron microscopy. A.F. and T.E. recruited patients and provided patient material. H.N. and T.S. isolated primary melanoma cells. N.S. and J.B. performed and interpreted comparative genomic hybridisation arrays. L.Z., D.Dau. and S.Z. generated gRNAs against Cdkn2a for CRISPR gene-editing technology and supervised the knock-out experiments. H.B. did the chromium release assay, L.Q-M. the immunohistochemistry, K.S.B. provided cell lines and data for reviewers. B.F.S. and B.J.P. established and carried out magnetic resonance imaging. M.E. did the statistical analyses (Fig. 1a, 4a and c). K.J.J. and A.B. performed two-dimensional light sheet fluorescence microscopy. E.B., T.W., L.Z., B.P., D.Sch., R.M., M.K. and M.R. discussed and interpreted the data. M.R. wrote the paper. All authors discussed the results and commented on the manuscript, and agreed with its content.

Competing interests

M.R., E.B. and T.W. are inventors of an European pending patent Number 13 826 993.1: "Use of active substance combinations for tumour senescence" and an United States patent Number US 10,046,029 B2: "Method of inducing senescence in tumour cells by administrating TNF-A in combination with IFN-A of IFN-Y". As chairperson M.R. has to sign all contracts of the department. M.R. receives grants for research projects or travel support and has the indicated shares. The authors B.P and M.K have research contracts with Imaging modality suppliers, and are members of the "ImmuneImage" consortium within the Horizon2020 IMI programme of the European Union. F.J.H reports institutional research support from Novartis. C.S. reports research support from Illumina and institutional research support from Novartis. All remaining authors declare no competing interests.

Additional information

Supplementary information is available for this paper at https://doi.org/10.1038/s41467-020-14987-6.

Correspondence and requests for materials should be addressed to M.Röc.

Peer review information *Nature Communications* thanks Raffaella Di Micco, Antoni Ribas and the other, anonymous, reviewer(s) for their contribution to the peer review of this work. Peer reviewer reports are available.

Reprints and permission information is available at http://www.nature.com/reprints

Publisher's note Springer Nature remains neutral with regard to jurisdictional claims in published maps and institutional affiliations.

Open Access This article is licensed under a Creative Commons Attribution 4.0 International License, which permits use, sharing, adaptation, distribution and reproduction in any medium or format, as long as you give appropriate credit to the original author(s) and the source, provide a link to the Creative Commons license, and indicate if changes were made. The images or other third party material in this article are included in the article's Creative Commons license, unless indicated otherwise in a credit line to the material. If material is not included in the article's Creative Commons license and your intended use is not permitted by statutory regulation or exceeds the permitted use, you will need to obtain permission directly from the copyright holder. To view a copy of this license, visit http://creativecommons.org/licenses/by/4.0/.

© The Author(s) 2020

cancers

MDPI

Article

MDM2, MDM4 and EGFR Amplifications and Hyperprogression in Metastatic Acral and Mucosal Melanoma

Andrea Forschner [1,*], Franz-Joachim Hilke [2], Irina Bonzheim [3], Axel Gschwind [2], German Demidov [2], Teresa Amaral [1,4], Stephan Ossowski [2,5], Olaf Riess [2,5], Christopher Schroeder [2], Peter Martus [6], Bernhard Klumpp [7], Irene Gonzalez-Menendez [3], Claus Garbe [1], Heike Niessner [1] and Tobias Sinnberg [1]

1 Center for Dermatooncology, Department of Dermatology, University Hospital Tübingen, 72076 Tübingen, Germany; Teresa.Amaral@med.uni-tuebingen.de (T.A.); Claus.Garbe@med.uni-tuebingen.de (C.G.); Heike.Niessner@med.uni-tuebingen.de (H.N.); Tobias.Sinnberg@med.uni-tuebingen.de (T.S.)
2 Institute of Medical Genetics and Applied Genomics, University Hospital Tübingen, 72076 Tübingen, Germany; Franz.hilke@charite.de (F.-J.H.); Axel.Gschwind@med.uni-tuebingen.de (A.G.); German.Demidov@med.uni-tuebingen.de (G.D.); Stephan.Ossowski@med.uni-tuebingen.de (S.O.); Olaf.Riess@med.uni-tuebingen.de (O.R.); Christopher.Schroeder@med.uni-tuebingen.de (C.S.)
3 Institute of Pathology and Neuropathology, University Hospital Tübingen, 72076 Tübingen, Germany; Irina.Bonzheim@med.uni-tuebingen.de (I.B.); Irene.Gonzalez-Menendez@med.uni-tuebingen.de (I.G.-M.)
4 Portuguese Air Force Health Care Direction, 1649-020 Lisbon, Portugal
5 German DFG NGS Competence Center, NCCT, 72076 Tübingen, Germany
6 Institute for Clinical Epidemiology and applied Biostatistics (IKEaB), 72076 Tuebingen, Germany; Peter.Martus@med.uni-tuebingen.de
7 Institute for Radiology, Rems-Murr-Kliniken, 71364 Winnenden, Germany; Bernhard.klumpp@kabelbw.de
* Correspondence: andrea.forschner@med.uni-tuebingen.de; Tel.: +49-(0)-7071-29-84555; Fax: +49-(0)-7071-29-4599

Received: 6 February 2020; Accepted: 24 February 2020; Published: 26 February 2020

Abstract: Background: Mucosal and acral melanoma respond worse to immune checkpoint inhibitors (ICI) than cutaneous melanoma. *MDM2/4* as well as *EGFR* amplifications are supposed to be associated with hyperprogression on ICI in diverse cancers. We therefore investigated the response of metastatic acral and mucosal melanoma to ICI in regard to *MDM2/4* or *EGFR* amplifications and melanoma type. Methods: We conducted a query of our melanoma registry, looking for patients with metastatic acral or mucosal melanoma treated by ICI. Whole exome sequencing, FISH and immunohistochemistry on melanoma tissue could be performed on 45 of the total cohort of 51 patients. Data were correlated with patients' responses to ICI and survival. Results: 22 out of 51 patients had hyperprogressive disease (an increase in tumor load of >50% at the first staging). Hyperprogression occurred more often in case of *MDM2/4* or *EGFR* amplification or <1% PD-L1 positive tumor cells. Nevertheless, this association was not significant. Interestingly, the anorectal melanoma type and the presence of liver metastases were significantly associated with worse survival. Conclusions: So far, we found no reliable predictive marker for patients who develop hyperprogression on ICI, specifically with regard to *MDM2/4* or *EGFR* amplifications. Nevertheless, patients with anorectal melanoma, liver metastases or melanoma with amplified *MYC* seem to have an increased risk of not benefitting from ICI.

Keywords: hyperprogression; immune checkpoint inhibitors; acral melanoma; mucosal melanoma; *MDM2*; *MDM4*; *EGFR*

1. Introduction

Although the introduction of anti-CTLA-4 and anti-PD-1 antibodies has significantly improved the prognosis of metastatic melanoma, primary therapy resistance is still present in about 40%–50% of patients [1–7]. Furthermore, up to 60% of melanoma patients treated with combined ipilimumab and nivolumab suffer severe, potentially life-threatening immune-related adverse events [8–11]. Therefore, there is a great need to determine parameters that make response to immunotherapy more predictable. Expression of Programmed cell death ligand 1 (PD-L1) on the tumor cell surface did not prove to be a reliable predictive biomarker for either response or survival, as checkpoint inhibitors are also efficient in PD-L1 negative tumors [12–14].

In addition, PD-L1 expression differed in about 50% of cases between primary tumors and metastases, or even between different metastases from one patient [15].

Patients with mucosal and acral melanoma respond worse to immunotherapy than patients with cutaneous melanoma [16,17]. The response rate to anti-PD-1 therapy in patients with mucosal melanoma is only about 23%, and is approximately 37% to combined immunotherapy [16]. Acral melanoma patients also show a reduced objective response rate to anti-PD-1 therapy of around 32% [17].

The situation of mucosal and acral melanoma patients is further complicated by the fact that these tumors are often triple wild-type tumors, i.e., without a *BRAFV600E/K*, *NRAS* or *NF1* mutation, and therefore not qualified for targeted therapy with *BRAF* and MEK inhibitors. On the other hand, triple wild-type melanoma was found to exhibit *MDM2/4* amplifications in about 15% of the cases [18,19]. *MDM2/4* as well as *EGFR* amplifications, have recently been described in association with hyperprogression on ICI in diverse cancers [20].

The term "hyperprogression" describes a fast and extensive progression following treatment with checkpoint inhibitors, but there is no precise and generally agreed definition. A common consensus is most likely to be an acceleration of the tumor growth rate by a factor ≥2 or an increase in tumor burden by more than 50% [21–24]. Others also considered times to treatment failure of less than two months after initiation of ICI [25]. Not all of these criteria were always met, such as when authors dealt with the term "hyperprogression". In some case series, staging intervals of three months and more were also included and progression speed was not always calculable [25,26].

We have recently reported a case of an acral melanoma patient with extensive *MDM2* amplification, suffering hyperprogression under combined checkpoint inhibition with ipilimumab and nivolumab. This was probably the first case of *MDM2* amplificated, hyperprogressive melanoma. [27]. Later, an anorectal melanoma patient with hyperprogressive disease under anti-PD-1 therapy was reported [26]. In this second case, however, no information was provided on *MDM2/4* or *EGFR* amplification.

In this study, we sought to evaluate the genomic pattern of mucosal and acral melanoma in relation to their response to checkpoint inhibitors. In particular, we intended to check whether *MDM2/4* or *EGFR* amplifications are associated with hyperprogression.

2. Materials and Methods

2.1. Patients and Clinical Data

We conducted a query of our melanoma registry and searched for patients with initial diagnosis of acral or mucosal melanoma in the period 01/01/2007 to 06/30/2017. All patients had given their written informed consent for data collection within the melanoma registry. Among all acral or mucosal melanoma patients identified in the query, all stage IV patients—at the time of first diagnosis or later on—were included for further evaluation if they had received at least two cycles of ICI and a radiological evaluation of response, i.e., CT, MRI or PET/CT scans (Figure 1). The ICI therapy regimes were as follows: ipilimumab (3 mg/kg) every 3 weeks, nivolumab (3 mg/kg) every 2 weeks, pembrolizumab (2 mg/kg) every 3 weeks or combined ipilimumab (3 mg/kg) every 3 weeks and nivolumab (1 mg/kg) every 3 weeks. Two patients had received combined immunotherapy in the frame of a study. The regimes for these two patients were either ipilimumab 3 mg/kg bw and nivolumab

1 mg/kg bw every 3 weeks or ipilimumab 1 mg/kg bw and nivolumab 3 mg/kg bw every 3 weeks. Therapy response was assessed at the first staging through a comparison to baseline evaluation before initiation of ICI. Baseline tumor load and response to therapy were assessed as the sum of long axis diameters of target lesions according to RECIST 1.1. [28]. In this study, complete or partial remission and stable disease (SD) were summarized to the disease control (DC) group. Progression was further classified, either as PD in the case of an increase of tumor load exceeding 20% but limited to 50% and as hyperprogressive disease (HPD) when the tumor burden increased by more than 50%.

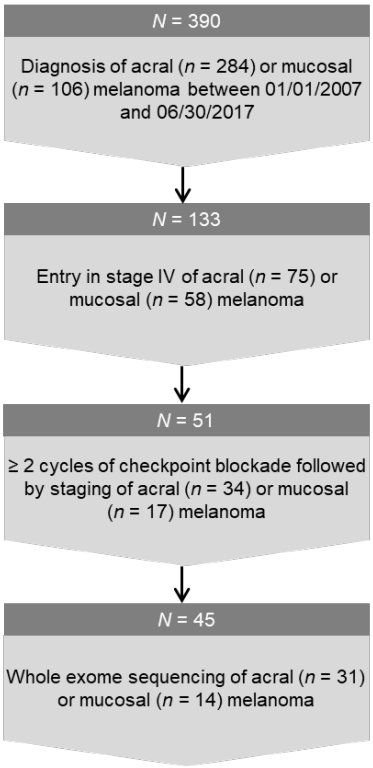

Figure 1. Flowchart of cohort generating.

Afterwards, the patients' responses to ICI were classified into 3 categories according to the percentage change in their tumor load:

(1) increase of tumor load of more than 50%: "hyperprogressive disease" (HPD),

(2) increase of tumor load exceeding 20% but limited to 50% "progressive disease" (PD) and (3) up to 20% increase or any decrease of tumor load: "disease control" (DC).

In 4 of the included patients, no CT score could be determined: Two patients had inoperable in-transit metastases, which were not located in the examination area of the CT. Therefore, these two patients were monitored additionally with photos and ultrasound. Both showed progressive findings and were classified as PD due to their clinical and sonographic change in tumor load. Two other patients had their staging outside our institution. Here, the radiology reports were used for response evaluation: one patient had DC and one had PD.

Local ethics committee approved this study (approval number 383/2017BO2). This study was performed in accordance with the Declaration of Helsinki.

2.2. Tumor Panel Analysis and Bioinformatics

2.2.1. Whole Exome Sequencing

Whole exome sequencing was performed on an Illumina NovaSeq6000 device (Illumina, San Diego, CA, USA). The library construction was done using the IDT xGen® Exome Research Panel

v1.0 (Integrated DNA Technologies, Inc., Carolville, IA, USA) according to the manufacturer's recommendations by pooling the DNA in batches of 8 samples for library capture. Due to the inadequate DNA integrity number (DIN), we had to adjust the DNA input for each sample. Instead of using 200 ng, we used the total available DNA for each sample. So, we ended up generating 11 pools with a starting amount ranging from 510–39 ng. The resulting 8 sample library pools were paired-end sequenced.

Whole exome sequencing quality control: An in-house developed pipline, called "megSAP" was used for data analysis (https://github.com/imgag/megSAP, vers. 0.1-484-g9ad29f4 and 0.1-614-g21d6cfe). In brief, sequencing reads were aligned to the human genome reference sequence (GRCh37) using BWA (vers. 0.7.15) [29]. Quality control parameters, like sample or data swaps as well as all meta data were collected during all analysis steps [30].

2.2.2. Somatic Mutation Analysis

Variants were called using Strelka2 (vers. 2.7.1) [31] and annotated with SNPeff/SnpSift (vers. 4.3i) [32]. For further interpretation, all somatic variants were uploaded to the Cancer Genome Interpreter [33].

2.2.3. Tumor Mutational Burden

The tumor mutational burden (TMB) was calculated as the number of all somatic alterations (coding SNVs and INDELs) based on the target size of the used exome enrichment system.

The formula was:

$$\left\lceil \frac{\left(\frac{Somatic-Known-Tumorgenes}{Target\ size} \times Genome\ size\right) + Tumorgenes}{Genome\ size} \right\rceil.$$

2.2.4. Copy Number Analysis

Copy number variants (CNVs) were identified using ClinCNV [34], an algorithm for multi-sample CNVs detection using targeted or whole-genome NGS data. Visual inspection of CNVs was performed. Samples were filtered out in case of a noisy coverage plot, large number of short homozygous deletions or complete absence of CNVs. Thus, we ended up with the calls of 40 patients. Ploidy was calculated as an average copy-number of the genomic regions within the sample. All CNVs calls were corrected for purity, cellularity and ploidy. Point mutations with the predicted loss-of-function effect were analyzed together with deletions. All detected CNVs were uploaded to CancerGenomeInterpreter.org for further interpretation. Copy numbers ≥4 were defined as amplifications in line with previous publications by Hayward et al. [18] and Liang et al. [35]. Copy numbers <1 were defined as deletions.

2.3. Immunochistochemistry and Fluorescence In-Situ Hybridization

2.3.1. Immunohistochemistry

Immunohistochemistry (IHC) was performed on formalin-fixed, paraffin-embedded (FFPE) tissue sections on the Ventana Ultra automated staining System (Ventana Medical Systems, Oro Valley, AZ, USA) using Ventana reagents, according to the manufacturer´s protocol. All cases were stained with an antibody against PD-L1 (clone 22C3, order no. M3653, 1:50, Dako, Cambridge, UK), MDM2 (clone 3G187, order no. 113-0230, 1:25, Zytomed, Berlin, Germany). Primary antibody detection was performed using the OptiView DAB IHC detection kit (Ventana). Appropriate positive and negative controls were used to confirm the adequacy of the staining. PD-L1 expression was evaluated using the MEL Score (PD-L1 positive tumor cells + PD-L1 positive mononuclear inflammatory cells/total tumor cells + total mononuclear cells). We classified PD-L1 staining into two groups: MEL score <1 and ≥1. MDM2 expression was specified as percentages of positive tumor cells. Images were acquired with a

Zeiss Axioskop 2 plus microscope equipped with a Jenoptik ProgRes C10 plus camera and software (Laser Optik System, Jena, Germany).

2.3.2. Fluorescence In-Situ Hybridization Analysis of MDM2

Fluorescence in-situ hybridization (FISH) analysis of *MDM2* gene amplification was performed using ZytoLight® SPEC *MDM2*/CEN 12 Dual Color Probe (order no. Z-2013, ZytoVision, Bremerhafen, Germany). Pretreatment and hybridization (HYbrite™, Abott, Wiesbaden, Germany) was done according to the manufacturer's manual. Assessment of results was carried out on the Axio Imager M2 (Zeiss, Oberkochen, Germany).

2.4. Statistical Analysis

Statistical analysis was performed using the statistical program for social sciences (SPSS) Version 25 (IBM, New York, NY, United States). STATA® v15 (StataCorp LLC, College Station, TX, USA) was used to generate the final version of the Kaplan-Meier survival curves. Differences between groups were tested using the Exact Fisher test and the exact version of the Chi-Square test for categorical variables (response and comparisons between potential predictors), and the Log rank test for overall survival. Survival curves were generated according to the Kaplan-Meier method. Overall survival was defined as the time between start of immunotherapy and death or censored at the last date of patient contact. For factors that were significant in the univariate log rank test, we performed a multivariate Cox regressions analysis. In this analysis, the three categorical variables "melanoma subtype" and "treatment response" were coded quantitatively as 1 = other mucosal melanoma, 2 = acral melanoma, 3 = anorectal melanoma (melanoma subtype), and 1 = disease control, 2 = progressive disease, 3 = hyperprogressive disease (treatment response). The level of significance was 0.05 (two-sided) in all analyses. In an ex post power analysis, we found that hazard ratios of 2.7 or higher and differences in frequencies of 42% could have been detected with 80% power in our sample (assuming equal group sizes).

3. Results

3.1. Patient Cohort and Clinical Parameters

The query of the melanoma registry identified 390 patients who had been diagnosed with acral (n = 284) or mucosal (n = 106) melanoma in the time between 01/01/2007 and 06/30/2017. About one third of the cohort (n = 133, 34%) entered stage IV during the course of the disease and 51 of these patients received at least 2 cycles of checkpoint inhibitors for unresectable metastases (Figure 1). Of these 51 cases, n = 34 were acral and n = 17 were mucosal melanoma.

The median age of the patients at the time of initiation of ICI was 71 years (IQR 58–77, range 40–87). About half of the patients were female (47%). Among the 17 mucosal melanomas, 8 were anorectal. About half of the patients (n = 27) had been treated by ipilimumab, 15 patients by anti-PD-1 therapy and 9 by a combination of ipilimumab and nivolumab. The median time between the start of immunotherapy and the first staging was 11 weeks (IQR 8–13).

The results of the first staging after starting the ICI were PD in the majority of the 51 patients (67%). Patients with anorectal melanoma responded particularly poorly: Of the eight patients with anorectal melanoma, seven had PD (88%). The patients with mucosal melanoma had a better response to therapy. Here only 33% had PD (Table 1). Six out of 8 patients (75%) with anorectal melanoma developed hyperprogression compared to 16 out of 43 patients (37%) with acral or other forms of mucosal melanoma.

A total of 37 out of 51 patients (73%) had already died at the time of the evaluation. Median overall survival of the total 51 patients since primary diagnosis of melanoma was 40 months, and the equivalent since the start of immunotherapy was 19 months. Anorectal melanoma patients had the worst prognosis with a median overall survival of 16 months and 8.5 months, respectively.

Table 1. Patient characteristics.

Patient Characteristics (n = 51)		**Median**	**IQR**
Age at first diagnosis of melanoma (years)		72	60–79
Tumor mutation burden (Mut/Mb)		2.8	1.8–4.7
Overall survival since primary diagnosis (months)		40	23–78
Overall survival since start of immunotherapy (months)		19	9–30
Time between tissue sampling and start of combined immunotherapy (months)		4	1–12
Time between start of combined immunotherapy and first staging (weeks)		11	8–13
		no. patients	%
Sex			
	Female	24	47
	Male	27	53
Melanoma type			
	Anorectal	8	15.7
	Acral	34	66.7
	Other mucosal	9	17.6
LDH at start of immunotherapy			
	LDH elevated	17	33.3
	LDH normal	32	62.7
	missing	2	4
Metastasis at start of Immunotherapy			
	Brain metastasis	6	11.8
	Liver metastasis	18	35.3
	Lung metastasis	31	60.8
Type of immunotherapy			
	Ipilimumab	27	53
	Nivolumab or Pembrolizumab	15	29.4
	Combined Ipilimumab + Nivolumab	9	17.6
Response to immunotherapy			
	Disease control	17	33.3
	Progressive disease	12	23.5
	Hyperprogressive disease	22	43.1
Origin of tissue sequenced			
	Metastasis	35	68.6
	Primary melanoma	10	19.6
	No tissue available	6	11.8

3.2. The Genomic Landscape of the Patients' Cohort

Of the final cohort of 51 cases, 45 patients had formalin-fixed tissue available for WES and IHC staining. For 6 patients, no tissue was accessible (Figure 1).

Paired tumor normal exome sequencing was performed with an average depth of 154× (range: 10.36–440.1) for the tumor tissue and 170× (range: 15.91–467.6) for normal tissue. We were able to call somatic single nucleotide variants (SNVs) and small insertions and deletion (INDELs) in all cases, but had to exclude five samples from the detection of the somatic copy number analysis due to poor tissue quality.

In total, we identified 8297 somatic SNVs. The analysis of the coding variants resulted in a median tumor mutation load of 2.83 mutations/Mb (range: 0.28–68.34). The tumor suppressor gene *NF1* and the oncogene *NRAS* were the most frequently mutated genes, each of them occurred in 18% (8 of 45) of the cases. The second most common gene concerned the oncogene *KIT* (5 of 45, 11%) (Figure 2A). We found driver mutations in the oncogene *BRAF* exclusively in patients with acral melanoma.

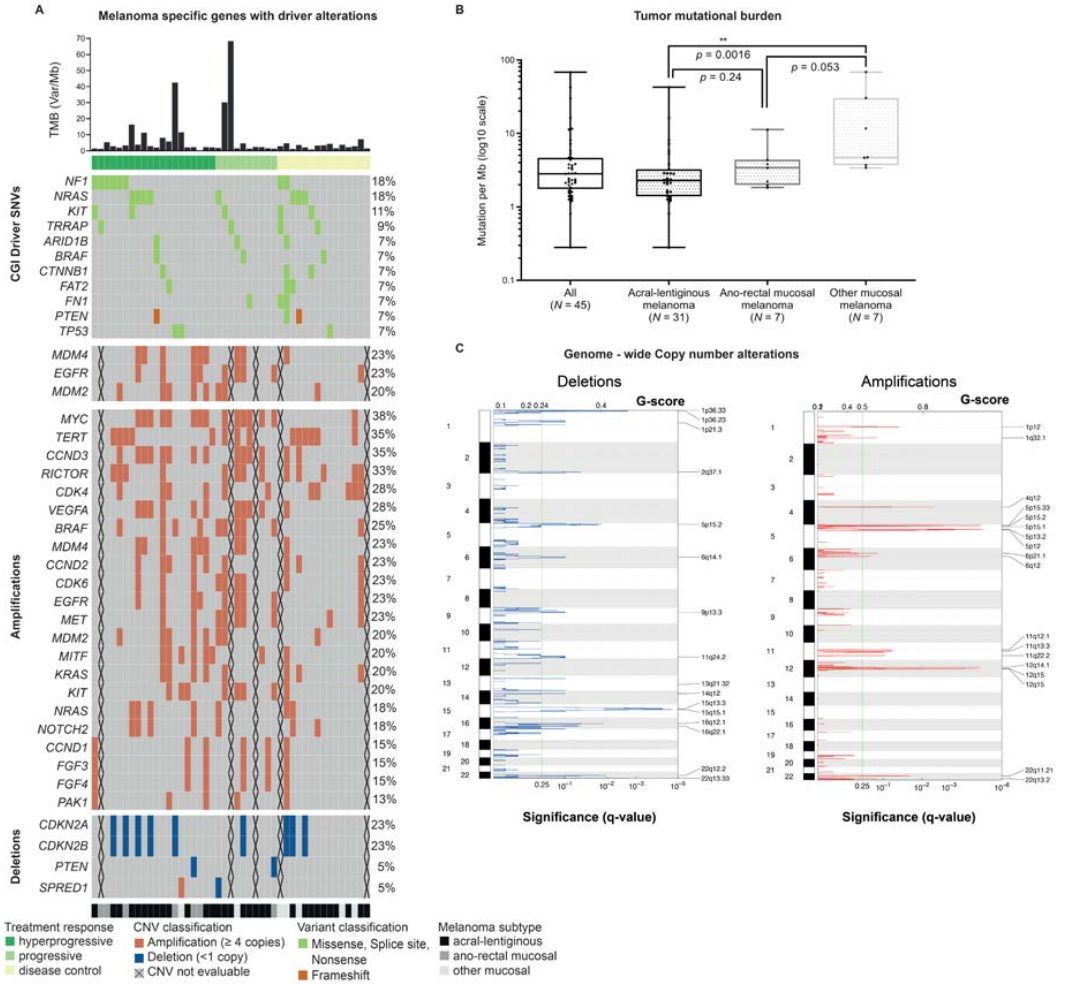

Figure 2. Mutational landscape of the cohort: tumor mutational burden (TMB), single nucleotide variants (SNVs), copy number variants (CNVs). The figure shows the most frequent alterations found in the 45 cases analyzed by whole-exome sequencing. The oncoplot (**A**) Melanoma specific genes with driver alterations depicts a list of genes filtered with the *Cancer Genome Interpreter* for known and predicted driver alterations. The upper part shows the tumor mutational burden (TMB) of each patient shown on a decimal scale (Mut/Mb). The oncoplot presents in the second panel from the top all genes with at least 3 mutations (SNVs and INDELs) in two different patients, translating to a minimal alteration frequency of 7%. The genes are sorted according to their alteration frequency and alphabetically. Each row represents a patient. The patients are sorted according to their melanoma subtype (acral-lentiginous, anorectal mucosal and other mucosal melanoma). Also, the response to the checkpoint inhibitors is shown (hyperprogression, progressive disease and disease control). In addition, the two lower panels depict somatic copy number alterations of particular interest. The lower panel shows somatic SNV and alteration frequency of all driver alterations found in the significantly altered genomic region shown in (**C**). The middle panel displays *MDM4*, *EGFR* and *MDM2*. On the right hand (**B**), the upper part Tumor mutational burden depicts the results of the comparison of the TMB between the three different melanoma subtypes. The boxplots show all data points, median, interquartile borders as well as minimum and maximum. The *t*-test (Wilcoxon-rank test) revealed a significant difference while comparing the TMB of acral-lentiginous (median: 2.28, range: 0.28–42.54) and other mucosal melanoma (median: 4.68, range: 3.38–68.34), meaning in acral-lentiginous melanoma, a significant lower TMB was observed compared to other mucosal melanoma. ** significant difference in the Wilcoxon-rank test. The lower part (**C**), Genome–wide Copy Number Alterations presents the results of the GISTIC analysis. GISTIC identified 16 regions on 11 chromosomes to be significantly deleted and 18 regions on 7 chromosomes to be significantly amplified. The cut-off for calling the regions is 0.25 (q-value).

Out of all 45 samples in which tumor mutation burden (TMB) determination was possible, 60% were classified as TMB low (<3.3 Mut/Mb), and about a third as intermediate (3.3–23.1 Mut/Mb). Only 3 patients (7%) had a high TMB (>23.1 Mut/Mb) [3].

The median TMB of the total cohort was 2.8 Mut/Mb (IQR 1.75–4.65). There was no significant difference in median TMB of patients with DC (2.4; IQR 1.3–4.6) and PD (2.8 Mut/Mb; IQR 2–5.4). The total cohort contained only three patients with a high TMB: one patient with acral melanoma who presented with PD and two patients with other types of mucosal melanoma and DC, respectively. There was no statistically significant difference between the three TMB groups and treatment response, classified in HPD, PD and DC. Interestingly, non-anorectal mucosal melanomas had a significantly higher TMB than anorectal or acral melanomas (Figure 2B).

Evaluation of copy number changes using GISTIC 2.0 showed that 18 regions were frequently amplified and 16 regions were frequently deleted ($q < 0.25$) (Figure 2C). The most frequently significantly ($q < 0.05$) amplified regions were located on chromosome 5p33.1, 12q14.1/15, 4q12 and 1p12 comprising the genes *TERT*, *CDK4*, *MDM2*, *KIT* and *NRAS*. The most frequently significantly deleted regions were located on chromosomes 15q15, 22q12/13, 1p36, 16q12/22, 5p15 and 2q37 affecting the tumor suppressor genes *SPRED1*, *CHEK2* and *NF2* (Figure 2C).

We furthermore evaluated other oncogenes or tumor suppressor genes, known to be frequently amplified or deleted in acral or mucosal melanoma [35,36] and performed a comparison with the Cancer Genome Interpreter database. Oncogenes with amplifications (copy number ≥4) and tumor suppressor genes with deletions (copy number <1), respectively are presented in Figure 2A. The five most common oncogenes concerned *MYC*, *TERT*, *CCND3*, *RICTOR* and *CDK4*. The most commonly affected tumor suppressor genes involved *CDKN2A/B*.

3.3. MDM2 FISH and PD-L1 Immunohistochemistry

FISH was performed using a *MDM2* specific probe to confirm the NGS results for copy number changes in *MDM2*. In the absence of a *MDM2* amplification, two positive signals are to be expected in both: the 12q15 (green) signals and the centromere (red) signals by FISH. An example of this is given in Figure 3A (left side). In contrast, numerous signals can be detected in the case of *MDM2* amplifications, as shown in Figure 3A (right side). Remarkably, the FISH results correlated very well with the results of the NGS study (Figure 3B). However, immunohistochemistry (IHC) for MDM2 did not correlate very well with the copy numbers determined by NGS or FISH (Pearson $r = 0.46$). This might be explained by a strong regulation of MDM2 expression e.g., by varying p53 activity or post-translational regulation in the tumor cells. Furthermore, no scoring of the staining intensity was used for the quantification of IHC. Immunohistochemistry for detection of PD-L1 expression was performed in all melanoma samples and further used to determine the PD-L1 score. Results of PD-L1 staining ranged from 0% to 40% of PD-L1 positive cells (IQR 0.875–6.25), Table S1 displays PD-L1 scores in detail. Furthermore, Figure S1 shows PD-L1 IHC and MDM2 IHC of a hyperprogressive case, and of a case with disease control.

3.4. Response to Immune Checkpoint Inhibitors-Anorectal Melanomas are Associated with Hyperprogressive Disease

Patients with the anorectal melanoma type often had significantly more hyperprogressive courses than the other two melanoma subtypes. Hyperprogression was observed in 75% of all anorectal melanoma patients, but only in 41% of the acral and in 22% of the other mucosal melanomas ($p = 0.012$).

About 90% of all patients whose tumors harbored amplification of *MDM2* (7 out of 8), *MDM4* (8 out of 9) or *EGFR* (8 out of 9) developed PD and 66% of the patients with *MDM4* amplification presented with HPD (6 out of 9).

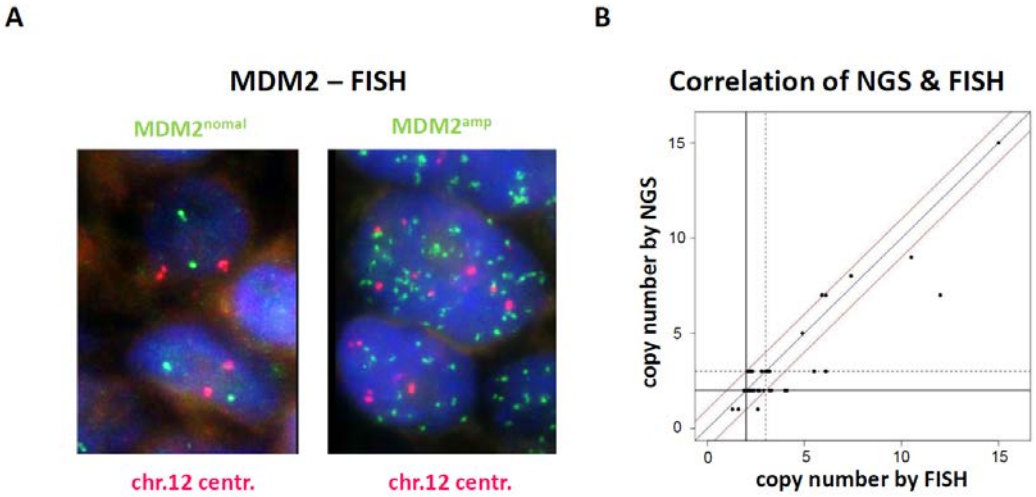

Figure 3. *MDM2* fluorescence in-situ hybridization (FISH). (**A**) Left microphotograph shows a representative case without *MDM2* amplification (*MDM2*^{normal}). On average, 2.7 copies of *MDM2* per tumor cell nucleus were detected by green fluorescence signals and 2.2 copies of centromer 12 per nucleus were detected by red fluorescence signals (*MDM2*/centromere 12 ration: 1.22). Right microphotograph shows a representative case with *MDM2* amplification (*MDM2*^{amp}). (**B**) Correlation diagram of *MDM2* copy numbers obtained by FISH and NGS.

Although we did not find a statistically significant difference, there was a trend towards a worse response in case of amplification (≥4 copies) of *MDM2*, *MDM4* or *EGFR* or PD-L1 score <1%. (Table 2). It should be pointed out that we have not obtained different results, even when combining the two groups HPD and PD to one single group of progressive patients (Table S2). Again, we only found a statistically significant difference when analyzing the melanoma subtype. Note that patients' age had no influence on treatment response (p = 0.40). However, *MYC* copy numbers ≥4 were significantly associated with PD (p = 0.013).

3.5. Survival Analysis-Anorectal Localization and Presence of Liver Metastases are Independent Negative Influencing Factors on Survival

The univariate survival analysis revealed significant negative influence factors for survival: the anorectal melanoma subtype, presence of liver metastases and HPD in the first staging (Figure 4). Patients with amplification (≥4 copies) of *MDM2*, *MDM4* or *EGFR* had no worse survival than patients without these amplifications (Figure S2). Note that patients' age was no influence factor for survival (HR = 0.99, CI 0.96–1.01).

The multivariate Cox regressions analysis revealed that liver metastases at start of ICI ((HR) 2.07; 95% confidence interval (CI) 1.05–4.08)), and the anorectal melanoma subtype ((HR 7.92; 95% CI 2.22–28.38)) are independent negative influencing factors on survival. Even after inclusion of the variable "treatment response", which is an intermediate variable (HR = 1.91, CI 1.24–2.93), both prognostic factors remained significant (liver metastasis HR = 2.44, CI 1.18–5.01, anorectal melanoma subtype HR = 2.13, CI 1.09–4.17).

Table 2. Characteristics and ICI treatment response. [a] Genetic pattern and clinical characteristics according to treatment response. [b] Genetic pattern and clinical characteristics according to melanoma subtype.

Category [a]	**Total** ***n*** **= 51**	**Hyperprogressive Disease** ***n*** **= 22**	**Progressive Disease** ***n*** **= 12**	**Disease Control** ***n*** **= 17**	***P*-value** [1]
MDM2 Amplification (≥4 copies) [2]					
Present	8	5	2	1	0.273
Absent	32	14	6	12	
MDM4 Amplification (≥4 copies) [2]					
Present	9	6	2	1	0.142
Absent	31	13	6	12	
EGFR Amplification (≥4 copies) [2]					
Present	9	4	4	1	0.534
Absent	31	15	4	12	
PD-L1 Score [3]					
<1%	11	7	2	2	0.190
≥1%	35	15	6	14	
Melanoma Type					
Other mucosal	9	2	1	6	0.012 *
Acral	34	14	10	10	
Anorectal	8	6	1	1	
Liver metastases					
Present	18	10	3	5	0.319
Absent	33	12	9	12	
Age (median 71 years)					
<71 years	24	8	3	13	0.397
≥71 years	27	9	9	9	
Category [b]	**Total** ***n*** **= 51**	**Anorectal Melanoma** ***n*** **= 8**	**Acral Melanoma** ***n*** **= 34**	**Other Mucosal Melanoma** ***n*** **= 9**	***P*-value** [1]
MDM2 Amplification (≥4 copies) [2]					
Present	8	1	7	0	0.721
Absent	32	5	21	6	
MDM4 Amplification (≥4 copies) [2]					
Present	9	2	5	2	1.0
Absent	31	4	23	4	
EGFR Amplification (≥4 copies) [2]					
Present	9	3	5	1	0.303
Absent	31	3	23	5	
PD-L1 Score [3]					
<1%	11	5	6	0	0.004 *
≥1%	35	3	23	9	
Liver metastases					
Present	18	4	12	2	0.316
Absent	33	4	22	7	
Age (median 71 years)					
<71 years	24	4	15	5	0.799
≥71 years	27	4	19	4	

* Significant. [1] Exact Chi-Square Test for Trend (Monte Carlo Simulation). [2] only cases where tissue was available and CNV were evaluable could be considered, therefore 11 cases are missing. [3] only cases where tissue was available could be considered, therefore 6 cases are missing.

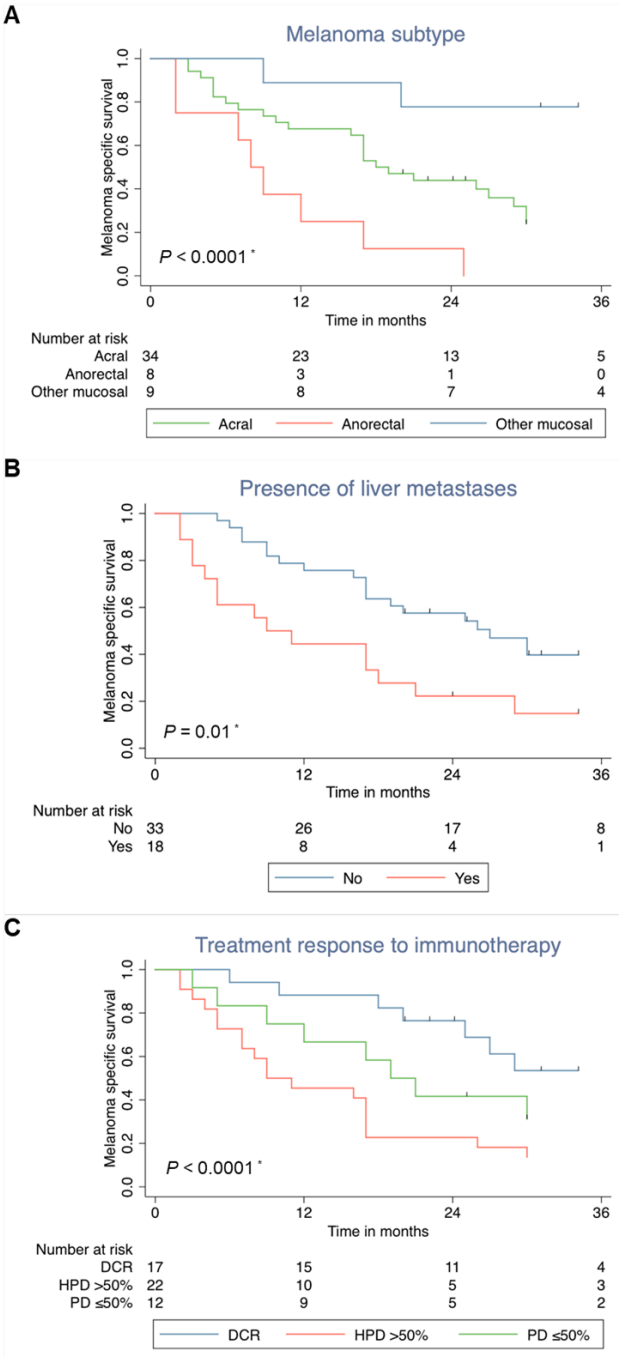

Figure 4. Melanoma specific survival according to (**A**) melanoma subtype (acral, anorectal, other mucosal melanoma), (**B**) liver metastases (present, absent) (**C**) response to checkpoint inhibitor (disease control, progressive disease, hyper-progressive disease). * significant difference in the Log rank test.

4. Discussion

The aim of this study was to check possible correlations between hyperprogression to checkpoint inhibitors and amplification (≥4 copies) of *MDM2*, *MDM4* or *EGFR* in acral and mucosal melanoma. We furthermore tested PD-L1 expression and clinical parameters such as liver metastases and specific melanoma subtypes and obtained relevant results. Although we could not see a statistically significant association between amplification of *MDM2*, *MDM4* or *EGFR* and the response to checkpoint inhibitors, we found a trend towards a lower chance of disease control in case of either *MDM2, MDM4* or *EGFR*

amplification. The anorectal melanoma subtype was associated with both significantly increased risk of having HPD and worse survival. Another factor for poor survival, which was independent of the anorectal type of melanoma, was the presence of liver metastases at the time of the start of ICI.

The influence of *MDM2/4* and *EGFR* amplification on response to immunotherapy is not completely clarified. *MDM2* and *MDM4* (an homologue of *MDM2*) inhibit the p53 tumor suppressor [37]. Likewise, it is known that *EGFR* activation might be associated with an upregulation of the checkpoints CTLA-1, PD-1 and PD-L1, which in turn, can cause resistance to checkpoint inhibitors [38]. Thus, *MDM2/4* and *EGFR* amplification have been brought into context with the development of hyperprogressive disease but the underlying mechanisms are not fully understood [20,27]. We found a trend but no significant correlation between worse response to checkpoint inhibition and either *MDM2, MDM4* or *EGFR* amplification, what is probably due to the relatively small number of cases. Furthermore, it has to be noted that only extremely effects (hazard ratios of 2.7 and differences of frequencies of 42%) could have been detected with our sample. Thus, negative results in our analysis do not confirm absence of true effects. In addition, it must be stated that we also had three different patients with disease control, despite the presence of *MDM2*, *MDM4* or *EGFR* amplification. Therefore, at the current state of knowledge, the presence of one of these amplifications should not be regarded as an exclusion criterion for checkpoint inhibitor therapy.

The NGS and FISH results showed a high degree of agreement, which confirmed the reliability of these two methods. The overall low TMB of our collective with a median of only 2.8 Mut/Mb fits well to other studies, according to which mucosal and acral melanoma are tumors with significant lower TMB than cutaneous melanoma [18,39]. Given the lower TMB of mucosal and acral melanoma compared to cutaneous melanoma, it might not be surprising that the response to checkpoint inhibition in these melanoma subtypes is lower. Retrospective analyses revealed 23% to 37% overall response rates for mucosal or acral melanoma patients treated by immunotherapy [16,17,39,40].

In a large study of 102,878 patients with different malignancies, NGS of tumor tissue revealed *MDM2* amplification in 3.5% of cases [41]. Tumors exhibiting *MDM2* amplification were less often associated with a high TMB than *MDM2* wild-type tumors [41]. We cannot validate this observation in our cohort, as only three patients had a high TMB and the median TMB in our cohort was very low. Nevertheless, there was no significant difference in the median TMB between patients with DC (2.4 Mut/Mb) and patients with PD (2.8 Mut/Mb).

It is noteworthy that most of the patients (75%) with anorectal melanoma developed hyperprogressive disease. We have also seen that PD-L1 expression was significantly lower in this subtype than in the others. Furthermore, it was shown by others, that anorectal melanoma is associated with low TMB and a low number of tumor infiltrating lymphocytes. Therefore, these tumors are probably less immunogenic and thus less responsive to checkpoint inhibitors [39]. Whether the hyperprogression was triggered by immunotherapy or simply by the natural course of the disease cannot be clarified.

In our cohort, patients with liver metastases had a significant worse rate of survival. The inferior outcome of patients with liver metastases treated by ICI has already been shown in other collectives, including patients treated with pembrolizumab and combined ipilimumab and nivolumab [42–44]. This might be due to a lower density of $CD8^+$ T cells in the liver metastases and also in the distant non-liver metastases of these patients [42]. In this context, it should be mentioned that an immunotolerance inducing effect resulting from the liver tissue is well-known in the field of liver transplantation. Even in the absence of histocompatibility, immunosuppression is not always required in case of transplanted liver tissue [45]. Furthermore, if several organs of one single donor are transplanted, the probability of successful transplantation increases if the liver is also transplanted [46]. This liver-induced immunotolerance might be disadvantageous in view of checkpoint inhibitors. In case of *BRAF V600* positive melanoma, treatment with BRAF and MEK inhibitors might be more suitable in case of liver metastases, as we did not find any reports indicating a worse response of liver metastases to targeted therapy.

Our study has several strengths. The systematic and wide-reaching query of our melanoma register provides an important basis, as all mucosal and acral melanomas that had received at least 2 cycles of checkpoint inhibitors could be identified and recorded in this study. Cases with only one cycle were omitted, because from our point of view in such cases the effect of the immunotherapy cannot be evaluated sufficiently. In our opinion, a representative collective was assembled and reported here.

Our study also presents some limitations. It should be noted that we could not exactly screen out patients for hyperprogression as defined by Champiat and colleagues [25] due to the retrospective character of our study. Response to therapy is normally performed every 12 weeks in as part of a daily routine. Therefore, we could not find a time to treatment failure of less than 2 months with simultaneous doubling of the growth rate in this time. Nevertheless, we were able to identify hyperprogressive patients by a >50 % increase in tumor mass in the first staging.

Next, it should be mentioned that only 18% of our patients were treated with the combination of ipilimumab and nivolumab. This is due to the systematic and far-reaching survey of cases with primary diagnosis between 2007 and 2017, which was necessary to generate a sufficiently large number of cases due to the rarity of these melanoma subtypes. The combination of ipilimumab and nivolumab was not approved in Germany until 2016, whereas ipilimumab had been approved since 2011. Since the combination of ipilimumab and nivolumab is superior to monotherapy with ipilimumab or nivolumab [10], it should be examined whether the worse response in the case of *MDM2*, *MDM4* or *EGFR* amplification also occurs in patients treated with combined immunotherapy.

Our finding that MYC amplifications are associated with ICI therapy failure suggests a potential biomarker role of MYC for primary resistance to ICI therapies. This is in line with recent experimental findings by others, who mentioned that MYC family members regulate the gene expression of immune checkpoints, including PD-L1 and CD47 [47].

Finally, the limited sample size of the study does not allow us to draw definite conclusions from negative results.

5. Conclusions

Patients with acral or mucosal melanoma harbor a high risk of not responding to checkpoint inhibitors and should be monitored closely. Patients with anorectal melanoma, melanoma with amplified *MYC* or liver metastases have an additional risk of not benefiting from checkpoint inhibitors and might have a significantly worse survival. In addition, in this collective, patients with *MDM2*, *MDM4* or *EGFR* amplification have an increased risk of not responding to checkpoint inhibitors. Despite this, a few patients with such amplifications did develop disease control. Therefore, these patients should not be excluded from immunotherapy in general. In these cases, the chance of response should be carefully weighed against possible risks, such as severe side effects, especially if the patients' performance status is reduced.

Further studies, including NGS in a sufficient lager number of patients with liver metastases and anorectal melanoma should be carried out to investigate the phenomenon of hyperprogression in melanoma.

Supplementary Materials: The following are available online at http://www.mdpi.com/2072-6694/12/3/540/s1, Table S1: PD-L1 scores of the cohort, Figure S1: MDM2 and PD-L1 immunostaining in a hyperprogressive case (39T) and in a case with disease control (30T) (original magnification, ×200), Table S2: Genetic pattern and clinical characteristics according to treatment response, Figure S2: Melanoma specific survival according to (A) MDM2 amplification (≥4 copies vs. <4 copies), (B) MDM4 amplification (≥4 copies vs. <4 copies) (C) EGFR amplification (≥4 copies vs. <4 copies), (D) PD-L1 scores (≥1% vs. <1% positive tumor cells).

Author Contributions: Conception and design: A.F., T.S. Development of methodology: A.F., F.-J.H., I.B., G.D., S.O., C.S., B.K., I.G.-M., C.G., H.N., T.S. Acquisition of data: A.F., F.-J.H., I.B., G.D., S.O., I.G.-M., C.S., B.K., C.G., H.N., T.S. Analysis and interpretation of data: A.F., F.-J.H., I.B., A.G., G.D., T.A., S.O., O.R., C.S., P.M., B.K., I.G.-M., C.G., H.N., T.S. Administrative, technical or material support: T.A. Study supervision: A.F., O.R., C.G., T.S. Writing, review, revision of the manuscript: A.F., F.-J.H., I.B., A.G., G.D., T.A., S.O., O.R., C.S., P.M., B.K., I.G.-M., C.G., H.N., T.S. All authors have read and agreed to the published version of the manuscript.

Funding: The study was supported by the Hiege foundation. A.F. was supported by the TÜFF Habilitation Program for Women of the Faculty of Medicine Tübingen, Germany, grant no° 2521-0-0. The authors acknowledge the support of the German Research Foundation (DFG) and the Open Access Publishing Fund of the University of Tübingen.

Acknowledgments: The authors thank the whole team of the melanoma outpatient department for their care for our melanoma patients and Ulrike Keim for conducting the search in the melanoma registry.

Conflicts of Interest: A.F. served as a consultant to Roche, Novartis, MSD and Pierre-Fabre; received travel support from Roche, Novartis, BMS and Pierre-Fabre; received speaker fees from Roche, Novartis, BMS, MSD and CeGaT. T.A. reports personal fees and travel grants from BMS; grants, personal fees and travel grants from Novartis; personal fees from Pierre Fabre; grants from Neracare; grants from Sanofi, outside the submitted work. C.G. reports grants and personal fees from Novartis, BMS and Roche; as well as personal fees from MSD. C.G. also reports personal fees from Amgen, Philogen, LEO and Incyte, outside the submitted work. F.-J.H., O.R. C.S. received an institutional grant from Novartis. The other authors state no conflict of interest.

References

1. Liu, D.; Jenkins, R.W.; Sullivan, R.J. Mechanisms of Resistance to Immune Checkpoint Blockade. *Am. J. Clin. Dermatol.* **2019**, *20*, 41–54. [CrossRef] [PubMed]
2. O'Donnell, J.S.; Long, G.V.; Scolyer, R.A.; Teng, M.W.; Smyth, M.J. Resistance to PD1/PDL1 checkpoint inhibition. *Cancer Treat. Rev.* **2017**, *52*, 71–81. [CrossRef] [PubMed]
3. Johnson, D.B.; Frampton, G.M.; Rioth, M.J.; Yusko, E.; Xu, Y.; Guo, X.; Ennis, R.C.; Fabrizio, D.; Chalmers, Z.R.; Greenbowe, J.; et al. Targeted Next Generation Sequencing Identifies Markers of Response to PD-1 Blockade. *Cancer Immunol. Res.* **2016**, *4*, 959–967. [CrossRef]
4. Hugo, W.; Zaretsky, J.M.; Sun, L.; Song, C.; Moreno, B.H.; Hu-Lieskovan, S.; Berent-Maoz, B.; Pang, J.; Chmielowski, B.; Cherry, G.; et al. Genomic and Transcriptomic Features of Response to Anti-PD-1 Therapy in Metastatic Melanoma. *Cell* **2016**, *165*, 35–44. [CrossRef] [PubMed]
5. Shin, D.S.; Zaretsky, J.M.; Escuin-Ordinas, H.; Garcia-Diaz, A.; Hu-Lieskovan, S.; Kalbasi, A.; Grasso, C.S.; Hugo, W.; Sandoval, S.; Torrejon, D.Y.; et al. Primary Resistance to PD-1 Blockade Mediated by JAK1/2 Mutations. *Cancer Discov.* **2017**, *7*, 188–201. [CrossRef]
6. Zaretsky, J.M.; Garcia-Diaz, A.; Shin, D.S.; Escuin-Ordinas, H.; Hugo, W.; Hu-Lieskovan, S.; Torrejon, D.Y.; Abril-Rodriguez, G.; Sandoval, S.; Barthly, L.; et al. Mutations Associated with Acquired Resistance to PD-1 Blockade in Melanoma. *N. Engl. J. Med.* **2016**, *375*, 819–829. [CrossRef]
7. Snyder, A.; Makarov, V.; Merghoub, T.; Yuan, J.; Zaretsky, J.M.; Desrichard, A.; Walsh, L.A.; Postow, M.A.; Wong, P.; Ho, T.S.; et al. Genetic basis for clinical response to CTLA-4 blockade in melanoma. *N. Engl. J. Med.* **2014**, *371*, 2189–2199. [CrossRef]
8. Ribas, A.; Hamid, O.; Daud, A.; Hodi, F.S.; Wolchok, J.D.; Kefford, R.; Joshua, A.M.; Patnaik, A.; Hwu, W.J.; Weber, J.S.; et al. Association of Pembrolizumab with Tumor Response and Survival Among Patients With Advanced Melanoma. *Jama* **2016**, *315*, 1600–1609. [CrossRef]
9. Robert, C.; Long, G.V.; Brady, B.; Dutriaux, C.; Maio, M.; Mortier, L.; Hassel, J.C.; Rutkowski, P.; McNeil, C.; Kalinka-Warzocha, E.; et al. Nivolumab in Previously Untreated Melanoma without BRAF Mutation. *N. Engl. J. Med.* **2015**, *372*, 320–330. [CrossRef]
10. Hodi, F.S.; Chiarion-Sileni, V.; Gonzalez, R.; Grob, J.J.; Rutkowski, P.; Cowey, C.L.; Lao, C.D.; Schadendorf, D.; Wagstaff, J.; Dummer, R.; et al. Nivolumab plus ipilimumab or nivolumab alone versus ipilimumab alone in advanced melanoma (CheckMate 067): 4-year outcomes of a multicentre, randomised, phase 3 trial. *Lancet. Oncol.* **2018**, *19*, 1840–1892. [CrossRef]
11. Wolchok, J.D.; Chiarion-Sileni, V.; Gonzalez, R.; Rutkowski, P.; Grob, J.J.; Cowey, C.L.; Lao, C.D.; Wagstaff, J.; Schadendorf, D.; Ferrucci, P.F.; et al. Overall Survival with Combined Nivolumab and Ipilimumab in Advanced Melanoma. *N. Engl. J. Med.* **2017**, *377*, 1345–1356. [CrossRef] [PubMed]
12. Larkin, J.; Chiarion-Sileni, V.; Gonzalez, R.; Grob, J.J.; Cowey, C.L.; Lao, C.D.; Schadendorf, D.; Dummer, R.; Smylie, M.; Rutkowski, P.; et al. Combined Nivolumab and Ipilimumab or Monotherapy in Untreated Melanoma. *N. Engl. J. Med.* **2015**, *373*, 23–34. [CrossRef] [PubMed]
13. Puzanov, I.; Dummer, R.; Schachter, J.; Pavlick, A.C.; Gonzalez, R.; Ascierto, P.A.; Margolin, K.A.; Hamid, O.; Agarwala, S.S.; Carlino, M.S.; et al. Efficacy based on tumor PD-L1 expression in KEYNOTE-002, a randomized comparison of pembrolizumab (pembro; MK-3475) versus chemotherapy in patients (pts) with ipilimumab-refractory (IPI-R) advanced melanoma (MEL). *J. Clin. Oncol.* **2015**, *33*, 3012. [CrossRef]

14. Weber, J.S.; D'Angelo, S.P.; Minor, D.; Hodi, F.S.; Gutzmer, R.; Neyns, B.; Hoeller, C.; Khushalani, N.I.; Miller, W.H., Jr.; Lao, C.D.; et al. Nivolumab versus chemotherapy in patients with advanced melanoma who progressed after anti-CTLA-4 treatment (CheckMate 037): A randomised, controlled, open-label, phase 3 trial. *Lancet. Oncol.* **2015**, *16*, 375–384. [CrossRef]
15. Madore, J.; Vilain, R.E.; Menzies, A.M.; Kakavand, H.; Wilmott, J.S.; Hyman, J.; Yearley, J.H.; Kefford, R.F.; Thompson, J.F.; Long, G.V.; et al. PD-L1 expression in melanoma shows marked heterogeneity within and between patients: Implications for anti-PD-1/PD-L1 clinical trials. *Pigment Cell Melanoma Res.* **2015**, *28*, 245–253. [CrossRef]
16. D'Angelo, S.P.; Larkin, J.; Sosman, J.A.; Lebbe, C.; Brady, B.; Neyns, B.; Schmidt, H.; Hassel, J.C.; Hodi, F.S.; Lorigan, P.; et al. Efficacy and Safety of Nivolumab Alone or in Combination with Ipilimumab in Patients with Mucosal Melanoma: A Pooled Analysis. *J. Clin. Oncol.* **2017**, *35*, 226–235. [CrossRef]
17. Shoushtari, A.N.; Munhoz, R.R.; Kuk, D.; Ott, P.A.; Johnson, D.B.; Tsai, K.K.; Rapisuwon, S.; Eroglu, Z.; Sullivan, R.J.; Luke, J.J.; et al. The efficacy of anti-PD-1 agents in acral and mucosal melanoma. *Cancer* **2016**, *122*, 3354–3362. [CrossRef]
18. Hayward, N.K.; Wilmott, J.S.; Waddell, N.; Johansson, P.A.; Field, M.A.; Nones, K.; Patch, A.M.; Kakavand, H.; Alexandrov, L.B.; Burke, H.; et al. Whole-genome landscapes of major melanoma subtypes. *Nature* **2017**, *545*, 175–180. [CrossRef]
19. Genomic Classification of Cutaneous Melanoma. *Cell* **2015**, *161*, 1681–1696. [CrossRef]
20. Kato, S.; Goodman, A.M.; Walavalkar, V.; Barkauskas, D.A.; Sharabi, A.; Kurzrock, R. Hyper-progressors after Immunotherapy: Analysis of Genomic Alterations Associated with Accelerated Growth Rate. *Clin. Cancer Res.* **2017**, *23*, 4242–4250. [CrossRef]
21. Kanjanapan, Y.; Day, D.; Wang, L.; Al-Sawaihey, H.; Abbas, E.; Namini, A.; Siu, L.L.; Hansen, A.; Razak, A.A.; Spreafico, A.; et al. Hyperprogressive disease in early-phase immunotherapy trials: Clinical predictors and association with immune-related toxicities. *Cancer* **2019**, *125*, 1341–1349. [CrossRef] [PubMed]
22. Sabio, E.; Chan, T.A. The good, the bad, and the ugly: Hyperprogression in cancer patients following immune checkpoint therapy. *Genome Med.* **2019**, *11*, 43. [CrossRef] [PubMed]
23. Ferrara, R.; Mezquita, L.; Texier, M.; Lahmar, J.; Audigier-Valette, C.; Tessonnier, L.; Mazieres, J.; Zalcman, G.; Brosseau, S.; Le Moulec, S.; et al. Hyperprogressive Disease in Patients With Advanced Non-Small Cell Lung Cancer Treated With PD-1/PD-L1 Inhibitors or With Single-Agent Chemotherapy. *Jama Oncol.* **2018**, *4*, 1543–1552. [CrossRef] [PubMed]
24. Sasaki, A.; Nakamura, Y.; Mishima, S.; Kawazoe, A.; Kuboki, Y.; Bando, H.; Kojima, T.; Doi, T.; Ohtsu, A.; Yoshino, T.; et al. Predictive factors for hyperprogressive disease during nivolumab as anti-PD1 treatment in patients with advanced gastric cancer. *Gastric Cancer* **2019**, *22*, 793–802. [CrossRef] [PubMed]
25. Champiat, S.; Dercle, L.; Ammari, S.; Massard, C.; Hollebecque, A.; Postel-Vinay, S.; Chaput, N.; Eggermont, A.; Marabelle, A.; Soria, J.C.; et al. Hyperprogressive Disease Is a New Pattern of Progression in Cancer Patients Treated by Anti-PD-1/PD-L1. *Clin. Cancer Res.* **2017**, *23*, 1920–1928. [CrossRef] [PubMed]
26. Faure, M.; Rochigneux, P.; Olive, D.; Taix, S.; Brenot-Rossi, I.; Gilabert, M. Hyperprogressive Disease in Anorectal Melanoma Treated by PD-1 Inhibitors. *Front. Immunol.* **2018**, *9*, 797. [CrossRef] [PubMed]
27. Forschner, A.; Niessner, H.; Moller, Y.; Horak, P.; Frohlich, M.; Warsow, G.; Stenzinger, A.; Frohling, S.; Glimm, H.; Klumpp, B.; et al. Genomics of Immunotherapy-Associated Hyperprogressors-Letter. *Clin. Cancer Res.* **2017**, *23*, 6374–6375. [CrossRef]
28. Eisenhauer, E.A.; Therasse, P.; Bogaerts, J.; Schwartz, L.H.; Sargent, D.; Ford, R.; Dancey, J.; Arbuck, S.; Gwyther, S.; Mooney, M.; et al. New response evaluation criteria in solid tumours: Revised RECIST guideline (version 1.1). *Eur. J. Cancer (Oxf. Engl. 1990)* **2009**, *45*, 228–247. [CrossRef]
29. Li, H.; Durbin, R. Fast and accurate short read alignment with Burrows-Wheeler transform. *Bioinform. (Oxf. Engl.)* **2009**, *25*, 1754–1760. [CrossRef]
30. Schroeder, C.M.; Hilke, F.J.; Loffler, M.W.; Bitzer, M.; Lenz, F.; Sturm, M. A comprehensive quality control workflow for paired tumor-normal NGS experiments. *Bioinform. (Oxf. Engl.)* **2017**, *33*, 1721–1722. [CrossRef]
31. Kim, S.; Scheffler, K.; Halpern, A.L.; Bekritsky, M.A.; Noh, E.; Kallberg, M.; Chen, X.; Kim, Y.; Beyter, D.; Krusche, P.; et al. Strelka2: Fast and accurate calling of germline and somatic variants. *Nat. Methods* **2018**, *15*, 591–594. [CrossRef] [PubMed]

32. Cingolani, P.; Platts, A.; Wang le, L.; Coon, M.; Nguyen, T.; Wang, L.; Land, S.J.; Lu, X.; Ruden, D.M. A program for annotating and predicting the effects of single nucleotide polymorphisms, SnpEff: SNPs in the genome of Drosophila melanogaster strain w1118; iso-2; iso-3. *Fly* **2012**, *6*, 80–92. [CrossRef] [PubMed]
33. Tamborero, D.; Rubio-Perez, C.; Deu-Pons, J.; Schroeder, M.P.; Vivancos, A.; Rovira, A.; Tusquets, I.; Albanell, J.; Rodon, J.; Tabernero, J.; et al. Cancer Genome Interpreter annotates the biological and clinical relevance of tumor alterations. *Genome Med.* **2018**, *10*, 25. [CrossRef] [PubMed]
34. Demidov, G.; Ossowski, S. ClinCNV: Novel method for allele-specific somatic copy-number alterations detection. *bioRxiv* **2019**. [CrossRef]
35. Liang, W.S.; Hendricks, W.; Kiefer, J.; Schmidt, J.; Sekar, S.; Carpten, J.; Craig, D.W.; Adkins, J.; Cuyugan, L.; Manojlovic, Z.; et al. Integrated genomic analyses reveal frequent TERT aberrations in acral melanoma. *Genome Res.* **2017**, *27*, 524–532. [CrossRef]
36. Newell, F.; Kong, Y.; Wilmott, J.S.; Johansson, P.A.; Ferguson, P.M.; Cui, C.; Li, Z.; Kazakoff, S.H.; Burke, H.; Dodds, T.J.; et al. Whole-genome landscape of mucosal melanoma reveals diverse drivers and therapeutic targets. *Nat. Commun.* **2019**, *10*, 3163. [CrossRef]
37. Wade, M.; Li, Y.C.; Wahl, G.M. MDM2, MDMX and p53 in oncogenesis and cancer therapy. *Nat. Rev. Cancer* **2013**, *13*, 83–96. [CrossRef]
38. Akbay, E.A.; Koyama, S.; Carretero, J.; Altabef, A.; Tchaicha, J.H.; Christensen, C.L.; Mikse, O.R.; Cherniack, A.D.; Beauchamp, E.M.; Pugh, T.J.; et al. Activation of the PD-1 pathway contributes to immune escape in EGFR-driven lung tumors. *Cancer Discov.* **2013**, *3*, 1355–1363. [CrossRef]
39. Dodds, T.J.; Wilmott, J.S.; Jackett, L.A.; Lo, S.N.; Long, G.V.; Thompson, J.F.; Scolyer, R.A. Primary anorectal melanoma: Clinical, immunohistology and DNA analysis of 43 cases. *Pathology* **2019**, *51*, 39–45. [CrossRef]
40. Postow, M.A.; Luke, J.J.; Bluth, M.J.; Ramaiya, N.; Panageas, K.S.; Lawrence, D.P.; Ibrahim, N.; Flaherty, K.T.; Sullivan, R.J.; Ott, P.A.; et al. Ipilimumab for patients with advanced mucosal melanoma. *Oncologist* **2013**, *18*, 726–732. [CrossRef]
41. Kato, S.; Ross, J.S.; Gay, L.; Dayyani, F.; Roszik, J.; Subbiah, V.; Kurzrock, R. Analysis of MDM2 Amplification: Next-Generation Sequencing of Patients With Diverse Malignancies. *Jco Precis. Oncol.* **2018**, *2018*, 1–14. [CrossRef] [PubMed]
42. Tumeh, P.C.; Hellmann, M.D.; Hamid, O.; Tsai, K.K.; Loo, K.L.; Gubens, M.A.; Rosenblum, M.; Harview, C.L.; Taube, J.M.; Handley, N.; et al. Liver Metastasis and Treatment Outcome with Anti-PD-1 Monoclonal Antibody in Patients with Melanoma and NSCLC. *Cancer Immunol. Res.* **2017**, *5*, 417–424. [CrossRef] [PubMed]
43. Forschner, A.; Battke, F.; Hadaschik, D.; Schulze, M.; Weissgraeber, S.; Han, C.T.; Kopp, M.; Frick, M.; Klumpp, B.; Tietze, N.; et al. Tumor mutation burden and circulating tumor DNA in combined CTLA-4 and PD-1 antibody therapy in metastatic melanoma—results of a prospective biomarker study. *J. Immunother. Cancer* **2019**, *7*, 180. [CrossRef] [PubMed]
44. Pires da Silva, I.; Lo, S.; Quek, C.; Gonzalez, M.; Carlino, M.S.; Long, G.V.; Menzies, A.M. Site-specific response patterns, pseudoprogression, and acquired resistance in patients with melanoma treated with ipilimumab combined with anti-PD-1 therapy. *Cancer* **2019**, *126*, 86–97. [CrossRef]
45. Calne, R.Y. Immunological tolerance—The liver effect. *Immunol. Rev.* **2000**, *174*, 280–282. [CrossRef] [PubMed]
46. Calne, R.Y.; Sells, R.A.; Pena, J.R.; Davis, D.R.; Millard, P.R.; Herbertson, B.M.; Binns, R.M.; Davies, D.A. Induction of immunological tolerance by porcine liver allografts. *Nature* **1969**, *223*, 472–476. [CrossRef]
47. Casey, S.C.; Tong, L.; Li, Y.; Do, R.; Walz, S.; Fitzgerald, K.N.; Gouw, A.M.; Baylot, V.; Gutgemann, I.; Eilers, M.; et al. MYC regulates the antitumor immune response through CD47 and PD-L1. *Sci. (New Yorkn. Y.)* **2016**, *352*, 227–231. [CrossRef]

© 2020 by the authors. Licensee MDPI, Basel, Switzerland. This article is an open access article distributed under the terms and conditions of the Creative Commons Attribution (CC BY) license (http://creativecommons.org/licenses/by/4.0/).

Dynamics of cell-free tumour DNA correlate with treatment response of head and neck cancer patients receiving radiochemotherapy

Franz J. Hilke[1, 2*], Francesc Muyas[1, 3*], Jakob Admard[1], Beate Kootz[1], Dominik Nann[4], Stefan Welz[5,6], Olaf Rieß[1,7], Daniel Zips[5,6], Stephan Ossowski[1,7], Christopher Schroeder[1], Kerstin Clasen[5]

[1] Institute of Medical Genetics and Applied Genomics, Medical Faculty and University Hospital, Eberhard Karls University Tübingen, Tübingen, Germany

[2] Department of Dermatology, Venereology and Allergology, Charité - Universitätsmedizin Berlin, Berlin, Germany.

[3] Universitat Pompeu Fabra (UPF), Barcelona, Spain

[4] Institute of Pathology and Neuropathology, Comprehensive Cancer Center and University Hospital Tübingen, Tübingen, Germany.

[5] Department of Radiation Oncology, Medical Faculty and University Hospital, Eberhard Karls University Tübingen, Tübingen, Germany

[6] German Cancer Consortium (DKTK), German Cancer Research Center (DKFZ) partner site Tübingen, Germany

[7] DFG NGS Competence Center Tübingen (NCCT), University of Tübingen, Tübingen, Germany.

* These authors contributed equally to this publication and are shared first authors.

Running title: CtDNA a potential biomarker in patients with HNSCC

Key words: Liquid biopsy, head and neck squamous cell carcinoma, radiochemotherapy, longitudinal analysis, dynamics of ctDNA/cvDNA

Financial support:

"Stiftung Tumorforschung Kopf-Hals" in Wiesbaden / Germany funded parts of the project.

Correspondence to:

Christopher Schroeder, M.D.

Institute of Medical Genetics and Applied Genomics

Eberhard-Karls-University of Tübingen

Calwerstr. 7

D-72076 Tübingen
Germany
Tel.: + 49 7071 29 72296
Christopher.schroeder@med.uni-tuebingen.de

Abstract

Purpose

Definitive radiochemotherapy (RCTX) with curative intent is one of the standard treatment options in patients with locally advanced head and neck squamous cell carcinoma (HNSCC). Despite this intensive therapy protocol, disease recurrence remains an issue. Therefore, we tested the predictive capacity of liquid biopsies as a novel biomarker during RCTX in patients with HNSCC.

Material and methods

We sequenced the tumour samples of 20 patients with locally advanced HNSCC to identify driver mutations. Subsequently, we performed a longitudinal analysis of circulating tumour DNA (ctDNA) dynamics during RCTX. Deep sequencing and UMI-based error suppression for the identification of driver mutations and HPV levels in the plasma enabled treatment-response monitoring prior, during and after RCTX.

Results

In 85% of all patients ctDNA was detectable, showing a significant correlation with the gross tumour volume (p-value 0.032). Additionally, the tumour allele fraction in the plasma was negatively correlated with the course of treatment (p-value < 0.05). If ctDNA was detectable at the first follow-up, disease recurrence was seen later on. Circulating HPV DNA (cvDNA) could be detected in three patients at high levels, showing a similar dynamic behaviour to the ctDNA throughout treatment, and disappeared after treatment.

Conclusions

Monitoring RCTX treatment-response using liquid biopsy in patients with locally advanced HNSCC is feasible. CtDNA can be seen as a surrogate marker of disease burden, tightly correlating with the gross tumour volume prior to the treatment start. The observed kinetic of

ctDNA and cvDNA showed a negative correlation with time and treatment dosage in most patients.

Introduction

Head and neck squamous cell carcinomas (HNSCC) represent a high number of cancer patients worldwide, with roughly 700,000 newly diagnosed cases in 2018 (1). The three major etiologies for the development of HNSCC are tobacco use, heavy alcohol consumption and infection with the human papillomavirus (HPV), especially associated with oropharyngeal squamous cell carcinomas (2, 3).

In unresectable, advanced HNSCC the primary combination of radiation and chemotherapy (RCTX) with curative intent is standard of care. The regimen includes a cumulative radiation dose of about 70 Gy within 6-7 weeks and a concomitant chemotherapy with cisplatin (4), optionally with 5-fluorouracil (5-FU) and mitomycin C (MMC) (5). Despite the intense treatment, the German Cancer Consortium Radiation Oncology Group reported a two-year overall survival (OS) rate of only 59.6% (6), recently. To date, active treatment monitoring during RCTX is not performed and the follow-up is based on clinical examinations and imaging modalities. This allows an approximation of the therapeutic success, but no insights into the existence of minimal residual disease (7).

In radiation oncology, the use of liquid biopsies could enable the detection of potential biomarkers for patient stratification, treatment response assessment and post-treatment surveillance in HNSCC patients (8-10). In addition, monitoring of HPV particles in plasma could be a marker for disease recurrence and of prognostic value (9, 11, 12).

Thus, in this study we tested the capacity of liquid biopsies to monitor treatment outcome in response to combined RCTX and to identify molecular residual disease (MRD) post treatment. The present study provides data of an ultra-sensitive NGS-approach to detect circulating cell-

free tumour (ctDNA) and viral DNA (cvDNA) and correlate the results with outcome parameters.

Materials and Methods

Patients and Clinical Samples

In this prospective pilot study 20 patients with locally advanced HNSCC were enrolled between 2015 and 2016. All participants declared written informed consent, and the study was approved by the local ethics committee (577/2014BO2). The patients received a definitive radiochemotherapy after primary diagnosis by intensity-modulated radiotherapy (IMRT) with a cumulative radiation dose of 70-77Gy and concomitant chemotherapy with cisplatin weekly or a combination therapy of 5-FU and MMC.

For the analysis of ctDNA, blood samples were collected prior to therapy as baseline (T1), three times during therapy to follow the ctDNA dynamics (T2-4) and subsequent to chemoradiation (T5) to evaluate the treatment outcome (time line shown in figure 1). Clinical investigations and computed tomography (CT) scans were performed six respectively twelve weeks after treatment for the first follow-up. Recurrent disease or progression were diagnosed by imaging and endoscopic follow-up and - if possible - by histology.

Targeted Panel Sequencing and Bioinformatics Analysis

A HNSCC specific cancer panel was used for the library preparation of DNA from formalin-fixed paraffin-embedded (FFPE) tumour tissues and blood samples were used as normal tissue control (13). All samples were processed and sequenced as previously published (14). Data analysis, quality control and calling of somatic single nucleotide variants, insertions and deletions were performed with an in-house pipeline, called “megSAP” (https://github.com/imgag/megSAP). Identification and clinical interpretation of driver mutations was performed using the Cancer Genome Interpreter (15).

CtDNA and HPV monitoring by ultra-deep sequencing with unique molecular barcodes

We collected peripheral blood samples for the isolation of cell-free DNA (cfDNA), using the QIAmp Circulating Nucleic Acid Kit (Qiagen, Hilden, Germany). We sequenced the genomic regions of all 127 driver mutations, identified in our patient cohort, and the E7 viral DNA sequence from the HPV16 and HPV18 strains (T1-T5; n = 99). The library preparation was done using the Agilent SureSelect$^{XT\text{-}HS}$ protocol, containing unique molecular identifiers (UMIs). Each unique DNA fragment is tagged with a unique 8bp UMI barcode prior to the first PCR amplification. These barcodes can subsequently be used to identify each PCR copy of an original DNA fragment.

Ultra-low frequency somatic variant calling using UMI-corrected deep-sequencing data

The input amount of cfDNA was limited to either 9 ng, 13 ng or 15 ng per patient and sample. This contains around 2700 – 4500 haploid genome equivalents. In order to identify mutations at ultra-low variant allele frequencies (VAF $\geq$ 0.1%) in cfDNA, we developed a UMI-based de-duplication and error correction procedure and a probabilistic model for mutation detection based on a beta-binomial distribution of errors (additional file 1). Our model detects mutations with a VAF as low as 0.043% (~1 mutated DNA per 2,325 reference-like DNA fragments in plasma). Variant allele frequencies and probabilities of each mutation per patient and time point were recorded for longitudinal analysis of ctDNA dynamics in plasma in relation to treatment dosage. Finally, we integrated VAF information and probabilities from multiple mutations per patient to substantially improve the detectability of residual ctDNA in plasma post-treatment (additional file 1).

Statistics and Data Correlation

Statistical significance was defined as $p < 0.05$. For longitudinal analysis of ctDNA levels we used a combination of linear regression for removal of confounding effects and Spearman correlation test for correlating ctDNA and treatment dosage or time since treatment start.

Results

Twenty patients with locally advanced HNSCC, located in the oropharynx (n=14), hypopharynx (n=4) or in the oral cavity (n=2), were included in this study. Of the 20 patients, 99 of 100 planned blood samples could be collected. One patient missed the first follow-up due to inpatient treatment in another clinic. The median follow-up was 823 days (range: 135 – 1168) with 13 patients still alive at the time of analysis. Ten patients showed a local or distant relapse, the majority of which already occurred in the first year. The genetic analysis revealed 667 somatic alterations of which 127 were classified as driver mutation, resulting in a median of four drivers per patient (min = 1, max = 52). The major affected signalling cascades were the TP53-, NOTCH-, HIPPO-, PI3K–pathway, or chromatin modifiers (suppl. Figure A1) (14). Additionally, immunohistochemistry revealed positivity for the $p16^{INK4a}$ protein in five patients (patients 2, 4, 8, 14 and 15).

Detection rate of ctDNA in the cohort

In order to monitor the response to treatment, we took blood samples from each patient at five consecutive time points (n = 99) and observed a positive detection rate of 85%. In three patients (2, 8 and 23) we could not detect ctDNA, likely due to variant calls of low quality or low variant allele frequency (VAF) in the solid tumour biopsy, undetectable levels of ctDNA, insufficient cfDNA fragment recovery from plasma, or insufficient depth of sequencing. Hence, these patients were excluded from further analysis.

Even though the total amount of cfDNA per sample (median: 9.98 ng/ml, range: 2.89 – 172.9 ng/ml) was limited, we achieved an average sequencing depth of 23,206x before and 2,049x after de-duplication of PCR copies (additional file 4), representing on average 2,049 haploid genome equivalents (hGEs). This enabled us to detect somatic alterations with variant allele fractions (VAF) as low as 0.05 percent (1 ctDNA per 2000 cfDNA) and different sensitivities depending on the sequencing depth and the number of UMI families (additional file 2&4).

Correlation of ctDNA in plasma with the gross tumour volume

We observed a positive correlation of the macroscopic tumour burden according to the gross tumour volumes (GTVs) in the planning CTs with the allele frequencies of driver mutations in cfDNA from plasma (referred to as 'ctDNA levels' from here on) observed before treatment initiation (T1) (p-value = 0.032 with Pearson correlation test). Bigger volumes of the primary tumours (PT) and their involved lymph nodes (LN) were associated with higher ctDNA levels (additional figure A2A). In addition to this, we observed that the fraction of short cfDNA fragments (≤ 150bp) correlated significantly and positively with ctDNA levels (p-value = 0.001 with Pearson correlation test, see additional figure figure A2B), supporting previous results (16).

Treatment surveillance and ctDNA kinetics

We next investigated the kinetics of ctDNA levels in response to the combined RCTX. To this end, we surveyed the level of ctDNA, the total cfDNA amount and the presence of a manifest infection during radiochemotherapy. The latter two measures are considered confounders influencing the proportion of ctDNA to total cfDNA in the bloodstream as previously published in this cohort (17). After removal of confounding effects we observed a ctDNA dynamic, showing a clear time and dosage dependency. Throughout the treatment, the allele frequency of the tumour- and patient-specific alterations decreased from a median of 1% at T1 to 0.01% at T5 (additional file 2 and figure 2). In seven patients (3, 7, 13, 14, 16, 18 and 20) we observed a significant negative correlation (p-value < 0.05) between the tumour allele fraction in the plasma and the course of treatment (Appendix table 1). Longitudinal analysis of another eight patients also showed a decrease in the ctDNA levels over time, although non-significant. One patient showed signs of therapeutic failure early in treatment, reflected by the increase in ctDNA levels over the course of treatment (patient 5; progressive disease at T5). Patient 11 was excluded from this correlation analysis, because only one mutation was monitored, which did

not reach the minimum sequencing depth for mutation detection at all time points (additional figure 3).

Detection of molecular residual disease (MRD)

The second major goal of this study was to detect residual ctDNA molecules with the help of liquid biopsy after therapy and to investigate the prognostic value of this observation. We refer to the significant observation of residual ctDNA molecules after treatment as 'molecular residual disease' (MRD) from here on. We included the 16 patients in the MRD analysis for which we successfully obtained plasma for T5 and which showed a significant ctDNA level for at least one earlier time (T1-T4). We compared the rate of observed MRD in the group of patients suffering from a relapse (patients 3, 5, 9, 10, 11, 13, 14, 21) with the rate in relapse-free patients (patients 4, 7, 15 – 20). We detected MRD in two out of eight patients (25%) suffering from a relapse (figure 3A and 3B), while none of the eight relapse-free patients showed MRD. Hence, 100% of patients with detectable MRD suffered a relapse, but 75% of relapsed patients did not show significant MRD after treatment.

Both MRD positive patients had a significant number of tumour fragments with MRD scores of 12.16 ($p < 10^{-12}$) and 2.44 ($p < 0.004$), respectively (see Figure 3A-B). They presented with either progressive disease within 101 days for patient 5 or distant relapse after 833 days for patient 10, respectively. Further analysis of the residual ctDNA fragments revealed that patient 5 still presented ctDNA fragments from five mutated driver genes with a global variant allele frequency of 0.27 % (Figure 3A). In patient 10 only the mutation in *TP53* was recovered (VAF = 0.09 %), while the mutation in *ATM* became undetectable (figure 3B).

HPV DNA in the plasma is a marker for therapy monitoring and prognosis in advanced HNSCC

HPV association in the solid tumour biopsies was assumed by positive immunohistochemical $p16^{INK4a}$ protein staining in three of the 17 patients for which liquid biopsy produced detectable levels of ctDNA. To evaluate the diagnostic potential of circulating cvDNA in plasma we screened the complete cohort at all five time points for the existence of the E7 sequence from

211 the HPV16 and HPV18 strains. We confirmed HPV-positivity in all three patients (100%), and
212 detected low levels of cvDNA in one additional patient. The number of viral fragments in
213 $p16^{INK4a}$ positive patients was very high, showing 2,229 to 11,671 reads per kilobase per million
214 reads (RPKM) at T1 (figure 4). Patient (5) had a negative $p16^{INK4a}$ test and showed only 352
215 RPKM at T1, and RPKM below 2 at later time points. All other $p16^{INK4a}$ negative patients had
216 RPKM values below 2 at all time points, indicating a complete absence of the E7 sequence. In
217 summary, we observed that HPV positive tumours show a more than 1000-fold enrichment of
218 viral sequence in plasma compared to HPV negative tumours.
219 Additionally, we assessed the cvDNA kinetics of the three patients (4, 14 and 15) during RCTX
220 treatment. The quantification of HPV fragments – normalized as RPKM values – showed a
221 steady decrease of the viral load throughout the therapy, mirroring the decrease of ctDNA levels
222 in the respective samples (figure 4). All three patients showed a significant correlation between
223 the longitudinal change of the normalized cvDNA counts and the administered treatment over
224 time (p-value < 0.05 with Spearman correlation test). Moreover, the longitudinal decrease in
225 normalized cvDNA counts (RPKM) correlated with the decrease of ctDNA levels in the
226 respective patients (p-value < 0.05 in patients 4 and 14, p-value $= 0.07$ in patient 15, using the
227 Pearson correlation test, figure 4). Finally, we estimated the number of HPV copies per cancer
228 cell in all three patients. Normalizing cvDNA coverage by genomic coverage we estimated
229 3.86, 2.95 and 11.69 HPV copies per cancer cell for patients 4, 14 and 15, respectively (suppl.
230 table 3). We observed that cvDNA levels became undetectable for all three patients at T3 or T4
231 and remained undetectable at T5, indicating only tumour cells harbor one or more copies of
232 HPV in their genome, while the majority of healthy cells have zero copies. Therefore, cvDNA
233 could be used as a highly sensitive marker for relapse screening.

Discussion

In this study, to the best of our knowledge, we document for the first time the dynamics of ctDNA and cvDNA and corresponding outcome parameters in patients with locally advanced HNSCC receiving primary chemoradiation. We tested the application of liquid biopsy to monitor the treatment response during RCTX and detection of molecular residual disease post-treatment. This led to several interesting findings, all of which could have relevance for the future clinical use of ctDNA as a biomarker in patients with advanced HNSCC under RCTX.

First of all, ctDNA can be seen as surrogate marker for the tumour burden, since ctDNA levels tightly correlate with gross tumour volumes as shown before (9-11). Moreover, we observed a time and dosage dependent dynamic of ctDNA levels in the plasma, and a decline of ctDNA levels corresponding with the primary success of the curative treatment intent. Therefore, we hope that surveilling the dynamic changes of ctDNA could be a new way to monitor and, if necessary, adjust the ongoing treatment regimen.

Interestingly, some of the patients showed a spike in ctDNA levels in the first liquid biopsy after treatment initiation (T2), followed by a rapid decline in T3 to T5. We speculate that this early spike reflects a strong increase in dying tumour cells after the first treatment dosages, as previously suggested in metastatic melanoma (18). However, it is unclear why other patients do not show an early spike, but a direct decline already after 4 to 7 days of treatment (T2). Based on our observations we can conclude that T3 (days 20-23) provides a more stable estimate of treatment response than T2.

Secondly, we observed that detectable post-treatment MRD and disease recurrence are indeed correlated, indicating that MRD could be a potent biomarker enabling stratification of patients into groups of high and low risk for disease recurrence, as it was shown in breast, lung, pancreatic, bladder, colon or rectal cancer (19-24). In those studies, the finding of residual ctDNA was associated with poorer overall survival and accelerated disease recurrence rates.

However, not all patients of our cohort suffering from relapse showed MRD. This could either be due to depth of sequencing applied, low number of monitored SNVs, or the absence of ctDNA despite later relapse. Further studies with increased numbers of monitored SNVs, higher sequencing depth or larger volumes of plasma will be necessary to better understand the sensitivity and specificity of the MRD approach.

Finally, we demonstrated the use of cvDNA as a highly sensitive biomarker for diagnosing HNSCC, monitoring of treatment response and detection of MRD or relapse. CvDNA showed the same dynamic properties during treatment as the ctDNA levels and our results indicate that cvDNA measurements are dramatically more sensitive than ctDNA measurements, with a thousand to ten thousand fold increase of detected cvDNA fragments compared to less than 100 ctDNA molecules per monitored SNV. In addition, we observed that cvDNA disappeared post treatment, indicating that only tumour cells harbor (at least one) copies of the virus. Therefore, we suggest using cvDNA as a blood based screening marker for the early detection of HNSCC, similar to EBV in nasopharyngeal carcinoma (25, 26). Moreover, a sustained detection of HPV following treatment could be predictive for disease recurrence (27-29).

A major limitation of liquid biopsy approaches is the limited amount of cfDNA extracted from a blood samples and the small fraction of ctDNA present in the total cfDNA convolute (30). With an average of 20 ng DNA per vial, representing roughly 6000 genome equivalents, the chance of detecting MRD by monitoring a single mutation is limited (31). This limitation can be overcome by targeting multiple independent mutations per individual (affecting different genes), which basically provides a multiplier of the number of detectable genome equivalents. Hence, the potential of our diagnostic strategy correlates with the total number of targeted mutations per individual, and an increase of the number of monitored mutations per individual significantly increases the power to detect tumour fragments at very low allele frequencies (19).

Conclusion

In this study, we could not detect MRD in all patients that suffered from a recurring disease, most probably due to the small number of mutations found by panel sequencing of the tumour biopsy. In future studies we will therefore utilise larger gene panels (>700 genes instead of 327 genes) or whole exome sequencing for biopsy analysis to substantially increase the number of monitored mutations in the liquid biopsy.

Acknowledgements

We would like to thank the "Stiftung Tumorforschung Kopf-Hals" in Wiesbaden / Germany for supporting this project by a grant to finance the genetic analysis. Besides, K. Clasen was supported by the intramural Fortüne / PATE Program of the Medical Faculty, Eberhard Karls University of Tübingen (Funding number: 2447-0-0). Francesc Muyas and Stephan Ossowski received funding from the European Union's H2020 research and innovation programme under grant agreement No 635290 (PanCanRisk).

References

1. Bray F, Ferlay J, Soerjomataram I, Siegel RL, Torre LA, Jemal A. Global cancer statistics 2018: GLOBOCAN estimates of incidence and mortality worldwide for 36 cancers in 185 countries. CA Cancer J Clin. 2018;68(6):394-424.

2. Leemans CR, Snijders PJF, Brakenhoff RH. The molecular landscape of head and neck cancer. Nat Rev Cancer. 2018;18(5):269-82.

3. Leemans CR, Braakhuis BJ, Brakenhoff RH. The molecular biology of head and neck cancer. Nat Rev Cancer. 2011;11(1):9-22.

4. Pignon JP, le Maitre A, Maillard E, Bourhis J, Group M-NC. Meta-analysis of chemotherapy in head and neck cancer (MACH-NC): an update on 93 randomised trials and 17,346 patients. Radiother Oncol. 2009;92(1):4-14.

5. Budach V, Stromberger C, Poettgen C, Baumann M, Budach W, Grabenbauer G, et al. Hyperfractionated accelerated radiation therapy (HART) of 70.6 Gy with concurrent 5-FU/Mitomycin C is superior to HART of 77.6 Gy alone in locally advanced head and neck cancer: long-term results of the ARO 95-06 randomized phase III trial. Int J Radiat Oncol Biol Phys. 2015;91(5):916-24.

6. Linge A, Lohaus F, Lock S, Nowak A, Gudziol V, Valentini C, et al. HPV status, cancer stem cell marker expression, hypoxia gene signatures and tumour volume identify good prognosis subgroups in patients with HNSCC after primary radiochemotherapy: A multicentre retrospective study of the German Cancer Consortium Radiation Oncology Group (DKTK-ROG). Radiother Oncol. 2016;121(3):364-73.

7. Chaudhuri AA, Binkley MS, Osmundson EC, Alizadeh AA, Diehn M. Predicting Radiotherapy Responses and Treatment Outcomes Through Analysis of Circulating Tumor DNA. Semin Radiat Oncol. 2015;25(4):305-12.

8. Tinhofer I, Staudte S. Circulating tumor cells as biomarkers in head and neck cancer: recent advances and future outlook. Expert Rev Mol Diagn. 2018;18(10):897-906.

9. Wang Y, Springer S, Mulvey CL, Silliman N, Schaefer J, Sausen M, et al. Detection of somatic mutations and HPV in the saliva and plasma of patients with head and neck squamous cell carcinomas. Sci Transl Med. 2015;7(293):293ra104.

10. Muhanna N, Di Grappa MA, Chan HHL, Khan T, Jin CS, Zheng Y, et al. Cell-Free DNA Kinetics in a Pre-Clinical Model of Head and Neck Cancer. Sci Rep. 2017;7(1):16723.

11. Ahn SM, Chan JY, Zhang Z, Wang H, Khan Z, Bishop JA, et al. Saliva and plasma quantitative polymerase chain reaction-based detection and surveillance of human papillomavirus-related head and neck cancer. JAMA Otolaryngol Head Neck Surg. 2014;140(9):846-54.

12. Jeannot E, Becette V, Campitelli M, Calmejane MA, Lappartient E, Ruff E, et al. Circulating human papillomavirus DNA detected using droplet digital PCR in the serum of patients diagnosed with early stage human papillomavirus-associated invasive carcinoma. J Pathol Clin Res. 2016;2(4):201-9.

13. Eder T, Hess AK, Konschak R, Stromberger C, Johrens K, Fleischer V, et al. Interference of tumour mutational burden with outcome of patients with head and neck cancer treated with definitive chemoradiation: a multicentre retrospective study of the German Cancer Consortium Radiation Oncology Group. Eur J Cancer. 2019;116:67-76.

14. Zwirner K, Hilke FJ, Demidov G, Socarras Fernandez J, Ossowski S, Gani C, et al. Radiogenomics in head and neck cancer: correlation of radiomic heterogeneity and somatic mutations in TP53, FAT1 and KMT2D. Strahlenther Onkol. 2019;195(9):771-9.

15. Tamborero D, Rubio-Perez C, Deu-Pons J, Schroeder MP, Vivancos A, Rovira A, et al. Cancer Genome Interpreter annotates the biological and clinical relevance of tumor alterations. Genome Med. 2018;10(1):25.

16. Mouliere F, Chandrananda D, Piskorz AM, Moore EK, Morris J, Ahlborn LB, et al. Enhanced detection of circulating tumor DNA by fragment size analysis. Sci Transl Med. 2018;10(466).

17. Zwirner K, Hilke FJ, Demidov G, Ossowski S, Gani C, Riess O, et al. Circulating cell-free DNA: A potential biomarker to differentiate inflammation and infection during radiochemotherapy. Radiother Oncol. 2018;129(3):575-81.

18. Xi L, Pham TH, Payabyab EC, Sherry RM, Rosenberg SA, Raffeld M. Circulating Tumor DNA as an Early Indicator of Response to T-cell Transfer Immunotherapy in Metastatic Melanoma. Clin Cancer Res. 2016;22(22):5480-6.

19. Chaudhuri AA, Chabon JJ, Lovejoy AF, Newman AM, Stehr H, Azad TD, et al. Early Detection of Molecular Residual Disease in Localized Lung Cancer by Circulating Tumor DNA Profiling. Cancer Discov. 2017;7(12):1394-403.

20. Tie J, Cohen JD, Wang Y, Li L, Christie M, Simons K, et al. Serial circulating tumour DNA analysis during multimodality treatment of locally advanced rectal cancer: a prospective biomarker study. Gut. 2019;68(4):663-71.

21. Christensen E, Birkenkamp-Demtroder K, Sethi H, Shchegrova S, Salari R, Nordentoft I, et al. Early Detection of Metastatic Relapse and Monitoring of Therapeutic Efficacy by Ultra-Deep Sequencing of Plasma Cell-Free DNA in Patients With Urothelial Bladder Carcinoma. J Clin Oncol. 2019;37(18):1547-57.

22. Garcia-Murillas I, Schiavon G, Weigelt B, Ng C, Hrebien S, Cutts RJ, et al. Mutation tracking in circulating tumor DNA predicts relapse in early breast cancer. Sci Transl Med. 2015;7(302):302ra133.

23. Sausen M, Phallen J, Adleff V, Jones S, Leary RJ, Barrett MT, et al. Clinical implications of genomic alterations in the tumour and circulation of pancreatic cancer patients. Nat Commun. 2015;6:7686.

24. Khakoo S, Carter PD, Brown G, Valeri N, Picchia S, Bali MA, et al. MRI Tumor Regression Grade and Circulating Tumor DNA as Complementary Tools to Assess Response and Guide Therapy Adaptation in Rectal Cancer. Clin Cancer Res. 2020;26(1):183-92.

25. Chan KC, Hung EC, Woo JK, Chan PK, Leung SF, Lai FP, et al. Early detection of nasopharyngeal carcinoma by plasma Epstein-Barr virus DNA analysis in a surveillance program. Cancer. 2013;119(10):1838-44.

26. Wang WY, Twu CW, Chen HH, Jiang RS, Wu CT, Liang KL, et al. Long-term survival analysis of nasopharyngeal carcinoma by plasma Epstein-Barr virus DNA levels. Cancer. 2013;119(5):963-70.

27. Lin JC, Wang WY, Chen KY, Wei YH, Liang WM, Jan JS, et al. Quantification of plasma Epstein-Barr virus DNA in patients with advanced nasopharyngeal carcinoma. N Engl J Med. 2004;350(24):2461-70.

28. Lo YM, Chan LY, Lo KW, Leung SF, Zhang J, Chan AT, et al. Quantitative analysis of cell-free Epstein-Barr virus DNA in plasma of patients with nasopharyngeal carcinoma. Cancer Res. 1999;59(6):1188-91.

29. Lo YM, Leung SF, Chan LY, Chan AT, Lo KW, Johnson PJ, et al. Kinetics of plasma Epstein-Barr virus DNA during radiation therapy for nasopharyngeal carcinoma. Cancer Res. 2000;60(9):2351-5.

30. Wan JCM, Massie C, Garcia-Corbacho J, Mouliere F, Brenton JD, Caldas C, et al. Liquid biopsies come of age: towards implementation of circulating tumour DNA. Nat Rev Cancer. 2017;17(4):223-38.

391 31. Chin RI, Chen K, Usmani A, Chua C, Harris PK, Binkley MS, et al. Detection of Solid
392 Tumor Molecular Residual Disease (MRD) Using Circulating Tumor DNA (ctDNA). Mol
393 Diagn Ther. 2019;23(3):311-31.
394

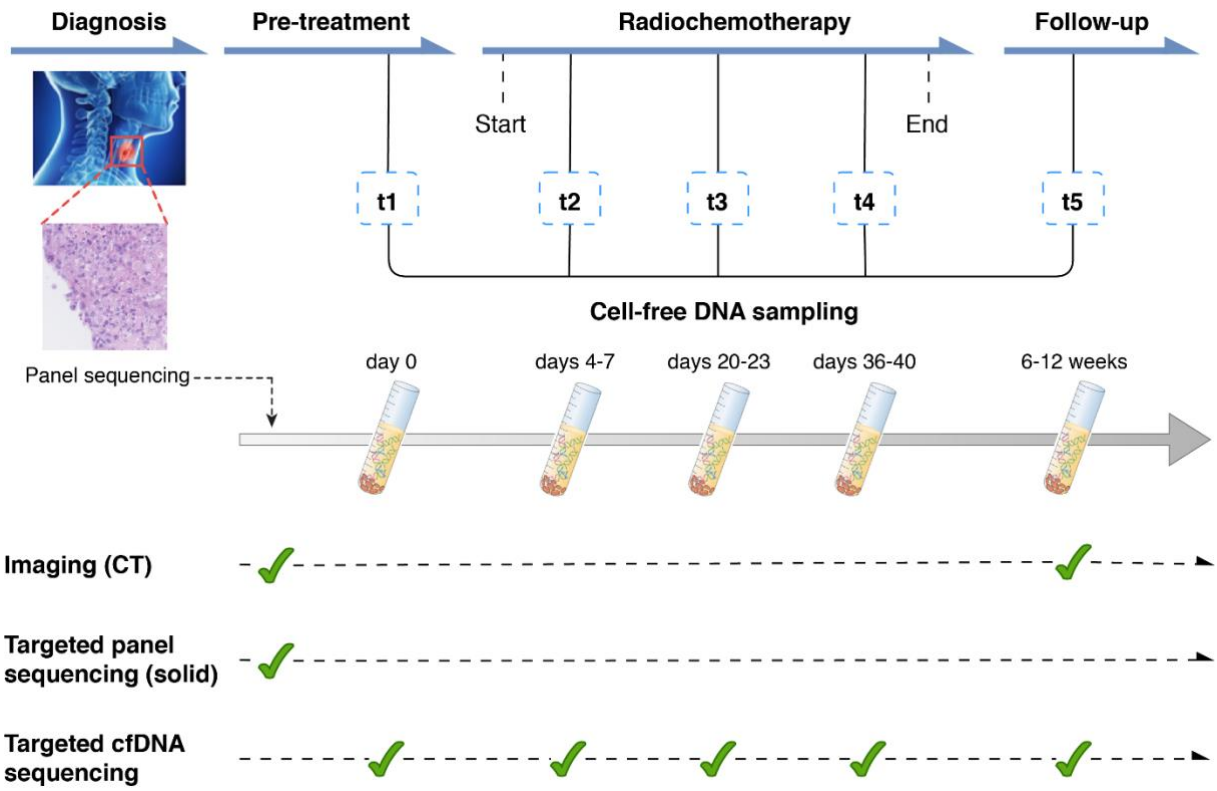

Figure 1

Overview of the study design, including diagnosis (imaging and biopsy NGS), treatment monitoring and the first follow-up. All solid tumour biopsies were sequenced using a cancer driver gene panel (327 genes) prior to the liquid biopsy. Based on the biopsy sequencing results suitable mutations were selected for monitoring in plasma. Five consecutive blood samples (T1 - T5) were taken prior, during and after treatment. The table in the lower part shows the diagnostic methods performed at each of the six time points.

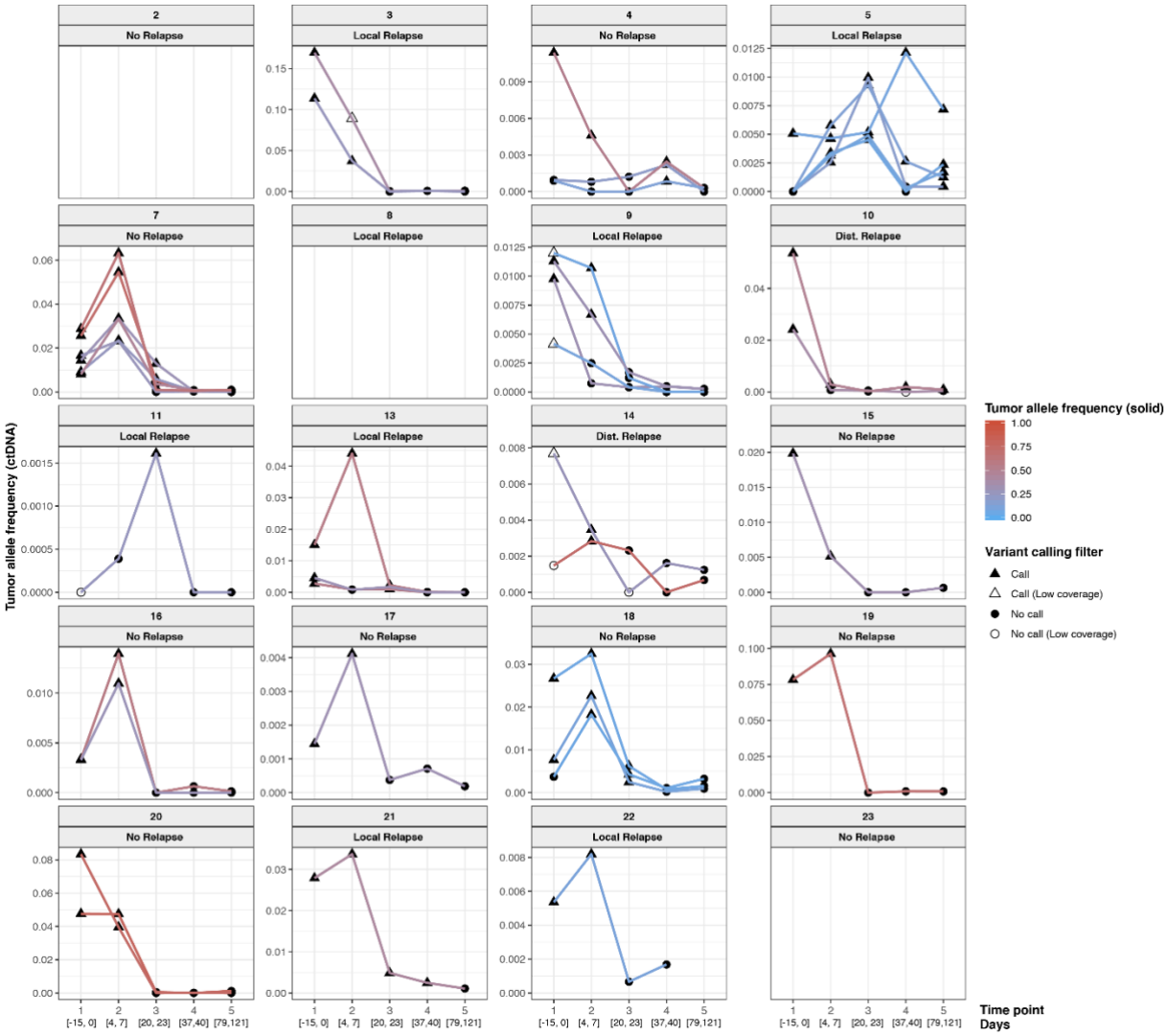

Figure 2

Variant allele frequencies (VAF) of monitored driver mutations in plasma at different times points during treatment. Each individual picture represents a patient and its relapse status. Lines connect VAF measures of the same mutation between time points and their colors represent their VAF in the solid tumour (*variant allele frequency (solid)* legend). The shapes of the points show the significance of variant calling (legend *Filter*).

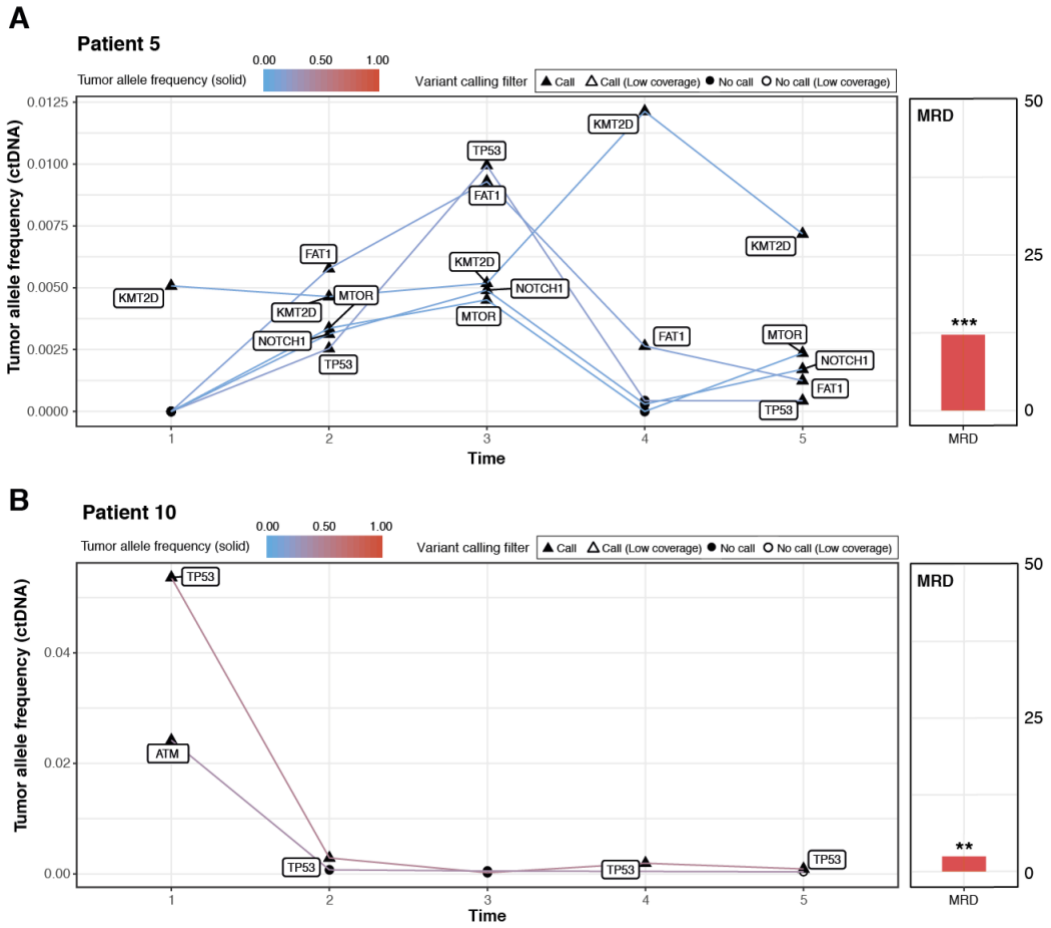

Figure 3

Longitudinal profiles of ctDNA levels in MRD patients. (A) Patient 5: Longitudinal profile of ctDNA levels for driver mutations (left) and the MRD value at the first follow-up (T5) after treatment. Lines connect identical mutations at different time points and boxes show gene names. The colour of the lines represents the VAF in the solid tumour and the shapes of the data points show the significance of the variant calling result. (B) Patient 10: Longitudinal profile of ctDNA levels for driver mutations (left) and the MRD value at the first follow-up (T5) after treatment. See (A) for plot description (** for p-value < 0.01 and *** for p-value < 0.001).

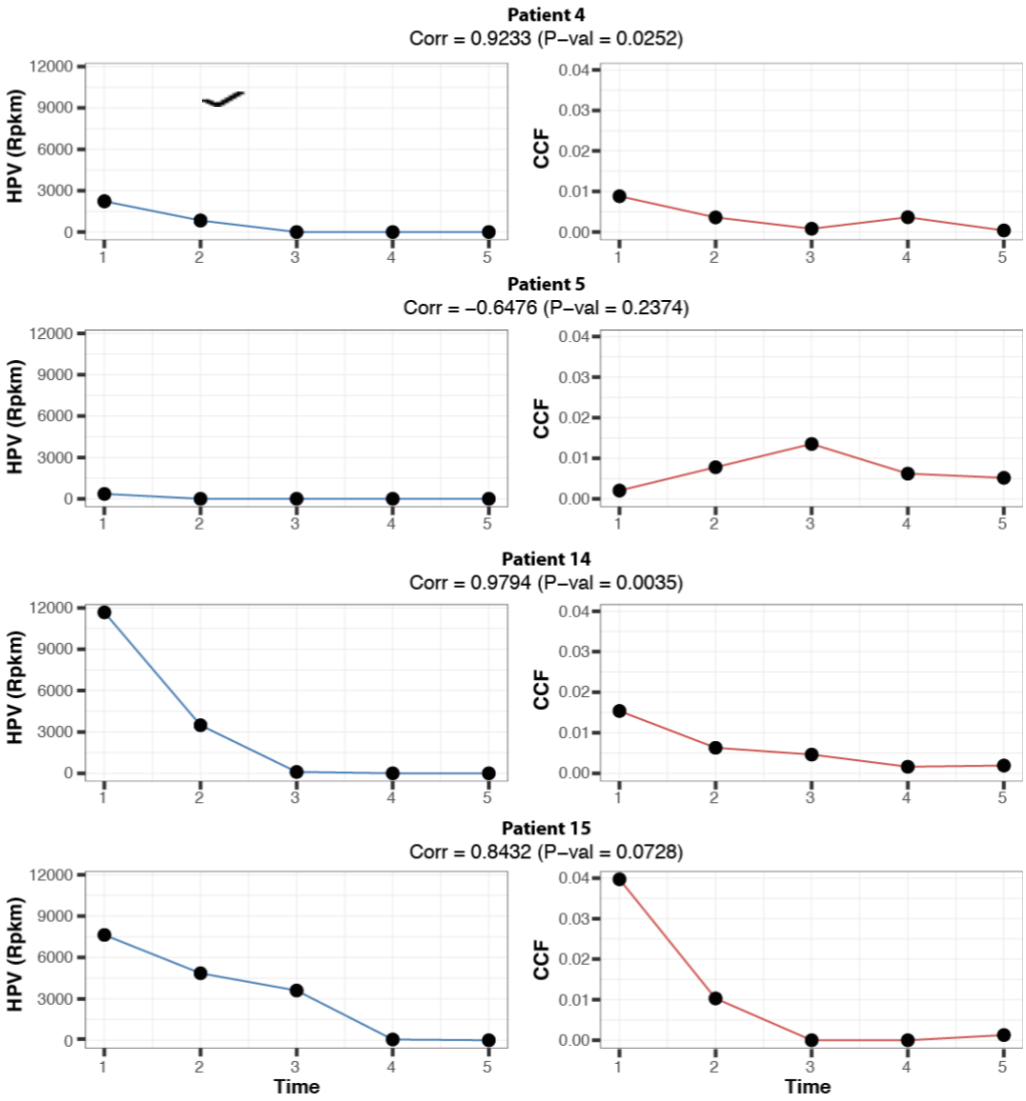

Figure 4

Longitudinal profiles of cvDNA levels in plasma. Left: normalized counts of HPV fragments observed in cfDNA at five time points for patients with at least HPV RPKM > 2 on average in all time points. Counts are normalized using the RPKM formula frequently applied for RNA-seq analysis. Right: Variant allele fractions (VAF) of driver mutations in cfDNA for the respective patients. Pearson correlation values between VAF and HPV (RPKM) are shown under patient label.

Next-generation sequencing in a real world cohort of 82 advanced melanoma patients identifies distinct mutation pattern in different melanoma subtypes

F. Hilke[1], T. Sinnberg[2], A. Gschwind[1], H. Niessner[2], G. Demidov[1], T. Amaral[2,3], S. Ossowski[1,4], I. Bonzheim[5], O. Riess[1,4], C. Garbe[2], C. Schroeder[1]*, A. Forschner[2]

[1] Institute of Medical Genetics and Applied Genomics, University Hospital Tübingen, Tübingen, Germany

[2] Center for Dermatooncology, Department of Dermatology, University Hospital Tübingen, Tübingen, Germany

[3] Portuguese Air Force Health Care Direction, Lisbon, Portugal

[4] German DFG NGS Competence Center, NCCT, Tübingen, Germany

[5] Institute of Pathology and Neuropathology, University Hospital Tübingen, Tübingen, Germany

*Correspondence:

Christopher Schroeder, M.D.
Institute of Medical Genetics and Applied Genomics
Eberhard-Karls-University of Tübingen
Calwerstr. 7, 72076 Tübingen, Germany
Tel.: + 49 7071 29 72296
christopher.schroeder@med.uni-tuebingen.de

Authors manuscript

Abstract

BACKGROUND

Next-generation sequencing (NGS) is becoming more and more important in the care of patients with advanced melanoma. To learn more about resistance to immune checkpoint inhibitors (ICI) and potential differences between melanoma subtypes, we evaluated the results of 82 melanoma patients who received NGS as part of routine clinical care in 2017.

PATIENTS AND METHODS

We determined the tumor mutation burden (TMB) and annotated all genetic driver alterations with the Cancer Genome Interpreter. Furthermore we searched for possible associations between mutated genes and different melanoma subtypes and patients` responses to ICI.

RESULTS

Melanoma of unknown primary had a similar mutation pattern and TMB like cutaneous melanoma, which hints at its cutaneous origin. Beside the typical hotspot mutation in *BRAF* and *NRAS* we observed frequently *CDKN2A* deletions. Acral and mucosal melanoma were dominated by CNV alterations affecting *PDGFRA*, *KIT*, *CDK4*, *RICTOR*, *CCND2* and *CHEK2*. Uveal melanoma typically had somatic SNVs in *GNA11/Q* and amplifications of *MYC* in all cases. A significantly higher incidence of *BRAF* V600 mutations and *EGFR* amplifications was found in patients progressive under ICI.

CONCLUCIONS

NGS might help to characterize melanoma subtypes more precisely and to identify possible resistance mechanisms for ICI therapy. Nevertheless, NGS based studies including larger cohorts are needed to proof potential genetic ICI resistance mechanisms.

Authors manuscript

Key words: Genome of advanced melanoma, acral, mucosal, uveal melanoma, melanoma of unknown origin, tumor mutation burden, TMB, immune checkpoint inhibitors, next generation sequencing

Authors manuscript

1. Introduction

In the last decade, multiple large-scale sequencing studies have elucidated the genetic landscape of melanoma and led to the classification of the genetic subtypes *BRAF* mutant, *RAS* mutant, *NF1* mutant or triple wild-type melanoma [1]. In conjunction with earlier exome sequencing studies [2,3] it was shown that the RTK, RAS/RAF/ERK, PI3K and cell cycle pathways were the major drivers for the oncogenesis of cutaneous melanoma. Over the past years multiple comprehensive sequencing studies have revealed the genetic landscape not only for cutaneous melanoma but also for acral and mucosal melanoma [4], resulting in the identification of further driver alterations and highlighting the impact of copy number changes in these subtypes [5,6]. Beyond the comprehensive genetic characterization, the identification of predictive and prognostic markers for treatment responses became a main focus over the past years [7,8]. Especially in the light of treatment failure in patients treated with immunotherapy certain genes and signaling cascades, like *MDM2* and *EGFR* amplifications [9-11], *PTEN* deletions and loss of functions mutations in *JAK2* or the interferon gamma signaling were identified as potential markers of primary or acquired resistance [12-15]. In addition, the recent work on the resistance mechanisms in melanoma patients treated with *BRAF* or *MEK* inhibitor therapy revealed new therapeutic strategies [7,8,16].

Therefore, we analyzed the results of next-generation sequencing of 82 patients with advanced melanoma, whose primary tumors or metastases had been sequenced as part of routine clinical care in 2017. We display the diversity of genetic mutations and affected pathways among this clinical cohort, highlighting both, genetic differences and similarities among the melanoma subtypes and show potential genetic resistance mechanisms to ICI.

Authors manuscript

2. Materials and Methods

2.1. Patients and tumor tissue

We included all melanoma patients of our Center for Dermatooncology whose tumors had been sequenced in 2017 as part of routine clinical care. All patients had been informed in a personal conversation with their dermato-oncologist and human geneticist about the procedure of tumor sequencing. Written consent was obtained from all patients. Clinical data were obtained from the patients` records. All patients had given their consent for their data to be made available for research. Local ethics committee of the University Tuebingen approved this study (approval number 103/2018BO2). The formalin fixed paraffin embedded tissue used for sequencing consisted in the latest available tissue, usually metastases that had been removed recently.

2.2. Sequencing

The sequencing panel was applied in three different versions, targeting 337 cancer associated genes in the primary setting (ssSCv2), 680 (ssSCv3) or 693 (ssSCv4) genes as well as intronic regions for the detection of distinct fusions in the updated versions (supplement table 4). As the sequencing panel changed in the course of this study, we focused the analysis on the 275 common genes present in all versions (s. supplement table 1-3). All samples were sequenced on an Illumina device (e.g. NextSeq500). Data processing was done by an in-house analysis pipeline using the open source tool BWA for mapping [17] and strelka2 for somatic variant detection [18]. The detection of somatic copy number alterations was done by our in-house software tool clinCNV [19]. Variants were annotated using SnpEff / SnpSift [20,21] and the publically available Cancer Genome Interpreter [22] for information about driver alterations. The R package MAFTOOLs version 2.0.16 was used for visualization [23].

Authors manuscript

2.3. Tumor mutation burden

Tumor mutation burden (TMB) was calculated as the number of all somatic alterations (coding SNVs and INDELs) based on the target size of the used panel. Since all three panel versions are designed to detect driver mutations in known tumor suppressor and oncogenes we had to adjust the calculation to avoid overrating the TMB.

Formula: $$\left[\frac{\left(\frac{Somatic - Known\_Tumorgenes}{Target\ size} \times Genome\ size\right) + Tumorgenes}{Genome\ size}\right]$$

2.4. Gene set enrichment analysis

The gene set enrichment was performed using either the clinical feature histopathological subtype or response to ICI, associated with the samples. The enrichment analysis was done using the gene set enrichment function of the R package MAFTOOLs version 2.0.16 [23]. It performs various groupwise and pairwise comparisons to identify enriched mutations for every category within a clinical feature.

2.5. Statistics

Statistical analysis was performed using the statistical program for social sciences SPSS Version 25 (IBM, New York, United States) as well as Graphpad Prism Version 8.3.0 (GraphPad Software, LLC). The distribution of TMB, SNVs and CNVs was compared between the different melanoma types using Mann-Whitney-U-test. The overall survival was calculated using the function overall survival in GraphPad Prism Version 8. Follow-up time was defined as the time between the initiation of immune checkpoint inhibition (ICI) and the date of the last follow-up or death from any cause.

Authors manuscript

3. Results

3.1 Patient cohort

In total 82 tumor tissues from 82 different patients were sequenced and analyzed. The cohort included cutaneous melanoma (n = 42), acral (n = 14), mucosal (n = 9) and uveal melanoma (n = 8), as well as melanoma of unknown primary (n = 9). The gender distribution was almost equal with 37 (45%) females and 45 (55%) males. The median age at the time of primary melanoma diagnosis was 57 years (IQR 46-67 years). The majority of patients (n = 75) had been treated with ICI, such as PD-1 antibody alone or in combination with CTLA-4 antibody (figure 1, table 1).

3.2. Driver alterations and signaling cascades

Comprehensive sequencing of the 82 tumor samples identified in total 1,650 somatic variants (SNVs and INDELs) and 2,137 somatic copy number alterations, such as amplifications or deletion of a complete gene (supplement table 4-5). We obtained a median number of 10 SNVs/INDELs per patient and a median TMB of 5.82 (range: 0-151.75). Furthermore, we referred to CancerGenomeInterpreter.org for the annotation of driver mutations and revealed a total number of 527 driver alterations, 283 SNVs and 244 CNVs, affecting 149 genes (supplement table 8-9).

The genomic classification of our cohort into *BRAF*-, *RAS*-, *NF1*-mutated or triple-wildtype showed that more than half of the patients carried a driver mutation in either one of the three genes (Fig. 1b). The serine/threonine kinase *BRAF* was the most frequently mutated gene of this cohort (28%). The vast majority were hotspot mutations V600E/K/R (91%). In addition, one patient had the *BRAF* G466E driver mutation and another had two simultaneous driver mutations at positions P367S and K601E. The second most frequent mutation was the GTPase *NRAS* (24%) with Q61K/L/R mutations. In two patients, we observed the rare combination of simultaneously occurring hotspot mutations in the gene *BRAF* (V600E) and *NRAS* (Q61K and

Authors manuscript

R, respectively). In addition hotspot mutations in *HRAS* (Q61R) and *KRAS* (G12D, D119H) were present in one and two patients respectively (not shown in figure 1). Driver mutations in the gene *NF1* were rare with 6%, while three of the patients either had a *BRAF* or *NRAS* hotspot mutation. The rest of the cohort, 36 patients (44%), were classified as triple wild type. Besides driver mutations in the genes *BRAF*, *NRAS* and *NF1* we found frequent activating amplifications in the receptor tyrosine kinases *ERBB3* and *MET*, as well as in the signal transducers *KRAS* and *PTPRD* (Fig. 1c). Thus, the RTK/RAS/MAP kinase-signaling pathway (hereafter RTK/RAS) is most frequently affected by driver mutations in our cohort overall (79%). Interestingly, the activating mutations in *ERBB3*, *MET* and *KRAS* were more abundant in the triple wildtype group.

The genes most frequently affected by copy number alterations (deletions or amplifications) were *CDKN2A* (24%) and *CCND3* (23%), both of which belong to the cell cycle control (Fig. 1c) and activating *MYC* amplifications that were detected in 24% of the patients. The PI3K signaling cascade was the third most frequent mutated signaling pathway (38%) with driver mutations in the genes *PTEN* (17%) and *RICTOR* (12%). Furthermore, we found frequent driver mutations in the Wnt and SWI/SNF signaling pathway (*CTNNB1*, *ARID2*, and *SMARCA4*).

3.3. Differences between melanoma subtypes

As part of the further analysis, we sought to identify possible genetic differences between the five histopathological melanoma subtypes. Interestingly, we found great similarities between the cutaneous melanoma and melanoma of unknown primary. Both subtypes were dominated by somatic SNVs, leading to the highest number of mutations (median = 7, range = 0-18) and a significantly higher TMB (median = 9.4, range = 0 - 36.4; $p < 0.003$) compared to the other subtypes (figure 2). The majority of the samples could be classified in the genomic subtypes *BRAF*, *RAS* and *NF1*. Only 19% of cutaneous or 33% melanoma of unknown primary were triple wild-type. In contrast, patients with acral and mucosal melanoma were mostly triple wild-

Authors manuscript

type (acral = 72%, mucosal = 78%) and had predominantly CNVs. In patients with mucosal melanoma we observed significantly more somatic CNVs (median = 177, range 144 – 186; $p < 0.03$) than in cutaneous melanoma (figure 2).

In order to identify possible genetic differences between the histopathological melanoma subtypes, we performed a gene set enrichment analysis (figure 3, supplement table 10-11) revealing several significant differences. The majority of significant differences were found in view to the uveal melanoma. In contrast to cutaneous, acral and mucosal melanoma, there was no enrichment of mutations in the RTK/RAS signaling pathway but frequent mutually exclusive mutations in the genes of the guanine nucleotide-binding protein subunits *GNA11* and *GNAQ* in combination with either the splicing factor *SF3B1* or the deubiquitinating enzyme *BAP1*. Of note, we found *MYC* amplifications in each of the uveal melanoma patients, which is a significant difference to the other melanoma subtypes ($p < 0.05$).

On the other hand, hotspot mutations in the genes *BRAF* and *NRAS*, in combination with homozygous deletions of the gene *CDKN2A*, were frequently found in cutaneous melanoma, whereas acral and mucosal melanoma were dominated by copy number changes affecting the RTK/RAS pathway and the regulators of cell cycle. The co-amplifications of the receptor tyrosine kinases *KIT* and *PDGFRA* on chromosome 4 as well as *CDK4* on chromosome 12 are of particular interest for acral melanoma, while mucosal melanoma had a significant accumulation of amplification in the regulator of the cell cycle control *CCND2*. Furthermore a member of the Fanconi anemia pathway, *CHEK2* was enriched for deletions in mucosal melanoma.

3.4. Genomic features of patients with resistance to immune checkpoint inhibitors

The majority of our cohort had been treated with ICI (75 of 82). Most of the patients (n=60) had received a combined immunotherapy with ipilimumab and nivolumab, and 15 patients had been treated with PD-1 antibodies alone. In order to identify possible genes associated with

Authors manuscript

resistance to ICI therapy, we classified treatment response according to RECIST [24] in the three groups: progressive disease (PD) (n = 45), stable disease (SD) (n = 12) and partial response (PR) (n = 18). Interestingly, most of the patients with PD and a *BRAF* mutation (16 of 18) had received therapy with *BRAF* and *MEK* inhibition (*BRAF/MEK*i) before initiation of ICI compared to those with a stable disease or partial response (2 of 4). As expected, the poorest survival was achieved by patients who suffered PD, followed by patients with SD and the best survival was that of patients with PR (suppl. Figure 1). The one-year survival rate was 51% for patients with PD compared to 83% for SD and 100% for PR (suppl. Figure 1).

As a next step, we performed a gene set enrichment analysis comparing the two response groups, progressive disease (PD, n=45) and disease control (DC, n=30) to identify significantly enriched genes for the PD group. The DC response group is the combination of the patients with either a stable disease (SD) or partial response (figure 4). We found that $BRAF^{V600}$ hotspot mutations and amplifications of the endothelial growth factor receptor (*EGFR*) were significantly enriched in patients with PD (18 of 45, p = 0.01 and 6 of 45, p = 0.04) compared to the DC group (4 respectively 0 of 30, figure 4, supplement table 13). The comparison of the overall survival between the patient groups *BRAF/MEK*i pre-treated (before ICI) and untreated *BRAF* mutant ($BRAF^{mut}$) melanoma respectively *BRAF* wildtype melanoma showed a significantly better OS for patients in the last two groups (p = 0.01) (figure 4, supplement table 14). The one-year survival rate was 72% for untreated $BRAF^{mut}$ and 80% for *BRAF*-WT compared to patients who received prior therapy with a *BRAF/MEK*i (63%).

In addition, we evaluated the abundance of mutated genes in the PD group, previously found to be associated with resistance to ICI. Among these genes are *CTNNB1, JAK2, MYC*, *MDM2*, *PTEN* and *TP53* [25] as well as *CDKN2A* [26]. Mutations in the genes *PTEN* and *TP53* were often found in the PD group with 24 % and 13 % respectively and occurred less frequent in the DC group (10% and 3%). Although alterations in *PTEN* and *TP53* were not found to be statistically enriched in our PD group we compared the signature of an alteration in at least one

Authors manuscript

of the three resistance-associated genes with the highest enrichment factors (*EGFR/PTEN/TP53*) in the PD versus the DC group. 23 of 45 PD cases had at least one mutation in any of the three genes whereas only 4 of 30 DC cases presented with a relevant mutation (two-tailed P = 0.0020; Yates's chi-square test). Accordingly, the relative risk to show PD in the first staging after starting with ICI was 1.86 for cases where the tumor harbors a mutation in *EGFR, PTEN* or *TP53*.

4. Discussion

In this study we aimed to evaluate TMB and driver mutations in a real world cohort of patients with cutaneous, acral, mucosal and uveal melanoma and melanoma of unknown primary. Employing a targeted cancer panel approach we found distinct genetic patterns for different histopathological subtypes. Furthermore, the comparison of driver gene mutations in patients with progressive disease compared to patients with a disease control treated with ICI, revealed an enrichment of *BRAF*, *EGFR*, *PTEN* and *TP53* gene mutations. All of them are potential markers of primary resistance to immune checkpoint blockade.

With the exception of patients with uveal melanoma, all subtypes were characterized by driver mutations in the genes of the RTK/RAS signaling pathway as well as cell cycle control and the PI3K pathway. In contrast, uveal melanoma was dominated by *MYC* amplifications and *GNA11* or *GNAQ* mutations in combination with the genes *BAP1* or *SF3B1*. The high frequency of *MYC* amplification has been described in previous work and it is known that high expression of *MYC* in tumors is associated with an increased risk of developing metastases and a worse prognosis [27-31]. Furthermore, we found mutual exclusivity of *SF3B1* or *BAP1* driver mutations in all patients with uveal melanoma. The splicing factor *SF3B1* is associated with an increased risk of metastasis and the deubiquitinase *BAP1* with a worse prognosis [31,32]. These

Authors manuscript

observations are in line with the clinical status of the included patients. All of them were already metastasized and characterized as highly advanced uveal melanomas.

The other three subtypes as well as melanoma of unknown primary were, as mentioned above, dominated by driver mutations in the genes of the cell cycle control (*CDKN2A*) and the RTK/RAS signaling pathway (*BRAF*, *NRAS*, *ERRB2*). In addition, cutaneous and occult melanoma have the highest tumor mutation burden compared to the other subtypes. Interestingly, they are also similar in terms of the number of CNVs and the frequency of genomic subgroups, *BRAF*-, *RAS*-, *NF1*-mutated or triple wild type. Taken together, these results support the existing assumption that the cutaneous and melanoma of unknown primary are similar and that latter probably originates from regressed or unrecognized primary cutaneous melanomas [33,34].

In comparison, the number of somatic CNVs was higher in acral and mucosal melanoma than in cutaneous melanoma. This result corresponds to the current state of knowledge [35,36], whereby a significantly higher number of CNVs could only be detected in mucosal melanoma. The driver mutations in the genes *RICTOR*, *CDK4*, *PDGFRA*, *KIT* are specific for acral melanoma and in mucosal melanoma it is the amplification or deletion of the genes *CCND2* and *CHEK2*. Our study confirms the observation of larger and more comprehensive studies from the near past [4-6].

In addition to the determination of subtype specific differences, the identification of driver mutations in genes with the potential to convey resistance towards immunotherapy was another focus of this study. Thus, driver mutations in the genes *BRAF* and *EGFR* were found significantly enriched in the group of patients with a progressive disease. Several studies in non-small-cell lung cancer have already shown the ineffectiveness of ICI in case of *EGFR* mutations in combination with a low TMB [37-39]. In addition, several retrospective studies have shown that the outcome of ICI is improved if these patients do not receive prior *BRAF* and

Authors manuscript

MEK inhibitor therapy [40-42]. In addition, an increased risk of a progressive disease at the first staging was associated with *PTEN* and *TP53* driver mutations. Both, if mutated, are potential genetic markers for a resistance towards ICI [25,26].

In addition, driver mutations in the cyclin-dependent kinases *CDKN2A*, *CDK4*, *CCND1/2/3* and the genes *MDM2/4* and *TP53* were abundant, which presumably contribute to a significant deregulation of cell cycle control. Deletions of gene *CDKN2A* appear to lead to resistance to immunotherapy and in combination with the deregulation of *CDK4*, worsen the prognosis in acral melanoma [13,43]. Therefore, the introduction of *CDK4/6* inhibitors could broaden treatment options [43-45]. Combined treatment with *MEK* and *CDK4/6* inhibitors could also be considered [46]. Another potential treatment target are driver mutations in the genes *ATM*, *CHEK2*, *FANCA*, *FANCC* and *BRCA2*, which belong to the DNA repair signaling pathway. One treatment option is a therapy with *PARP* inhibitors or alternatively platinum-based chemotherapy [47].

One of the limitations of the study is the fact that we evaluated a cohort of patients collected in daily clinical practice without specific inclusion criteria. This means that all patients were in an advanced stage of disease including distant metastases and most of them had already received several systemic therapies. With regards to the differences between the melanoma subtypes [48,49] and the identification of potential druggable targets, this is probably not that relevant. Although there might be differences between primary melanoma and metastasis [82], it still seems to be appropriate to tailor the therapy regime to the genomic pattern of the metastases. In regard to the advanced tumor stages of the patients and prior systemic therapies, the interpretation of genetic patterns for ICI resistance might be difficult. Sequencing the tumor tissue at an earlier stage without pre-treatment might be more appropriate to detect possible genetic resistance mechanisms.

Authors manuscript

Finally, we observed, that the TMB of cutaneous melanoma in our cohort was lower than that of TCGA [50]. This difference might be due to the fact that the estimated TMB of our cohort is based on a panel of genes and therefore different from the whole-exome approach used in the TCGA cohort. Furthermore, we probably have a negative selection of patients in our cohort as most of our patients had not responded to ICI, which is likely to be more common when the TMB is lower [48,49,51,52].

5. Conclusion

NGS might help to characterize melanoma subtypes more precisely and to better understand ICI failure in some points. Nevertheless, prospective studies are urgently needed to learn more about potential ICI resistance mechanisms and further effort should be made to introduce targeted therapies beyond *BRAF*, *MEK* or *KIT* inhibitors, such as *MYC* or *MDM2* inhibitors for metastasized melanoma.

Authors manuscript

Declarations

Ethics approval Local ethics committee of the Eberhard Karls University approved this study (approval number 103/2018BO2). This study was performed in accordance with the Declaration of Helsinki

Availability of data and material Datasets used and/or analyzed during the current study are available from the corresponding author on reasonable request.

Authors' contributions Conception and design: AF, F-J H, CG, CS. Development of methodology: AF, F-J H, GD, SO, CS, CG. Acquisition of data: AF, F-J H, SO, CS. Analysis and interpretation of data: all authors. Study supervision: AF, F-J H, CG, CS. Writing, review, revision of the manuscript: all authors. All authors have read and agreed the submitted version of the manuscript.

Funding AF was supported by the TÜFF Habilitation Program for Women of the Faculty of Medicine Tübingen, Germany, grant no° 2521-0-0.

Acknowledgements We thank the whole team of the melanoma outpatient department for their care for our melanoma patients.

Conflict of interest statement: AF served as consultant to Roche, Novartis, MSD, Pierre-Fabre; received travel support from Roche, Novartis, BMS, Pierre-Fabre, received speaker fees from Roche, Novartis, BMS, MSD and CeGaT. TA reports personal fees and travel grants from BMS, grants, personal fees and travel grants from Novartis, personal fees from Pierre Fabre, grants from Neracare, grants from Sanofi, outside the submitted work. CG reports grants and personal fees from Novartis, BMS, Roche, personal fees from MSD. Personal fees from Amgen, Philogen, LEO, Incyte, outside the submitted work. F-JH, OR and CS received an institutional grant from Novartis. The other authors declared no competing interests.

Authors manuscript

References

1. Cancer Genome Atlas, N. Genomic Classification of Cutaneous Melanoma. *Cell* **2015**, *161*, 1681-1696, doi:10.1016/j.cell.2015.05.044.
2. Krauthammer, M.; Kong, Y.; Bacchiocchi, A.; Evans, P.; Pornputtapong, N.; Wu, C.; McCusker, J.P.; Ma, S.; Cheng, E.; Straub, R., et al. Exome sequencing identifies recurrent mutations in NF1 and RASopathy genes in sun-exposed melanomas. *Nat Genet* **2015**, *47*, 996-1002, doi:10.1038/ng.3361.
3. Hodis, E.; Watson, I.R.; Kryukov, G.V.; Arold, S.T.; Imielinski, M.; Theurillat, J.P.; Nickerson, E.; Auclair, D.; Li, L.; Place, C., et al. A landscape of driver mutations in melanoma. *Cell* **2012**, *150*, 251-263, doi:10.1016/j.cell.2012.06.024.
4. Hayward, N.K.; Wilmott, J.S.; Waddell, N.; Johansson, P.A.; Field, M.A.; Nones, K.; Patch, A.M.; Kakavand, H.; Alexandrov, L.B.; Burke, H., et al. Whole-genome landscapes of major melanoma subtypes. *Nature* **2017**, *545*, 175-180, doi:10.1038/nature22071.
5. Liang, W.S.; Hendricks, W.; Kiefer, J.; Schmidt, J.; Sekar, S.; Carpten, J.; Craig, D.W.; Adkins, J.; Cuyugan, L.; Manojlovic, Z., et al. Integrated genomic analyses reveal frequent TERT aberrations in acral melanoma. *Genome Res* **2017**, *27*, 524-532, doi:10.1101/gr.213348.116.
6. Newell, F.; Kong, Y.; Wilmott, J.S.; Johansson, P.A.; Ferguson, P.M.; Cui, C.; Li, Z.; Kazakoff, S.H.; Burke, H.; Dodds, T.J., et al. Whole-genome landscape of mucosal melanoma reveals diverse drivers and therapeutic targets. *Nat Commun* **2019**, *10*, 3163, doi:10.1038/s41467-019-11107-x.
7. Garman, B.; Anastopoulos, I.N.; Krepler, C.; Brafford, P.; Sproesser, K.; Jiang, Y.; Wubbenhorst, B.; Amaravadi, R.; Bennett, J.; Beqiri, M., et al. Genetic and Genomic Characterization of 462 Melanoma Patient-Derived Xenografts, Tumor Biopsies, and Cell Lines. *Cell Rep* **2017**, *21*, 1936-1952, doi:10.1016/j.celrep.2017.10.052.
8. Krepler, C.; Sproesser, K.; Brafford, P.; Beqiri, M.; Garman, B.; Xiao, M.; Shannan, B.; Watters, A.; Perego, M.; Zhang, G., et al. A Comprehensive Patient-Derived Xenograft Collection Representing the Heterogeneity of Melanoma. *Cell Rep* **2017**, *21*, 1953-1967, doi:10.1016/j.celrep.2017.10.021.
9. Kato, S.; Goodman, A.; Walavalkar, V.; Barkauskas, D.A.; Sharabi, A.; Kurzrock, R. Hyperprogressors after Immunotherapy: Analysis of Genomic Alterations Associated with Accelerated Growth Rate. *Clin Cancer Res* **2017**, *23*, 4242-4250, doi:10.1158/1078-0432.CCR-16-3133.
10. Forschner, A.; Niessner, H.; Moller, Y.; Horak, P.; Frohlich, M.; Warsow, G.; Stenzinger, A.; Frohling, S.; Glimm, H.; Klumpp, B., et al. Genomics of Immunotherapy-Associated Hyperprogressors-Letter. *Clinical cancer research : an official journal of the American Association for Cancer Research* **2017**, *23*, 6374-6375, doi:10.1158/1078-0432.Ccr-17-1480.
11. Forschner, A.; Hilke, F.J.; Bonzheim, I.; Gschwind, A.; Demidov, G.; Amaral, T.; Ossowski, S.; Riess, O.; Schroeder, C.; Martus, P., et al. MDM2, MDM4 and EGFR Amplifications and Hyperprogression in Metastatic Acral and Mucosal Melanoma. *Cancers (Basel)* **2020**, *12*, doi:10.3390/cancers12030540.
12. Trujillo, J.A.; Luke, J.J.; Zha, Y.; Segal, J.P.; Ritterhouse, L.L.; Spranger, S.; Matijevich, K.; Gajewski, T.F. Secondary resistance to immunotherapy associated with beta-catenin pathway activation or PTEN loss in metastatic melanoma. *J Immunother Cancer* **2019**, *7*, 295, doi:10.1186/s40425-019-0780-0.

Author manuscript

13. Horn, S.; Leonardelli, S.; Sucker, A.; Schadendorf, D.; Griewank, K.G.; Paschen, A. Tumor CDKN2A-Associated JAK2 Loss and Susceptibility to Immunotherapy Resistance. *Journal of the National Cancer Institute* **2018**, *110*, 677-681, doi:10.1093/jnci/djx271.
14. Zaretsky, J.M.; Garcia-Diaz, A.; Shin, D.S.; Escuin-Ordinas, H.; Hugo, W.; Hu-Lieskovan, S.; Torrejon, D.Y.; Abril-Rodriguez, G.; Sandoval, S.; Barthly, L., et al. Mutations Associated with Acquired Resistance to PD-1 Blockade in Melanoma. *N Engl J Med* **2016**, *375*, 819-829, doi:10.1056/NEJMoa1604958.
15. Gao, J.; Shi, L.Z.; Zhao, H.; Chen, J.; Xiong, L.; He, Q.; Chen, T.; Roszik, J.; Bernatchez, C.; Woodman, S.E., et al. Loss of IFN-gamma Pathway Genes in Tumor Cells as a Mechanism of Resistance to Anti-CTLA-4 Therapy. *Cell* **2016**, *167*, 397-404 e399, doi:10.1016/j.cell.2016.08.069.
16. Boshuizen, J.; Koopman, L.A.; Krijgsman, O.; Shahrabi, A.; van den Heuvel, E.G.; Ligtenberg, M.A.; Vredevoogd, D.W.; Kemper, K.; Kuilman, T.; Song, J.Y., et al. Cooperative targeting of melanoma heterogeneity with an AXL antibody-drug conjugate and BRAF/MEK inhibitors. *Nat Med* **2018**, *24*, 203-212, doi:10.1038/nm.4472.
17. Li, H.; Durbin, R. Fast and accurate short read alignment with Burrows-Wheeler transform. *Bioinformatics (Oxford, England)* **2009**, *25*, 1754-1760, doi:10.1093/bioinformatics/btp324.
18. Kim, S.; Scheffler, K.; Halpern, A.L.; Bekritsky, M.A.; Noh, E.; Kallberg, M.; Chen, X.; Kim, Y.; Beyter, D.; Krusche, P., et al. Strelka2: fast and accurate calling of germline and somatic variants. *Nat Methods* **2018**, *15*, 591-594, doi:10.1038/s41592-018-0051-x.
19. Demidov, G.; Ossowski, S. ClinCNV: novel method for allele-specific somatic copy-number alterations detection. *bioRxiv* **2019**, 10.1101/837971, 837971, doi:10.1101/837971.
20. Cingolani, P.; Platts, A.; Wang le, L.; Coon, M.; Nguyen, T.; Wang, L.; Land, S.J.; Lu, X.; Ruden, D.M. A program for annotating and predicting the effects of single nucleotide polymorphisms, SnpEff: SNPs in the genome of Drosophila melanogaster strain w1118; iso-2; iso-3. *Fly (Austin)* **2012**, *6*, 80-92, doi:10.4161/fly.19695.
21. Cingolani, P.; Patel, V.M.; Coon, M.; Nguyen, T.; Land, S.J.; Ruden, D.M.; Lu, X. Using Drosophila melanogaster as a Model for Genotoxic Chemical Mutational Studies with a New Program, SnpSift. *Frontiers in genetics* **2012**, *3*, 35, doi:10.3389/fgene.2012.00035.
22. Tamborero, D.; Rubio-Perez, C.; Deu-Pons, J.; Schroeder, M.P.; Vivancos, A.; Rovira, A.; Tusquets, I.; Albanell, J.; Rodon, J.; Tabernero, J., et al. Cancer Genome Interpreter annotates the biological and clinical relevance of tumor alterations. *Genome medicine* **2018**, *10*, 25, doi:10.1186/s13073-018-0531-8.
23. Mayakonda, A.; Lin, D.C.; Assenov, Y.; Plass, C.; Koeffler, H.P. Maftools: efficient and comprehensive analysis of somatic variants in cancer. *Genome research* **2018**, *28*, 1747-1756, doi:10.1101/gr.239244.118.
24. Eisenhauer, E.A.; Therasse, P.; Bogaerts, J.; Schwartz, L.H.; Sargent, D.; Ford, R.; Dancey, J.; Arbuck, S.; Gwyther, S.; Mooney, M., et al. New response evaluation criteria in solid tumours: revised RECIST guideline (version 1.1). *European journal of cancer (Oxford, England : 1990)* **2009**, *45*, 228-247, doi:10.1016/j.ejca.2008.10.026.
25. Fares, C.M.; Van Allen, E.M.; Drake, C.G.; Allison, J.P.; Hu-Lieskovan, S. Mechanisms of Resistance to Immune Checkpoint Blockade: Why Does Checkpoint Inhibitor

Authors manuscript

Immunotherapy Not Work for All Patients? *American Society of Clinical Oncology educational book / ASCO. American Society of Clinical Oncology. Meeting* **2019**, *39*, 147-164, doi:10.1200/edbk_240837.
26. Brenner, E.; Schorg, B.F.; Ahmetlic, F.; Wieder, T.; Hilke, F.J.; Simon, N.; Schroeder, C.; Demidov, G.; Riedel, T.; Fehrenbacher, B., et al. Cancer immune control needs senescence induction by interferon-dependent cell cycle regulator pathways in tumours. *Nature communications* **2020**, *11*, 1335, doi:10.1038/s41467-020-14987-6.
27. Parrella, P.; Caballero, O.L.; Sidransky, D.; Merbs, S.L. Detection of c-myc amplification in uveal melanoma by fluorescent in situ hybridization. *Investigative ophthalmology & visual science* **2001**, *42*, 1679-1684.
28. Lin, X.; Sun, R.; Zhao, X.; Zhu, D.; Zhao, X.; Gu, Q.; Dong, X.; Zhang, D.; Zhang, Y.; Li, Y., et al. C-myc overexpression drives melanoma metastasis by promoting vasculogenic mimicry via c-myc/snail/Bax signaling. *Journal of molecular medicine (Berlin, Germany)* **2017**, *95*, 53-67, doi:10.1007/s00109-016-1452-x.
29. Wolfer, A.; Ramaswamy, S. MYC and metastasis. *Cancer research* **2011**, *71*, 2034-2037, doi:10.1158/0008-5472.can-10-3776.
30. McCarthy, C.; Kalirai, H.; Lake, S.L.; Dodson, A.; Damato, B.E.; Coupland, S.E. Insights into genetic alterations of liver metastases from uveal melanoma. *Pigment cell & melanoma research* **2016**, *29*, 60-67, doi:10.1111/pcmr.12433.
31. Robertson, A.G.; Shih, J.; Yau, C.; Gibb, E.A.; Oba, J.; Mungall, K.L.; Hess, J.M.; Uzunangelov, V.; Walter, V.; Danilova, L., et al. Integrative Analysis Identifies Four Molecular and Clinical Subsets in Uveal Melanoma. *Cancer cell* **2017**, *32*, 204-220.e215, doi:10.1016/j.ccell.2017.07.003.
32. Park, J.J.; Diefenbach, R.J.; Joshua, A.M.; Kefford, R.F.; Carlino, M.S.; Rizos, H. Oncogenic signaling in uveal melanoma. *Pigment cell & melanoma research* **2018**, *31*, 661-672, doi:10.1111/pcmr.12708.
33. Egberts, F.; Bergner, I.; Kruger, S.; Haag, J.; Behrens, H.M.; Hauschild, A.; Rocken, C. Metastatic melanoma of unknown primary resembles the genotype of cutaneous melanomas. *Annals of oncology : official journal of the European Society for Medical Oncology / ESMO* **2014**, *25*, 246-250, doi:10.1093/annonc/mdt411.
34. Heppt, M.V.; Tietze, J.K.; Reinholz, M.; Rahimi, F.; Jung, A.; Kirchner, T.; Ruzicka, T.; Flaig, M.J.; Berking, C. Disease kinetics but not disease burden is relevant for survival in melanoma of unknown primary tumor. *Discovery medicine* **2015**, *20*, 231-237.
35. Curtin, J.A.; Fridlyand, J.; Kageshita, T.; Patel, H.N.; Busam, K.J.; Kutzner, H.; Cho, K.H.; Aiba, S.; Brocker, E.B.; LeBoit, P.E., et al. Distinct sets of genetic alterations in melanoma. *The New England journal of medicine* **2005**, *353*, 2135-2147, doi:10.1056/NEJMoa050092.
36. Furney, S.J.; Pedersen, M.; Gentien, D.; Dumont, A.G.; Rapinat, A.; Desjardins, L.; Turajlic, S.; Piperno-Neumann, S.; de la Grange, P.; Roman-Roman, S., et al. SF3B1 mutations are associated with alternative splicing in uveal melanoma. *Cancer discovery* **2013**, *3*, 1122-1129, doi:10.1158/2159-8290.cd-13-0330.
37. Fruh, M.; Peters, S. EGFR mutation subtype impacts efficacy of immune checkpoint inhibitors in non-small-cell lung cancer. *Annals of oncology : official journal of the European Society for Medical Oncology / ESMO* **2019**, *30*, 1190-1192, doi:10.1093/annonc/mdz185.
38. Lee, C.K.; Man, J.; Lord, S.; Links, M.; Gebski, V.; Mok, T.; Yang, J.C. Checkpoint Inhibitors in Metastatic EGFR-Mutated Non-Small Cell Lung Cancer-A Meta-Analysis.

Authors manuscript

Journal of thoracic oncology : official publication of the International Association for the Study of Lung Cancer **2017**, *12*, 403-407, doi:10.1016/j.jtho.2016.10.007.
39. Ozaki, Y.; Muto, S.; Takagi, H.; Watanabe, M.; Inoue, T.; Fukuhara, M.; Yamaura, T.; Okabe, N.; Matsumura, Y.; Hasegawa, T., et al. Tumor mutation burden and immunological, genomic, and clinicopathological factors as biomarkers for checkpoint inhibitor treatment of patients with non-small-cell lung cancer. *Cancer Immunol Immunother* **2020**, *69*, 127-134, doi:10.1007/s00262-019-02446-1.
40. Johnson, D.B.; Pectasides, E.; Feld, E.; Ye, F.; Zhao, S.; Johnpulle, R.; Merritt, R.; McDermott, D.F.; Puzanov, I.; Lawrence, D., et al. Sequencing Treatment in BRAFV600 Mutant Melanoma: Anti-PD-1 Before and After BRAF Inhibition. *Journal of immunotherapy (Hagerstown, Md. : 1997)* **2017**, *40*, 31-35, doi:10.1097/cji.0000000000000148.
41. Moser, J.C.; Chen, D.; Hu-Lieskovan, S.; Grossmann, K.F.; Patel, S.; Colonna, S.V.; Ying, J.; Hyngstrom, J.R. Real-world survival of patients with advanced BRAF V600 mutated melanoma treated with front-line BRAF/MEK inhibitors, anti-PD-1 antibodies, or nivolumab/ipilimumab. *Cancer Med* **2019**, *8*, 7637-7643, doi:10.1002/cam4.2625.
42. Schilling, B.; Martens, A.; Geukes Foppen, M.H.; Gebhardt, C.; Hassel, J.C.; Rozeman, E.A.; Gesierich, A.; Gutzmer, R.; Kahler, K.C.; Livingstone, E., et al. First-line therapy-stratified survival in BRAF-mutant melanoma: a retrospective multicenter analysis. *Cancer Immunol Immunother* **2019**, *68*, 765-772, doi:10.1007/s00262-019-02311-1.
43. Kong, Y.; Sheng, X.; Wu, X.; Yan, J.; Ma, M.; Yu, J.; Si, L.; Chi, Z.; Cui, C.; Dai, J., et al. Frequent Genetic Aberrations in the CDK4 Pathway in Acral Melanoma indicate the potential for CDK4/6 Inhibitors in Targeted Therapy. *Clinical cancer research : an official journal of the American Association for Cancer Research* **2017**, 10.1158/1078-0432.ccr-17-0070, doi:10.1158/1078-0432.ccr-17-0070.
44. Tang, B.; Sheng, X.; Kong, Y.; Chi, Z.; Si, L.; Cui, C.; Yan, X.; Mao, L.; Lian, B.; Li, S., et al. Palbociclib for treatment of metastatic melanoma with copy number variations of CDK4 pathway: case report. *Chinese clinical oncology* **2018**, 10.21037/cco.2018.06.08, doi:10.21037/cco.2018.06.08.
45. Young, R.J.; Waldeck, K.; Martin, C.; Foo, J.H.; Cameron, D.P.; Kirby, L.; Do, H.; Mitchell, C.; Cullinane, C.; Liu, W., et al. Loss of CDKN2A expression is a frequent event in primary invasive melanoma and correlates with sensitivity to the CDK4/6 inhibitor PD0332991 in melanoma cell lines. *Pigment cell & melanoma research* **2014**, *27*, 590-600, doi:10.1111/pcmr.12228.
46. Posch, C.; Sanlorenzo, M.; Ma, J.; Kim, S.T.; Zekhtser, M.; Ortiz-Urda, S. MEK/CDK4,6 co-targeting is effective in a subset of NRAS, BRAF and 'wild type' melanomas. *Oncotarget* **2018**, *9*, 34990-34995, doi:10.18632/oncotarget.26204.
47. Mateo, J.; Lord, C.J.; Serra, V.; Tutt, A.; Balmana, J.; Castroviejo-Bermejo, M.; Cruz, C.; Oaknin, A.; Kaye, S.B.; de Bono, J.S. A decade of clinical development of PARP inhibitors in perspective. *Annals of oncology : official journal of the European Society for Medical Oncology / ESMO* **2019**, *30*, 1437-1447, doi:10.1093/annonc/mdz192.
48. Van Allen, E.M.; Miao, D.; Schilling, B.; Shukla, S.A.; Blank, C.; Zimmer, L.; Sucker, A.; Hillen, U.; Foppen, M.H.G.; Goldinger, S.M., et al. Genomic correlates of response to CTLA-4 blockade in metastatic melanoma. *Science (New York, N.Y.)* **2015**, *350*, 207-211, doi:10.1126/science.aad0095.
49. Johnson, D.B.; Frampton, G.M.; Rioth, M.J.; Yusko, E.; Xu, Y.; Guo, X.; Ennis, R.C.; Fabrizio, D.; Chalmers, Z.R.; Greenbowe, J., et al. Targeted Next Generation

Author manuscript

Sequencing Identifies Markers of Response to PD-1 Blockade. *Cancer immunology research* **2016**, *4*, 959-967, doi:10.1158/2326-6066.cir-16-0143.
50. Network, C.G.A. Genomic classification of cutaneous melanoma. *Cell* **2015**, *161*, 1681-1696, doi:10.1016/j.cell.2015.05.044.
51. Snyder, A.; Makarov, V.; Merghoub, T.; Yuan, J.; Zaretsky, J.M.; Desrichard, A.; Walsh, L.A.; Postow, M.A.; Wong, P.; Ho, T.S., et al. Genetic basis for clinical response to CTLA-4 blockade in melanoma. *The New England journal of medicine* **2014**, *371*, 2189-2199, doi:10.1056/NEJMoa1406498.
52. Forschner, A.; Battke, F.; Hadaschik, D.; Schulze, M.; Weissgraeber, S.; Han, C.T.; Kopp, M.; Frick, M.; Klumpp, B.; Tietze, N., et al. Tumor mutation burden and circulating tumor DNA in combined CTLA-4 and PD-1 antibody therapy in metastatic melanoma - results of a prospective biomarker study. *Journal for immunotherapy of cancer* **2019**, *7*, 180, doi:10.1186/s40425-019-0659-0.

Authors manuscript

Table and figure legends

Table 1: Patient cohort

The collective with details on the patients, their primary tumors, disease courses and sequenced tissues are presented here

Table 2: Tumor mutation burden, number of SNVs and CNVs of melanoma subtypes

Melanoma of unknown primary did not differ in tumor mutation burden, number of somatic single nucleotide variants (SNVs) or somatic copy number variants (CNVs) from cutaneous melanoma whereas tumor mutation burden / number of SNVs of cutaneous melanoma were significant higher than tumor mutation burden / number of SNVs of acral melanoma, mucosal melanoma, and uveal melanoma. Mucosal melanoma had significant more CNVs than cutaneous melanoma. The p-values were calculated using the Mann-Whitney-U Test.

Figure 1-Oncoplot of the most frequently mutated genes with driver mutations

Figure 1 shows a summary of the driver mutations of the melanoma cohort most frequently found, based on the 275 genes contained in all 3 panel versions (ssSCv2/v3/v4). The Oncoplot shows the patients in horizontal orientation and the gene and the corresponding driver mutations per patient in vertical orientation. The plot is divided into three parts, in the upper area (a) all somatic single nucleotide variants (SNVs) and small insertions and deletions (INDELs) per patient, including the synonymous variants, are shown. The middle panel (b) summarizes all somatic SNVs found with a frequency of at least five percent, plus the two genes *GNAQ* and *BAP1*. The lower panel (c) summarizes the 15 most mutated genes with somatic copy number changes (CNVs). For both panel (b) and (c), only mutations that were annotated as drivers or druggable biomarkers by the Cancer Genome Interpreter (CGI) are shown. The entire cohort is sorted by the histopathological subtype in a gray scale (cutaneous, acral-lentiginous, mucosal, uveal, melanoma of unknown primary = occult). In addition the type of therapy is annotated

Authors manuscript

(red: combined immunotherapy, n = 60; blue: anti-PD-1, n = 15; green: no immunotherapy, n = 7).

Figure 2- Tumor mutation burden, copy number variants and genetic subtypes

Figure 2 shows the comparison of tumor mutation burden (TMB), number of somatic copy number changes (CNVs) and the frequency of the genetic subtypes *BRAF*, *NRAS*, *NF1* and Triple wild-type (triple-WT) between the four histopathological subtypes (cutaneous, acral-lentiginous, mucosal, uveal) and the melanoma of unknown primary (occult). The figure consists of 3 histograms (a, b, c), whereby the y-axis always represents the histopathological subtypes. On the x-axis the TMB is indicated in (a), as mutations per megabase (Mut/Mb), in (b) the number of somatic CNVs, in absolute numbers related to the 275 common genes and in (c) the genetic subtype in absolute numbers. Patients with cutaneous melanoma have the most somatic SNVs and thus the highest median TMB compared to the remaining three subtypes ($p \leq 0.003$). The median TMB of occult and cutaneous melanoma is only slightly different with 7.5 var/Mb versus 9.4 var/Mb, respectively. The mucosal melanoma clearly has the most somatic CNVs with a median of 33 and there is a significant difference between the mucosal and cutaneous melanoma ($p = 0.025$) and the uveal and occult melanoma ($p = 0.025$). Cutaneous melanoma shows an even distribution of *BRAF* and RAS mutated patients (40% each) and patients with melanoma of unknown primary are also in 45% *BRAF* mutated. The other three subtypes show a clear overweight of tumors with the status triple-WT.

Figure 3- Gene set enrichment analysis of histopathological subtypes

Figure 3 summarizes the genetic differences, based on the gene set enrichment analysis (subtype versus rest of the cohort), of the four histopathological subtypes and the melanoma of unknown primary (occult). The figure consists of a histogram (a) showing the number of somatic changes (SNVs), including synonymous variants, and the median (m) of each subtype. Below is the Oncoplot (b). It is sorted by histopathological subtypes cutaneous, acral-lentiginous, mucosal,

Authors manuscript

occult and uveal melanoma (gray scale). It summarizes the genes that are significant ($p < 0.05$) for each subtype. In vertical alignment, the patients are summarized and in horizontal alignment the genes and the corresponding changes. On the left side the frequency, as a histogram in percent, of the somatic mutations (drivers) per gene, related to the total cohort, is shown. The panel (c) shows the frequency (in percent) of mutations per gene related to the subtypes (gray scale) compared to the rest of the cohort. For cutaneous melanoma, the genes *BRAF* ($p = 0.009$), *NRAS* ($p = 0.0004$) and *CDKN2A* ($p = 0.03$) are significantly enriched mutated compared to the rest of the cohort. For the acral-lentiginous melanoma the genes *RICTOR* ($p = 0.01$), *CDK4* ($p = 0.04$), *PDGFRA* ($p = 0.03$) and *KIT* ($p = 0.03$) are enriched mutated, for the mucosal melanoma the genes *CCND2* ($p = 0.01$) and *CHEK2* ($p = 0.03$) are enriched mutated, for the melanoma of unknown primary the gene *ERBB2* ($p = 0.03$) is enriched mutated and for the uveal melanoma the genes *GNAQ* ($p = 0.0006$), *GNA11* ($p = 0.00001$), *BAP1* ($p = 0.0006$), *MYC* ($p = 0.000003$) and *SF3B1* ($p = 0.0000002$) are enriched mutated.

Figure 4- Gene set enrichment analysis according to treatment response to immune checkpoint inhibitors

Figure 4 shows the result of the gene set enrichment analysis (a) related to the three response groups (progressive and stable disease, partial response), as well as the overall survival of the three groups (b) and the influence of pre-therapy with BRAF/MEK inhibitors before the start of immunotherapy (c). For patients categorized as progressive disease at first staging, mutations in the genes *BRAF* ($p = 0.01$) and *EGFR* ($p = 0.04$) were enriched mutated compared to patients with a stable disease or partial response. In 89% of cases (16 out of 18), patients with *BRAF* mutations had previously received BRAF/MEK inhibition before receiving immunotherapy. When using this information for the comparison of overall survival, the patients who had previously received BRAF/MEK inhibitor therapy showed a significantly worse overall survival ($p = 0.015$, log-rank Mantel-Cox test) of 435 days and a one-year survival rate of 51%

Authors manuscript

compared to patients who had mutated *BRAF* but did not receive prior therapy with BRAF/MEK inhibitors (OS = undefined only two death occurred, 1 year survival rate = 72%) or who are BRAF wild-type (OS = 809 days, 1 year survival rate = 80%).

Authors manuscript

List of supporting information

Supplement table 1 - Cancer panel version ssSCv2

Supplement table 2 - Cancer panel version ssSCv3

Supplemental table 3 - Cancer panel version ssSCv4

Supplement table 4 - List of common 275 genes present in all three panel versions

Supplement table 5 - List of all somatic mutation (SNVs and INDELs) identified in all 82 patients unfiltered for the common 275 genes

Supplement table 6 - List of all somatic copy number variants (Amp & Del) identified in all 82 patients unfiltered for the common 275 genes

Supplement table 7 - Tumor mutation burden [Mut/Mb] of all 82 patients

Supplement table 8 - List of all somatic mutation (SNVs and INDELs) filtered for the common 275 genes and driver mutations

Supplement table 9 - List of all somatic copy number variants (Amp & Del) identified in all 82 patients filtered for the common 275 genes and driver mutations

Supplement table 10 - genomic subtype

Supplement table 11 - gene set enrichment based on histopathological subtype

Supplement table 12 - Overall survival based on disease groups

Supplement table 13 - gene set enrichment based on disease group

Supplement table 14 - Overall survival based on BRAF mutation status and pre-treatment with BRAF/MEK inhibitors

Authors manuscript

Next-generation sequencing in a real world cohort of 82 advanced melanoma patients indentifies distinct mutation pattern in different melanoma subtypes
Figure 1

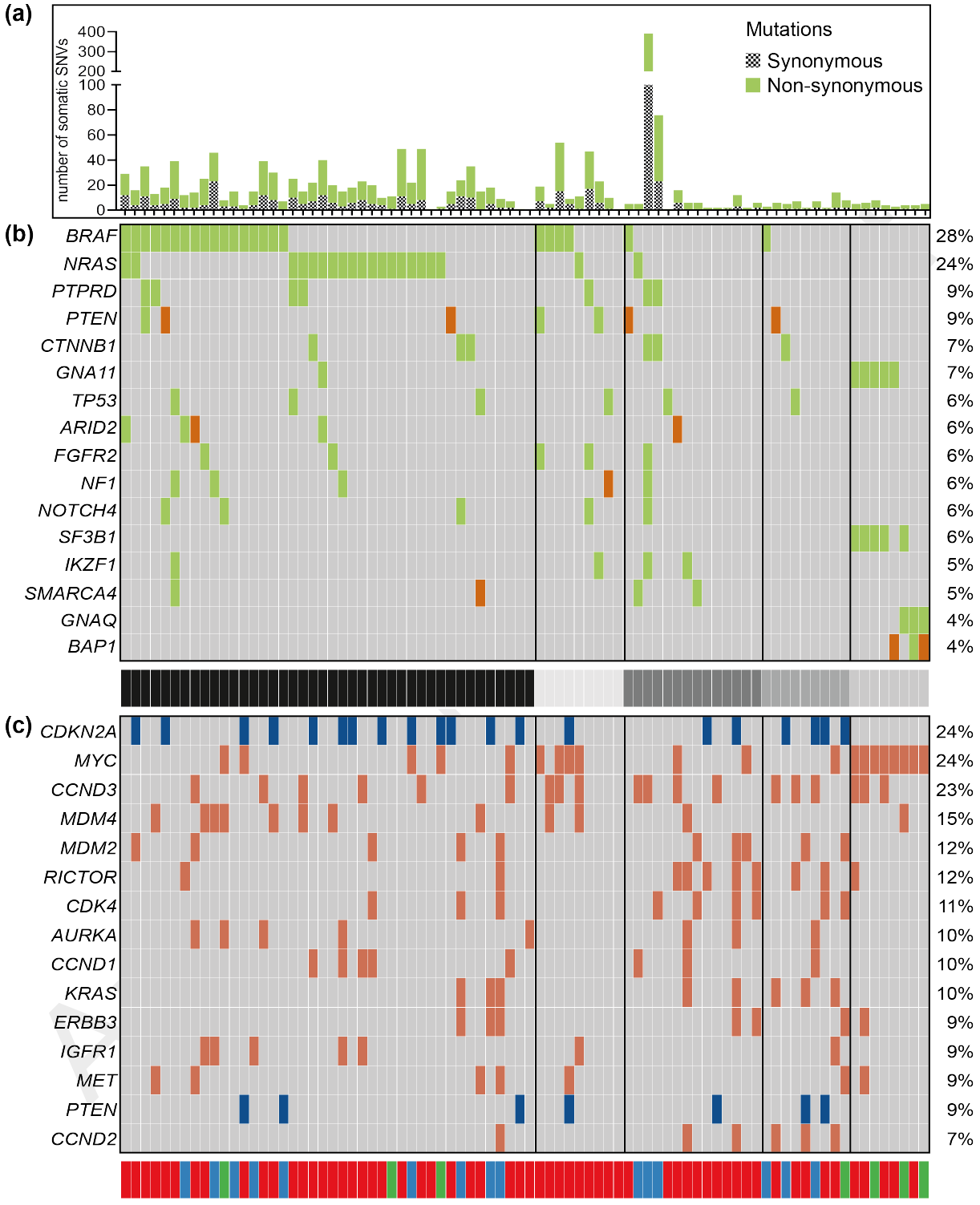

642

Next-generation sequencing in a real world cohort of 82 advanced melanoma patients identifies distinct mutation pattern in different melanoma subtypes
Figure 2

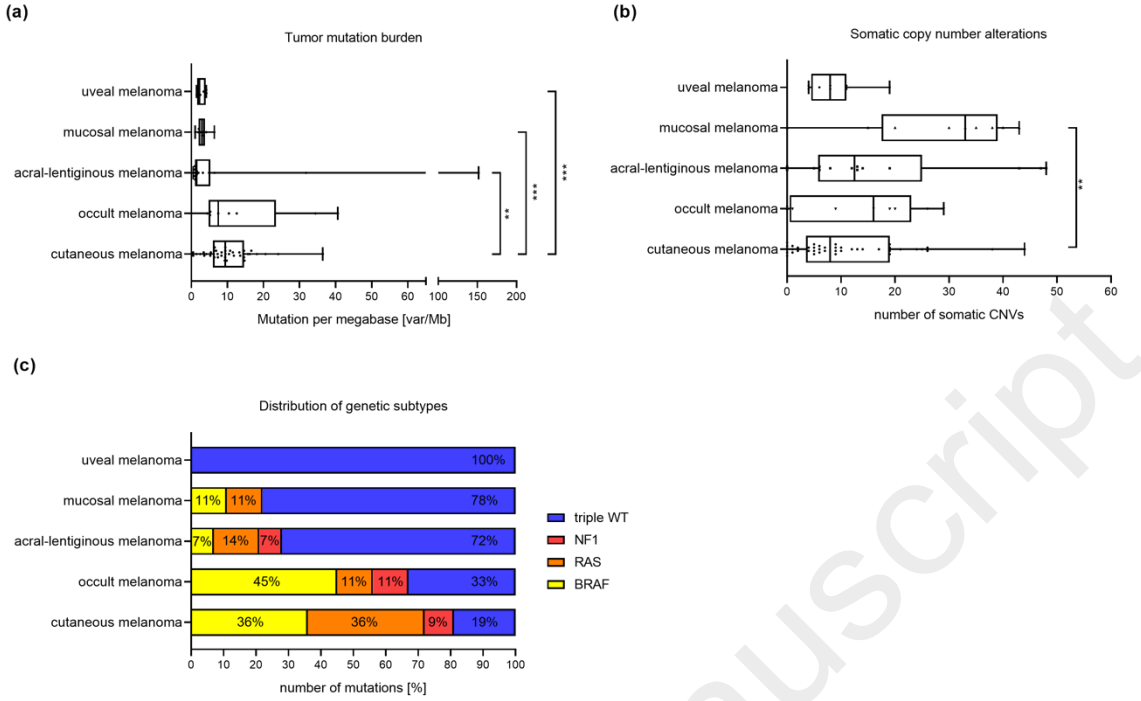

643

Authors manuscript

Next-generation sequencing in a real world cohort of 82 advanced melanoma patients indentifies distinct mutation pattern in different melanoma subtypes
Figure 3

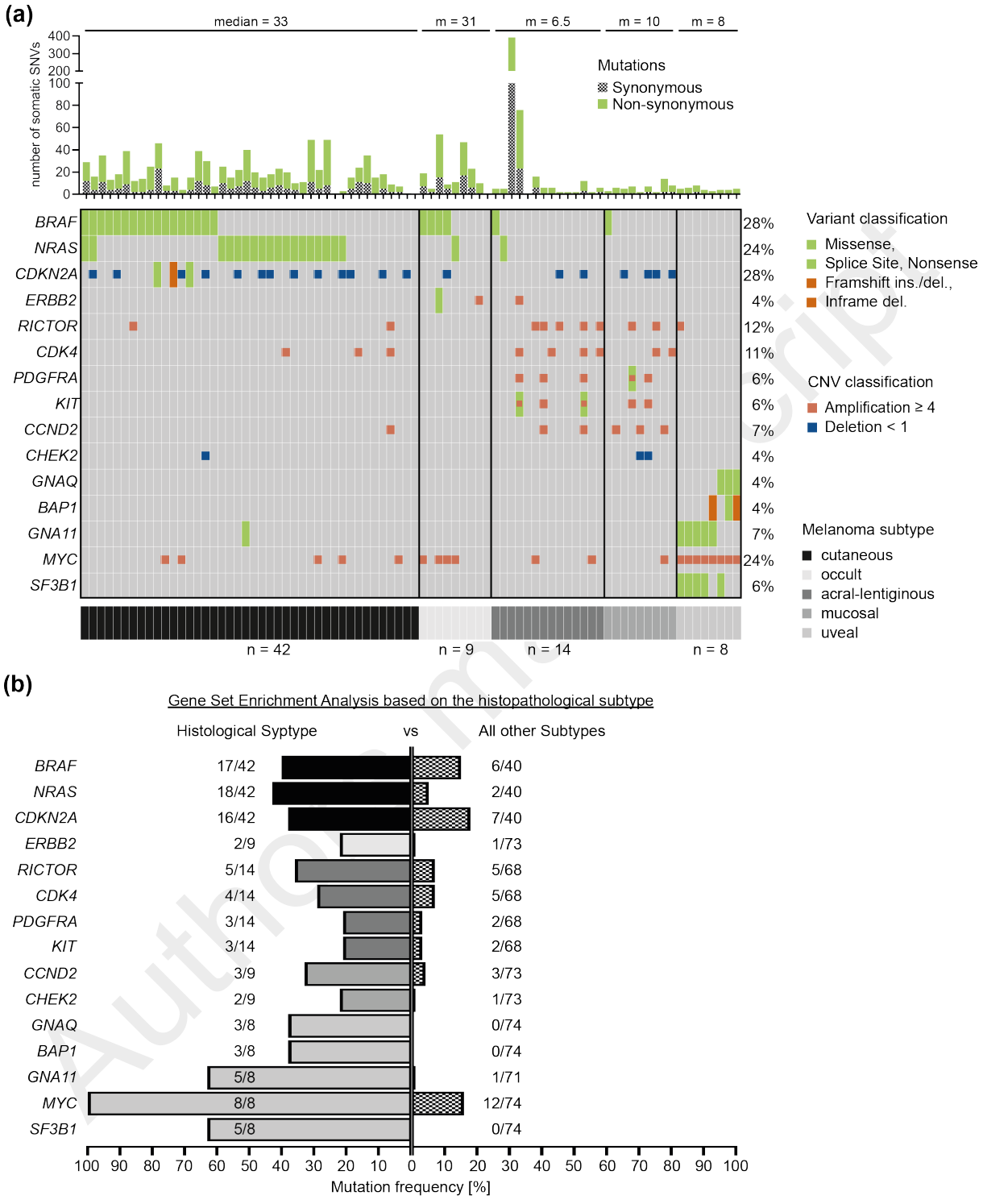

644

Author manuscript

Next-generation sequencing in a real world cohort of 82 advanced melanoma patients indentifies distinct mutation pattern in different melanoma subtypes
Figure 4

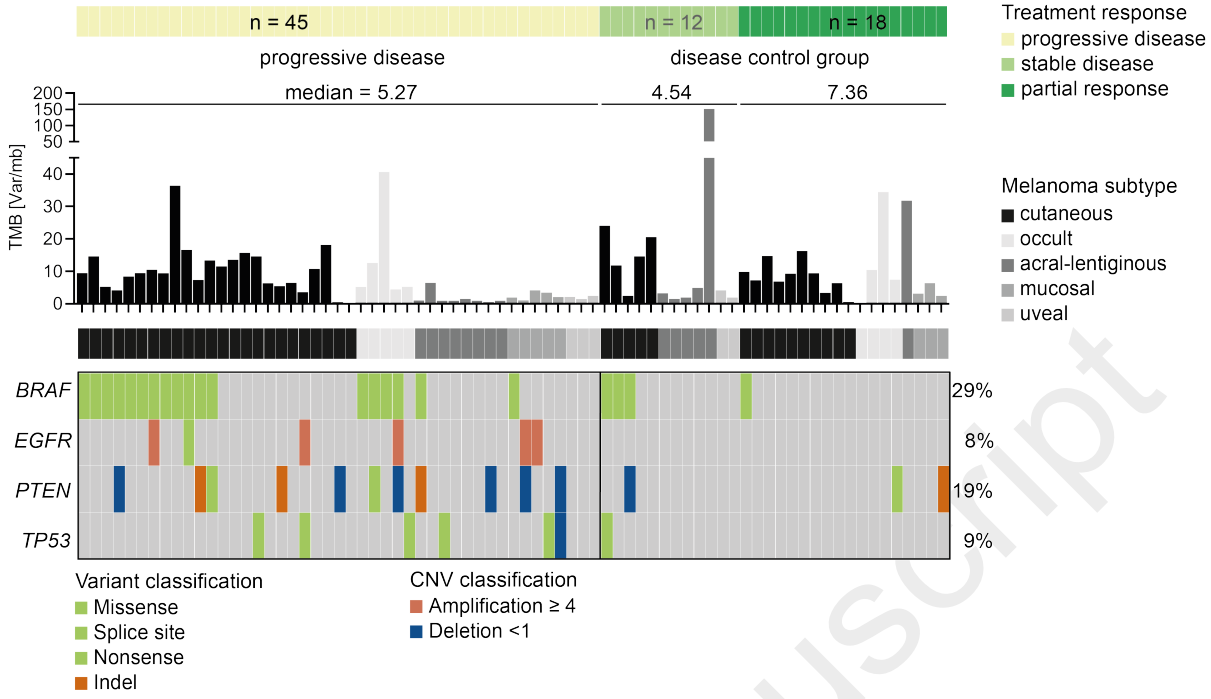

645

Authors manuscript